TRMM

A SATELLITE MISSION TO MEASURE TROPICAL RAINFALL

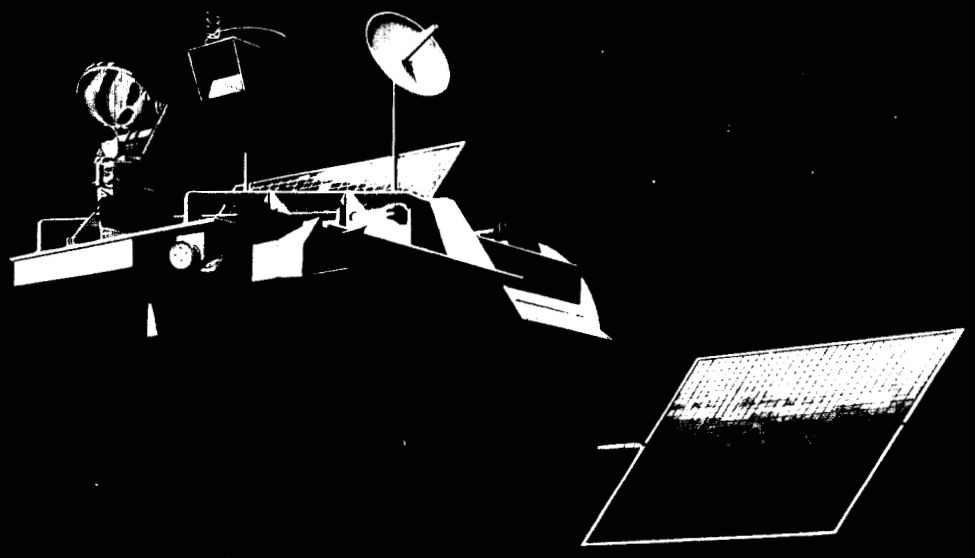

Report of the Science Steering Group

NASA
National Aeronautics and Space Administration

REPORT OF THE SCIENCE STEERING GROUP

FOR A

TROPICAL RAINFALL MEASURING MISSION

(TRMM)

Edited by

JOANNE SIMPSON
Goddard Space Flight Center
Greenbelt, Maryland 20771

AUGUST 1988

TROPICAL RAINFALL MEASURING MISSION SCIENCE STEERING GROUP

PHILIP ARKIN
National Oceanic and Atmos. Admin.

DAVID ATLAS
Consultant

GEOFFREY AUSTIN
McGill University

CHARLES ELACHI
Jet Propulsion Laboratory

NOBUYOSHI FUGONO
Communications Research Laboratory, Japan

MICHAEL GARSTANG
University of Virginia

ROBERT HOUZE
University of Washington

MICHAEL HUDLOW
National Oceanic and Atmos. Admin.

TAROH MATSUNO
University of Tokyo

GERALD NORTH
Texas A&M University

EUGENE RASMUSSON, Chairman
University of Maryland

JAGADISH SHUKLA
University of Maryland

JOANNE SIMPSON, Study Scientist
Goddard Space Flight Center

ROY SPENCER
Marshall Space Flight Center

VERNER SUOMI
University of Wisconsin

OTTO THIELE, Executive Secretary
Goddard Space Flight Center

PETER WEBSTER
Pennsylvania State University

JAMES WEINMAN
Applied Research Corporation

THOMAS WILHEIT
Goddard Space Flight Center

EDWARD ZIPSER
National Center for Atmos. Research

PREFACE

The Tropical Rainfall Measuring Mission (TRMM), a satellite program now being studied jointly by the United States and Japan, would carry out the systematic study of tropical rainfall required for major strides in weather and climate research. As the first of National Aeronautics and Space Administration's (NASA's) planned Earth Probe series of research satellites, TRMM could be launched as a free flyer as early as 1994. TRMM could also be one of the first major elements on the Space Station in the late 1990's. The Earth Probe program is a series of small, specialized Earth Science satellite missions which was outlined in the overall strategy developed by the Earth System Science Committee.

The present report has been prepared by the TRMM Science Steering Group (SSG), which is a team of 19 experts in atmospheric, oceanic, and remote sensing sciences. This report presents the scientific justification for TRMM and outlines the implementation process for the scientific community, NASA management, and the other decision-makers and advisory persons who are expected to evaluate the priority of this project.

John S. Theon
Chief, Atmospheric Dynamics and Radiation Branch
Earth Science and Applications Division
Office of Space Science and Applications

EXECUTIVE SUMMARY

The Tropical Rainfall Measuring Mission (TRMM) is a proposed space system for measuring tropical rainfall and its variations. Such measurements are essential for the progress of our knowledge of the overall Earth system. Evaporation of water vapor into the atmosphere and its condensation to produce rainfall are at the heart of the Earth's habitability for man and other species. For instance, the placements of human settlements have been dictated more by the availability of an ample water supply than by any other factor. The nature of the Earth's vegetative cover is also controlled, to a very large extent, by the moisture conditions. Rainfall, of course, is central to the water supply.

Condensation of water vapor releases heat inside the Earth's atmosphere, and this is a principal driver for global-scale motions in the troposphere. The nature of this heat release coupled with the resulting motions concentrates the tropical rainfall largely into a latitudinally thin region called the intertropical convergence zone (ITCZ). Within this circumglobal zone, the rain falls from roughly 30 individual cloud clusters, each several hundred kilometers across. Within these cloud clusters, the vertical energy transports and about 60 percent of the rainfall are further concentrated into about 2,000 towering cumulonimbus clouds called "hot towers," which carry high energy air up to the upper troposphere, a function essential in driving the large world-wide meridional circulation called the Hadley cell. These towers contain updrafts ranging from about 5 to more than 30 m/s and sometimes generate rain rates above 100 mm/hr over 4 km by 4 km areas. The remainder of the rain has been recently found to fall at much more gradual rates from the large "anvils" or stratiform extrusions from the "hot towers." The fraction of anvil precipitation increases as the cloud system ages. The number, size, and preferred location of these cloud clusters varies considerably, on time scales ranging from days to years and longer, so that the atmospheric heat engine maintains a variable "fire box." The year-to-year variability of the latent heat released by these cloud clusters is now appreciated to be a leading cause for year-to-year global climate variations, most notably those variations which are linked to the El Niño-Southern Oscillation (ENSO).

The members of the Science Steering Group (SSG) who have jointly authored this report began their work in early 1986. In early 1987, the National Aeronautics and Space Administration (NASA) and the Science and Technology Agency of Japan instituted a study of the feasibility of implementing TRMM as a joint space mission. The main goal is to obtain a minimum of 3 years of climatological determinations of rainfall in the tropics, producing a data set of 30-day average rainfall over 5° by 5° areas, along with estimates of the vertical distribution of latent heat release.

There is presently tremendous uncertainty as to both the horizontal and vertical distribution of the tropical condensational heat source from month to month and year to year. Knowledge of the quantitative distribution of rainfall over the tropical oceans has been uncertain to a factor of about two. Quantitative dynamic models of year-to-year climate variability (e.g., models which include the ENSO phenomenon, which involves the tropical Pacific Ocean as well as the atmosphere) require better observations of tropical rainfall for their verification and improvement. Atmospheric general circulation models (GCMs) for both research and large-scale weather prediction are in dire need of better rainfall information for initialization and testing, while models of the 30-60 day tropical oscillation and models of the tropical atmosphere's impacts on distant air motion patterns (teleconnections) need more information on the vertical profile of latent heating in the tropics. We now know that this profile differs depending on the proportion of hot tower versus anvil precipitation present. Furthermore, the tropical ocean and atmosphere are closely coupled. It is estimated that both cloud radiation and the fresh water input from rainfall may have significant effects on ocean circulations and the marine biomass, while the associated variations in low-level winds determine whether or not upwelling of nutrient-rich water will take place.

The measurement of rainfall has always represented one of the most difficult challenges in meteorology. This is due to its high spatial variability on the meso- and smaller scales, together with its high time variability, both of which make measurements from existing sparse surface networks questionable in terms of representativeness. Also, it is true that most of the tropical rainfall occurs in regions that are relatively inaccessible to *in situ* measurements. The most ambitious field study of tropical rainfall that has been carried out to date, the 1974 *G*lobal Atmospheric Research Program *A*tlantic *T*ropical *E*xperiment (GATE) observations in the eastern Atlantic portion of the ITCZ, confirmed that tropical rainfall shows diurnal variations with different phase structure over the land and ocean as well as differing phase structure over different parts of the world's oceans. These regional differences in diurnal variability must be considered in the design of a mission to measure tropical rainfall.

It is clear that space measurement is the only means to a more accurate global documentation of tropical rainfall. Even now, space measurements have proven to be very useful. For instance, measurements of outgoing longwave radiation (OLR) from visible/infrared (VIS/IR) sensors on operational satellites have provided a proxy variable which serves as our current best estimator of rainfall variability over the tropical oceans. Also, passive microwave measurements from the Electrically Scanning Microwave Radiometer (ESMR) instrument on Nimbus-5, from the Scanning Multichannel Microwave Radiometer (SMMR) instrument on Nimbus-7, and from the Special Sensor Microwave/Imager (SSM/I) instrument on the Defense Meteorological Satellite Program (DMSP) have provided, and the latter will continue to provide, valuable information on rainfall. These passive microwave measurements have all been obtained from polar sun-synchronous orbits, so they cannot give representative estimates of daily or monthly average rainfalls in the presence of the large diurnal variations. The same will be true for the passive microwave measurements to be made on the Earth Observation System (Eos) polar platforms, which will also be in sun-synchronous orbit.

The current plans for the TRMM include three principal types of instruments. The most innovative of these is the first quantitative precipitation radar to be flown in space. The proposed TRMM radar will provide good measurements of

rain rates over both land and ocean. When properly constrained by the passive microwave measurements, the radar will be instrumental in obtaining the height profile of the precipitation content, from which the profile of latent heat release can be estimated. The second type instrument is a combination of a cross-track scanning multichannel dual-polarized passive microwave radiometer and a single-channel radiometer scanning in a similar mode. The radiometers will give good measurements of rainfall rates over the oceans, but such measurements are less reliable over land where the surface emissivity inhomogeneities make interpretation difficult. An Advanced Very High Resolution Radiometer (AVHRR) is also included in the TRMM instrument complement so that the rainfall measurements from the radar and passive microwave instruments can be used to better interpret VIS/IR measurements from past and future operational satellites. For this reason, TRMM is often referred to as a "flying rain gauge," with a high potential contribution to the World Climate Research Program's (WCRP's) rain climatology initiative.

The TRMM orbit is presently planned to be circular at an altitude of 350 km and at an inclination of 35°. This orbit will give intensive coverage in the tropics and will permit extraction of the diurnal cycle in climatological rainfall. The relatively low altitude also allows for much smaller instrumental footprints than those of previous microwave space sensors, leading to substantially more accurate retrieval capabilities of the rain variations, which normally occur over rather small space scales. Power and antenna size limitations currently limit the radar swath to about 220 km, which is a little more than one-third of the 600 km swath of the other instruments. The overlap region will be important for comparison studies between the different instruments and retrieval techniques. An extensive TRMM surface validation or "ground truth" program, supplemented by instrumented aircraft flights, is being developed for further refinement and testing of the remote sensing algorithms.

The first two chapters of this Report of the TRMM SSG are devoted to the scientific background and the deficiencies in our knowledge which lead to the need for TRMM. Chapter III states the science requirements, in terms of priority science questions, related important science and remote sensing questions, and the accuracy and resolution requirements. Chapter IV poses the overall approach to be adopted, addressing the question of whether tropical rainfall can be adequately sampled by a low Earth orbiter with the planned instrument swaths. The skewed distributions and autocorrelations characteristic of tropical rainfall are taken into account, as are important known relationships between rain areas and rain amounts. With the reservation that nearly all the sampling analyses to date are based on the GATE data, results indicate that the sampling error will be 10 percent or less, and it could be substantially reduced if polar orbiter microwave data were simultaneously available.

Chapter V describes the instrument complement, spacecraft, and the proposed system concept, including command, data relay, and tracking. The chapter concludes with an error analysis which considers the radar and passive microwave instruments together, combines both the sampling errors and an assumed instrument error, larger than expected, but uncorrelated among the different ranges of rain rate. The combined errors are estimated to be roughly 13 percent over oceans and roughly 20 percent over land. In the heavy rain ITCZ zone, these errors would amount to about 1.2 and 1.7 mm/day, respectively.

Chapter VI is a summary of the relevant work on rain retrieval methods and their testing, which has advanced substantially during 1988. The new retrieval methods make it possible to meet the TRMM science requirements with a single-frequency radar and a combination of the ESMR and SSM/I for the passive microwave complement. This chapter begins by presenting the complementarity of the TRMM instrument set, showing how the errors introduced by any one of the instruments tend to be mitigated by the capability of the other parts of the payload. Then multichannel passive microwave retrievals of several types are described with examples of applications to actual cloud systems. A summary of radar algorithms depending on attenuation and reflectivity is made, including the conditions under which each is applicable and brief results from an aircraft test are shown. A radar algorithm relating rain area to rain amount has been adapted for space and improved by relating it to the rain probability distribution function, leading to the algorithm now called the HART (Height Area Rainfall Threshold) technique. Another new algorithm development combining multichannel passive microwave techniques to constrain the radar equation for vertical hydrometeor profiling is outlined next. The value of the VIS/IR capability in pattern recognition, as well as in providing linkages with operational rain estimates, is summarized. Finally, algorithm development and testing by means of coupling cloud dynamical/microphysical models to cloud radiative models is illustrated, in combination with actual observational tests with high-level aircraft microwave data in a continuing program.

Chapter VII outlines the validation or "ground truth" program involving combinations of remote and *in situ* measurements from the surface supplemented by special experiments with instrumented aircraft. Pre-mission "ground truth" data gathering is already well underway to aid mission sampling analysis studies and to develop key regional climatologies. Data are currently being collected at the primary site in Florida, at a monsoon site in northern Australia, and at an ocean site in the western Pacific, i.e., Kwajalein Atoll, Marshall Islands. At the Florida site, centered near the Cape Canaveral area, both on-shore and off-shore (ocean) rain measurement research has begun to develop a standard rainfall measurement and data assimilation technology that can be transferred to a number of validation sites around the globe. At the Darwin, Australia site, rain data are being gathered during two rainy seasons from a calibrated dopplerized radar. These data sets are comparable to GATE data sets both in regard to duration and to radar operation. Beginning in 1988, DMSP's SSM/I, and possibly NASA aircraft overflights, will provide further tests of microwave algorithms against the calibrated radars in Florida, Darwin, and Kwajalein.

Chapter VIII describes the structure of an end-to-end data flow scheme for TRMM including key elements of the science data processing approach. The instrument data will be transmitted to the Tracking and Data Relay Satellite System (TDRSS) once per orbit and then relayed through the White Sands Ground Tracking (WSGT) facility to the Mission and Data Operations facility at the NASA/Goddard Space Flight Center (GSFC) via Domsat. After formatting (processed raw data—Level 0), the data will be transmitted to Japan and to

the TRMM Science Data Processing Center (SDPC) at GSFC via the NASA Communications Network (NASCOM). The SDPC will then process the data to generate several levels of science data products. Most of the data will be processed to basic physical parameters within 24 hours after receiving the Level 0 data. Analyzed products may be produced by TRMM Science Team members or by SDPC when the Team members provide models and analysis tools. Ancillary "ground truth" data and data from supporting field experiments required for the data processing and validation will be stored at SDPC. Data processed by the SDPC will be available to the TRMM Science Team members in the local area as well as to Japan and remote sites via telecommunication lines or through physical transfer of other storage media. Once the TRMM Science Team approves the release of data, products will be transferred to the National Space Science Data Center (NSSDC) at GSFC for archiving and distribution to general users.

ACKNOWLEDGMENTS

The TRMM SSG is grateful to many other scientists for substantial contributions to this report. In particular, we acknowledge the contributions of the TRMM Study Manager, Mr. T. Keating, who provided the materials for Chapter V on instruments and spacecraft and to the Executive Secretary to the SSG, Mr. O. Thiele, who developed Chapter VII on ground truth. Dr. C. Kummerow made a significant contribution on rainfall retrievals in Chapter VI, as did Dr. Daesoo Han on science data handling in Chapter VIII.

We are additionally grateful to the following persons who contributed important text, figures, and criticisms: Drs. R. Adler, T. Bell, L. Chiu, R. Gurney, W.-K. Lau, R. Meneghini,T. Nakazawa, T. Nitta, D. Rosenfeld, K.-S. Shin, and R. Schiffer. Dr. M. Geller, Chief of the Goddard Laboratory for Atmospheres, contributed text, constructive criticisms, and strong support throughout the TRMM study and report preparation.

CONTENTS

CONTENTS (continued)

CONTENTS (continued)

I. INTRODUCTION

There is a growing recognition (NASA Advisory Council, 1986) of the importance of the interactions of the atmosphere, the oceans, the land masses, and the biosphere. To obtain a comprehensive understanding of the Earth system as a whole, each of the components must be observed, understood, and modeled in the context of its impacts upon and control by others.

The hydrological cycle is the centerpiece of the Earth system and the key to understanding its behavior. It is the presence of the world ocean and water substance in the atmosphere and on land that makes the climate of planet Earth uniquely suited for the sustenance of life. The importance of the hydrological cycle arises from the Earth's unique juxtaposition with the triple point of water. It is the phase changes that water undergoes, and the fact that the Earth's energy fluxes are to a large extent in the form of latent heat of water vapor that, compared to other planets, restricts the latitudinal temperature gradients and the prevailing planetary wind intensities, as illustrated in Table 1.

Table 1. Planetary Wind Speeds

Planet	Net Solar Input (Earth = 1)	Average Wind (m/s)	Maximum Wind (m/s)
Earth	1	10	110
Mars	0.52	100	160
Venus	0.41	90	130
Jupiter	0.02	50	160
Saturn	0.006	170	500
Uranus	0.001	80	130

In the table, the solar input measured at the outer limit of the planet's atmosphere (Jastrow and Thompson, 1972) is multiplied by 1 minus the planetary albedo, then all values are normalized relative to that of the Earth, which is set at 1. The mean wind is the average over the whole planetary atmosphere, and the maximum wind is the highest value, frequently found in the upper-tropospheric jet streams.

In addition to the importance of the mean hydrological cycle for the average climate of our planet, variations in the hydrological cycle are crucial for describing and explaining changes in the global circulations, on time scales varying from days to decades and longer. Rainfall in the tropics and subtropics is particularly important. Two-thirds of global precipitation falls in the tropics and subtropics (Sellers, 1969; Jaeger, 1976). Moreover, the rain-associated energy release is a primary driver for tropical circulations, and the variability of tropical precipitation plays a key role in the variability of global circulations and in the short-term changes in climate.

One of the most crucial and least-known components of the global hydrological cycle is the precipitation over the tropical oceans, which has never been measured before; indirect estimates can disagree by as much as 100 percent or more. For example, results of extrapolation from gauges on coastlines and islands (affected by land-sea circulations) differ from inferences from ship observations of rain frequency and from inferences using the infrared channels on geosynchronous or polar orbiting satellites.

TRMM is a highly-focussed, limited-objective program aimed at measuring monthly and seasonal rainfall averaged over areas of about 10^5 km^2 over the global tropics and subtropics. Its radar data will provide the first opportunity to estimate the vertical profile of latent heat release, which is increasingly recognized as essential in determining the structure and dynamics of important large-scale circulation features.

The TRMM is planned to have a low altitude (350 km) orbit in order to have high spatial resolution data from passive and active (radar) microwave sensors, together with high-resolution VIS/IR channels to obtain more accurate measurements of tropical rainfall than ever previously obtained. The low inclination (35°) will permit documentation of the important diurnal rainfall cycle. The measurements are intended to improve our understanding and knowledge of the mechanisms of intra-annual and interannual variability of the Earth's climate. In particular, a multi-year data set of tropical rainfall will help in providing a hitherto non-existent quantitative description of the global hydrological cycle and validation of climate models, helping to explain how varying sea, air, and land mass interactions produce climate changes. Also equally important, the TRMM satellite will provide a "flying rain gauge" to test and improve geosynchronous satellite rainfall estimation techniques; the latter techniques can then be more useful in validation of dynamic models of circulations on scales from the mesoscale up to that of the main planetary circulations.

A large body of observational and modeling evidence has accumulated during the past decade, which shows significant relationships, particularly in the Pacific Basin, between changes in tropical sea surface temperature (SST), tropical rainfall and global circulation, and short-term climate variability. Global models have apparently shown remarkable success in simulating important aspects of these changes in circulation and rainfall. However, a main obstacle in verification and improvement is posed by the necessity to use proxy variables, such as low values of Outgoing Longwave Radiation (OLR), instead of more direct measurements of oceanic precipitation. For example, a crucial relationship is suggested in Figure 1. The interannual variability of observed OLR (proxy variable for observed rainfall) and model-simulated precipitation both show that the variability is largest over the tropical regions and especially over the tropical oceans. It is clear that such large interannual changes in the intensity of tropical heat sources are related to large interannual changes in tropical as well as extra-tropical circulations, but adequate model tests and quantitative clarification of the mechanisms involved cannot be achieved without more direct and more accurate specification of tropical precipitation.

Thus, in order to make further progress in the areas of climate modeling and prediction, it is urgent to document the space-time variability of rainfall over the tropical oceans. Finally, in order to obtain a reliable climatology for the global tropics and a quantitative description of the hydrological cycle, the TRMM will also provide, for the first time, an application of space technology specifically for the measurement of rainfall employing a rain radar.

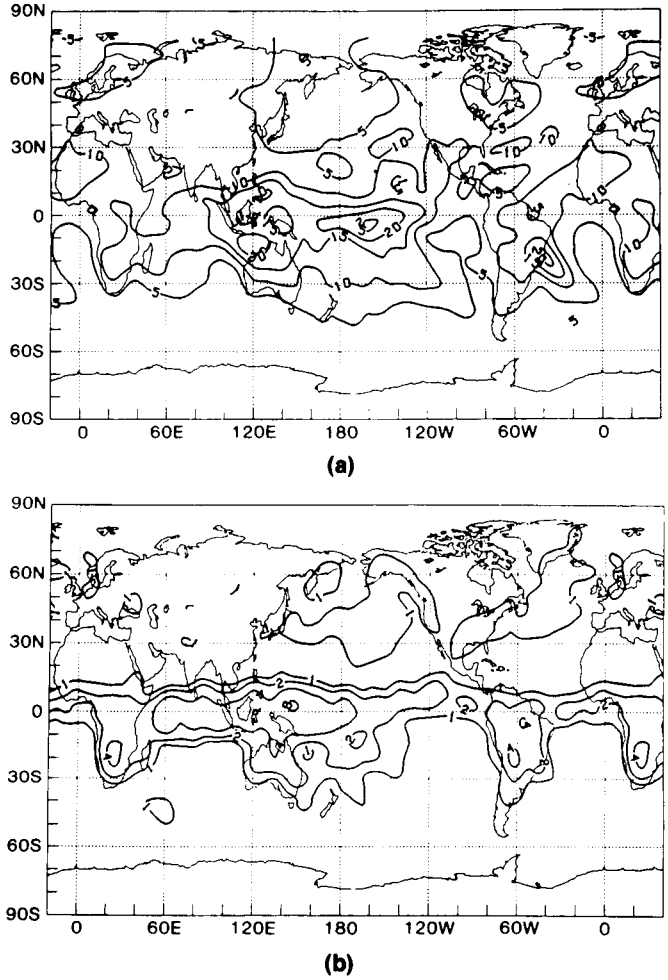

Figure 1. Inferred interannual precipitation variability. Note the concentration in the tropics, particularly in the Pacific and "maritime continent" areas. (a) Standard deviation of monthly mean OLR (W m^{-2}) for January for 12 years (1975-1986) (Shukla, 1987). (b) Standard deviation of model-simulated January rainfall (mm day^{-1}) for 6 years (1979-1984). Model used was Goddard Laboratory for Atmospheric Sciences (GLAS) model described by Fennessy *et al.* (1985).

TRMM has already been building much of its science background on the results of the First GARP Global Experiment (FGGE) program (particularly upon GATE[1] and MONEX[2]) and is utilizing the results of EMEX[3] for a sample of rain structure and distribution in an important monsoon regime. The planned cooperative effort with Japan (and resulting low cost to the U.S. Space Program) is hoped to expedite an early launch date (1994). TRMM is being planned in close conjunction with the ongoing (1985-1995) international Tropical Ocean and Global Atmosphere (TOGA) program, which is designed to improve our understanding of ocean-atmosphere interaction and to develop coupled models for long-range forecasting and climate prediction. A critical element in the TOGA observational strategy is the accurate determination of rainfall over the entire tropics. Joint experiments are being designed between TOGA and TRMM to obtain "ground truth" measurements of oceanic precipitation.

TRMM, with its 3-year minimum of data from a low-inclination, low-orbit satellite is also an important component of the Eos, in which further advanced microwave sensors are planned for two U.S. polar orbiting satellites. Analysis of data from these satellites will need diurnal variability information from TRMM. In the longer range, TRMM is a necessary predecessor for a much more ambitious multi-satellite system, the Global Energy and Water Cycle Experiment (GEWEX) which is part of the Global Change initiative planned for the early 21st century.

Intrinsic to a space mission of this nature is a substantial "ground truth" program to support the infra-structure of an organized precipitation research program, including rain measurement technology development and application during the mission-planning phase, and to validate (and probably calibrate) the spaceborne remotely-sensed parameters during the mission. The pre-mission phase must focus on rain measurement research, rain processes and variability studies, and development of transfer standards (measurement and procedural techniques) for calibrating the mission validation sites. Also, a primary surface-based rain research facility is crucial to flight instrumentation and algorithm development. Aircraft experiments, including high-level flights with multichannel microwave sensors, are an important part of this effort.

For the mission phase, representative "ground truth" sites must be selected and developed for key types of precipitation regimes, e.g., tropical oceans, tropical continents (jungle and arid), monsoonal regions, etc. In addition to their primary role of validation and calibration, mission "ground truth" measurements will significantly enhance the TRMM data sets.

SUMMARY OF TRMM GOALS AND MISSION CONCEPT

TRMM Goals

The SSG has agreed that the main TRMM goals are to:

- advance the Earth system science objective of understanding the global energy and water cycle by means of providing distributions of rainfall and inferred heating over the globe,
- understand the mechanisms through which tropical rainfall and its variability influence global circulation and to improve our ability to model these processes in order to predict global circulation and rainfall variability at monthly and longer time scales, and

[1]GATE stands for GARP Atlantic Tropical Experiment. Its field phase was in 1974. GARP stands for Global Atmospheric Research Program.
[2]MONEX stands for Monsoon Experiment. It was also part of GARP. Its field phases were in 1978-79.
[3]EMEX stands for Equatorial Mesoscale Experiment. Its field phase took place in 1987.

- evaluate a space-based system for rainfall measurement.

A secondary goal closely connected to the main goals is to better model and understand convectively driven precipitating cloud systems in the tropics, their organization on the mesoscale, and their interactions with the ocean and the ambient atmosphere.

TRMM Mission Concept

The complement of TRMM sensors and their orbit parameters are summarized in Table 2. The rationale for their selection to accomplish the mission goals is discussed later in Chapters V and VI. The items in italics are desired features to be incorporated if resources permit.

Table 2. TRMM Sensor Summary

Microwave Radiometers	Radar	Visible/Infrared Radiometer	Orbit
19, 37, 90 GHz (dual polarized)	14 GHz	VIS and 10 μm IR	35° inclination
10 km resolution	4 km footprint	1 km resolution	350 km altitude (high resolution)
600 km swath	250 m range resolution	600 km swath	Rapid precession
	220 km swath		
10 GHz at 20 km resolution	*24 GHz*	*Moonlight visible*	
5 GHz at 40 km resolution	*600 km swath*	*1.6 mm (phase of H_2O)*	
		6.7 mm, split window	

Note: Items in italics desired if resources permit but are not necessary to achieve main TRMM objectives.

II. SCIENTIFIC BACKGROUND AND ITS DEFICIENCIES

GLOBAL HYDROLOGICAL CYCLE

In fulfilling its life-sustaining functions, water circulates freely between its oceanic, atmospheric, and terrestrial reservoirs. Compared to the ocean, the atmosphere is an insignificant reservoir of water substance. An average air column of 1 square centimeter in area contains only around 3 gm of precipitable water, in the form of water vapor; even in the tropics, the vapor content rarely exceeds twice this value. Since the globally averaged annual rainfall is estimated to be around 1 m, the average elapsed time between evaporation or transpiration and the return of a water parcel to the Earth's surface in the form of precipitation is only around 10 days.

Nevertheless, in contrast to the transport by ocean currents, river flow, or the even slower percolation through the soil, a water molecule may be carried thousands of kilometers from its terrestrial source during its short residence within the atmosphere. During this brief period, the water molecule acts as an efficient "solar collector," having received energy during evaporation from the Earth's surface and later releasing the latent heat in concentrated regions of local intense precipitation. Consequently, it is the atmosphere, with its great mobility, that provides the rapid, global transport of water necessary to sustain the weather and climate regimes and biological systems of our planet.

A knowledge of the variations in the hydrological cycle is crucial for describing and explaining changes in the global atmospheric circulation, on time scales varying from weeks to decades and longer. Through its intimate links with the energy fluxes, the hydrological cycle couples the various components of the global climate system (Figure 2). For example, the fact that the Earth's energy flux is mainly in the form of latent heat of water vapor results in smaller latitudinal temperature gradients and prevailing planetary wind intensities than those which would prevail on a dry planet (Mintz and Leovy, 1969).

The hydrological cycle is most intense in the tropics and subtropics. Most of the absorption of incoming solar radiation in the tropics occurs in the ocean. About half of this energy is transported poleward by ocean currents (Riehl and Simpson, 1979); the remainder is returned by evaporation to the tropical atmosphere in the form of latent heat. Over three-fourths of this latent energy is released in the deep tropics by condensation occurring in the towering convective systems that populate the Equatorial Trough Zone, often referred to as the Intertropical Convergence Zone (ITCZ), that girdles the globe. The concentration of condensation processes (in a small precipitating region) of water vapor which has been evaporated over a wide area is the "solar collector" property of the hydrological cycle discussed earlier. Thus, rainfall in the ITCZ is particularly important as a forcing mechanism of the atmosphere's large-scale circulation and climate.

The tropical rain forests represent the world's greatest concentration of living things. The rain forests are centers of intense convective activity. They are simultaneously source regions of biogenic gases and aerosols and regions of strong photochemical activity. The collective effect is one of rapid mixing and oxidation of trace gases which impacts global tropospheric chemistry and climate. The rain forests play a complex role in the total water budget of the planet, capturing, storing, and ultimately recycling water through evapotranspiration back to the atmosphere. Knowledge of these sources,

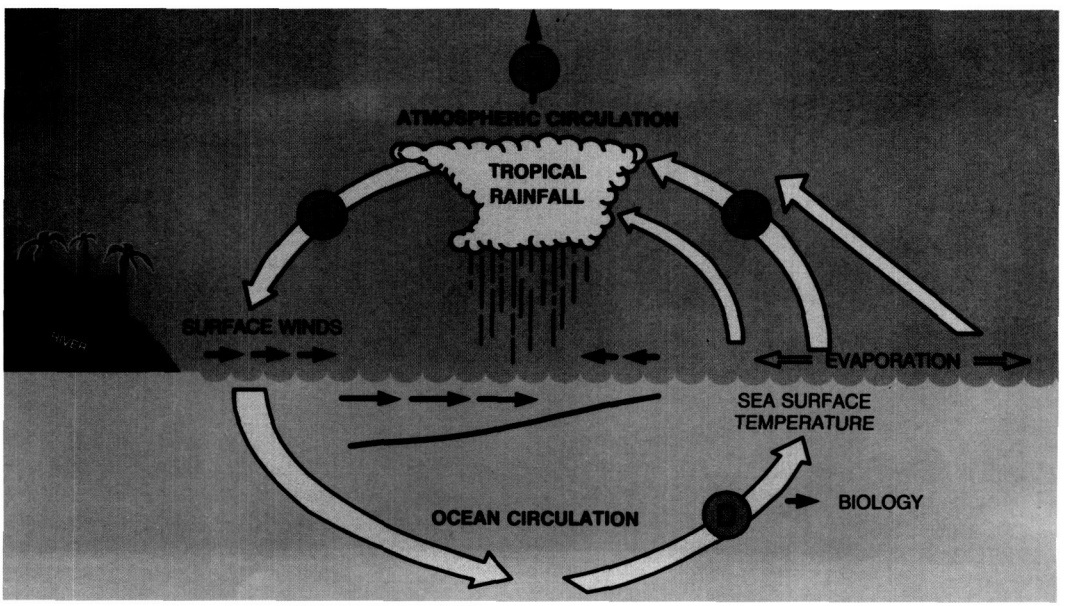

Figure 2. Schematic diagram showing the key role of tropical rain systems in ocean-atmosphere and land interactions.

sinks, and pathways of water must include knowledge of rainfall over the vast trackless rain forest centered in the global tropics (Harriss *et al.*, 1988).

The primary driving force for the time-averaged planetary scale motions in the Earth's atmosphere is provided by the quasi-stationary heat sources which result from the combination of latent heat release and radiative processes. Both observational studies and GCM experiments indicate that the non-uniform distribution of cloudiness and precipitation provides the largest asymmetric component of diabatic[4] forcing in the tropics.

A schematic diagram of the coupled ocean-atmosphere system in which clouds are allowed to become fully interactive with the radiation field is shown in Figure 3 (Webster, 1987). This replaces the traditional view in which the radiation budget and clouds were viewed as essentially passive, with the radiative heating approximately a function of latitude only. To help understand the importance of this advance, Figure 4 shows the contributions of latent heat gradient and radiative flux convergence gradient separately. In the last few years it has become possible to treat the radiative and latent heating aspect of clouds interactively, which can lead to much improved understanding of how they significantly alter the basic driving forces of the ocean and the atmosphere.

Clouds tend to heat the atmospheric column through radiative flux convergence (Webster and Stephens, 1980; Stephens and Webster, 1984). The resultant radiational heating gradient between climatological clear and cloudy regions is at least half the magnitude of the latent heating gradient. While they

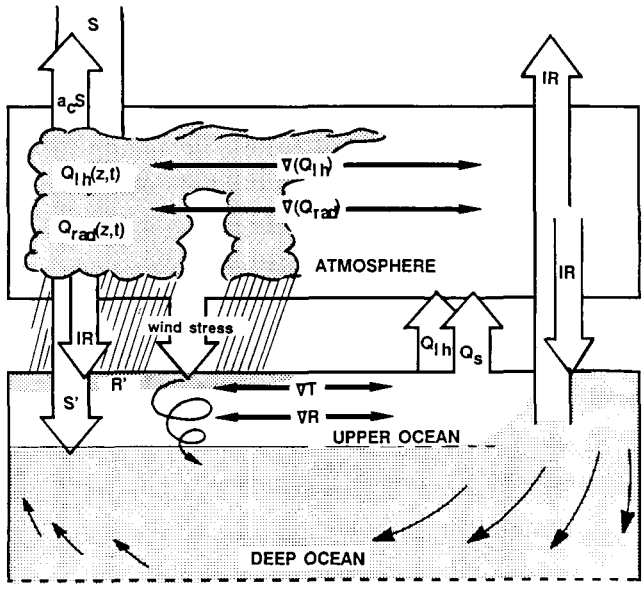

Figure 3. Schematic diagram of the coupled ocean-atmosphere system where the atmospheric part of the hydrosphere (clouds) is allowed to become fully interactive with the radiation field. The ocean-atmosphere interaction occurs through wind stress and surface heat fluxes. Clouds significantly alter the basic driving forces of the atmosphere by heating, relative to the clear regions. Clouds, however, cool the surface below them and also change the proportion of visible to long-wave radiation reaching the surface, thus altering the radiative heating distribution in the upper layer of the ocean. Precipitation is a source of fresh water which alters the density gradient in the ocean, driving circulations and contributing to changes in the SST gradient. In turn, the ocean temperature gradient and radiation distribution determine the evaporation and, eventually, influence where cloudiness and precipitation occur. The combined latent and radiative heating gradient drive the atmospheric motions which, in turn, affect the ocean. (Webster, 1987a, 1987b).

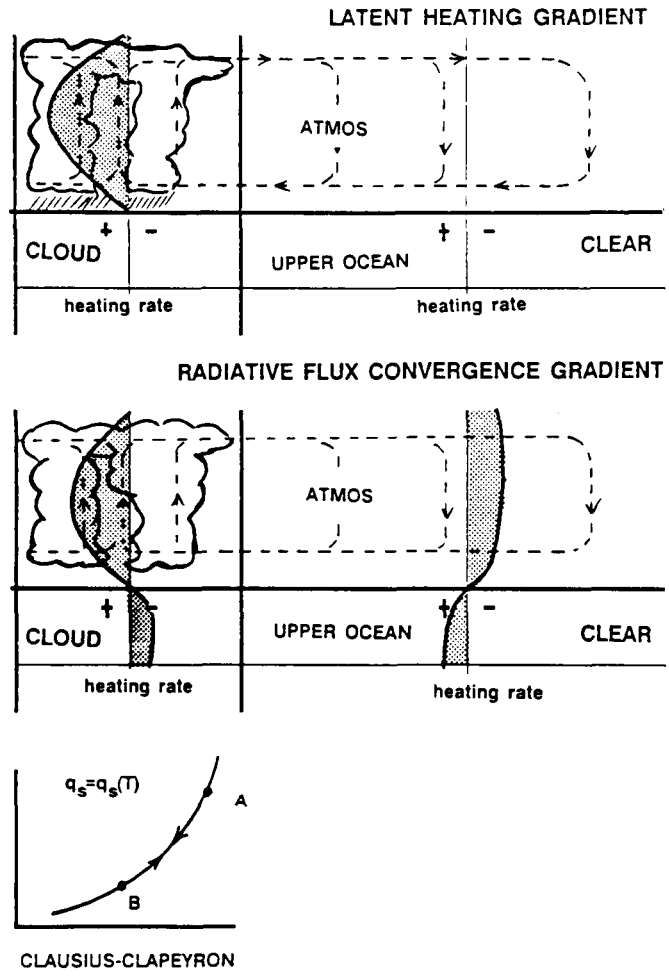

Figure 4. Comparison of the latent heating gradient and radiative heat flux divergence gradient between clear and cloudy regions. The effect of both processes on the atmospheric gradient is in the same sense. However, in the upper ocean layer below cloudy regions there is substantial cooling at about 0.5°C per month. The Clausius-Clapeyron curve indicates the direction and non-linear magnitude change of q_s, the saturation mixing ratio of water vapor in air, in warm SST cloudy regions (A) and in cool SST clear regions (B). (After Webster, personal communication).

[4]A diabatic process is a thermodynamic change of state (of pressure, temperature, or specific volume) of a gaseous system in which there is a transfer of heat across the boundaries of the system or there is an addition or removal of heat by a source or sink within the system.

heat the atmospheric column, clouds also cool the surface below them. It is estimated that the differential cooling rate of a 100 m-deep ocean surface layer between cloudy and clear regions is about 1°C per month (Ramanathan, 1987). Clouds also change the proportion of visible to long-wave radiation reaching the surface and, thus, change the radiative heating distribution in the upper layer of the ocean. It should be noted that the ocean surface layer heating gradient imposed by the cloudiness differences is in the opposite sense from the atmospheric radiation and latent heat gradients, which reinforce each other. Webster (1987) has provided evidence that this component of ocean heating is a significant factor in the coupled ocean-atmosphere variability.

Finally, the input of fresh water in the precipitating cloudy regions alters the density gradient in the ocean. The change of the ocean density gradient through the variations in salinity resulting from evaporation and precipitation differences may, in some regions, be as large as the effect of temperature variations, implying a substantial effect in inducing thermohaline circulations, which in turn can change the SST's (Taft and Kessler, 1987). Webster (1987a,b) and others have shown that small changes in ocean temperature where the ocean is warmest can invoke very large changes in the atmospheric hydrological cycle. Clearly, more precise precipitation information is needed to document the magnitudes and variabilities and to quantify the important feedback mechanisms.

The disparity in scales of the processes resulting in the interactions illustrated in Figures 2 to 4 presents a major challenge. The release of latent heat occurs in individual cloud elements whose space scale is only a few kilometers and whose life cycle is a few hours or less. These individual convective elements are not randomly distributed but are organized on a variety of time and space scales. The basic building blocks are the cloud clusters and other mesoscale systems associated with synoptic disturbances. The frequency and intensity of these disturbances are, in turn, modulated on intraseasonal time scales. The distribution of tropical precipitation exhibits a pronounced annual cycle, but the climatologically preferred regions or zones of convective activity are also modulated or shifted on interannual time scales. Like the annual cycle, the year-to-year variations in rainfall are often coupled to changes in the upper ocean that result in anomalous SST's. Such coupled ocean-atmosphere interactions are particularly pronounced over the tropical oceans. The manner in which low-frequency modes of rainfall variability are related to changing surface conditions, both SST and land surface anomalies, is a major focus of current climate research. (See World Climate Research Program (WCRP), 1985.)

THE IMPORTANCE OF TROPICAL RAIN SYSTEMS

Cloud Clusters and Tropical Storms

Most of the rain that falls in the tropics is produced by convective processes which result in cloud "clusters" several hundred kilometers in horizontal dimension, which may last for hours, days, or, rarely, weeks. As seen from geostationary orbit (Figure 5), tropical cloud clusters tend to concentrate in the Equatorial Trough Zone. On the one-third of the Earth depicted in Figure 5, there are about 10-12 of these clusters. A number of roughly 30 cloud clusters around the global tropical belt at any one time is typical. In certain favored locations (see, e.g., Simpson and Riehl, 1981), about 1 in 10 of these clusters may deepen into a tropical cyclone, which is named as a tropical storm when the maximum sustained windspeed reaches 17.5 ms^{-1} and as a full hurricane or typhoon when the windspeed exceeds 33 ms^{-1}. These systems, on approaching landfall, may inundate the coastal region by storm surges as high as 4 to 8 m, causing heavy losses of lives and property. Six storms, each wreaking damage estimated in excess of 1 billion dollars, have struck the United States since 1972. Nevertheless, tropical cyclone rain may be as large as 35 percent of the annual average rain in many parts of the tropics and subtropics; consequently, Japan considers itself a nation "blessed by typhoons."

Continental Versus Maritime Precipitation

It is well known that oceanic cumuli produce precipitation by coalescence at a shallow depth of 1-3 km, while continental cumuli must generally have greater thickness to precipitate and may do so either by coalescence or ice processes or both. (See, e.g., Battan, 1973; Rogers, 1979.) Evaporation of precipitation between cloud base and the surface is greater over land, increasing as aridity increases (Rosenfeld and Mintz, 1988). Over oceans, most cumulonimbus clouds form in organized disturbances, while over land storms can be generated locally. In many parts of the world, rainfall is initiated and enhanced by the forced ascent of moist air over elevated terrain. This is orographic rain, and most of the world's truly exceptionally high rainfall is orographic. Examples abound from the windward slopes of the Hawaiian Islands (over 10 m of annual rain) to the hills of southeast Asia intercepting the monsoon airflow (1-2 m per month is not unusual).

Monsoon Rainfall

The monsoon is a global phenomenon affecting over 50 percent of the world population inhabiting the main continents of east and southeast Asia, Japan, India, parts of west Africa and northern Australia, which cover an area comprising 25 percent of the globe, or half of the tropics. In these monsoon regions, the rainfall season is very well defined. Over India and southeast Asia, the summer monsoon rain occurring between June through August contributes over 80 percent of the annual rainfall. The high concentration of rainfall during the monsoon season and the generally inadequate irrigation facilities found in these regions cause the economy and prosperity of the monsoon belt to be critically dependent on the variability of the monsoon rainfall.

Many rain-producing disturbances are known to exist over the monsoon region. In the Indian subcontinent and vicinity, these include the Bay of Bengal disturbances, the vortices that often accompany the local monsoon onset in southwestern India, and rainfall associated with disturbances in the so-called monsoon trough which sweeps north and south across the entire subcontinent accompanying the advance and retreat of the monsoon (Figure 6). Over east Asia, a similar migration of the monsoon trough and the accompanying rainband is also

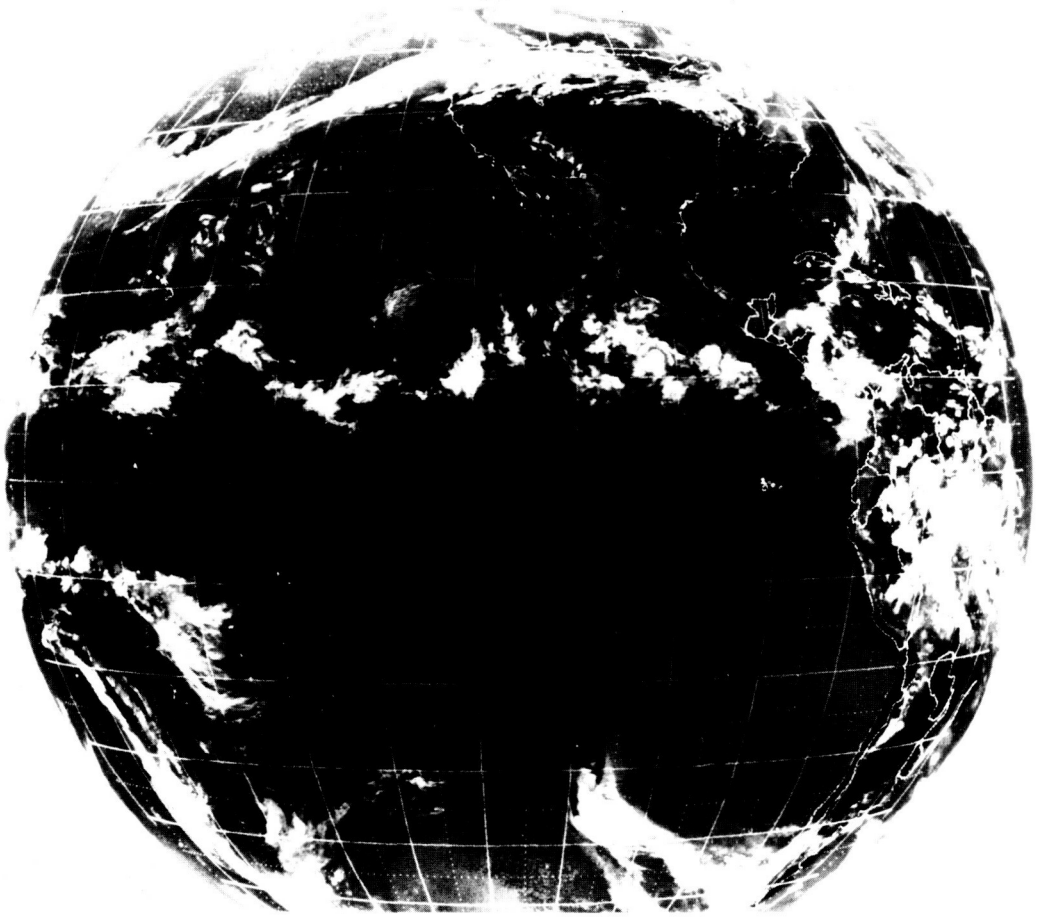

Figure 5. Infrared geostationary satellite picture for October 20, 1975. Latitude and longitude interval is 10 degrees (solid lines). About one-third of the globe is visible. Note that there are about 10 cloud clusters seen in the band located in the Equatorial Trough Zone.

found (Lau and Li, 1984; Lau *et al.*, 1987). This is known as the "Mei-Yu" trough or "Baiu" in Japan. Figure 7 shows the three typical stages of development of the Baiu. From May to June, a quasi-stationary front associated with the Baiu trough establishes itself in a southwest to northeast direction stretching from southern China to Japan bringing copious rain to these regions. From late June to early July, the Baiu front abruptly shifts northward accompanied by a similar shift of the subtropical high and the low-level southerly wind, which brings in a large amount of warm, moist air from the western Pacific (Tanaka *et al.*, 1987). Rainfall in the Baiu frontal zone is often organized into mesoscale structures with extremely large variability in space and time. Rainfall rates as high as several hundred millimeters per day are frequently observed during peak periods. Yet simultaneously over other parts of the system, dry conditions may prevail. It is clear that understanding of rainfall variability in the monsoon region is crucial in any attempt to make reliable monsoon rainfall forecasts.

Rainfall and the Tropical Large-Scale Circulation

Three decades ago, it was brought out by Riehl (1954) that a large fraction of the total rainfall at any location in the tropics is caused by only a few heavy rainfall events. In looking at the percentage of rainstorms in terms of how large a percentage of the monthly rain they produce, it is typical that only about 10-15 percent of the days with rain account for half of the total monthly rain, while the remaining 85-90 percent of the rainy days contribute to the other half. Water resource analyses (e.g., Ulanski and Garstang, 1978) show that the difference between an adequate rainy season and a severe drought over an area of about 10^3 km^2 can be brought about by the absence of just two or three substantial rain events. Over a substantially larger area in South Africa, Garstang and Emmitt (1983) show a similar concentration of rainfall. The fact that the major fraction of the precipitation at most tropical locations is produced by just a few large rainstorms clearly represents a sampling challenge facing adequate detection of total monthly rainfall by an orbiting satellite; it leads to the need for large averaging areas and ingenious use of the rain distributions and their spatial and temporal correlations, as discussed in Chapter IV.

Tropical convective clouds, as well as producing life-giving rain and the rare but often devastating flood associated with hurricanes or typhoons, carry out many essential functions in the global Earth-atmosphere system, as summarized in Table 3.

Among the largest-scale planetary atmospheric circulations in the tropics are the meridional Hadley cells, which girdle the globe in both northern and southern hemispheres. In the

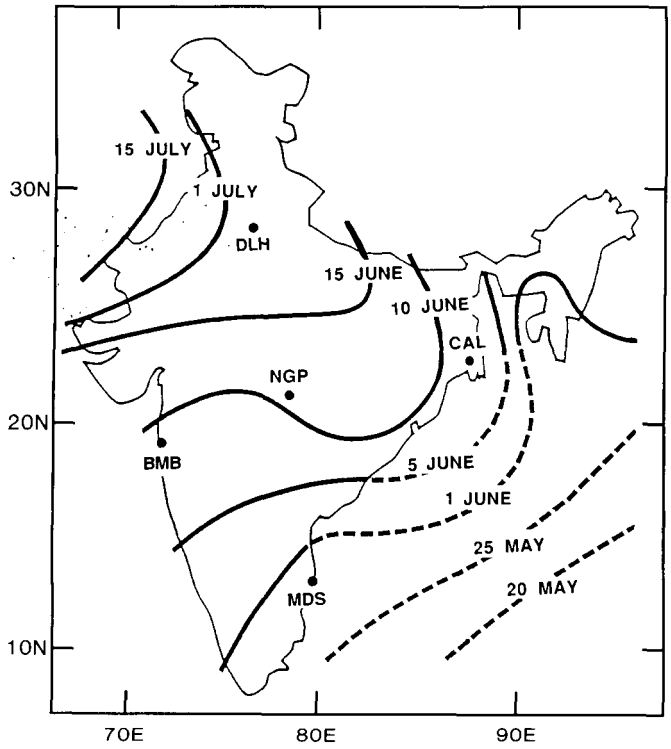

Figure 6. Mean date of onset of summer monsoon over India based on the arrival of heavy monsoon rain. Broken lines denote isolines based on inadequate data (Mooley and Shukla, 1987).

Hadley cells, there is highly concentrated ascent in the region of the equatorial trough and slow widespread descent in the subtropical high-pressure cells, at about 30° north and south. The low-level equatorial component of the flow is 2-3 ms^{-1}.

Figure 8a shows a schematic meridional cross section, depicting the average Hadley cell circulation with typical convective clouds. The sinking motions associated with the subtropical high pressure cells and their easterly trade-wind-dominated equatorward fringes appear in the left half of the diagram, where the trade-wind inversion commonly restricts the growth of cumuli. Even though these trade-wind cumuli are shallow and undramatic looking, they play a significant role in maintaining the trade-wind circulation and its steadiness, as shown originally by Riehl *et al.* (1951). These clouds release only about 25 percent of the latent energy received by the lower air from ocean fluxes but export most of it equatorward into the Equatorial Trough Zone. Even so, their vertical pumping action and "cut off" towers cause the observed deepening of the moist convective layer in the downstream direction, and their latent heat conversion plays a major part in sustaining the downstream pressure drop which maintains and accelerates the trade winds as they flow toward the equator. Recently, Betts and Ridgway (1988) have helped to build a quantitative physical linkage between tropical radiative processes, subsidence, and sea-air fluxes, which can enable numerical models to better simulate the complex interactions of these processes in the important trade-wind zones of the tropics. Direct measurement of the rainfall from these trade-wind cloud systems, some of which may be quite shallow, is an important need in this improved understanding and simulation.

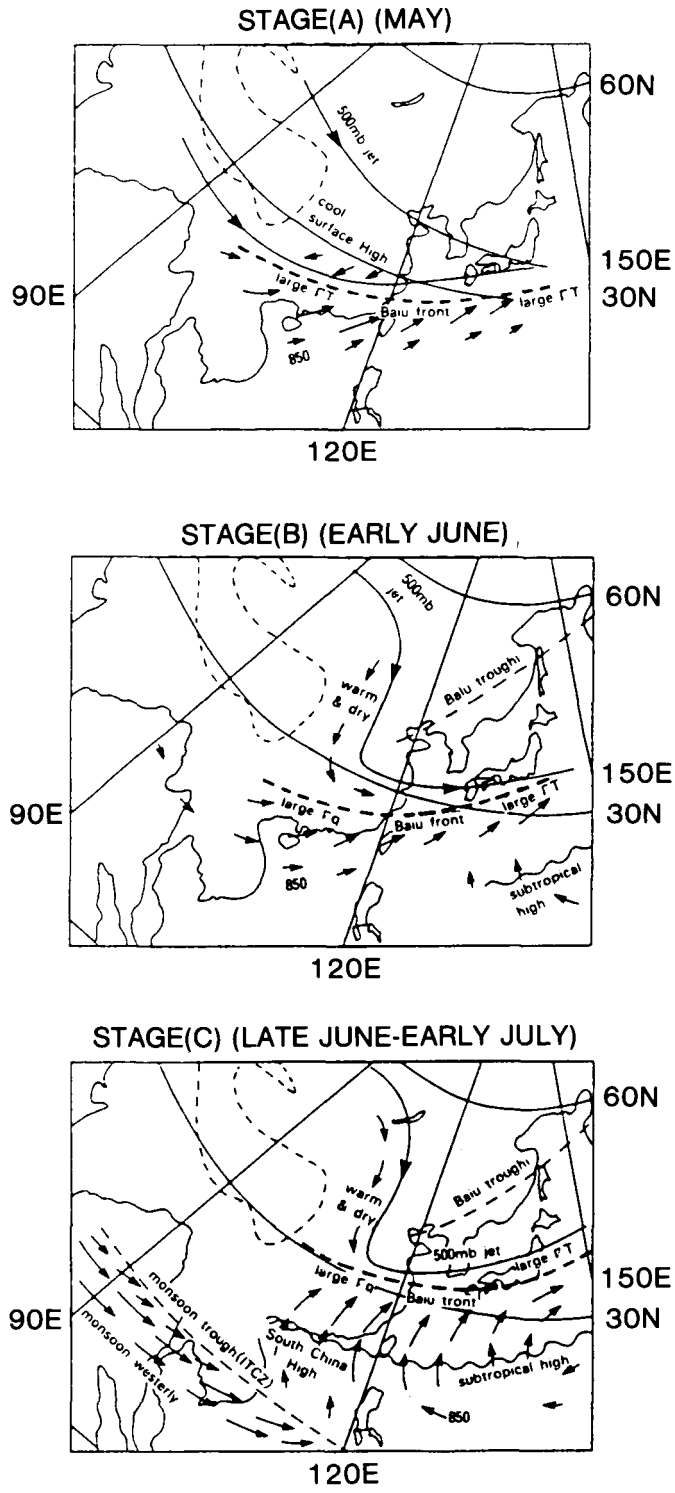

Figure 7. Typical pattern of surface and 500 mb flow in relation to the Baiu front during stages (A), (B), and (C) of this development.

The largest tropical circulation is the zonal Walker cell of the Pacific Basin, shown in Figure 8b in interaction with the east Asian portion of the Hadley cell. The low-level westward component of the circulation has speeds up to a few meters per second.

Table 3. The Importance of Tropical Rain Systems

Life-giving resource for world's largest biomass (the tropical rain forest) and for billons of humans
Exhibits dangerous variability (drought/flood seesaw) circulations
Firebox of atmospheric heat engine (latent heat release in equatorial zone) driving atmospheric circulations
Vertical transports of heat, moisture, momentum affect large-scale circulations
Occasional destructive storms (typhoons, floods)
Important coupling between ocean and atmosphere
Key link in climate change (ENSO's)
Mechanisms for troposphere to stratosphere fluxes
Electric charge separation between Earth and ionosphere
Chemical scavenging, rain-out, acid rain

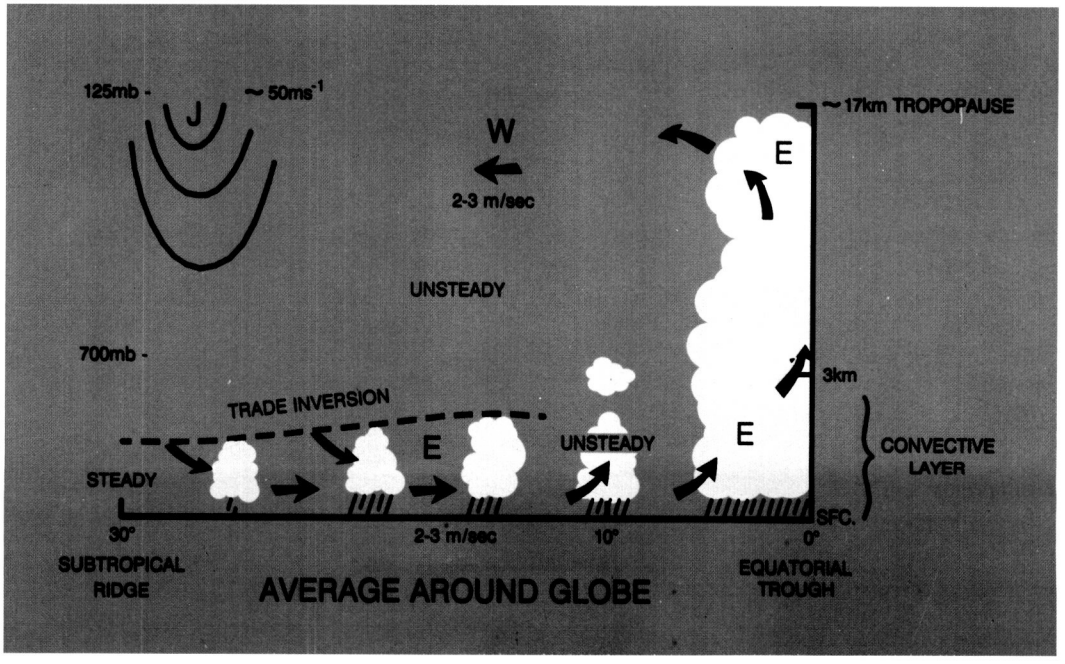

Figure 8a. Schematic illustration of the meridional Hadley circulation, averaged over longitude. The latitude coordinates are located relative to the equatorial trough, specified as 0 degrees and the subtropical ridge line, specified as 30 degrees. The thick arrows denote the mean circulation, with subsidence in the equatorward-flowing trades and rising motion in the equatorial trough, which is concentrated into the cloudy zones depicted in Figure 5. The subtropical westerly jet aloft is denoted by J. The trade winds are steady, while the remaining circulations are much more variable.

Tropical Rainfall and Energy Transport

To see what happens to the latent heat energy when the trade winds export it to the Equatorial Trough Zone, we refer to the extreme right side of Figure 8a. There we see a schematic "hot tower" typical of the convection within the equatorial firebox of the atmosphere. Some typical photographs made from mapping aircraft are shown in Figure 9 (from Malkus and Riehl, 1964). These tall cumulonimbus clouds, frequently towering 17 km into the stratosphere, have strong updrafts which convert the latent heat stored in water vapor into sensible heat (heat as measured directly by a thermometer) and potential energy, thereby acting as the "combustion cylinders" of the atmospheric heat engine. That the firebox function of

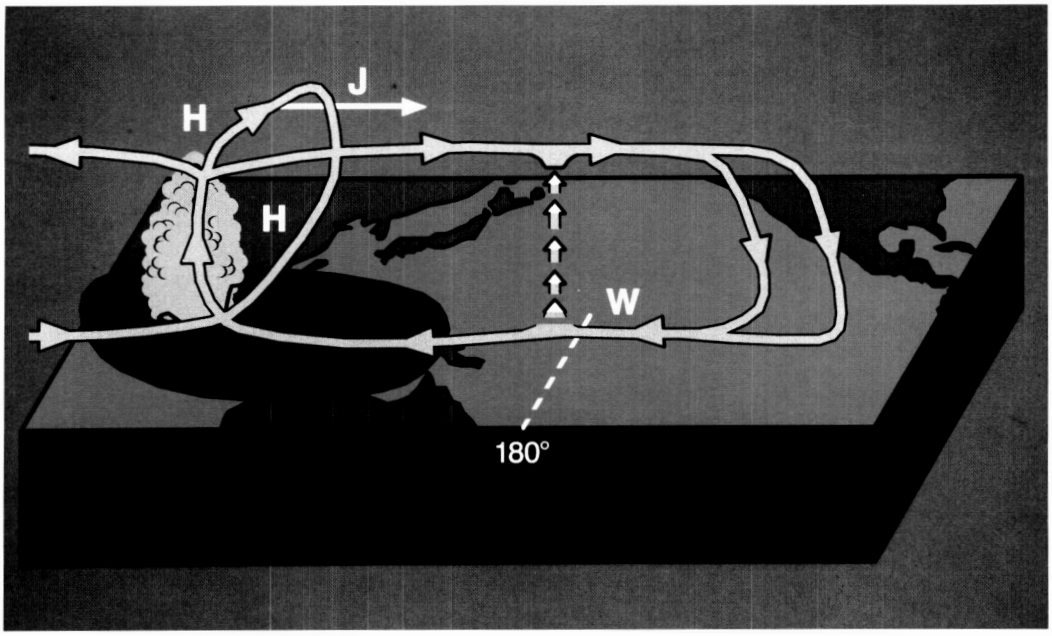

Figure 8b. Schematic illustration (not to scale) of the Walker circulation in the Pacific Basin and its interaction to reinforce (under non-El Niño conditions) the east Asian branch of the Hadley cell. The red area denotes the normally warm SST's in the region of the "maritime continent," which are associated with intense convective rain, as indicated by the cloud. The dashed line just east of the date line depicts the eastward shift of the axis of the upward branch of the Walker cell during an ENSO situation.

the atmosphere is concentrated into a very narrow latitudinal band is shown in Figures 5 and 10. Figure 10 shows a pre-satellite map of oceanic precipitation (Malkus, 1962) constructed by extrapolating from land and island stations, with the results adjusted so that global water and heat energy budgets are balanced. The lack of precipitation measurements to substantially improve Figure 10, which may have significant errors, has been a major obstacle to the development of Earth system science during the past quarter century. Figure 10 again brings home the latitudinal concentration of the precipitation[5] heat release and shows that it is the major supply providing the source for the huge poleward export of heat and potential energy; precipitation heating is also the major term which acts toward balancing outgoing radiative heat losses at all latitudes.

In studying the heat budget of the Equatorial Trough Zone and investigating the mechanisms and interacting scales of motion which maintain it, Riehl and Malkus (1958) found the necessity to postulate their "hot tower" hypothesis, which in the past three decades has gained many applications and gradual acceptance in tropical meteorology. They recently repeated the same analyses with vastly more extensive and improved data sources and arrived at essentially the same results (Riehl and Simpson, 1979). A result relevant to TRMM is summarized in Table 4.

One of the most important findings concerning mechanisms in the atmosphere's Equatorial Trough Zone was that the vertical transports must be effected by large buoyant cumulonimbus cores or "hot towers," which have undergone little or no dilution from the mixing in, or entrainment, of the drier outside air. In conducting their budget study, Riehl and Simpson (1979, *loc. cit.*) were able to estimate the vertical energy flux from the undilute hot towers, and using typical cloud measurements, were able to specify how many towers are needed at one time. This figure comes out to be about 1,600-2,400 cloud towers. The interacting scales involved and the extreme concentration of the "firebox" (or heat release) is brought home by the decadal hierarchy of numbers in Table 4. Clearly, since there are so few cloud cylinders in the atmosphere firebox, and cloud growth is highly dependent on their forcing and their environment, one might expect large circulation variabilities related to variation in the high towers and their latent heat release.

Only now, with the prospect of the TRMM satellite, has it become realistic to expect to begin documenting variabilities in these intense convective cores, their top heights, together

[5]The heat is initially released by the condensation of gaseous water vapor into very small liquid cloud droplets, about 5 to 10 mm in diameter. These droplets must grow by coalescence or other processes to 100 to 300 mm (0.1 to 0.3 mm) before they have sufficient terminal velocities to fall as rain. The rain must reach the Earth or ocean surface to add a net amount of latent heat to the air, for if the small drops remain airborne and evaporate, the condensation heating is reabsorbed. Hence, the shorter expression "precipitation heating" is commonly used.

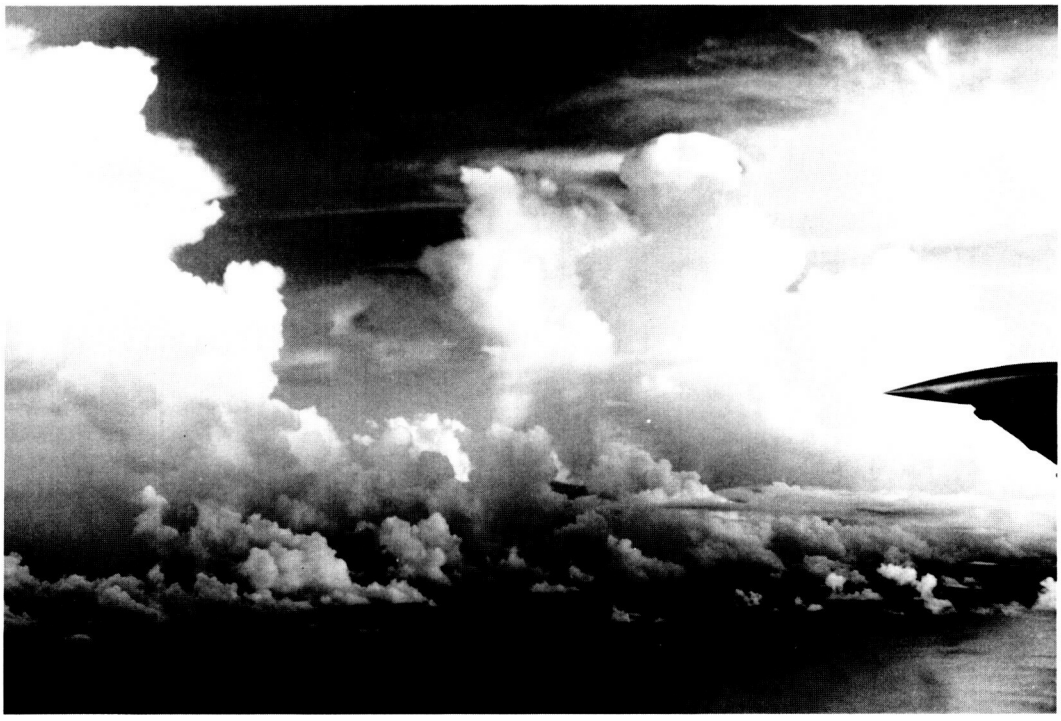

Figure 9a. Photograph from an aircraft flying at an altitude of about 3 km of the active convective portion of a typical cloud cluster in the Equatorial Trough Zone of the Pacific Ocean (Malkus and Riehl, 1964).

Figure 9b. Photograph taken a few minutes later of the older, more stratified portion of the same cloud cluster (Malkus and Riehl, 1964).

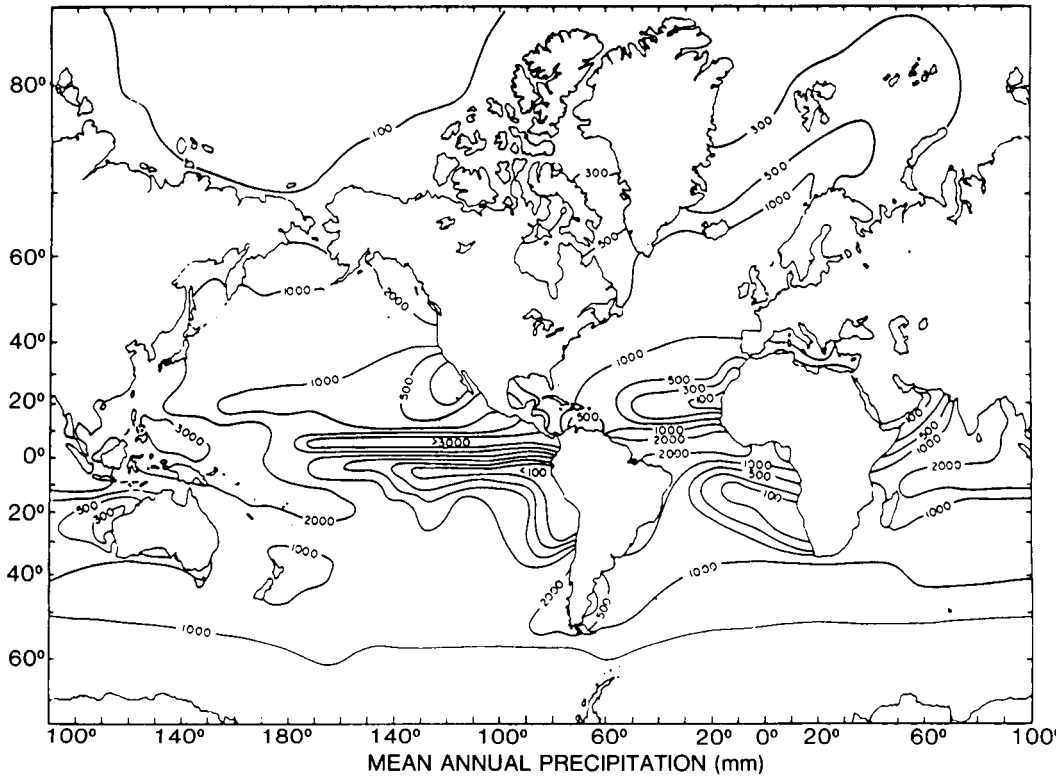

Figure 10. Pre-satellite map (after Malkus, 1962) of the mean oceanic precipitation in millimeters. The map was constructed by extrapolation from coastal and island stations and adjusted to balance the global water budget.

with rainfall areas, amounts and vertical profiles. Developing relationships of these cloud properties to those of the large-scale environment should greatly aid in the parameterization of convective processes in large-scale circulation models.

Structure of Cloud Clusters

The cloud photographs in Figures 9a and 9b show a tropical oceanic cloud cluster in two different stages of its life cycle.

Table 4. The Atmosphere's Concentrated Firebox

Summary of "Hot Towers" in the Equatorial Trough Zone	
A	Area of Equatorial Trough Zone = 1
10^{-1}A	Occupied by synoptic systems (satellite identified) ~30
10^{-2}A	Occupied by mesoscale convective systems (on radar, average area ~2,500 km^2)
10^{-3}A	Undilute towers reaching high troposphere (satellite IR temperatures 240 to < 210 K)
	Number of Hot Towers Required is 1,600-2,400, if a Single Tower is:
	5 × 5 km
	Ascent speed = 2-3 ms^{-1}
	50-80 towers per synoptic disturbance

The tall cumuli in Figure 9a has rounded towers; their tops were still actively rising as they neared the tropopause level. In Figure 9b, taken a few minutes later, we are looking at an older portion of the cloud system. The rounded towers are no longer seen; the picture is dominated by stratiform anvils and shelf clouds, most of which are precipitating but at a much slower and more horizontally uniform rate than are the heavily showering high towers. A very important result from the radar studies undertaken in the GATE and winter MONEX experiments is the finding that a large fraction of the precipitation in convectively-driven rain systems comes from the anvil and stratus layers. Figure 11 shows a schematic diagram of a tropical oceanic cloud cluster typical of GATE conditions (after Houze and Betts, 1981). Table 5 (after Leary and Houze, 1980) shows some properties of this idealized cloud cluster and the large-scale area containing the cloud cluster.

In the example shown in Table 5, the stratiform portion of the cloud cluster contributes more than 40 percent of the total cluster rainfall in 1 hour. There is incomplete evidence that the relative contributions of convective versus stratiform rain depends on the system size, its age, and ambient conditions. For example, using radar observations in GATE and winter MONEX, the fraction of the total precipitation contributed by the stratiform portions of the cloud systems normally ranged between about 30 to 60 percent. Examining smaller cloud clusters in south Florida, Adler and Negri (1988) found an average 20 percent stratiform precipitation contribution with a marked late-afternoon maximum, while in intense At-

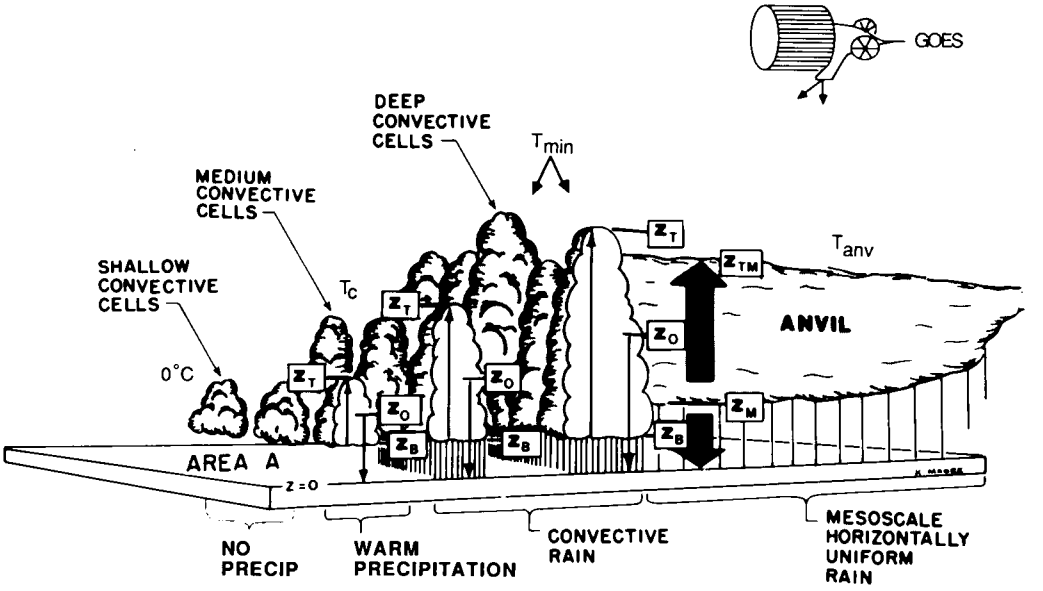

Figure 11. Schematic diagram of a tropical oceanic convective cloud cluster (after Houze and Betts, 1981) showing the younger, wholly convective portion on the left and the older portion, with more stratiform and anvil rain, on the right. The diagram relates to Table 5. The z's denote heights and the T's, temperatures.

Table 5. Properties of Idealized Cloud Cluster and Large-Scale Area Containing the Cloud Cluster

	Area Covered	Rainfall in 1 Hour
Areas of convective towers (A_h)	0.5×10^4 km^2	1.5×10^{11} kg
Stratiform precipitation area (A_s)	2.0×10^4 km^2	1.0×10^{11} kg
Upper level cloud overhang (A_o)	7.5×10^4 km^2	0
Total area of cloud cluster ($A_h + A_s + A_o$)	10^5 km^2	2.5×10^{11} kg
Area of large-scale region containing cloud cluster (A)	2.0×10^5 km^2	2.5×10^{11} kg

lantic hurricane Allen, 1980, Jorgensen (1984) reported that the stratiform precipitation contribution was about 60 percent of the total during many hours of observation by airborne radar. In midlatitudes, mesoscale convective systems sometimes have structures similar to cloud clusters, with a high stratiform component (Houze and Hobbs, 1982). In a case recently documented in the 1985 PRE-STORM program, Johnson and Hamilton (1987) found 29 percent of the rain to be stratiform.

Figures 12a and 12b are from GATE observations, while Figure 12c is from a numerical model of a GATE squall line (Tao and Simpson, 1988). In both, the overall stratiform contribution is significant (25 and 32 percent, respectively); note the gradual stratiform increase as the convective updrafts with their heavier rain rates die out. The sizable stratiform rain contribution from tropical convective systems is of major importance to the TRMM program. It provides a measurement challenge to space instrumentation but offers an immense

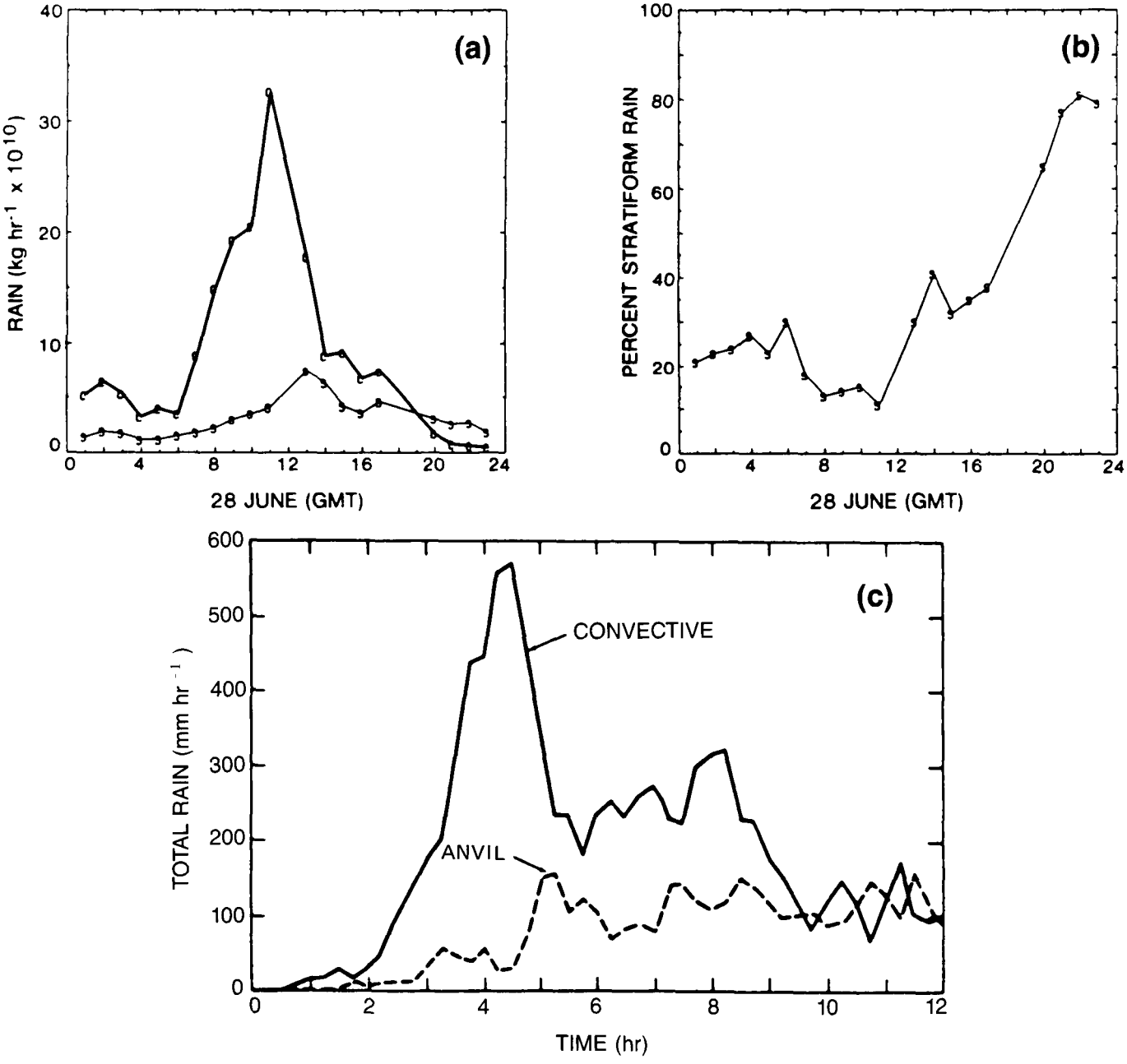

Figure 12. (a) Convective (C) and stratiform (S) volume rain rates (kg hr^{-1}) on GATE day 179, derived from the integration of rain rates >6 mm hr^{-1} (convective) and <6 mm hr^{-1} (stratiform) over an area 400 km in diameter centered on communication. (b) The contribution by the stratiform rain, expressed as a percentage of the total rain volume as a function of time. The weighted percentage for the 24-hour period is 25 percent. (Negri, personal communication). (c) Cloud population model simulation of convective versus anvil stratiform rain in a GATE squall line. The ordinate is the total rain rate over the entire area of convective cores (solid) and anvil (dashed). It should be noted that three classes of ice are required in the model to realistically simulate the bright melting band and stratiform precipitation. (After Tao and Simpson, 1988).

scientific benefit if the challenge can be met. The anvils release latent heat as their ice particles form and grow (Houze and Hobbs, 1982). In addition, melting and evaporation of precipitation below the anvil cool the environment (Leary and Houze, 1979), and the anvils are important absorbers and emitters of radiation (Webster and Stephens, 1980). Houze (1982) has postulated that the vertical profile of the latent heating which clouds provide to the surrounding atmosphere differs widely between convective and stratiform precipitation, as illustrated in Figure 13. The lower diagram of Figure 13 contrasts the heating profiles of isolated active cumuli with those of a mesoscale cluster like that in Figure 11, which includes anvils.

Different vertical heating profiles are associated with differences in the forces controlling important large-scale circulation features. Recently there has been a great interest in studies of the so-called 30-60 day oscillation in the tropics and its possible connection with the ENSO phenomenon (Lau and Chan, 1986). One of the key issues in these studies is the manner in which tropical convection and the large-scale wind field may interact. It is found that the propagation speed of atmospheric Kelvin waves,[6] which are believed to be intimately related to the 30-60 day oscillation, is strongly affected by the shape and structure of the vertical heating profile (Lau and Peng, 1987). Also a higher-level centroid of the heating function gives a more realistic structure of the mean tropical east-west circulation such as the Walker cell (Hartmann *et al.*, 1984).

THE CLIMATOLOGICAL IMPORTANCE OF TROPICAL RAIN VARIABILITY

Satellite "snapshots," e.g., Figure 5, reveal the basic mesoscale character of the convective systems associated with tropical synoptic disturbances. However, when these patterns are averaged over several weeks or longer, large-scale, coherent patterns of variability emerge. These time-averaged planetary-scale features are associated with the seasonal monsoons, trade-wind systems and oceanic convergence zones, whose spatial scales are much larger than the transient disturbances appearing on daily weather maps. Multi-week to multi-year variations in these planetary features also exhibit large-scale, coherent features, a factor of great significance to climate

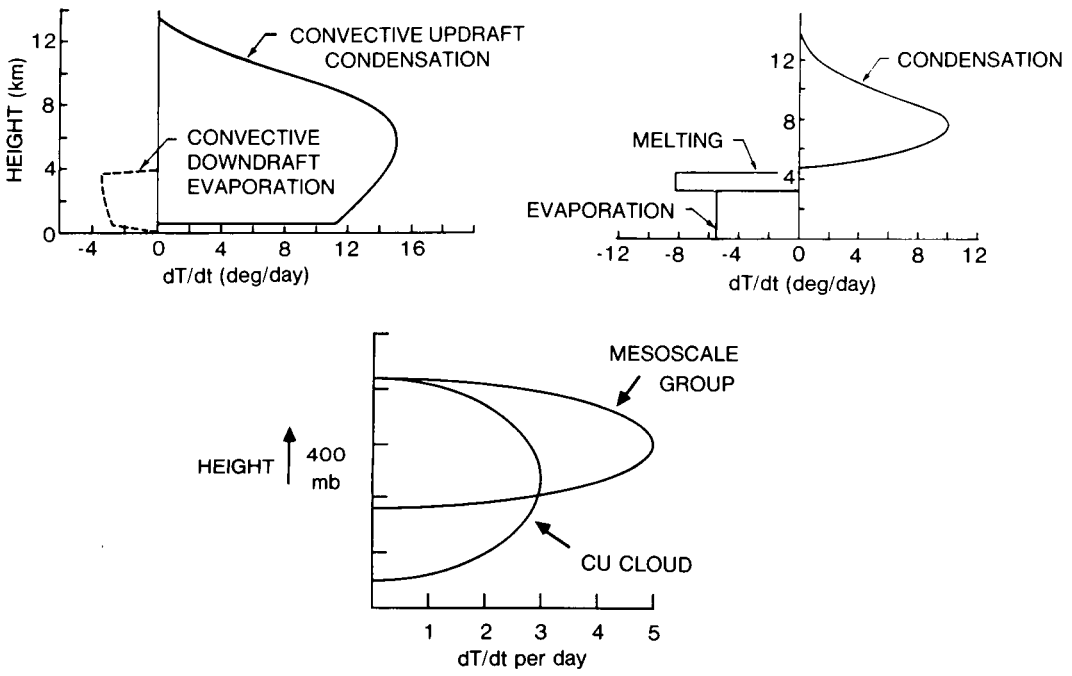

Figure 13. Schematic diagrams (after Houze, 1982) illustrating the differences between the vertical heating profiles associated with convective (left top) and stratiform (right top) precipitation. The lower diagram contrasts the hypothesized heating profile that would be associated with active convective cells only against that postulated to be produced by a cluster such as illustrated in Figures 9a and b and 12a and b, where there is a significant contribution from stratiform rain. Note that the more realistic cluster has a higher level at which the maximum heat release is hypothesized to occur. Note also that the detection of precipitation by radar is not necessarily the location of the actual condensation heating and that considerably more modeling work and observations are needed to specify heating profiles and their variability.

[6]These Kelvin waves are a special kind of tropical gravity wave mode, limited to a narrow band in the "equatorial wave guide region." Their motion field is in the zonal-vertical plane.

prediction and to the development of sampling strategies for estimating accumulated precipitation.

Annual Cycle

Although the annual cycle in tropical surface temperatures is on the whole much less than that found in the extratropics, the variation in the large-scale precipitation regimes is more pronounced; so much so that in much of the tropics the annual cycle is characterized in terms of rainy and dry, rather than summer and winter seasons. It is the seasonal variations in the location and intensity of precipitation, and the associated changes in atmospheric heating—the latent heat release and radiational heating related to cloudiness—which strongly amplify the otherwise weak effect on the circulation of the annual cycle in surface temperature.

Aided by satellites over the past two decades, atmosphere and ocean scientists have been able to work out tantalizing qualitative relationships between variability in rainfall, SST's, and large-scale circulations in both media. These have depended upon defining a proxy variable for tropical rainfall. One of the most useful of these proxy variables has been OLR derived from the National Oceanic and Atmospheric Administration (NOAA) operational polar orbiter satellite measurements. Average values over 9 years for the two solstice seasons are shown in Figure 14. Experience suggests that areas in the tropics where time-averaged OLR values are less than 240 W m^{-2}, namely those areas where the largest amount of OLR originates from the cold cloud tops of convective systems, bear a general qualitative correspondence with regions of heavy convective rainfall and mean upward motion. These areas are shaded in the figure. One maximum is centered over Africa, another over South America/Central America; both migrate north-south with the "high sun" season. The third and most extensive area is centered over the land areas and adjacent warm waters of the Indonesian-Australian-east Asian monsoon region, with eastward extensions along the the ITCZ north of the equator, and the South Pacific Convergence Zone (SPCZ) in the southwest Pacific.

That the inferred regions of heavy precipitation do indeed mark the upward branches of time-averaged direct thermal circulations (warm, moist air rising; cool, dry air sinking) is supported by Figure 15. This figure shows an estimate of the 200 mb velocity potential, which reflects the irrotational, divergent part of the circulation. Thus, it can be used to infer the horizontal branches of these circulations in the upper troposphere. The broad-scale, time-averaged features and major year-to-year variations of the velocity potential field, which are now routinely produced by major meteorological analysis centers, are related to crucial energy conversions maintaining the large-scale atmospheric circulation (Rasmusson and Arkin, 1985). The large-scale patterns shown on Figure 15 appear each year. Consistent with Figure 14, the dominant feature is the massive upper tropospheric outflow region associated with the precipitation systems of the Asian-Australian monsoons. Note that this feature migrates seasonally along a northwest-southeast axis, in a manner similar to the migration of the OLR minimum, with which it appears

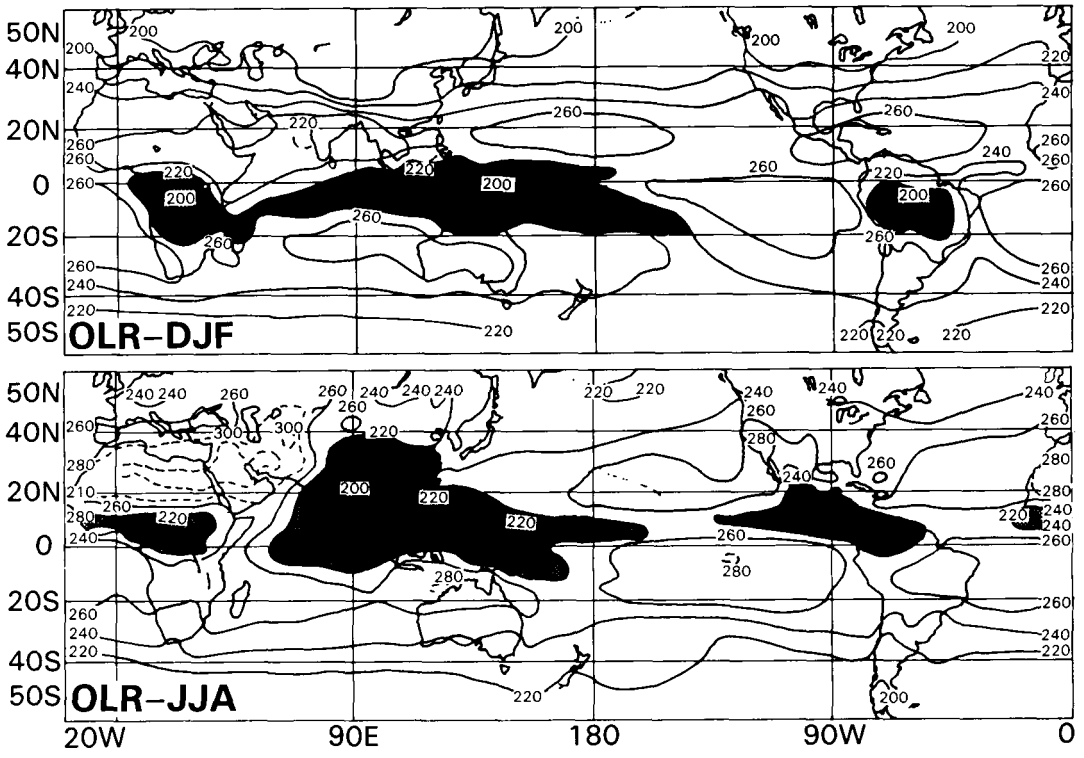

Figure 14. Mean OLR for December-February (upper) and June-August (lower). Areas where OLR is less than 240 W m^{-1} are shaded (Janowiak *et al.*, 1985).

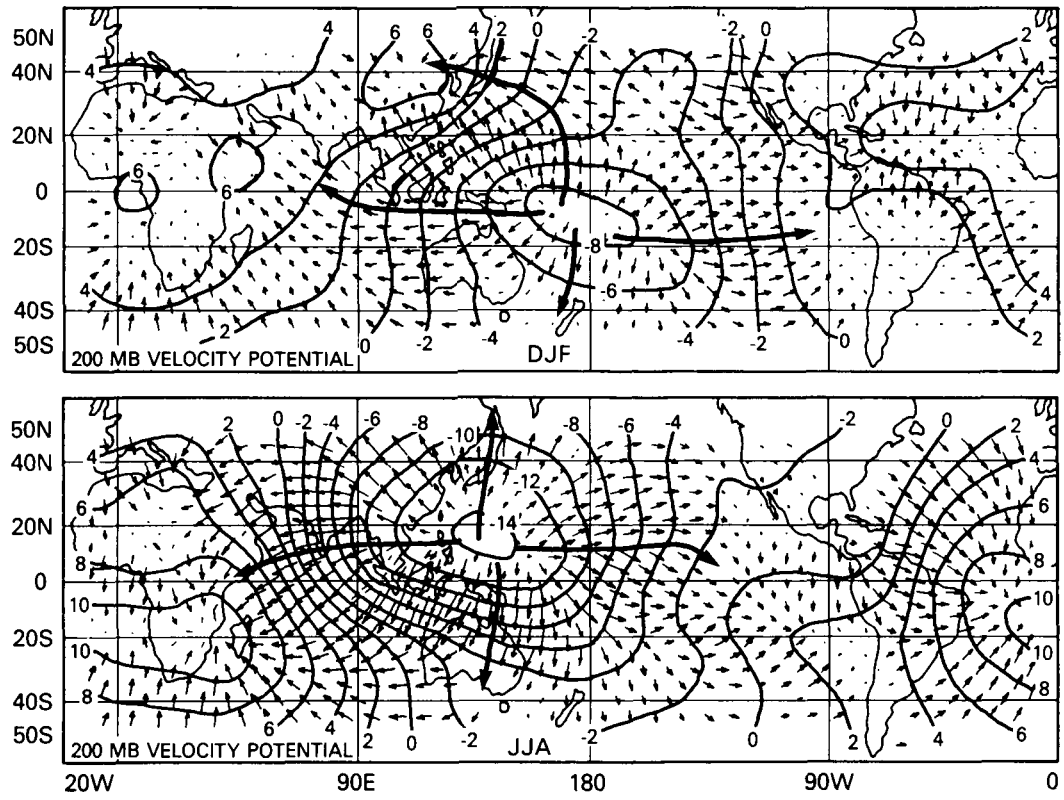

Figure 15. Mean 200 mb velocity potential for December-February (upper) and June-August (lower) (From Arkin *et al.*, 1986).

to be linked. The weaker but more widespread upper level inflow-subsidence regions largely coincide with radiative sink regions: the winter continents, the subtropics and the cold waters of the eastern equatorial Pacific.

The annual cycle in tropical circulation and rainfall is closely coupled with the annual cycle of SST (not shown). The longitudinal temperature difference between the upwelling region of the eastern equatorial Pacific and the huge "warm pool" that overlies the west Pacific-eastern Indian Ocean monsoon region is particularly important. There is a good correspondence between the location and seasonal migration of the warm pool and the monsoon precipitation regime. More generally, the tropical oceanic regions of OLR less than 240 W m^{-2} remain primarily within the areas enclosed by the 28°C SST isotherm. However, there are large regions where the SST exceeds 28°C but OLR is greater than 240 W m^{-2}. This is particularly true during the northern summer. Gadgil *et al.* (1984) have demonstrated that an SST threshold around 28°C is a necessary but not sufficient condition for widespread, recurrent convection. Thus, the time-averaged planetary-scale thermal circulations not only reflect the classical land-sea monsoon contrasts but also reflect an east-west Walker Circulation response to SST gradients.

The circulation systems of the atmosphere and the ocean are coupled through interactions at the air-sea interface. However, it is only in the deep tropics, where the time scale of the oceans is relatively short, and that of the planetary scale atmospheric circulations, i.e., the monsoons, tradewind systems, and convergence zones, are relatively long, that there is a close dynamic coupling on time scales shorter than 1 year (Philander, 1979). As illustrated in Figures 3 and 4, the thermal coupling associated with SST anomalies is strongly amplified by the apparent associated changes in the large-scale rainfall regime, leading to changes in the low-level atmospheric circulation, which in turn leads to changes in the ocean upwelling and current systems, and to further changes in the SST, thus closing an interactive feedback loop.

The fresh water cycling in the tropical-subtropical atmosphere generates substantial buoyancy fluxes at the ocean surface. A fresh water input from rain of 1 m per year is approximately equivalent to a heat input of 40 W m^{-2} at 25°C or 30 W m^{-2} at 30°C surface temperature. This implies that the subtropical evaporation approximately balances the heating as far as density effects are concerned. The tropical rainbelt (ITCZ) provides the ocean a substantial buoyancy input from rain, increasing the stability against overturning of the upper ocean layer. This stabilizing will modify the strength of the mixing processes in the upper ocean, with consequences for the thermal feedback effects and biological productivity in the marine zone under the atmospheric ITCZ. These effects may relate most critically to biogeochemical controls and to the interaction of the atmosphere and ocean on climate time scales. There is clearly a need to document them through more accurate rainfall determinations.

The fresh water anomaly budget in the west equatorial Pacific-Indonesian-maritime continent belt plays a central role in current thoughts on the global salinity balances (Piola and Gordon, 1984). The precipitation distribution in that geographic belt is an essential element in a critical analysis of

the Pacific-Indian Ocean inter-ocean transport north of Australia and its manifestations. Similarly, the excess salt flux in the Gulf Stream cannot be adequately modeled without knowledge of the fraction of subtropical evaporation which is removed in the ITCZ rain zone. The whole subtropical oceanic gyre stratification is affected.

Interannual Variability

The 1980's have been a decade of major climatic events which have drawn attention to the socio-economic consequences of unusual regional and global fluctuations. Of particular significance were the global dislocations associated with the major 1982-83 ENSO episode, the catastrophic effects of the Ethiopian drought and the continuing, multi-decadal scale downturn in Sahelian rainfall.

There is persuasive evidence from both observational studies and model simulations (Bjerknes, 1969; Horel and Wallace, 1981; Webster, 1981, 1982; Shukla and Wallace, 1983) that the massive shifts in tropical precipitation regimes are related to large-scale SST anomaly patterns, and perhaps to land surface changes as well. An outstanding and particularly important example is the ENSO cycle.

Strictly speaking, the term "El Niño" refers to an anomalous warming of the surface water of the eastern equatorial Pacific, but it is often applied to the related basin-scale equatorial Pacific warming. The Southern Oscillation (Walker and Bliss, 1932) is a global-scale seesaw in atmospheric surface pressure with centers of action around Indonesia-north Australia and the southeast Pacific. The two phenomena are atmospheric and oceanic parts of an elegant and pervasive global system of climate fluctuations now referred to as ENSO. (For a review and bibliography, see Rasmusson 1985.) ENSO is the most notable and pronounced example of global climate variability on the interannual time scale. The nearly simultaneous appearance of pronounced climate anomalies around the world, together with the disruption of the marine ecosystems along the west coast of the Americas, can have serious weather and climate consequences and major adverse effects on regional and global food production.

It is believed that the ENSO cycle owes its existence to large-scale, ocean-atmosphere interactions in the equatorial Pacific, with a possible contribution from the Indian Ocean. The entire longitude belt extending from the eastern Indian Ocean through the eastern tropical Pacific participates in the seesaw pattern of atmospheric variability associated with the ENSO cycle. While the largest ENSO signals are found in this sector, it is now clear that the Atlantic basin often responds as well.

During the cold water phase of the cycle (Figure 16, lower), the equatorial easterlies are strong, and the Walker circulation spans the breadth of the Pacific, so that dry conditions prevail over the central and eastern equatorial zone. The persistent easterly winds over the broad expanse of the central equatorial Pacific exert a westward frictional drag on the ocean, which requires a balancing east-west slope in sea level of about 0.5 m across the basin (Wyrtki, 1975). The thermocline layer, which separates the warm mixed surface layer from the colder, stratified water below takes on an opposite slope, reflecting high SST and a deep, warm, mixed layer (~150 m) in the western Pacific and a very shallow or non-existent mixed layer along the South American coast.

It is, however, the warm phase of the cycle which has received the most attention. These "warm" or "ENSO" episodes often begin early in the year, reach their mature phase around the end of that year (Figure 17) and decay during the following 6 months (Rasmusson and Carpenter, 1982). The most important contributor to the appearance of anomalous warm surface waters in the central equatorial Pacific is the weakening of the equatorial surface easterlies (Figure 16 upper). When this occurs, the westward frictional drag on the ocean surface diminishes, and the equilibrium with the sea level slope is disrupted. Warm surface waters move eastward. The west Pacific warm pool expands eastward, accompanied by an eastward extension of the associated region of heavy rainfall and westerly low-level wind anomalies. The anomalous distribution of rainfall also contributes to changes in ocean stratification and circulation through its effect on ocean salinity (and thus, density). These effects may constitute a significant and generally neglected perturbation of ocean dynamics (Webster, 1987a).

While the tropical circulation response to heating is quite well understood in terms of simple equatorial wave dynamics, e.g., Gill (1980), the way in which tropical heating influences extratropical climate is rather complex, being strongly dependent on the climatological mean circulation and the location and distribution of the heating itself. The teleconnection[7] process, through which an atmospheric response is generated outside the region of direct forcing, has been the subject of intense study and lively debate during the past few years. The Pacific-North American circulation anomaly pattern (Figure 18) serves as a good example of a teleconnection observed during the northern winter of a warm episode (Wallace and Gutzler, 1981). On the other hand, another teleconnection has recently been found in the western Pacific (Figure 19) which appears during the northern summer. Various hypotheses for the underlying mechanism of these teleconnection patterns have been proposed, e.g., Horel and Wallace (1981); Simmons *et al.* (1983); Palmer and Owen (1986); Nitta (1987), but the issue is yet to be resolved.

Although the typical ENSO-related drought pattern which occurred over southern Africa during the rainy season of 1982-83 was among the worst of the century, it was merely one aspect of a continental-scale longer-lasting period of drought that afflicted much of Africa between 1982-84 (Rasmusson, 1987). This illustrates the fact that many aspects of tropical rainfall variability, including the multi-year droughts of the Sahel, and the recurrent droughts of northeast Brazil are related to factors in addition to ENSO. For these and other features of tropical variability, one must adopt an even broader view, which involves the entire tropics, both land and ocean, as well as possible links with the extratropics.

[7]Defined as coherent variability between distantly separated centers of action. Definition provided by personal communication from Dr. R. Livezy, Climate Analysis Center, NOAA.

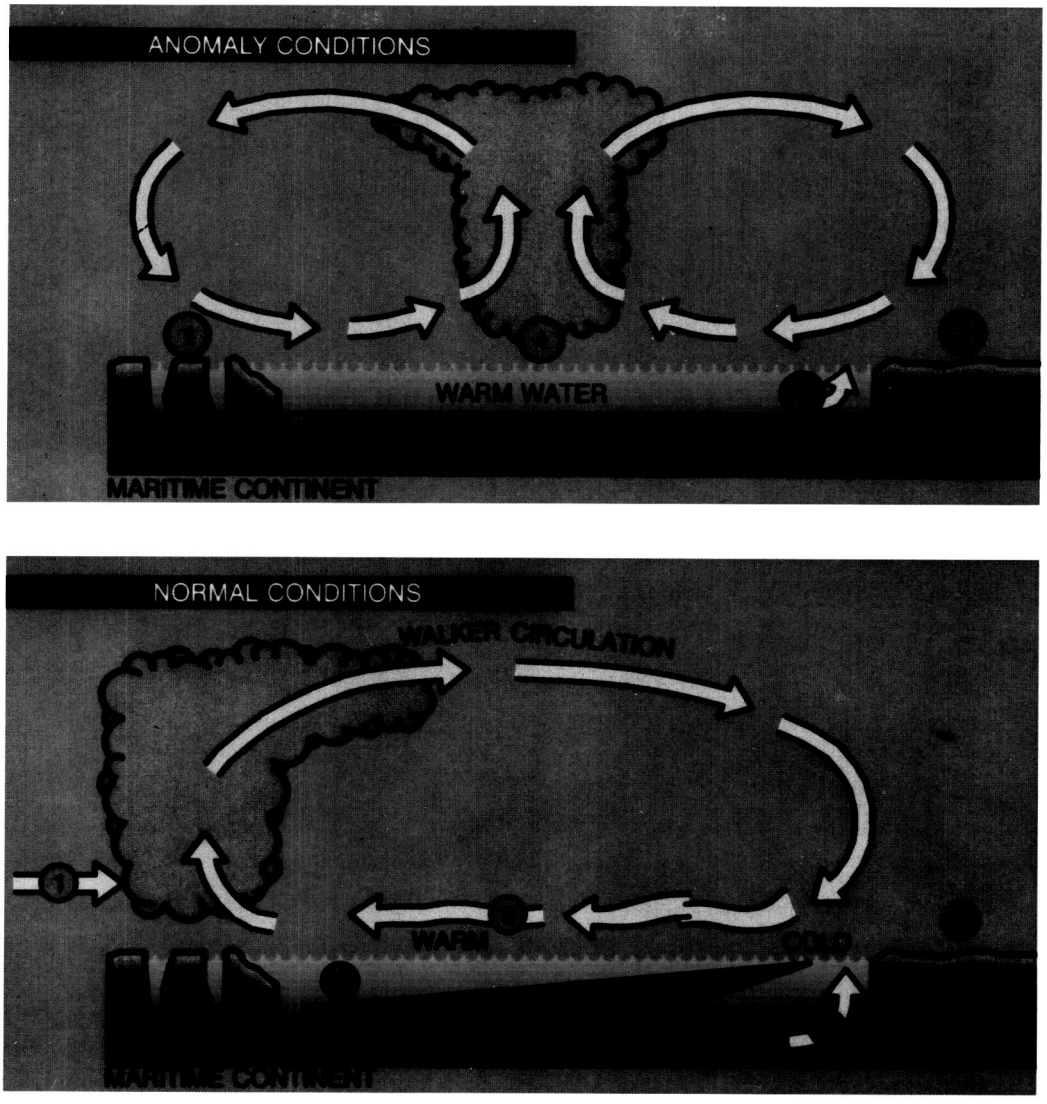

Figure 16. Schematic east-west (zonal) sections across the Pacific basin in normal (bottom) and anomaly (top) conditions. Note that under normal conditions the Walker cell is a single zonal cell (with ascent over the maritime continent) superimposed on the meridional Hadley circulation, which exists on a global average. Under El Niño conditions, the Walker cell is split, with ascent over the mid-Pacific warm temperature anomalies. For explanation of the coupled ocean-atmosphere processes, see text.

Intraseasonal Variability

There is also a high degree of coherent atmospheric variability on time scales of about 30-60 days (centered around 40-50 days) which exhibits a remarkable degree of similarity to the lower frequency ENSO cycle. The first evidence of organized large-amplitude intraseasonal oscillations was reported by Madden and Julian (1971, 1972). The oscillations are particularly evident in rainfall and wind fluctuations over the Indian Ocean and the Indonesian-north Australian sector of the low-latitude tropics. During the past several years, the global aspects of this oscillation have become more apparent through the work of Lau and Chan (1985, 1986, 1987), Lorenc (1984), Weickmann *et al.* (1985), Knutson and Weickmann (1987), and others.

Analysis of high-resolution time series of OLR data (Nakazawa, 1986) shows that the oscillations first appear in the western equatorial Indian Ocean as convective outbursts consisting of large aggregrates of cloud clusters, each of which has a dimension of about 3,000 km and a time scale of several days. These "superclusters" then migrate eastward, although the component individual clusters move westward (Figure 20). The speed of forward migration is about 5 m sec^{-1}, consistent with that associated with the 30-60 day oscillation. Maximum convective activity occurs in the Indonesian-north Australian region, after which the clusters weaken or disappear over the central and eastern Pacific. However, the oscillation in the upper tropospheric wind field can often be traced around the entire equatorial belt. The oscillation strongly influences climate in the equatorial regions and has a profound influence

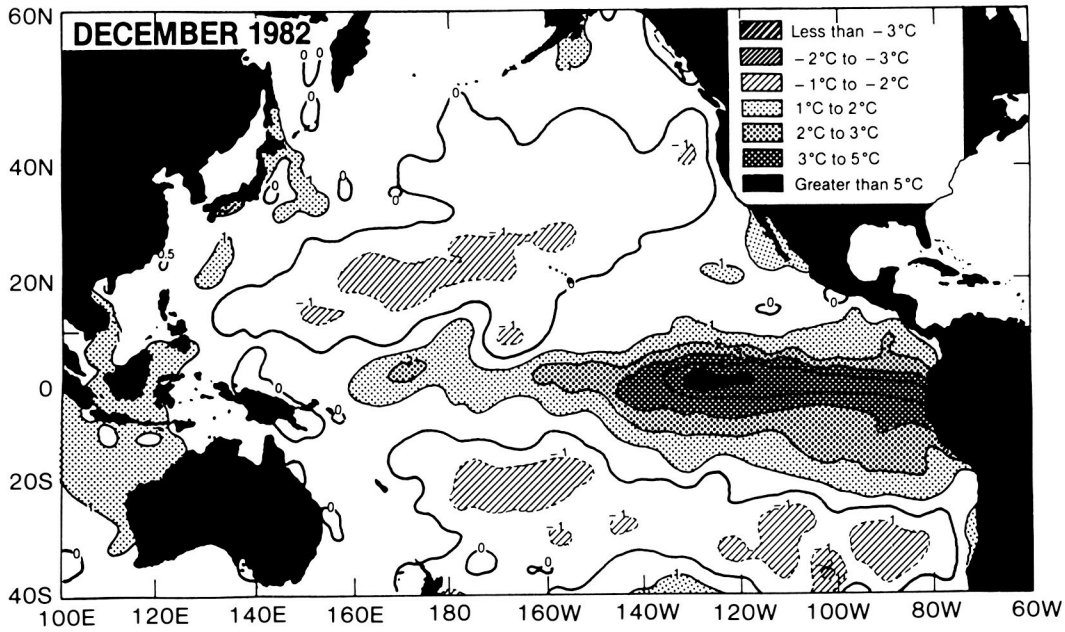

Figure 17. SST anomalies for December 1982, during the maximum development of the 1982-1983 ENSO event.

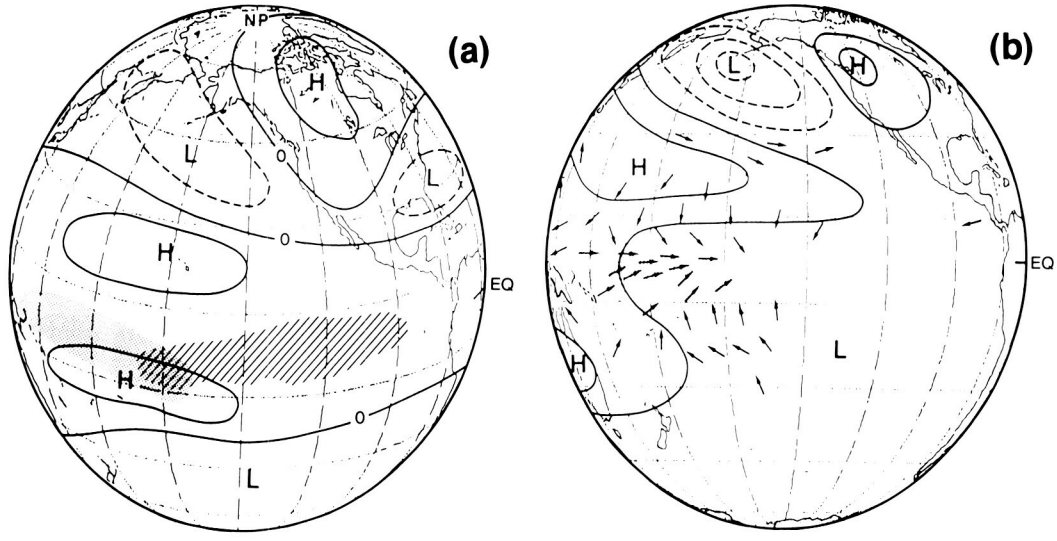

Figure 18. Schematic representation of teleconnection patterns associated with the equatorial sea-surface temperature anomalies (Shukla and Wallace, 1983). (a) Upper tropospheric geopotential height. Hatched area represents warm sea-surface temperature anomaly; stippled area shows region of enhanced rainfall. (b) Sea level pressure and surface winds (arrows).

on the monsoon regions of east Asia, India, and Australia as well. There is evidence that it also affects the extratropical winter hemisphere (Lau and Chan, 1986; Lau and Phillips, 1986; Knutson and Weickmann, 1987). Thus, this mode of variability is of vital importance to both medium-range weather prediction and short-term climate variability.

There has been significant progress in our theoretical understanding of the 30-60 day oscillation since 1985. GCM experiments (Lau and Lau, 1986) have pointed to internal atmospheric dynamics associated with tropical convection as the basic cause of these oscillations. A numerical experimental study by Hayashi and Sumi (1986) first suggested the existence

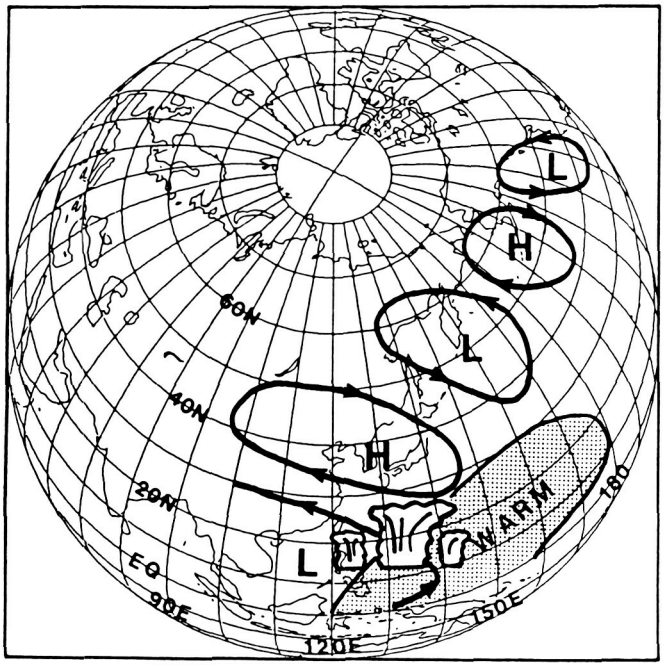

Figure 19. A newly discovered teleconnection characteristic of anti-El Niño years. Schematic pictures show the relationships between SST anomalies, convective activities and atmospheric Rossby wave trains. During summers corresponding to anti-El Niño years in which SST in the tropical western Pacific is warmer than normal, intense convection regions are shifted northward by about 5° to 10° latitude from the normal position south of the Philippines. Atmospheric Rossby waves respond to this tropical heating and propagate downstream over the North Pacific to North America. As a result of the Rossby wave response, east Asian regions including continental China and Japan are covered by anticyclonic circulations, resulting in extremely hot days (Nitta, 1987).

of "superclusters." Theoretical studies of Lau and Peng (1987) have suggested specifically the importance of a nonlinear wave-amplification mechanism[8] by which the rainfall interacts positively with the wave intensity. Recent studies suggest that the details of the vertical heating profile from convection and low-level heating from boundary layer processes, and surface evaporation may be important in modifying the time scale of the oscillation (Lau *et al.*, 1987). The importance of these processes is consistent with the observed collocation of regions of large amplitude of the oscillation and high SST, in particular regions where the SST is higher than 28°C (Gadgil *et al.*, 1984). Since the regions of intense convection are apparently positioned by the SST field, the amplitude and propagation speed of the 30-60 day mode, which is dependent on the interaction of convection and circulation, should also be associated with the SST field. The maximum response occurs in the Indian Ocean-western Pacific monsoon sector, but, during major ENSO episodes, the area of maximum amplitude shifts eastward with the eastward migration of the 28°C isotherm.

While the origin of the 30-60 day oscillations does not appear to depend on coupled ocean-atmosphere dynamics, the oscillations themselves may nevertheless be related to interannual ENSO variability. For example, through their integrated effect over several cycles, they may provide a mechanism for conditioning the ocean on the interannual time scale, or they may act as a triggering or timing mechanism for major ENSO cycle turnabouts. This is at present an active and lively topic of research.

One of the most intriguing observations of the 30-60 day oscillation is the remarkable similarity between the spatial structure and evolution of the atmospheric anomalies with those observed during ENSO. Recently, Lau and Chan (1987) showed evidence from OLR data that the 30-60 day oscillation may be an "intrinsic climate mode" in the tropical ocean-atmosphere, which occurs on both intraseasonal and interannual time scales. The latter can be identified with the ENSO cycle, when an instability in the tropical ocean-atmosphere system related to this intrinsic mode becomes excited. An emerging perspective is that scale interactions may be important between intraseasonal and interannual time scales, and the annual cycle interactions may be important between intraseasonal and interannual time scales and the annual cycle.

DIURNAL VARIABILITY

The diurnal changes in insolation, surface temperature, humidity, and low-level stability modulate and sometimes even dominate the variability in rainfall. Even in those coastal and land areas with large-amplitude cycles and optimal radar and gauge data, diurnal variability has rarely been documented for a long enough period for its interaction with the prevailing large-scale flows and surface conditions to be well understood and modeled.

Over the oceans, a single nighttime maximum was tentatively believed to prevail (Riehl, 1954) owing to destabilization by outgoing radiation from cloud tops. Evidence supporting this hypothesis was reported by Kraus (1963) from a weather ship site in the eastern tropical Pacific. Later, a superimposed semi-diurnal variation was indicated in some tropical locations with three-hourly data (Lavoie, 1963; Malkus, 1963) with maxima just before sunrise and sunset. Using long records of surface gauge and pressure data from Batavia and Wake Island, Brier and Simpson (1969) related the semi-diurnal component to the lunar-solar tide.

The GATE area off West Africa, on the other hand, showed a pronounced afternoon maximum, which McGarry and Reed (1978) hypothesized might be attributable to the passage of easterly waves at a preferred time of day. Winter MONEX (Houze *et al.*, 1981) radar studies revealed quite different cycles over Borneo and the nearby ocean, which appear to be associated with the unique local orography.

Using the proxy variable of cold infrared (IR) radiation cloud tops, Augustine (1984) undertook a Pacific-wide study

[8]This mechanism is called wave-CISK, where CISK stands for "conditional instability of the second kind." Physically, it means that the cloud scale and the large storm scale of motion are interacting in a cooperative manner, intensifying each other. For a pioneering paper on wave-CISK, see Bates (1973).

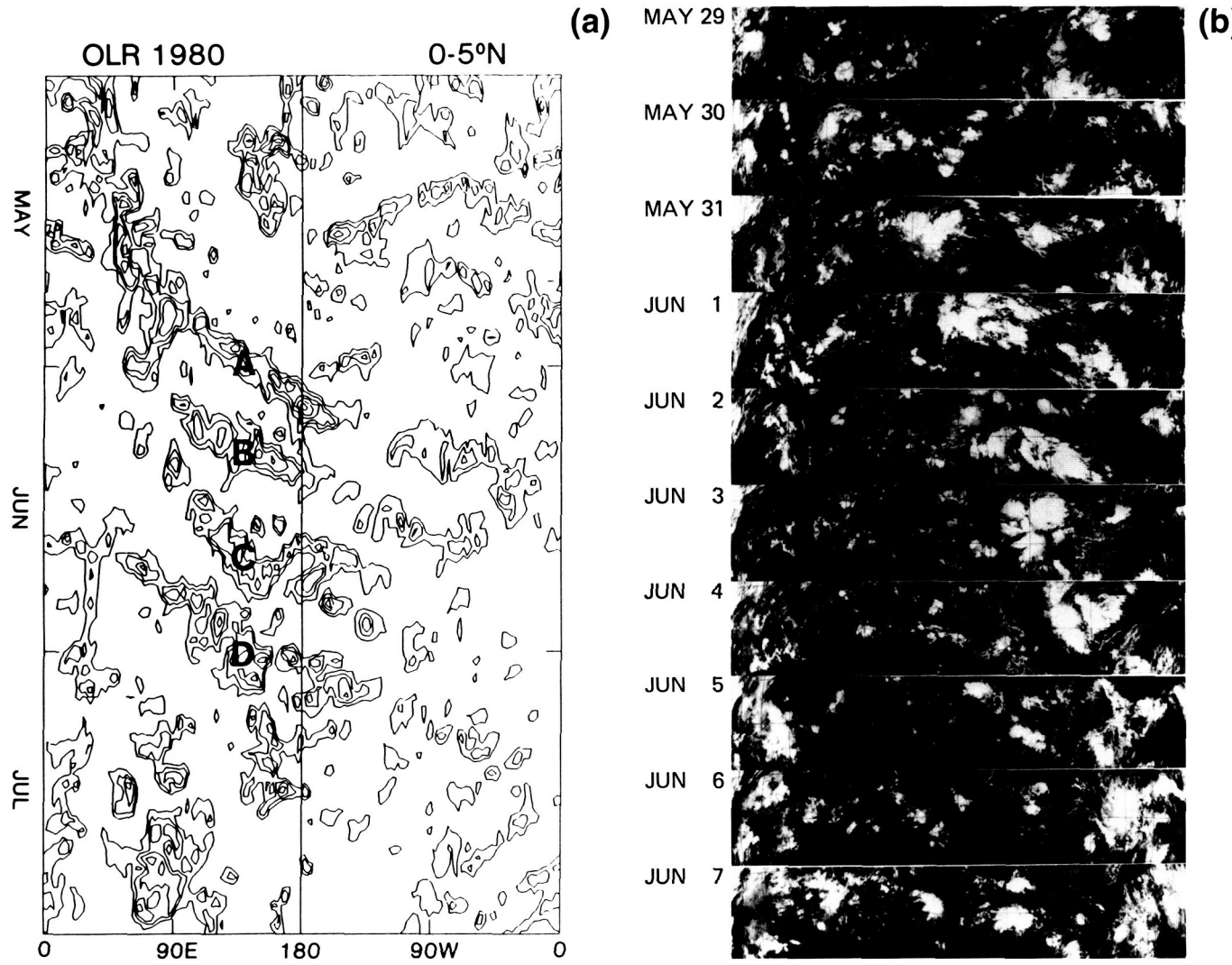

Figure 20. (a) Time-longitude section of transient (seasonal trend removed) OLR anomaly averaged between the equator and 5°N from May to July 1980. Negative (active convective) regions are contoured. Contour interval is in decrements of 30 W m^{-2} starting at -15 W m^{-2}. Symbols A to D indicate superclusters. (b) Daily geosynchronous meteorological satellite (GMS) (Japan) IR images stripped between 10°N and 10°S at 00 GMT from May 29 to June 7, 1980. Centered longitude and latitude are 140°E and the equator, respectively (Nakazawa, 1987).

for August 1979 which showed both a diurnal and semi-diurnal component for four out of five sub-areas, while the fifth sub-area (centered at 150°W) had a morning maximum only. On the whole, less rain was inferred for the hours of darkness than those of daylight! A study using a similar method by Albright *et al.* (1985) gave a comparable picture. Caution must be exercised, however, in using results based upon cold IR cloud tops, since there is a bias between times of convective growth compared with times of convective decay and extensive layer clouds. After years of controversy and tantalizing partial evidence, we can only conclude that diurnal rain variations over the tropical oceans are important, since they may reach or exceed half of the mean value, that they appear to vary with location in a manner which may depend on nearby land mass configuration and that it is not yet demonstrated whether a daytime or nighttime maximum is prevalent over the open oceans! For the necessary documentation, repeated and extensive long-period sampling over the global tropics is required with a more direct measurement method than the proxy IR estimation.

MESOSCALE AND CLOUD SCALE PROCESSES

Although the main goals of TRMM concern short-term climate variability and a primary TRMM product by which to study these are to be monthly rainfall averages over substantial areas, it must be kept in mind that the rain is produced by convective systems. Precipitating cumulus clouds have dimensions of 2 to nearly 20 km, although associated precipitating stratiform regions may extend 500 km or even 1,000

km (see Table 5). The clouds are usually organized in systems on the mesoscale, in lines or clusters which persist for only hours or days. The cloud systems are modulated or even triggered by local inhomogeneities in the winds and/or the lower boundary conditions.

In considering the ENSO, which is one of the most exciting problems involving interplay between all the components of the variable Earth system, we must consider scales smaller than ocean basins or months to understand and model the apparent coupling between the inferred precipitation anomalies and those in SST. For example, a warm ocean surface is not enough to produce tall clouds (Gadgil *et al.*, 1984) unless there is also conditionally unstable air overhead (which is common in the deep tropics) and *unless there also are conditions permitting or forcing low-level convergence of moist air and those initiating and sustaining upper-level outflow* (which are restricted to limited areas and not yet fully understood).

Fortunately, two- and three-dimensional numerical models of tropical convective clouds have made vast progress as a result of the GATE observations and increased available computer power (Simpson *et al.*, 1977, 1982). Cloud population models have been developed and successfully applied to computing vertical fluxes of heat, moisture, and momentum in the equatorial zone (Soong and Tao, 1980), to explaining the relation between outflows, mergers, and the propagation of cloud systems (Tao and Simpson, 1984, 1988) and to simulate the rainfall and other distributions of cloud system properties in the GATE environment (Tao *et al.*, 1987). However, despite the progress, the models must still use untested assumptions about cloud forcing by environmental processes. Limited computer power and fragmentary observations greatly restrict the necessary sophistication in treatment of the physical processes involving the cloud hydrometeors, namely the cloud drops, raindrops, and ice particles. These microphysical processes within a cloud occur on a still smaller scale, down to meters and even centimeters. Computer simulations which can simultaneously treat interacting events on scales ranging from a few centimeters up to thousands of kilometers are still mainly in the future, although some progress is underway in "nesting" higher resolution grids for the small-scale cloud processes within larger model grids dealing with mesoscale and regional scale events.

Even with the above limitations, the presently available cloud models are adequate to move ahead on two frontiers crucial to TRMM. The first is the development and testing of rainfall retrieval algorithms by coupling radiative and dynamic/microphysical models, as described by Simpson *et al.* (1988) and later in Chapter VI. The second is in the need to derive a quantitative relationship between the measured vertical distribution of precipitation-sized hydrometeors and the profiles of latent heat release needed by modelers of large-scale circulation and its variations on several scales, including the 30-60 day time period.

TOWARD A GLOBAL PRECIPITATION CLIMATOLOGY: CRITICAL DEFICIENCIES

Lack of Quantitative Numbers, Error Bounds, Scale Mismatch

The important role played by tropical rainfall in the global hydrological cycle has been made clear. A major roadblock holding back progress in Earth system science is a lack of accurate quantitative numbers regarding the hydrological cycle, a key part of which is rainfall and its variability. Qualitative relationships have been developed relating SST anomalies to hemispheric circulation alterations, with large amplification effects provided by the linkage with tropical convective rainfall. So far, this important link has been deduced indirectly from OLR, or the changes in the cloud top temperatures as sensed from infrared sensors on satellites.

Arkin and Meisner (1987) have shown how a simple algorithm to estimate rainfall from satellite IR temperatures, when "tuned" by the sparse surface observations in one region, can give systematic errors of at least 50 percent in other land areas for 3-year averages. A major problem[9] is to determine the error bounds from the quality and quantity of data available for validation efforts.

The operational World Weather Watch (WWW) surface meteorological network was primarily designed to resolve synoptic-scale variability. In contrast, precipitation is an episodic process, which varies markedly over short distances and time spans. There is a wide variety of structure and organization on the meso- and smaller scales associated with both tropical and extra-tropical precipitation systems.

Precipitation has been accurately measured over only a few well-instrumented areas of the world, most of which were connected with short-duration field programs such as GATE and EMEX. Even over land areas where conventional meteorological observations may appear relatively dense, there is often a fundamental mismatch between the routine synoptic-scale sampling and the much smaller precipitation variability. These may be associated with terrain, diurnal variability, and planetary boundary layer processes as well as the intermittent, subsynoptic character of precipitation systems. *In situ* measurement deficiencies are even more pronounced over oceans where, except for scattered and often unreliable ship reports and non-representative island stations, conventional surface data are essentially nonexistent.

A related scale mismatch, influencing the TRMM strategy, contrasts the desired monthly average over large areas 500 by 500 km in size, with the small size and high variability of the processes that produce that average.

[9]See Proceedings of a Workshop "Validation of satellite-derived precipitation measurements for the Global Precipitation Climatology Project," WCRP, WMO/TD-No. 203, Washington, DC. The main conclusion was that there is no standard ground truth for precipitation. Recommendations were for numerous sites in key regions with calibrated radars and gauge networks over land. Techniques such as hydrophones below the ocean surface, radar, and optical gauges on ships, were recommended for the much more difficult problem of oceanic validation.

Need for Increased Knowledge Concerning Differences Between Continental and Maritime Precipitation

All current estimates of rainfall distribution suffer from the critical deficiency that we do not know the extent to which land/ocean differences are biased. Furthermore, near coastlines evidence suggests that rain processes may differ from those far at sea. In a recent radar study comparing rain clouds in the GATE region of the tropical Atlantic with those over Florida, Texas, Israel, and South Africa, Rosenfeld[10] has found that, for rain cells having the same depth, the continental cells have: 1) higher radar reflectivities, 2) shorter lifetimes, 3) smaller areas, 4) smaller rainfall yield, and 5) a smaller fraction of their total precipitation in stratiform rain. Similar detailed quantitative comparisons of GATE rain cells with those over different tropical ocean areas are not presently available.

It is difficult to estimate the contribution of orographic rain to the seasonal and annual totals in the tropics. Places where such rains are highest are often rain forests with few inhabitants and fewer rain gauges. However, enough is known about orographic rain to expect a large bias in satellite estimates using IR products. Overflying sensors which can determine the depth of the rain layer are clearly required.

Lacking the information to estimate the bias, we cannot now estimate the quantitative difference between continental and oceanic rainfall in the tropics. It is suspected that the zonal rainfall is dominated by three peaks in the "continental" regions (South America, Africa, and the Indonesian region), but we have no present way of knowing that with sufficient accuracy. This is crucial information for determining the distribution of tropical heating and its seasonal distribution.

Coastline-Dominated Regimes: The "Maritime Continent"

The maritime region including Indonesia and tropical Australia probably generates more deep tropical convection than any other part of the world. Sprawling across 60 degrees of longitude, one sixth of the Earth's circumference, from southeast Asia through Malaysia and Indonesia to northern Australia and New Guinea, thunderstorms can be found with or without larger-scale disturbances on any day of the year. Several studies (Krishnamurti, 1971; Krishnamurti *et al.*, 1973; Rasmusson and Arkin, 1985; Webster, 1982, 1983) have demonstrated that this region is a principal sink for low-level inflow and a principal source for high-level outflow (refer back to Figure 15) for both the Hadley (north-south) and Walker (east-west) circulations. Variations in convective latent heat release and circulation in this atmospheric "boiler box" are of central importance to ENSO events and their widespread impacts and teleconnections. Figure 21 relates the altered boiler box convection to an associated wave pattern in the upper-level jetstream, which brings about the Pacific-North America (PNA) teleconnection illustrated in Figure 18.

The boiler box region is characterized by numerous islands of various sizes, bays, seas, and peninsulas, to such an extent

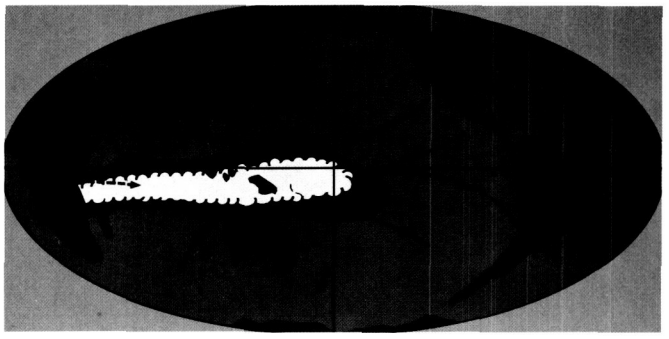

NON-EL NIÑO

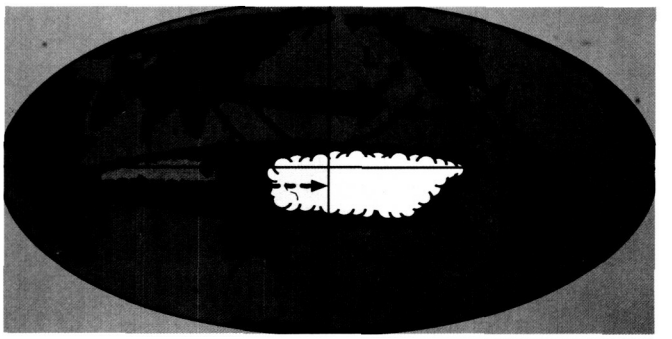

EL NIÑO

Figure 21. Comparison between normal, non-El Niño, conditions (above) with 1982/1983 El Niño conditions during the northern winter season (below). The light stippled areas are those of high cold clouds, assumed to be locations of precipitation heat release. The underlying hatched areas are warm sea-surface temperatures. Note how the warm, convective "boiler box" extends eastward when the ENSO occurs, resulting in a weaker Walker circulation but a more zonally uniform Hadley cell overturning. The thin arrows denote low-level windflow; the northeast and southeast (surface) tradewinds are dashed, while the cold surges in the winter hemisphere are the slightly heavier solid arrows. The upper-level outflow from the boiler box (not shown) has pronounced impacts on the high-tropospheric jet streams (heavy solid arrows). In an ENSO situation, the altered upper-level outflow from the boiler box leads to an eastward extension of the east Asian subtropical jet, and associated eastward shift of the Aleutian low and further downstream adjustments in the midlatitude westerlies. This results in the circulation anomaly pattern shown in Figure 18. As a consequence, the extra-tropical weather is altered significantly, frequently with disastrous consequences (Rasmusson and Webster, 1988, personal communication).

[10]Paper in preparation for publication at the Goddard Space Flight Center.

as to earn its name "maritime continent." As Ramage (1968) pointed out, its atmosphere is dominated by land-sea breeze circulations which, in turn, strongly modulate the cumulonimbus convection. Using winter MONEX data, Houze *et al.* (1981) showed the extent of this modulation in the Borneo region; more recently, Williams and Houze (1987) have demonstrated it over a much larger time and space domain, with cloud areas over land and sea varying by a factor of five between day and night! Their analyses further suggest that the character of the land rain systems differs from those over water. Results from the EMEX/AMEX (Australian Monsoon Experiment) program in 1986/1987 should help clarify some of the processes at work during one season. The rainfall and associated interactions there are too important to the Earth system behavior to neglect to follow up with a longer period of data.

Roadblocks to Improved Models

The inability to measure tropical rainfall is a roadblock in the path toward more credible models for elements of the hydrological cycle and toward more accurate models for medium-range (5-10 day) weather forecasts. The mid-latitude numerical forecasts could also be improved if rainfall, latent heat release, and winds were made available for model initialization. These observations are also required to validate model dynamics and energetics, as well as the forecasts and simulations which result.

Today's state-of-the-art GCM's produce plausible simulations of climate and climate variability. For example, estimates of the vertically integrated diabatic forcing obtained from a GCM experiment look virtually identical to the model-generated rainfall map for the same period (Shukla, 1984). Figure 22 indicates that latent heat is the dominant component of the diabatic forcing and is thus primarily responsible for driving atmospheric motions. Yet these results cannot yet be verified quantitatively.

PROGRAMMATIC BACKGROUND AND RELATIONSHIPS

Benefits and Background from Global Atmospheric Research Program (GARP)

Important background knowledge and answers to key questions on several scales of motion have been developed by analyses of GARP observational programs, particularly the FGGE, which advanced the use, data requirements, and understanding of global models, and the GATE and MONEX on the regional, mesoscale, and cloud-scale processes in two key regions of the tropics. To date, virtually all the rain data upon which the TRMM sampling requirements have been based were derived from the GATE ship radar observations (see Thiele, 1987, Section 1.2; McConnell and North, 1987; and Kedem *et al.*, 1987) although similar analyses of EMEX and other tropical radar data are currently in progress.

Among the many other important GATE findings upon which tropical rain research must be based is that by Houze and colleagues (see, e.g., Houze and Betts, 1981; Houze and Hobbs, 1982) showing that a major part of the rain area and a substantial fraction of the rain amount from tropical convective systems falls from the anvil and stratus layers formed by convection. GATE had two other major impacts on tropical convection studies that have a driving role in the plans for TRMM. The first was the adaptation and testing of three-dimensional cloud models (see Simpson and Van Helvoirt, 1980; Simpson *et al.*,1982) and the development of cloud population models in a tropical environment (Soong and Tao, 1980; Tao *et al.*, 1987; Tao and Simpson, 1984, 1988). The second was that the well-documented, apparently anomalous diurnal rain variation in the GATE region led to wider recognition of the importance and complexity of diurnal variability in tropical rainfall.

The impacts of winter and summer MONEX on tropical rain research have been reviewed by Johnson and Houze (1987). Winter MONEX confirmed many of the GATE findings and also emphasized the importance of land-sea interactions in understanding tropical rainfall and its variability. In summer MONEX, the precipitation structure of Bay of Bengal depressions, which are the major rain and flood producers over northern India, are documented. The depressions were found to be populated by mesoscale rain areas similar to those in GATE, with large stratiform areas attached to areas and lines of deep convection (Houze and Churchill, 1987).

Tropical Ocean Global Atmosphere Program (TOGA)

The TOGA (WCRP, 1985; National Academy of Sciences, 1986) is an international effort aimed at establishing the predictability of the future state of the coupled tropical ocean-atmosphere system and the impact of that system on the global climate on time scales of months to years. There are two principal thrusts. The first is the diagnosis and forecasting of an ongoing climate event, in particular the ENSO phenomenon of the Pacific Ocean regions. The second thrust is aimed at the understanding of the physical principles that govern a sequence of these climate events.

TOGA calls for a 10-year program (1985-1995) of atmospheric and oceanic observations and will undertake, for the first time, the determination of the time-dependent heat storage and circulation of the tropical oceans using a combination of real-time analysis of oceanic and atmospheric fields and the modeling of the combined ocean-atmosphere system.

Central to the TOGA observation, diagnosis, and modeling efforts is careful determination of the vertical and horizontal structure of atmospheric precipitants. This is because a key element of the coupled ocean-atmosphere variation is the vast latent heating occurring in the warm ocean region of the tropics, coupled with the radiative heating and cooling associated with the cloudy regions. Atmospheric circulation responses appear very sensitive to the horizontal and vertical distribution of the latent heating. Furthermore, a significant part of the density gradient which drives the density currents of the tropical oceans may arise from variations in salinity in the surface layer imparted by precipitation. Consequently, a major requirement for TOGA is the accurate determination of the magnitude and horizontal and vertical gradients of tropical precipitation and heating. These data are essential for both

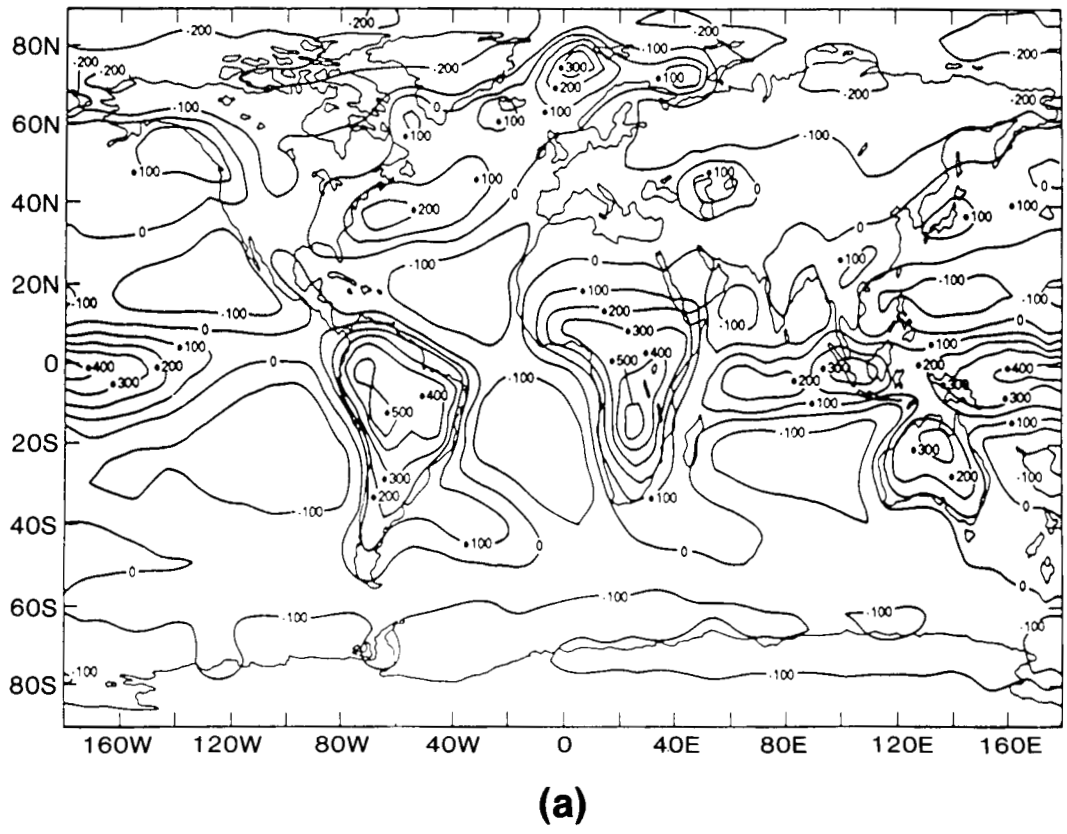

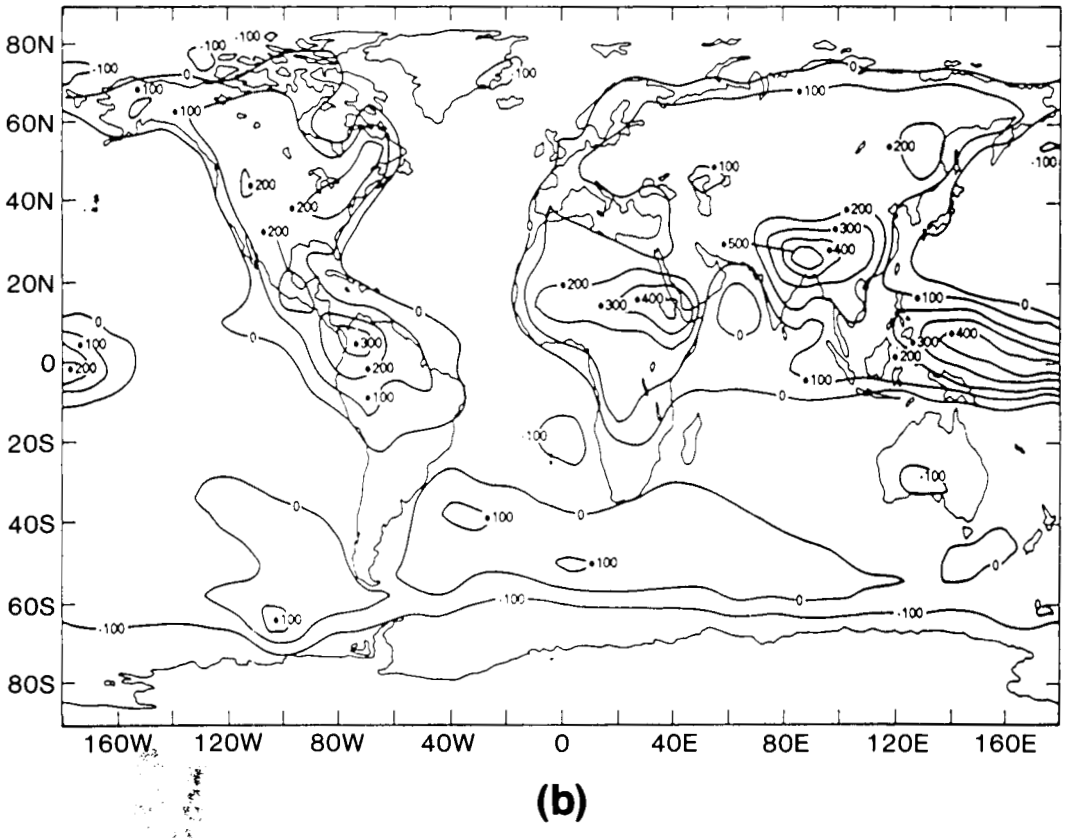

Figure 22. (a) Vertically integrated net diabatic heating (calories cm^{-2} day) of the atmosphere during winter as simulated by the GLAS climate model. (b) Similar diagram for summer (Shukla, 1984).

diagnostic studies and for model validation. Unfortunately, quantitative precipitation data are at present unavailable over most of the tropics, and this constitutes a major deficiency in the TOGA observational program. The TRMM would directly address this deficiency. The TRMM plans to obtain "ground truth" validation by surface and budget-type rain determinations; these, as well as the planned pre-mission experiments related to tropical rainfall, should be of immense benefit to TOGA.

Global Change Studies

The Earth sciences have developed to the point where each component of the Earth system, such as the ocean, the land surface, the cryosphere, and the atmosphere can no longer be treated in isolation. It has long been known that the ocean provides sensible and latent heat to the atmosphere, which in turn helps to drive ocean currents by wind stresses. Rainfall and continental runoff at the ocean margins change the surface salinity and thus buoyancy and also contribute thereby to ocean circulation forcing. The land is also a source of moisture and drives the atmosphere through topographic forcing and latent and sensible heat transfers. The interaction of the biosphere, both on the ocean and on the land, with the physical environment is only beginning to be understood quantitatively. Indeed, what is new in Earth sciences is not the qualitative understanding that these processes are mutually important, but the realization that it is beginning to be possible to measure and model these interactions quantitatively, even at a global scale.

This realization has spawned many new programs, such as the International Geosphere/Biosphere Program (National Academy of Sciences, 1986a) under the aegis of the International Council of Scientific Unions. As the name suggests, this international program aims to promote the quantitative study of the Earth. For the reasons already given in the preceding chapters, tropical rainfall is being recognized as one of the important parts of the system which must be known better.

Within the United States, several recent studies have stated the significance of tropical precipitation for studies of the Earth system. For instance, in a recent report (National Academy of Sciences, 1985), the Committee on Earth Sciences of the National Research Council noted (pp. 32-33), "Precipitation is central to the hydrological cycle.... Improved understanding of the physical processes that determine the amount and spatial distribution of precipitation is recognized by the committee and in other studies (National Academy of Sciences, 1980) as one of the fundamental problems of meteorology..." Similarly, a NASA study recently concluded (NASA Advisory Council, 1986, p. 20) that "The measurement of global moisture must ...be made a primary objective within studies of the fluid and biological Earth in the years ahead," and further (p. 39), "There is a critical requirement for space measurements of global precipitation. An exploratory mission is needed to test the feasibility of using active and passive microwave data, together with VIS/IR imagery, to derive useful estimates of rainfall amounts and distribution. A low-inclination orbit will permit study of the diurnal cycle of rainfall over the tropics and an assessment of the relationship of heat released into the atmosphere to anomalies in atmospheric circulation."

The Global Energy and Water Cycle Experiment (GEWEX)

The GEWEX, a new initiative of the WCRP (see WCRP, 1987), will concentrate on improving our knowledge of the transport of water and energy within the atmospheric system. Its scientific objectives are:

- to describe and understand the transport of water (vapor, liquid, and solid) and energy in the global atmosphere and at the underlying surface; and
- to develop methods of predicting changes in the distribution of water (vapor, liquid, and solid) within the global atmosphere and at the underlying surface which may occur naturally or through the influence of man's activities.

A further objective of GEWEX is to promote scientific advances and technical developments, such as the deployment of new satellite systems and orbital testing of new remote sensing instruments, which would find operational applications for improved weather forecasting and climate prediction. In addition, GEWEX will also promote the development of time-dependent representations and predictive models of the global transport and ground storage of water and validation of these models against the observed annual and multi-annual evolution of available water resources and river discharge in several selected continent-scale domains.

The overall research strategy of the WCRP is formulated into three specific objectives or "streams" (Schiffer, 1987):

- Stream 1: Establishing the physical basis of long-range weather prediction (Atmospheric Prediction Research);
- Stream 2: Understanding the predictable aspect of global climate variations over periods of several months to several years (TOGA); and
- Stream 3: Assessing the response of climate to natural or manmade influences over periods of several decades (World Ocean Circulation Experiment, WOCE).

The TOGA and WOCE programs are already underway so we can expect, by the mid-1990's, significant progress in our knowledge of the oceans and their interaction with the atmosphere. One of the largest problems will then be the transports of water and energy within the atmosphere.

The present operational World Weather Watch (WWW) observing system does not meet the observational requirements of GEWEX with respect to describing the global distribution of precipitation, evaporation, and water transport. A number of special WCRP data projects, based on existing observations, have been implemented in an attempt to improve the data coverage, but the total of available information remains inadequate. The situation is further aggravated by the fact that the global hydrological processes are not adequately described by present GCM's. Thus GEWEX has been proposed to be the central project in WCRP Stream 1 to address these problems.

The GEWEX observing system, planned to start late this century or early in the next, includes five geostationary satellites with improved resolution Visible-Infrared Spin Scan

Radiometer (VISSR) imagers and combined IR and microwave sounders for temperature and moisture. There will be a number of low Earth orbiting satellites. Among the many measurement packages aboard these orbiters, there will be one to measure winds and cloud structure, and a precipitation package with an instrument complement similar to TRMM but more advanced, which will be flown on both low-inclination and polar platforms.

The WCRP's GEWEX (described in greater detail by Schiffer, 1987) will need to build upon the TRMM results for a more comprehensive documentation of global hydrological interactions and for the better design of an advanced precipitation package. This TRMM document attempts to define a shortly achievable mission, which can be the first in a series of space missions necessary to meet the objectives laid down in the Earth system science planning documents.

Earth Observing System (Eos)

Eos is a science mission whose goal is to advance the understanding of the entire Earth system on the global scale through developing a deeper understanding of the components of that system, the interactions among them, and how the Earth system is changing. The Eos mission will create an integrated scientific observing system which will enable multidisciplinary study of the Earth, including the atmosphere, the oceans, the land surface, and the solid Earth. In order to quantify changes in the Earth system, Eos will be a long-term mission providing systematic, continuing observations from low Earth orbit, including conventional observations and data from a set of satellite instruments that are proposed to fly in the Space Station era, starting in 1995. These instruments, jointly developed by NASA, the European Space Agency (ESA), and Japanese investigators, are planned to fly on a set of satellites in sun-synchronous polar orbit and will consist both of research instruments and successors to the current NOAA operational instruments.

The goal of Eos is to provide a much improved understanding of the Earth as a system and of the sensitivity of different parts of the system to changes elsewhere. Calibrating models of the Earth or components of it, assimilating data into the models, and using data to validate these models are complicated tasks that will require a comprehensive data and information system and the assembly of a global data base for a period of 10 or more years.

Beyond the radiative components, the water budget is the next important unknown needed to determine the overall energy balance of the Earth; as yet none of its components have been adequately determined. Considerable work is needed, both in improved observations and in improved modeling. Many of the new Eos instruments will make observations pertaining to the hydrological cycle. However, because the platforms will be in polar orbit, little information will be provided about diurnal effects. Since diurnal variability is high for tropical rainfall, one of the least-known components of the hydrological cycle, the information from TRMM on these diurnal changes is essential if the Eos observations are to be interpreted correctly.

Given the necessity for substantial improvements in the estimation of the hydrological fluxes, it may be seen that Eos cannot just be a set of instruments in polar orbit, however good their specifications. Conventional and other satellite data will also be required. The unique information provided by TRMM is, therefore, an extremely important data set that must be available for the Eos information system if the Eos project is to be successful.

III. SCIENCE REQUIREMENTS

SCIENCE QUESTIONS

Priority Science Questions

The TRMM SSG gave priority to tractable questions concerning the relationships of tropical rainfall to short-term climate variability, particularly those in which the coupled ocean-atmosphere system is believed to play a predominant role. Keeping in mind the knowledge deficiencies summarized in the previous sections, the near-term state of space technology and its verification opportunities, and the modest budget expected for TRMM, the SSG agreed upon the priority science questions listed in Table 6.

Chapter V. The approach to acquiring the primary data set and its use in answering some of the priority science questions, together with associated sampling problems, are addressed in Chapter IV.

In examining the questions in Table 6, it is clear that models, of many types and scales, will be essential ingredients in working from the data sets toward their answers. In the case of Questions 3 and 4, coupled ocean-atmosphere models can be improved by knowledge of the rain input, and the improved models, in turn, will help to understand sea-air interaction better. This understanding can then be used to improve prediction models. In using the TRMM data toward answering Question 4, the mesoscale atmospheric processes which initiate and sustain cloud clusters become better understood.

Table 6. TRMM Priority Science Questions

1) What is the four-dimensional structure of latent heating in the tropical atmosphere? How does it vary diurnally, intraseasonally, seasonally, and annually?

2) What is the role of latent heat released in the tropics in both tropical and extra-tropical circulations?

3) What is the monthly average rainfall over tropical ocean areas of about 10^5 km^2 and how does this rain and its variability affect the structure and circulation of the tropical oceans?

4) What is the relationship between precipitation and changes in the boundary conditions at the Earth's surface (e.g., SST's, soil properties, vegetation)?

5) What is the diurnal cycle of tropical rainfall and how does it vary in space?

6) What are the relative contributions of convective and stratiform precipitation and how does their ratio vary in different parts of the tropics and in different seasons?

7) How can improved documentation of rainfall improve understanding of the hydrological cycle in the tropics?

These questions can be addressed with the aid of space-time smoothed data sets. For example, a 3-year time series of rain rates over 500-600 km square boxes (or rectangular area equivalents) and through a month will be adequate for the main scientific purposes and hence will be the primary mission data product. The smoothing leads to an advantage not shared by most missions: we are able to tolerate fairly large random errors in the individual measurements so long as the errors are not biased. It also means that if the properties of rain fields are not too disagreeable, we can tolerate the sampling gaps inevitably associated with low Earth-orbiting satellites. Such a low Earth orbiter takes a snapshot of a large averaging area consisting of thousands of individual pixels then returns to the same averaging box about 12 hours later for another look, and so on. The ensemble of pixels collected from each latitude-longitude box are then to be pooled at the end of each 30-day period and used for an estimate of the month-long rain rate. Configurations of instruments and spacecraft which will meet the data set requirements are described in detail in

For another example of improved understanding of scale linkages, Question 1 concerning the structure of latent heating and Question 6 concerning the relative contribution of convective and stratiform precipitation are clearly related, but there is no one-to-one relationship between where the precipitation-sized hydrometeors are found and where the latent heat has actually been released by condensation. Houze and collaborators (e.g., Houze, 1982) have presented qualitative diagrams (see Figure 13), derived from surface-based radar, and calculations from a conceptual model that suggest that the latent heating should peak at a higher altitude when a cloud cluster has a large contribution from stratiform anvil precipitation than would occur if all the precipitation fell from active convective towers. It is clearly necessary to combine the most sophisticated dynamical/microphysical numerical models of cloud populations with data from individual TRMM passes over validation sites to work out these relationships more quantitatively. The objective would be to find out how vertical profiles of latent heat release are related to the hydrometeor

distribution and how these profiles are jointly controlled by the larger-scale environment of the clouds.[11]

A valuable by-product of this part of the TRMM analyses could be improved parameterization of cumulus effects in large-scale numerical prediction models. These examples illustrate how, in the process of obtaining the TRMM data set and of using it toward answering the priority science questions, the solutions to many related important questions concerning interactions in the tropics may be achieved.

Related Important Science Questions and Remote Sensing Questions

In addition to the mission-driving science questions listed in Table 6, which are to be addressed with the basic data set of area-wide monthly rainfalls, there are other important questions to which the TRMM, including its rain retrieval algorithm development, its verification efforts (with special field programs), and its technological systems integration and data processing, can be expected to contribute. In the science area, these questions mainly concern time and space scales smaller than those of the primary data set and their interactions within the atmosphere, with the underlying Earth and ocean, and with the biosphere. Models and other data sources will be needed to address them, and their pursuit should contribute to the main TRMM questions and, more broadly, to tropical Earth system science. Some of these questions are listed in Table 7. Others, equally important, will be formulated during the pre-mission research and as the mission data become available.

Nearly all the questions in Table 7, which should be regarded as illustrative examples rather than as a comprehensive list, involve combining other data with the observations from the TRMM satellite. The oceanic data expected from TOGA will provide a first-time opportunity to address questions such as the first two, although addressing the first question will involve both models and measurements at and close to the air-sea interface. Examining the scales of droughts and the air-Earth-precipitation interactions under increasingly arid conditions can contribute not only to weather and climate prediction but to the use of weather information in economic and resource management decisions.

TRMM is a pioneering mission in measuring tropical rainfall from space, particularly since it will be the first space mission to fly a quantitative weather radar. In that sense, it is an exploratory mission in space science, application, and technology. TRMM will provide the experience upon which to base many successor missions, such as the Eos and GEWEX, which may be expected to build upon the TRMM results to construct more sophisticated and comprehensive measuring systems to detect on a global basis all phases of water substance as their transformations and motions drive the hydrological cycle. Table 8 lists some of the important

Table 7. Related Science Questions

1) What are the mesoscale and cumulus scale linkages between SST, its variation in space and time, and the characteristics of precipitating cloud systems in the tropics?

2) How does the precipitation structure and its variability impact the ocean surface layers and thereby surface salinity, oceanic circulation, and the marine biological habitats?

3) Under what conditions are droughts over land areas associated with alterations in precipitation amounts and structure over the nearby oceans?

4) What are the differences in the structure and life cycles of tropical precipitating cloud systems over different portions of the tropical oceans, and can these differences be explained in terms of large-scale ocean and atmospheric environments?

5) Over land, how are atmospheric rain and ice layer thicknesses related to soil moisture, evaporation, runoff, and vegetation status? How do these thicknesses and relationships vary as aridity increases?

6) How can the TRMM data be used to incorporate radiative processes in dynamical/microphysical cloud models, and how can these interactively modeled processes be included or parameterized in GCM's?

7) How do the three-dimensional wind fields as sensed by the very high frequency (VHF) profilers on the mid-Pacific atolls relate on various time scales to the corresponding precipitation structure?

8) How does varying tropical rainfall affect tropical wetlands, and thus the main chemically reducing environment on the surface of the planet?

[11]There is indirect evidence from other remote sensors (Balsley *et al.*, 1988) that these heating profiles may vary between the eastern Atlantic GATE region and the central Pacific, which, if supported by TRMM results, could have important impacts on understanding climate and large-scale circulation characteristics.

Table 8. Remote Sensing Science Goals

1) Development, test, and validation of improved rain retrieval algorithms from space
2) Tests of and improved methods for rain estimation from geosynchronous satellites—past, present, and future
3) Further development of multi-data source analysis techniques, blending several types of space and *in situ* sources with different coverage of cloud systems
4) Use of improved knowledge and models of internal precipitating cloud structure to relate to radiative signals received in different microwave channels (active and passive)
5) Parameterization of diurnal cycle for potential future sun-synchronous measurement opportunities
6) Better precipitation statistics for planning future spaceborne precipitation measurement systems
7) Use of mission-obtained improved knowledge of convective/stratiform rain ratio to improve sampling techniques for future space missions
8) Use of mission- and otherwise-obtained improved knowledge of ice phase structure and variability in raining cloud systems to design improved instrument complement for future space missions
9) Improved ways to achieve large dynamic range for spaceborne rain radar, which still stays within achievable power, good resolution for passive microwave

goals regarding environmental observations from space toward which the TRMM may be expected to help provide progress.

EXPECTED ACCOMPLISHMENTS AND REQUIRED ACCURACY

Expected Accomplishments

The TRMM program will provide monthly rainfall over the global tropics and subtropics for a continuous period of 3 years or more. This will be a key data set for successful completion of the ongoing international programs of TOGA and WOCE and the planned Eos and GEWEX.

The expected scientific and technological accomplishments are listed below:

1. *Validation of Global Circulation Models:* At present there are no reliable data sets for either monthly and seasonal mean rainfall or for their interannual variability to validate the global atmospheric models. A reliable rainfall data set will help identify possible weaknesses of the current parameterization schemes and suggest possible ways to improve the parameterization of marine boundary layer and moist convection.

2. *Space-Time Variability of Vertically Integrated Latent Heating:* A reliable measurement of rainfall, particularly over the oceans, will provide for the first time space-time variability of vertically integrated latent heating. This, coupled with information on the nature of synoptic disturbances in different regions of the tropics, can help determine the vertical structure of the diabatic heating.

3. *Calibration of Archived and Future IR Rainfall Estimates:* Currently useful indices of tropical rainfall are being prepared to describe its interannual variability. The TRMM program will provide a unique data set to calibrate the IR-based indices of rainfall, and that can help in producing a longer time series of tropical rainfall.

4. *Fresh Water Forcing for Ocean Models:* By combining the direct measurements of oceanic precipitation with estimates of evaporation and salinity, the net fresh water forcing can be calculated and used for simulation and validation of thermohaline oceanic circulation.

5. *Quantitative Description of Hydrological Cycle:* Rainfall over the global tropics is an important component of the hydrological cycle; however, there are no reliable estimates of rainfall over the tropical oceans. The TRMM program will provide the necessary rainfall data over the oceans to describe the hydrological cycle quantitatively.

6. *Relationship Between SST Anomaly and Rainfall Anomaly Over the Tropical Oceans:* One of the central premises of TOGA is a deterministic relationship between the SST variations and rainfall anomalies. There are sufficient ship and satellite data for defining the space-time variability of SST; however, similar data for rainfall was never available. The TRMM program

will provide, for the first time, a quantitative description of the space-time variability of rainfall. This will enable us to carry out sensitivity studies with global GCM's and verify our earlier notions of SST-rainfall relationship based on empirical studies.

7. *Space-Based Measurement of Rainfall:* In addition to the various possible scientific accomplishments, TRMM will advance the technology of measurement of rain from space. It will be the first time that a quantitative precipitation radar[12] will be flown in space. The TRMM program will also help in the development of techniques for analysis of space data and development of retrieval algorithms.

Accuracy and Resolution Requirements

The accuracy requirements for measurement of rainfall depend upon the nature of the scientific problem being addressed. The major scientific problems to be addressed by TRMM are validation of global models, documentation of diurnal, intraseasonal and interannual variability over land and oceans, and vertical structure of diabatic heating. For GCM applications, the required anticipated resolution would be about 500 m. However, in order to calculate the statistics of convective and stratiform clouds separately, the required vertical resolution (at nadir only) will be 250 m. The main TRMM accuracy requirements are summarized in Table 9, in Items 1 through 6. Items 7 and 8 concern phenomena of smaller scale than those to which the primary requirements are addressed. The SSG wished to note, however, that TRMM will provide more accurate information on these scales than is presently available from geosynchronous or polar orbiting satellites, while recognizing the limitations posed by only two passes per day over each site. It was not considered reasonable to specify a percentage accuracy requirement on the latter two items, especially since rainfall verification by surface radars and other methods may differ by as much as 30 to 50 percent on these scales.

[12]The Soviet Union has had an X-band radar on its COSMOS 1500 satellite for the primary purpose of measuring sea-surface winds. The radar has a viewing angle ranging from 20° to 40° from nadir with a swath width of 500 km and a resolution of 1 to 2.5 km. A picture obtained from a hurricane Diana overflight in 1984 showed echoes in good qualitative agreement with aircraft-determined echo locations. We have not yet been able to obtain further data from this radar. (Personal communication from Dr. Peter Black, Hurricane Research Division, NOAA, Miami, FL.)

Table 9. TRMM Accuracy Requirements

1) *Climate Models and GCM Validation*	
Space:	(500 × 500 km) or ~10^5 km^2
Time:	Monthly mean
Accuracy:	1 mm/day (10 percent in heavy rain)
2) *Documentation of Intraseasonal Variability (the 30- to 60-Day Oscillation — Signal ~4 mm/day)*	
Space:	10^6 km^2
Time:	15 days
Accuracy:	20 percent (0.8 mm/day)
3) *Sahel Drought*	
Space:	2.5 x 10^6 km^2 (2° latitude × 10° longitude)
Time:	Seasonal
Accuracy:	20 percent
4) *Monsoons*	
Space:	10^6 km^2
Time:	Monthly
Accuracy:	10 percent
5) *Diurnal Cycle Over Ocean*	
Space:	20° longitude, 5° latitude
Time:	Bimonthly
Accuracy:	10 percent of first harmonic amplitude, 20 percent of the second amplitude
6) *Vertical Resolution (Portion of Swath Covered by Radar)*	
For GCM's:	500 m (only possible out to about 6 scan angle, or 60 km swath)
For cloud statistics:	250 m (nadir only)
7) *Tropical Rain Systems: Structure and Evolution*	
Space:	~20 km
Time:	~12 hr
Accuracy:	Much better than current (~30-50 percent)
Vertical resolution:	500 m to 4 km
8) *Tropical Dynamics (Input to Regional Models and GCM's)*	
Space:	~20 km
Time:	~12 hr
Accuracy:	Much better than current (~30-50 percent)
Vertical resolution:	500 m to 4 km

IV. SCIENTIFIC APPROACH

RELEVANT CHARACTERISTICS OF TROPICAL RAIN

In approaching the design of any spaceborne rain measuring system, it is important to determine how the total rainfall in the regions of interest is distributed among the different rain rates. Does most of the rain fall fairly uniformly at light to moderate rain rates, or is a large fraction concentrated into a few large rain systems with high rain rates? What are the times and distances over which rainfall is correlated? Quantitative answers to these questions are essential to prescribe and evaluate the sampling strategy of a low Earth-orbiting satellite and also affect the choice of instrument complement.

The frequency of occurrence of rain intensities in different rate categories over a specified area can be plotted as a histogram or expressed as a smoothed curve which fits the histogram. In either case, there is a spike of strength $1 - P_r$ at zero rain rate, representing the no-rain observations and a rainy portion which integrates to P_r. P_r is the probability of observing rain in any measurement. Figure 23 shows both histogram and continuous curve of the rainy portion for rain rates observed in GATE. The curve is called the probability density function (pdf) of the rain rates. In the case of tropical rainfall, the pdf's are always highly skewed such that a large fraction of the total rainfall is concentrated into a relatively small number of storms of high intensity or in a small fraction of the time or of the area in which it is raining.

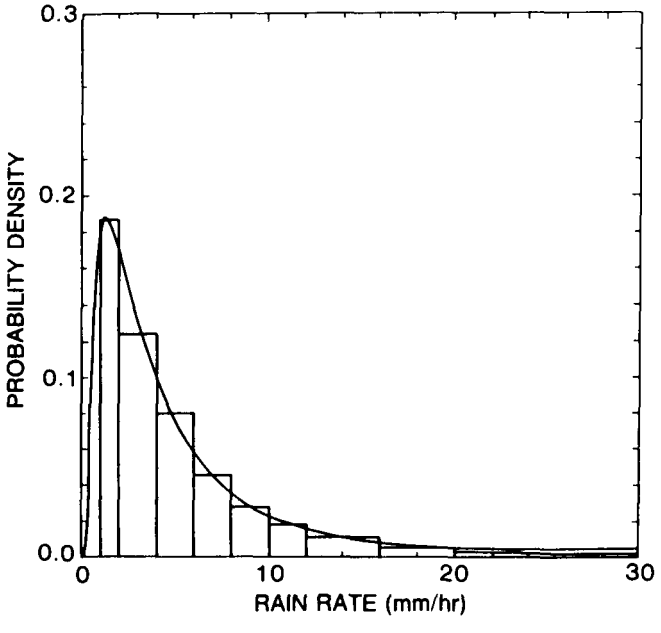

Figure 23. A fit of the log-normal pdf to the continuum of rain rates above zero for complete visits to the entire GATE area but sampled every 12 hours. The GATE rainfalls were averaged over 4 km by 4 km areas and sampled at 15-minute intervals.

The existence of skewed rain distributions at individual locations in the tropics and subtropics has been well known since the end of World War II (Riehl, 1954; Garstang, 1972). However, our knowledge of the importance and implications of this skewness has been extended to rain cell properties and made more useful and quantitative by the use of surface-based radars. Important advances were made in the 1970's when several researchers (Biondini, 1976; Lopez 1977) showed that the probability distribution of many convective cloud variables, including rain rates, cloud radar echo heights, rain cell echo areas and other features, could be well fitted by the lognormal distribution,[13] which is illustrated by the curve in Figure 23. This distribution is well known in other scientific problems; it has the feature of being a normal or Gaussian distribution when plotted on a logarithmic scale. The lognormal probability density is:

$$P(r)\,dr = \frac{P_r}{[\sigma\sqrt{2\pi}]} \exp\left(-\frac{\left(\ln\left(\frac{r}{r_o}\right)\right)^2}{2\sigma^2}\right) d(\ln(r)) \qquad (1)$$

where r_o is the median of r and σ^2, variance $= r_o^2 \exp(\sigma^2)[\exp(\sigma^2) - 1] = 52$ mm^2 hr^{-2}, the logarithm of r. The average rain rate can be expressed

$$\bar{r} = P_r\, r_o \exp\left\{\frac{\sigma^2}{2}\right\} \qquad (2)$$

As expressed here $\bar{r}$ is the average rain rate including the times when it is not raining, but, if P_r is set equal to one, it becomes the average rain rate when it is raining. This latter average for the GATE distribution shown in Figure 23 is 5.3 mm hr^{-1}. Other useful properties of a distribution are the median (which is the rain rate below and above which one-half the total rain events occur), the mode (the most common or frequently-measured rain rate) and the variance. For the lognormal distribution of Equation (1) and Figure 23, when P_r is 1, these are:

[13]Other statistical distributions have also been shown to fit rainfall data well (e.g., Simpson, 1972). The arguments presented here would not change substantially if a different distribution were used, even though some statistical details would.

- Median = r_0 = 3.1 mm hr^{-1} (50 percent of the time with rain, the rain rate is lower than this value; the other 50 percent of occasions with rain, the rain rate is higher)
- Mode = $r_0 \exp[-\beta^2]$ = 1.1 mm hr^{-1}

The standard deviation of the rain rate, which is the square root of the variance, is 7.2 mm hr^{-1} for the distribution in Figure 23. The standard deviation is 1.4 times the mean. This order of variability is typical for tropical rainfall in all areas.

For designing a tropical rainfall measuring system, it is important to know how much of the total rain volume (RV) is contributed by various rain-rate intervals. To obtain this result, the right hand side of Equation (1) is multiplied by r and integrated from zero to the rain rate desired. Figure 24 gives the result for GATE data. The rain rates below which 10, 50, and 90 percent of the cumulative rain occurs are easily calculated or read from this diagram to be:

$$r_{50} = r_0 \exp(\sigma^2) = 8.8 \text{ mm hr}^{-1}$$

$$r_{10} = r_{50} \exp(-1.28\,\sigma) = 2.4 \text{ mm hr}^{-1} \quad (3)$$

$$r_{90} = r_{50} \exp(1.28\,\sigma) = 32.4 \text{ mm hr}^{-1}$$

Fortuitously, the GATE data available for our analyses were averages over areas of 4 by 4 km,[14] approximately the resolution of the planned spaceborne radar (see Table 3). These results have important implications for the TRMM approach.

For example, Chiu (1987) has shown that with these 4 by 4 km averages, while 50 percent of the cumulative rainfall occurs at rates in excess of 9 mm hr^{-1}, this rain falls in only 10 percent of the total radar echo areas. Similarly, only about 10 percent of the GATE rainfall occurs at rates less than 2 mm hr^{-1}, although such rates cover about 50 percent of the rainy area. Woodley *et al.* (1975) found similar results for the 1.3×10^4 km^2 area instrumented for the Florida Area Cumulus Experiment (FACE).

The GATE and FACE radar rain distributions tell us where to concentrate our attention in the TRMM instrument design. For example, in GATE-type rainfall, we need not overly concern ourselves with accurate measurement of rates less than about 2 mm hr^{-1}. This is fortunate, because the accuracy of most remote sensing systems degrades at the lighter rain rates. On the other hand, the instrument should be capable of a dynamic range of about 2 to 50 mm hr^{-1}, the interval within which more than 90 percent of the GATE rainfall occurred.

This background material is provided for several purposes. First of all, it describes some of the key statistical characteristics of the precipitation which TRMM is intended to measure. Secondly, by so doing, it permits the system designer to better specify the parameters and performance of the observing system. Thirdly, it provides a basis for supporting modes of rainfall inference to strengthen the VIS/IR, microwave radiometric and radar methods described in a later chapter. In this chapter, we concentrate on the sampling strategy, which will be implicitly based on these characteristics of tropical rainfall throughout, and will in some aspects make direct use of the lognormal distribution.

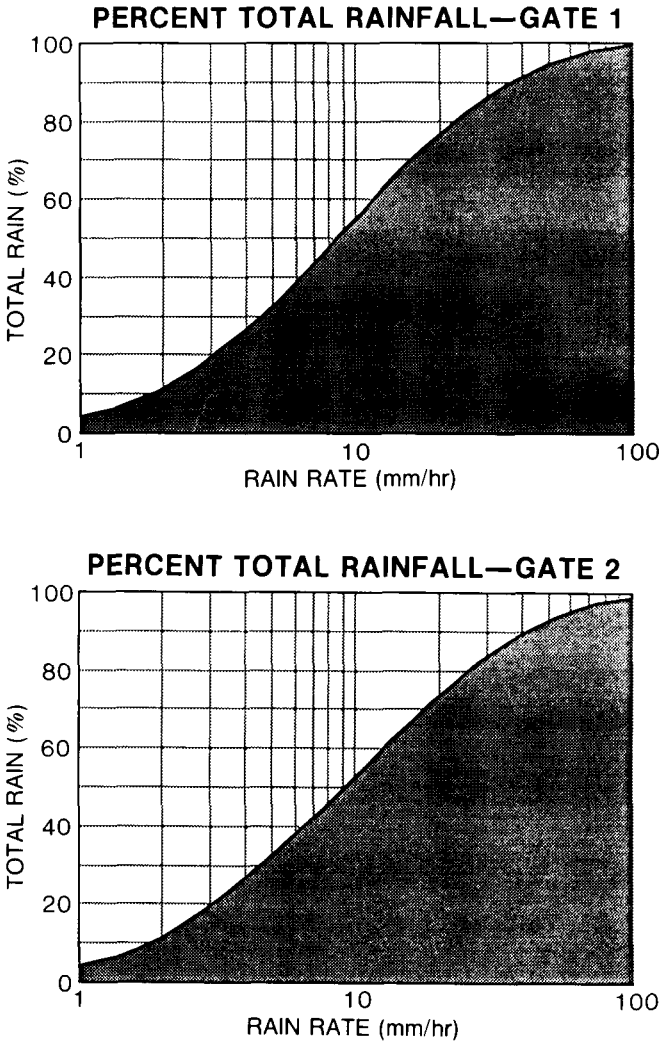

Figure 24. Percent of total rain as a function of rain rate for Phase I and II of the GATE. These logarithmic curves are obtained by multiplying Equation (1) by rain rate, r, and integrating over all rain rates.

PRECIPITATION DATA SET

A precipitation data set meeting the scientific requirements set out in previous sections of this report can be obtained by an analysis of data from passive and active microwave scanning instruments flown on a low-altitude Earth orbiter restricted to tropical and near-tropical latitudes (TRMM). The product is considerably enhanced when data are combined with information from operational satellites and conventional surface measurements. The primary scientific requirements call for a time series of space-time smoothed fields of rain

[14]Analysis of the highest resolution version of the GATE radar data, namely 1 km range by 1° azimuth (or roughly 1 km by 1 km) shows rain rates up to 100 mm hr, with r_{90} about twice as large as in Equation (3). See paper by Wang *et al.* (1988).

rates and a climatology of vertical distributions of rain. The strategy for achieving these goals consists of combining essential rainfall information from TRMM with the existing operational precipitation data stream. By choosing multichannel scanning passive microwave radiometers (swath width approximately 2 times the satellite altitude) and a scanning active microwave radiometer (swath width ½ satellite altitude) we provide a physical basis for the precipitation retrieval algorithms and thereby provide a transfer standard for calibrating the more empirical methods used with operational satellites. This flying rain gauge then allows the tuning of VIS/IR precipitation algorithms over regions of the globe where no *in situ* data are available.

By restricting the TRMM orbit to the tropics and near tropics, we increase the sampling rates over those for comparable altitude polar orbiters, especially in the subtropics, where they are more than doubled. Furthermore, the diurnal cycle is densely sampled by TRMM passages in the course of about 1 month, allowing removal of this important bias in mean rain rate estimation. By choosing a low altitude for the satellite, the footprints of the individual radar and passive microwave pixels can be kept small (see Table 3) with antennas of feasible size.

SAMPLING ERRORS

While it is recognized that data products will be greatly improved when TRMM rain map data are integrated with operational data, it is of interest to see how closely TRMM alone comes to meeting the scientific requirements for rain maps. Much of the rest of this chapter will be devoted to arguments that the TRMM satellite outfitted with hypothetically perfect scanning instruments can provide satisfactory estimates of rain rate averaged over a month and over 500-600 km squares.

Arguments presented in the Error Analysis section of Chapter V on instruments and their associated errors suggest that sampling errors are the largest single component of the overall error budget. Hence, it is imperative that detailed sampling studies be conducted for TRMM over a range of orbit parameter choices.

Most methods of estimating space-time average rain rate are limited by errors due to gaps in the space-time volume for which rain rate is measured. Figure 25 shows a schematic diagram of a single blob of rain in a space-time volume. The object of any sampling strategy is to find a suitable approximation to the average rain rate over the space-time volume. Figure 26 shows some typical sampling designs of interest. The first is a rain gauge network which appears in the diagram as a matrix of rods running parallel to the time axis (upper right in the figure). Clearly, the important rain field parameter for this design is the spatial variability of time averages. If the horizontal length scale for these time averages is large compared to gauge spacing, we expect to have good estimates of the space-time average using the rain gauge design.

The upper left diagram in Figure 26 shows the kind of sampling encountered in a polar low Earth-orbiting satellite design. The measurements are analogous to snapshots taken at finite intervals. An actual satellite orbit with low inclination would make only partial visits to these plane squares at a

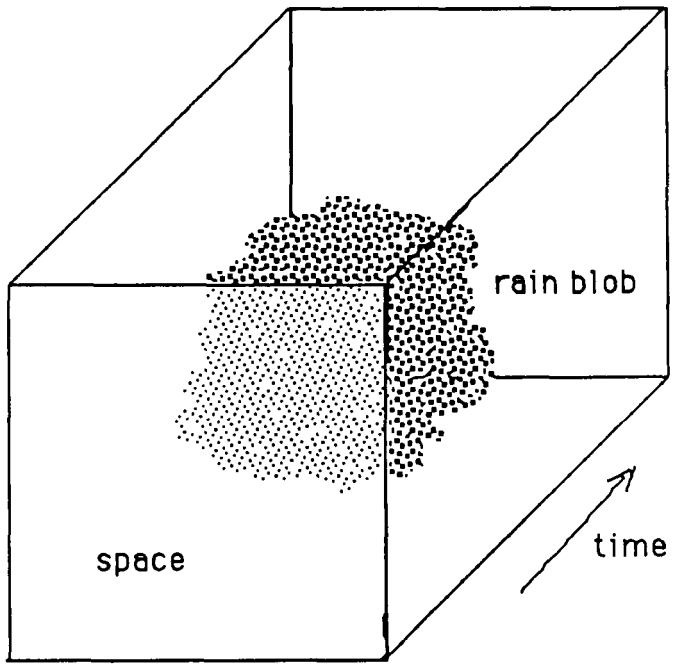

Figure 25. Schematic diagram of a blob of rain in a space-time volume. The goal of the rainfall estimation is to compute the space-time integral of rain rate through the volume.

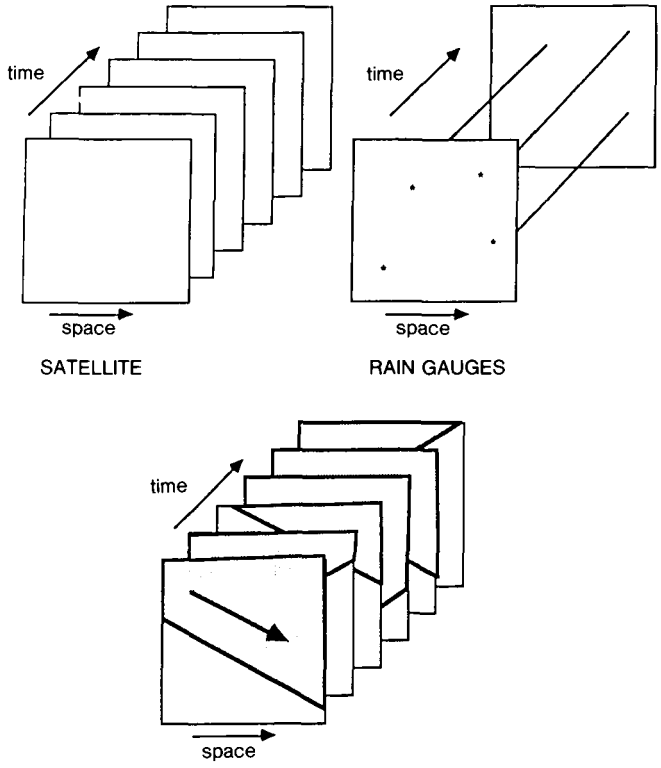

Figure 26. Sampling designs for space-time means of rain. Upper left: Low Earth polar orbit data from scanning instruments consists of snapshots at fixed intervals. Upper right: An array of point rain gauges consists of rod-like spikes through the volume. Lower: A schematic of the overpasses of a low-inclination satellite such as TRMM.

sequence of intervals depending upon latitude as shown in the lower diagram in Figure 26. Note that in the satellite design case the important quantity is the time scale for variation of spatial averages.

Sampling Studies Using the GATE Data

Studies (Laughlin, 1981) with an oceanic tropical rain data set (GATE) suggest that the autocorrelation time for rain averaged over 280 km squares is about 8 hours and extrapolation to 500 km squares leads to a value of perhaps 12 or more hours (Bell, 1987a). For the purpose of estimating the mean rain rate, one independent sampling interval is twice the autocorrelation time (Leith, 1973). This time scale for 500 km boxes suggests that returns to the box twice per day should provide reasonable estimates for monthly averages. Our calculations show that the errors are fairly sensitive to the choice of 8 versus 12 hours for the autocorrelation time of a 500 km averaging box, errors being about 40 percent larger for the smaller time constant.

Laughlin (1981) fit the lagged autocorrelation to an exponential. He then calculated the expected sampling errors of different discrete sampling visit intervals and various averaging spans. Figure 27 shows his results for a square 280 km on a side. Laughlin's study is based upon the autocorrelation time taken from the GATE data. It is interesting that the Laughlin model makes no assumption about the probability distribution of rain rates. Nor is it necessary to assume statistical homogeneity in the space variables. The main assumption is that the autocorrelation function for area mean rain rate is a decaying exponential and this seems to describe the GATE data reasonably well for square areas ranging from 4 to 280 km on a side. Laughlin also finds sampling errors to be proportional to the standard deviation of the area average rain rates.

Note that in Figure 27 the sampling error for a TRMM orbit returning with flush visits every 12 hours is slightly less than 10 percent. Since TRMM averaging boxes are to have about four times this area we might divide the error by two. On the other hand, a 30-degree inclined orbit will give rise to about 80 partial visits in a month equivalent to 30 flush visits which increases the error at most by a factor of 1.41. Laughlin's results then suggest that we might expect random sampling errors of about 7 percent.

While Laughlin's approach suggests that discrete sampling by a low Earth orbiter will lead to sampling errors of 10 percent or less, which probably are acceptable for the TRMM, the model is simplistic; the sampling problem need more different types of analysis. It is clearly advisable to develop and use other sampling models which adopt different assumptions. However, until the Darwin rain radar data becomes available in 1988, we have been restricted to the GATE data set for model tuning, since there have been no other comparable time series of rain over oceans.

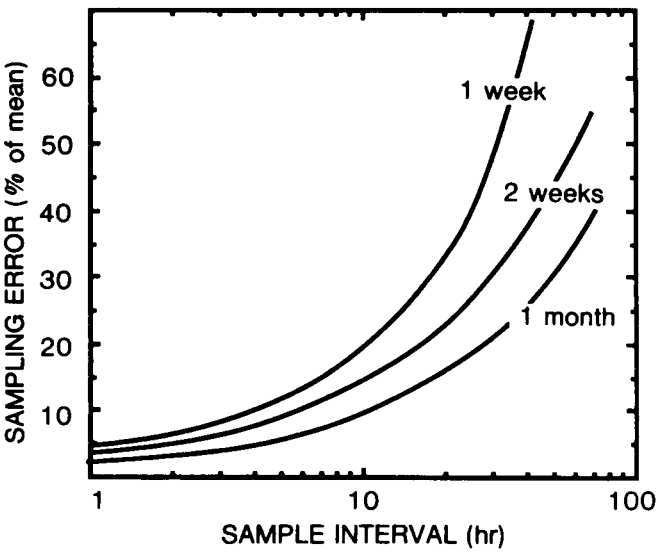

Figure 27. Laughlin's Markov model results for sampling error for complete visits to a 280 km square at various intervals (abscissa) and for various averaging times (curves).

Possible Limitations of GATE Data Set and Other Data Sets

Because all of the statistical models have so far been based upon the GATE, we need to describe the data set briefly. The experiment took place in the summer of 1974. The data were taken from two ships, one at 8.5° North and 23.5° West, about 700 km southwest of Dakar, Senegal, West Africa. The other was located about 160 km south of the first. These ships were equipped with radar, rain gauges and other relevant atmospheric probes. GATE rain data were collected in three periods of which only the first two are used here. GATE I provided 18 days of data, while GATE II produced data for 15 days. The question of the degree to which these eastern Atlantic data are characteristic of tropical rain processes is clearly an important one. The eastern Atlantic ITCZ passed through the central GATE area. The lower cloud layer there was more stable than that of the western Atlantic (Simpson *et al.*, 1977), so that updrafts and rain rates may have been weaker than elsewhere over tropical oceans. Also, some disturbances clearly originated on the land mass of Africa and propagated westward into the experimental area. Comparative radar studies in GATE and at several tropical continental locations were summarized in Chapter II; comparisons between GATE and monsoon rain systems near Darwin, Australia are in progress.[15] The key results from sampling analyses for one or more additional oceanic regions should be available by 1989.

Spatial Rain Rate Correlations in the GATE

During the GATE, instantaneous rain rate data were collected every 15 minutes. Hudlow and Patterson (1979) binned

[15]In progress by Rosenfeld at the Goddard Space Flight Center.

the data spatially into 4 by 4 km squares over the entire area which covered a circle 400 km in diameter. The filtering into spatial averages limits its usefulness, but this was all the information available for the initial studies. Based upon this data set, we can estimate the spatial autocorrelation function, which is consistent with a $-\frac{2}{3}$ power law as a function of separation out to distances of about 70 km; after that it falls approximately exponentially (Bell *et al.*, 1988). This rather weak decay suggests that rain rates are correlated over great distances and that an integral length scale may not be easily determined. This result is of great importance to the TRMM sampling strategy, so clearly spatial autocorrelations must and will be examined with other tropical radar rain data sets.

Other Sampling Approaches Using GATE Data

Three other approaches were made to the sampling problem. These may be summarized quite briefly here because conclusions based upon them are consistent with the Laughlin work.

McConnell and North (1987) partitioned the rain rates into four categories and flew an imaginary satellite over the GATE data, finding the average contribution to the space-time average from each rate category. An ensemble of seven orbits similar to TRMM was constructed by varying the starting time. The satellite was flown over making flush visits in each pass. The standard deviation of errors was less than or about 10 percent for the ensemble in each category.

Kedem, Chiu, and North (1987) used a mixed distribution approach. The idea was to sample the GATE data according to various space-time designs, fit the rate histogram to a spike at zero rate and a continuum lognormal density distribution and then *calculate* the space/time average from the fit. Figure 27 gives an idea about the quality of the fit to a lognormal density for satellite visits (about once every 12 hours). Again for designs that were similar to that of a TRMM satellite, the results agreed with Laughlin. Note that the above two studies are for 15 or 18 days as opposed to a month contemplated for TRMM, and for an area about a quarter of the 500 $\times$ 500 km resolution required of TRMM; all visits, however, were flush (100 percent coverage by the snapshots).

Two recent studies have attempted to go beyond the GATE overflight studies described above. They attempt to make the orbital visits more realistic, including the partial intersections of swath with averaging box, and they attempt to include the effects of the larger (500 km) TRMM averaging boxes. Shin and North (1987) have extended the Laughlin method to approximate partial visits by using exact orbital calculation and when a partial visit occurs, it is given a weight proportional to the area of intersection of the swath and the averaging box. In this work, two quantities must be extrapolated from the GATE data: 1) the autocorrelation time is taken to be 12 hours for the 500 km box, and 2) the ratio of standard deviation to mean for the 500 km box is taken to be 1 hour. These two values are based upon fitting curves to GATE data and extrapolating to boxes of 500-km width. The results indicate that sampling errors of less than 10 percent are to be expected for month-long averages. The latitude dependence of the errors is weak. Sampling errors for a range of orbit altitudes and inclinations are shown later in Figure 31.

Finally, Bell (1987a) has devised a stochastic rainfield model that has many of the statistical properties observed in GATE rain. The advantage of this approach is that long Monte Carlo runs can be performed with artificial diurnal cycles and other variables. Also a code has been developed which simulates the exact overpasses of a satellite. Bell *et al.* (1988) have shown that for this model the area averages are well simulated by a first-order Markov process consistent with Laughlin. Similarly, the Kedem *et al.* (1987) mixed distribution approach works well. In the case of 30-day averages with the TRMM boxes, the sampling errors are consistent with the Shin and North (1987) work but slightly smaller at high latitudes. The latter discrepancy is caused by the conservative assumptions made by Shin and North about fractional visits when more than one visit to a box occurs within a few hours. The Bell modeling results support the value of one for the coefficient of variation for 500 km boxes.

Studies are continuing with GATE data to further understand the problems of nonequidistant visitation times of the satellite as the averaging box is taken away from the equator. Parameter variation studies are also being conducted to determine the effects of satellite altitude and inclination changes. A study is in progress on the ESMR-5 data to determine the representativeness of GATE data compared to other longitudes along the ITCZ. Studies with geosynchronous data are beginning to examine the diurnal cycle to be expected throughout the tropics.

TRMM Sampling Over Land

Over land the most reliable measurement technique for monthly averaged rain is likely to be the radar on TRMM. In this case the radar swath, being only one-third the width of the passive microwave swath, will lead to sampling errors that are about 1.3 times as large. However, there are several factors which can mitigate this situation. Firstly, over land some of the requirements (African drought, for example) are weaker, with seasonal averages and 10-degree squares being sufficient. Secondly, the pioneering work of Spencer *et al.* (1983a) suggests that rain over land can be deduced reasonably well using passive microwave frequencies with ice-scattering dominated radiative processes (for example, 37 and 85 GHz, which will be on TRMM). Since then, airborne data have suggested that rain rates may be quite well estimated with these frequencies, provided they are "calibrated" for different precipitation regimes (Hakkarinen and Adler, 1987; Simpson *et al.*, 1988; see also Chapter VI on algorithm development). The calibration could be done using the TRMM radar and/or the TRMM surface validation sites. Also over land a sparse but nonetheless usable network of rain radars and gauges exists.

DIURNAL CYCLE

The TRMM orbit (Figure 28) is designed to sample the local hours over the course of several weeks. Figure 29 shows the visitation diagram for a 30-degree inclination orbit for an averaging box located at 15 degrees latitude. For the entire month, the satellite makes partial visits to the box 80 times, but the total area visited is only equivalent to 30 full visits.

ORIGINAL PAGE
COLOR PHOTOGRAPH

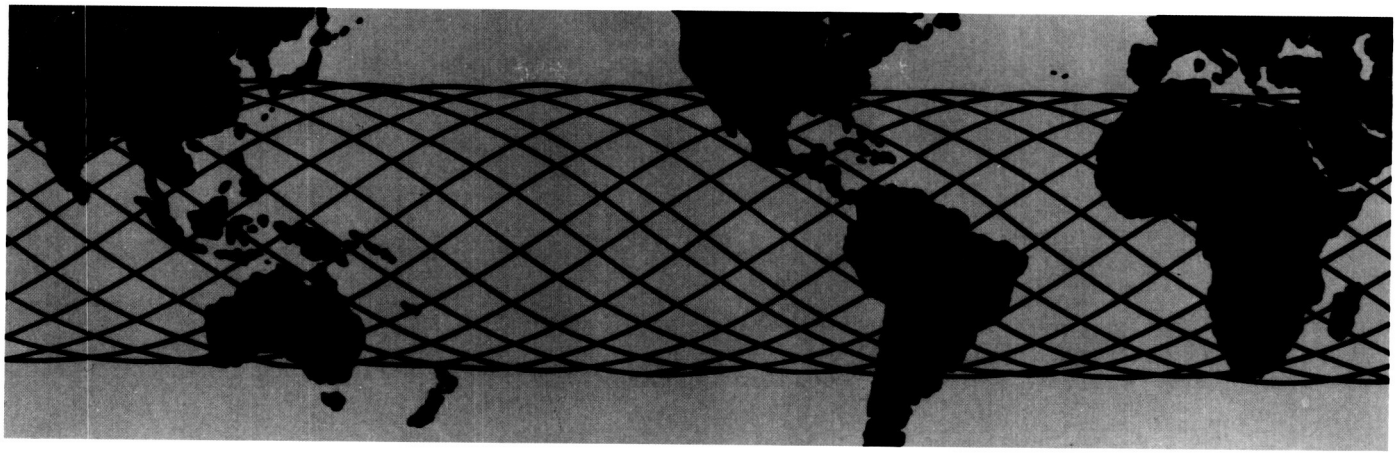

Figure 28. Schematic diagram of TRMM orbits during a 1-day period (angle of orbit inclination 35°).

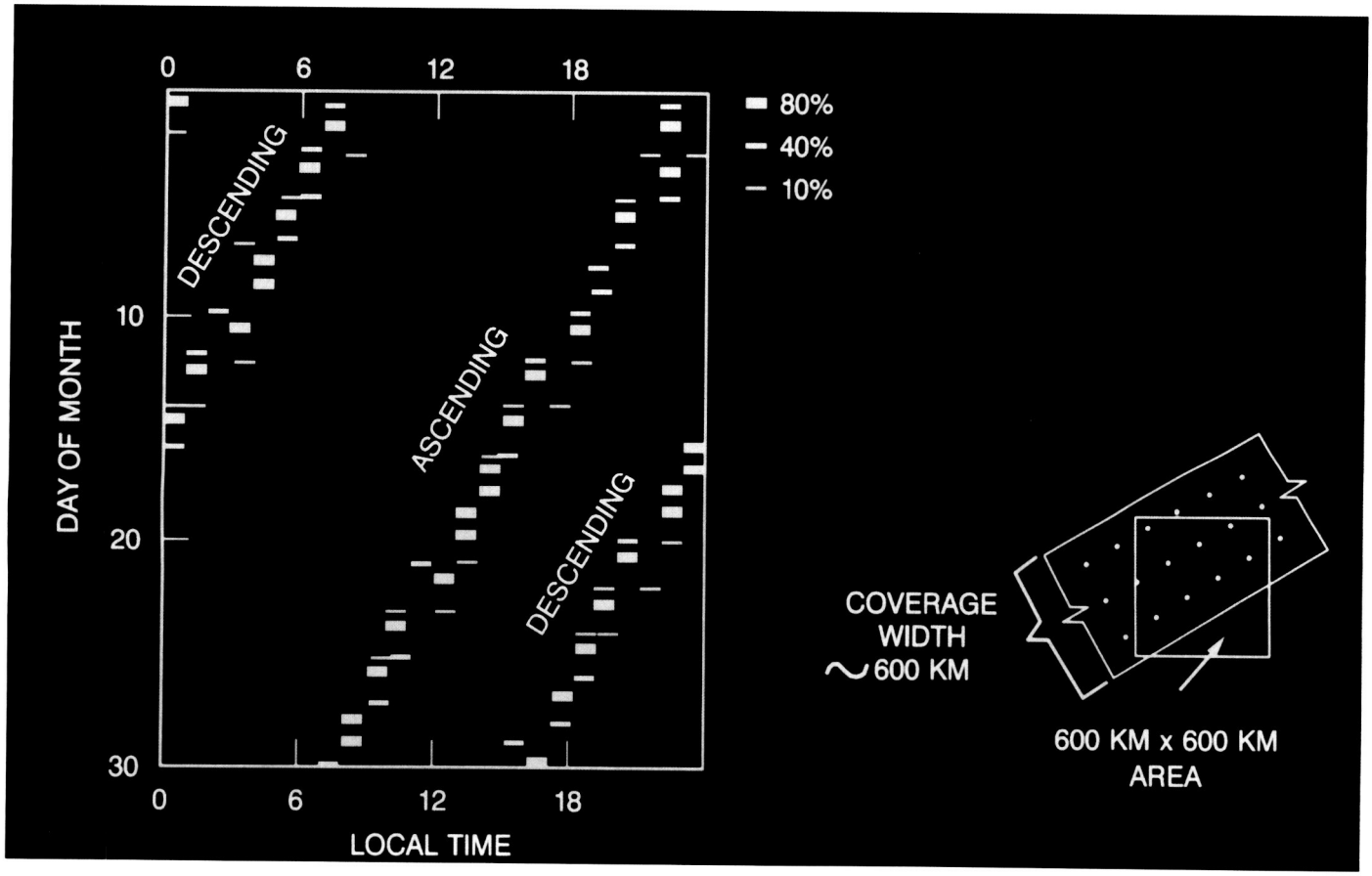

Figure 29. Diagram of the visits of TRMM to an averaging box located at 15°N. The ordinate shows the day of a hypothetical month and the abscissa shows the local time of day. The fraction of the box covered by the swath on a particular visit is indicated by the area of the corresponding rectangle in the diagram.

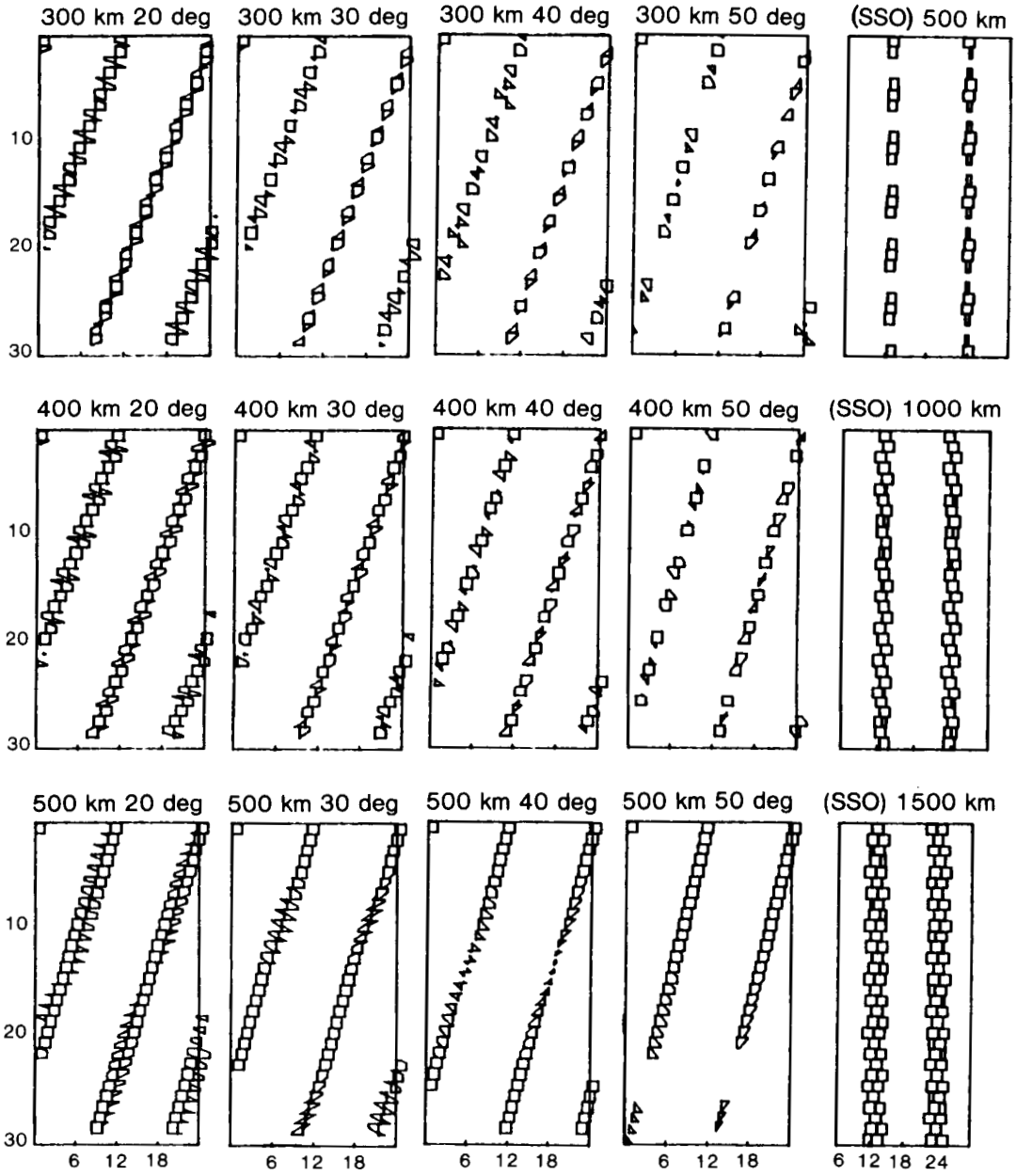

Figure 30. The visiting sequence and fractional coverages through a month for some selected orbits from 300 to 500 km altitude and from 20° to 50° inclination. In each orbit, the ordinate indicates the day of the month and the abscissa indicates the local time of day. The right-hand column illustrates sun-synchronous orbits (SSO) at three different altitudes.

For this box the entire diurnal cycle is sampled in about 3 weeks if both ascending and descending nodes are included.

Figure 30 shows the effect of changing the satellite altitude (increasing swath width) as well as the inclination. Clearly, low inclination and high altitude are best for sampling, although resolution is sacrificed at higher altitudes. Figure 31 shows the sampling error as a function of orbit altitude and inclination. Note that increasing the altitude from 300 to 350 km very nearly offsets the increase in sampling error caused by increasing the inclination from 30° to 35°.

The diurnal cycle is of interest in itself from an atmospheric dynamics point of view. It is useful to know how well we can estimate the amplitude and phase of the first few harmonics of the diurnal cycle from TRMM data. Bell (1987b) has estimated that (for rain with GATE-like statistics) the amplitude of the first harmonic can be obtained to an accuracy of about 10 percent of the mean rainfall over a TRMM box with about three seasons of data. One can, of course, obtain similar accuracies from fewer seasons of data by averaging over larger areas.

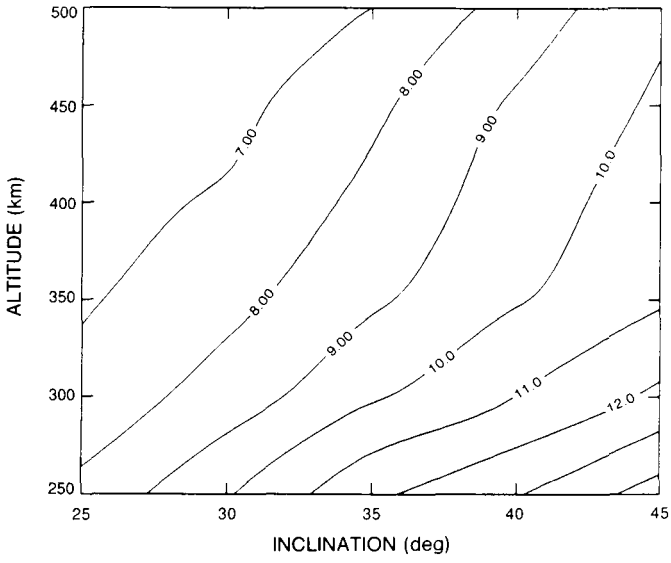

Figure 31. Diagram showing the isopleths of average sampling error (percent) for averaging boxes ranging from the equator to 20° latitude for different orbital inclinations (abscissa) and different altitudes (ordinate). These errors are derived from the Shin and North (1988) model and are for ESMR-5 swath width (±50 across nadir). Errors tend to be about two percentage points higher for the SSM/I instrument which has a narrower swath. The value used for the coefficient of variation for the 500 × 500 boxes was 1.0, and the value used for the autocorrelation time for the rain field for this area was 12 hours.

VERTICAL DISTRIBUTIONS

The vertical distribution of hydrometeors in a column of tropical oceanic rain is presently poorly known except in a few case studies. Data on the vertical distribution is needed for the development of accurate passive microwave retrieval algorithms and for fundamental atmospheric science studies. The radar flying on board TRMM will provide vertical distribution data along-track with a swath about one third of the width of the passive microwave swath. This horizontally high resolution data (~4 km) can be used in conjunction with passive microwave data to sharpen the retrieval estimate along the swath or it can be archived to form a climatology of vertical distributions for different locations and seasons to be used in any passive microwave retrievals in the future. The optimum vertical resolution for this application is about 250 m at nadir. This resolution should suffice for fundamental atmospheric dynamics studies as well.

SUMMARY OF TRMM SAMPLING ERROR STUDY

A summary of the sampling studies relative to TRMM is given in Table 10.

Table 10. Sampling Research Summary

Sampling studies based upon imaginary overflights of GATE radar ship area (280 × 280 km) lead to errors of ±8 percent for 30-day averages.
Extrapolation to 500 km grid boxes requires untested assumptions about the behavior of autocorrelation times and variances for large area average rain rates.
Preliminary modeling studies for large grid boxes and realistic orbits making partial visits to the boxes suggest sampling errors of 7 to 12 percent depending on values taken for the extrapolated parameters.
Addition of a single, perfect sun-synchronous satellite with wide swath can essentially halve the sampling errors.
More work is in progress to check the statistical representativeness of GATE rainfall and to better understand the large-area extrapolations.

V. INSTRUMENT COMPLEMENT AND SPACECRAFT

MEASUREMENT REQUIREMENTS

In pursuing the fundamental goal of TRMM (understanding the role of tropical rainfall in global weather and climate variability), specific science questions were posed, as outlined in Tables 6 and 7. The kind of observational data needed to address these questions then led to the measurement and accuracy requirements set forth in Table 9. Based on these requirements, a study was made of current and expected new remote sensing technology that could be suitably deployed in space in a configuration that could achieve the desired results yet remain within reasonable budget constraints.

Proposed System Concept

The proposed system consists of a spacecraft with a single frequency radar and multifrequency microwave and VIS/IR radiometers in a circular orbit at an altitude of 350 km inclined at 35° relative to the equator. The unique combination of sensor wavelengths, coverages, and resolving capabilities proposed, together with the low-altitude, non-sun-synchronous orbit, provides an overall sampling capability that is expected to meet the measurement requirements already set forth as shown conceptually in Figure 32.

SPACECRAFT

The TRMM spacecraft is planned to be a free-flyer launched on an expendable launch vehicle (ELV). It is anticipated that the spacecraft bus will be an adaptation of existing spacecraft designs and available equipment and modules to minimize the mission costs. For example, there is the possible design adaptation of previously flown research, commercial, or military satellites, including possible use of modular components designed for the NASA Multimission Modular Spacecraft (MMS). A key consideration of TRMM is maintaining the low-altitude orbit, which is planned in order to achieve the desired measurement resolution. The resulting high drag dictates a substantial propulsion system. Table 11 outlines the key features of the proposed free-flyer.

INSTRUMENT COMPLEMENT

The instrument module will be separate from the spacecraft bus. It will contain the Precipitation Radar instrument, a modified AVHRR, and two passive microwave radiometers. One will be a single channel ESMR and the other will be a multi-frequency SSM/I.

Precipitation Radar

A radar is required that will use algorithms based on either rain reflectivity or on relative attenuation. All specifications of sensitivity at a given rain rate are assumed to be relative to a 5 km deep rain layer with a 0.5 km bright band. It is also assumed that the Ulbrich Z-R and K-R relationships hold. It is further assumed that the attenuation in the bright band (dB/km) is twice that of the rain. Key elements of desired performance specifications are:

- A single frequency radar with frequency near 14 GHz.
- Minimum signal-to-noise (S/N) ratio of unity for a rain rate of 0.5 mm hr^{-1} for the backscatter from the top of the rain. (Note that if one designs to this value, the S/N at a particular frequency is automatically determined at all other rain rates and ranges within the storm.)
- Sufficient dynamic range of the radar receiver so that both the rain and surface returns can be measured at the minimum rain rate of 0.5 mm hr^{-1}.
- The surface return along the antenna side lobes is to be less than the rain return at 0.5 mm hr^{-1} for all relevant angles of incidence and all relevant range gates.
- Horizontal resolution (instantaneous field of view (IFOV)) to be equal to or better than 5 km at nadir incidence (3 dB, one-way gain). This resolution will inevitably be degraded as a function of scan angle due to geometric effects.
- Minimum vertical resolution of 250 m at nadir.
- For off-nadir angles, the range resolution can exceed 250 m as long as the net vertical resolution due to the combined effects of range resolution and beamwidth of the antenna is not degraded by more than 10 percent over the vertical resolution due to the antenna effects alone.
- Minimum of 64 independent samples at each resolution cell, where the resolution cell is defined by the above three requirements. (Independent samples can be achieved by pulse averaging and/or by summing contiguous range gates. A sufficient number of independent samples is needed both to reduce the fluctuations in the backscattered power and to increase the effective S/N by subtracting the system noise from the signal-plus-noise measurement.)
- Contiguous coverage over the raining areas required over a minimum swath width of 200 km.
- The maximum observable range must be sufficiently large to observe precipitation echoes up to a height of at least 15 km above the surface and to include the surface echo within the observable range. (This requirement applies to all relevant incidence angles.) At nadir, there is also a requirement to observe the radar return echo at least 5 km beyond the surface echo for the purpose of measuring the so-called "mirror image" return power.
- To achieve a signal-to-noise ratio of unity or better for the backscattered rain signal from the lowest levels of the storm for a rain rate of 10 mm hr^{-1}. This condition should be satisfied for all relevant incidence angles.
- To include adaptive scanning as a means of decreasing the average radar power consumption, increasing the

maximum available peak transmit power, increasing the maximum scan angle, and/or increasing the number of independent samples. (Note: If an appropriate adaptive scan strategy is adopted, the contiguous coverage requirement can be relaxed to: All areas of significant rain rates are to be measured over a minimum swath width of 200 km. Significant rain rates are defined as those rain rates which account for the upper 95 percent of the cumulative distribution of tropical rain rates as represented in the GATE data or other appropriate data sets or those rates determined dynamically by the instrument.)

In a planned cooperative effort, Japan is investigating three potential radar designs, the key features of which are shown in Table 12. The options correspond to various combinations of antennas and transmitters: Options 1 and 2 employ a planar array antenna with a Traveling Wave Tube Amplifier (TWTA) for Option 1 and solid state power amplifiers for Option 2. In Option 3, a TWTA is used along with a parabolic cylindrical antenna. These combinations presently are being studied with respect to cost, reliability, and performance.

Microwave Radiometer

TRMM planning is based on utilization of an existing single-channel ESMR and a copy of the multifrequency SSM/I radiometer developed for the operational DMSP to meet minimal mission requirements at the lowest possible cost. A copy of the SSM/I has been flying on a DMSP spacecraft that was launched in 1987.

The ESMR is a space-qualified flight prototype left over from the Nimbus series of research satellites. The instrument will require refurbishment and possibly some modification to be compatible with TRMM. A study is presently underway

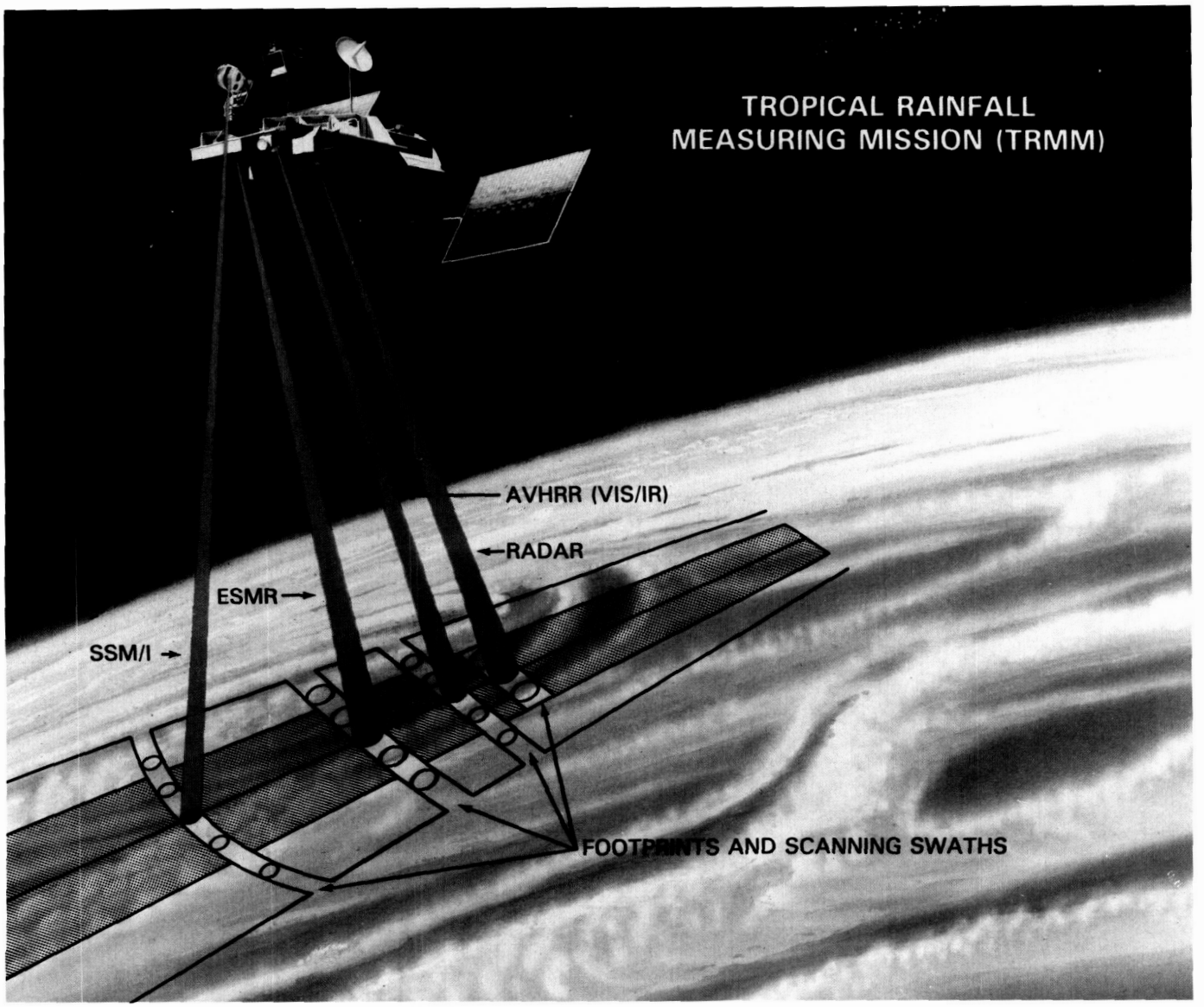

Figure 32. Artist's concept of the spacecraft and instruments showing the relative Earth coverage of each instrument.

to determine what has to be done to the ESMR. Only minor modifications to the production model SSM/I are anticipated.

The performance features and interface specifications for the two passive microwave instruments are listed in Table 13.

Table 11. Proposed Generic Spacecraft System

Mass	1,942 kg (2,195 kg at launch)
Fuel mass	253 kg
Fuel	Hydrazine
Attitude control	Vertical ± 0.2°
Power	1,000 W total (minimum, end of life)
Command and data handling (C&DH) for engineering functions	
• Frequency	S-band single access (SSA)
• Command	1 kbps
• Telemetry	2 kbps

Table 12. Japan Radar Salient Performance and Interface Specifications

	Option (1)	Option (2)	Option (3)
Mass (kg)	323	328	273
Power, average (W)	224	224	224
Power amplifier	TWTA	Solid state	TWTA
Frequency (GHz)	14	14	14
Radar dimensions (m)	2.1(l) × 2.1(w) × 0.65(h)	2.3(l) × 2.3(w) × 0.65(h)	3(l) × 1.55(w) × 2.5(h)
Antenna design	Planar array	Planar array	Parabolic cylindrical
Data rate (kbps)	85	85	85
Storage (Mb/orbit)	467	467	467
IFOV (degree)	0.71	0.71	0.71
Footprint, maximum (km)	5.0 × 4.5	5.0 × 4.5	5.0 × 4.5
Footprint, minimum (km)	4.3 (dia.)	4.3 (dia.)	4.3 (dia.)
FOV (degree)	± 17.4	± 17.4	± 17.4
Swath width (km)	220	220	220
Number of channels	1	1	1
Scan	Electronic	Electronic	Electronic

Table 13. ESMR and SSM/I Performance and Interface Specifications

Parameter	ESMR	SSM/I
Frequency (GHz)	19.35	19.35, 22.235, 37, 85.5
Polarization	Horizontal	Horizontal/vertical, except 22
Mass (kg)	34	55
Power (W)	47	33
Outline dimensions (cm)	94 × 92 × 11	61 × 66 (antenna), 36 × 41 (drum)
Data rate (kbps)	1	3.3
Data storage (Mb/orbit)	5.4	18
IFOV (degree)	1.4 nadir, 2.0 at 45°	1.88, 1.60, 1.08, 0.42
Footprint, maximum (km)	12 × 24 (45°)	16 × 23 (for 19 GHz channel)
Footprint, minimum (km)	9 (nadir)	4 × 5 (for 85 GHz channel)
FOV (degree)	± 45 (cross-track scanning)	± 56 azimuth, conical scan with 45° half-cone
Swath width (km)	700	580 km
Number of channels	1	7
Scan method	Electronic	Mechanical
Attitude stability (deg/sec)	0.15	0.5
Attitude knowledge (degree)	0.3	0.1
Orbit position (km)	2.0 in-track, 3.0 radial	1.0 in-track, 1.5 radial
Time accuracy (ms)	250	250

Visible and Infrared (VIS/IR) Radiometer

The data from the VIS/IR radiometer on TRMM will be used for three main purposes. First, the instrument will serve as the background imager and will provide the cloud context within which the passive microwave and radar observations are made. Second, data from the VIS/IR radiometer will be used in TRMM rain estimation algorithms based primarily on the passive and active microwave sensors. For example, VIS/IR cloud observations will be useful in discriminating surface effects from cloud/rain effects in the microwave observations. Cloud-top height information will also be useful in the microwave precipitation retrievals. The third purpose of this radiometer, and possibly the most important, is to serve as a "bridge" from TRMM rainfall estimates to estimates made with geostationary and low Earth-orbiting satellites using VIS/IR techniques. The TRMM rainfall estimates can therefore be used as a calibration, for example, of the geostationary infrared rainfall estimates.

The VIS/IR imaging radiometer proposed for the TRMM is presently planned as a modification of the NOAA AVHRR-3. The AVHRR-3 is a six-channel version of the original four-channel AVHRR that has been flown on the Television and Infrared Observation Satellite-N (Tiros-N) and the operational NOAA weather satellites since October 1978. AVHRR-3 is planned for the NOAA-K, -L, -M series and should be developed well in advance of the TRMM version. A study contract was initiated with the International Telephone and Telegraph (ITT) Corporation, Aerospace/Optical Division, and manufacturers of the AVHRR, to examine the impact of moving the AVHRR from the 824 km sun-synchronous orbit of the NOAA satellites to the 350 km, 35 degree-inclined (non-sun-synchronous) orbit planned for TRMM. The results of this study are given in detail in the final report dated

September 1986. There were no major obstacles to such an operational change. The required sensor modifications are well understood and will result in a minimal increase in cost.

The six channels of the AVHRR-3 are shown in Table 14, along with signal-to-noise ratio (SNR) and the noise equivalent delta temperature (NEDT).

Because of cost considerations, only two channels could be selected for the TRMM mission. However, a third night visible is desired if resources should become available. Channel 5 at 10.7 mm is used for determination of cloud-top temperature (and thereby top height inference). It is the primary channel for transfer of information to single-channel geostationary rainfall estimation techniques (Arkin, 1979). Visible Channels 1 (daylight, 0.665 mm) and 2 (nighttime, 0.650 mm, if included) are used for cloud identification and structure information.

Channels 4 and 6 would both be important to TRMM objectives in similar ways, although they do not presently appear affordable. In the absence of clouds, these channels can provide information about atmospheric water vapor. The 6.7 mm channel is sensitive to water vapor in the middle and upper troposphere, while the 12.0 mm channel, in combination with the window channel at 10.7 mm, is related to lower-tropospheric moisture (Chesters *et al.*, 1983). This type of moisture information would be important in terms of incorporating cloud environmental information, in this case atmospheric humidity, into TRMM rain algorithms. More importantly, these two channels may be significant in the transfer function of TRMM precipitation information to other satellite systems using only infrared techniques. By the mid-1990's, geostationary infrared rain estimation may be based on more than just the 11 mm channel. Channels such as 6.7 mm or the split-window technique using both the 10.7 and 12.0 mm channels may be used to better identify rain areas with geostationary satellite data. The frequencies in both Channels 4 and 6 have proven useful in identifying thin, non-precipitating cirrus clouds and in discriminating those clouds from convectively precipitating areas. This has been shown by Szejwach (1982) at 6.7 mm and recently by Inoue (1987) using the 12.0 mm channel.

To maintain a reasonable data rate (i.e., approximately 80 kbps for the AVHRR) a channel priority of data transmission is planned. The highest priority is for continuous visible data and a thermal channel. Thus, Channel 1 or 2 (if available) will be transmitting at all times, with Channel 1 on in daylight and Channel 2 serving as the night visible channel. Channel 5 will transmit thermal data both day and night. Plans for transmitting any other channels have presently been set aside. Table 15 gives salient performance features and interface specifications for the AVHRR.

The possibility of adding a tropospheric wind measuring capability to the TRMM AVHRR has been suggested. This would consist of adding a second facet to the 45° inclined scan mirror of the AVHRR. The new surface would view the Earth 180° after the original mirror and would be mounted at a 67.5° inclination angle so as to view either 45° fore or aft of nadir. Each side of the scan mirror would image the surface continuously with one image being approximately 300 km (or 40 sec) displaced along track from the other. By examining the off-nadir scene at nadir (or vice-versa), cloud motions could be converted to wind fields. Rough calculations indicate that the minimum detectable wind speed is approximately 10 m/sec. However, resource limitations have precluded a design incorporating the proposed feature.

COMMAND, DATA HANDLING, AND TRACKING

The primary C&DH link for the TRMM payload will be the S-band Single Access (SSA) channel through the Tracking and Data Relay Satellite System (TDRSS). Spacecraft housekeeping command and telemetry and back-up for the science data will be via the TDRSS S-band Multiple Access (SMA) channel. The orbital position of the spacecraft will be determined by the TDRSS ranging system. The major components of the C&DH subsystem are:

- two TDRSS standard transponders with 5 W transmitters,
- two NASA standard type recorders with dual transports (1,000 Mb capacity),
- one S-band TDRSS two-axis gimbaled antenna (SSA), and
- two S-band Omni antennas.

Table 14. AVHRR-3 Channels and Sensitivity

Channel	Wavelength (mm)	Bandwidth (mm)	Sensitivity
1	0.665	0.02	SNR > 100:1 at 0.5% albedo
2	0.650	0.50	SNR > 10:1 at 8×10^{-9} W/(cm^2 sr)
3	1.61	0.06	SNR > 100:1 at 0.5% albedo
4	6.72	0.36	NEDT < 0.24K at 240K
5	10.7	1.0	NEDT < 0.015K at 300K
6	12.0	1.0	NEDT < 0.015K at 300K

Table 15. AVHRR Salient Performance Features and Interface Specifications

Parameter	AVHRR (Modified)
Mass (kg)	40
Power, average (W)	30
Outline dimensions (cm)	118 × 54 × 97
Data rate (kbps)	80
Storage (Mb/orbit)	650 maximum
IFOV (degree)	± 0.17
Footprint, maximum (km)	2 × 3
Footprint, minimum (km)	1
FOV (degree)	± 57
Swath width (km)*	1,100
Number of channels	2 (real-time)
Scan	Mechanical
Attitude stability (degree)	0.2
Attitude knowledge (degree)	0.1
Orbit position (km)	1 (in- and cross-track), 10 (radial)
Time accuracy (ms)	1.0
Time stability (ms)	5 in 10^9

*Useful swath width may be limited to 700 km.

The C&DH system as currently planned is for a total real-time data rate capacity of 170 kbps plus 30 kbps for Reed-Solomon Coding (1.0×10^9 bits per orbit). This data level requires one dual transport tape recorder. An additional recorder system will be included for back-up. The tape recorder will be played back simultaneously with the total 200 kbps real-time data (via the TDRSS at SSA) at a rate of 2.0 Mbps. The playback time will be 8.4 minutes, and the duty cycle will be once per orbit. The limit of 170 kbps is established based on allowing only two AVHRR channels with a single-frequency radar (Table 16). One thermal (IR) channel of the AVHRR would be on at all times, and the second channel will be within the daytime visible spectrum. Possibly, an additional nighttime visible channel will be added, but transmission time would be shared with the daytime channel.

More complete details on the TRMM data flow and data processing are contained in Chapter VIII of this report. Table 16 also shows the playback specifications.

ERROR ANALYSIS

In this analysis we will concentrate on the primary mission goal, the determination of the rainfall on climatological time and space scales. In particular, estimates will be derived of the uncertainty of the monthly average rainfall determination in 5 degree squares. The results can be scaled to other space-time scales.

In this estimation of the errors of the monthly rainfall estimates, two radar and two microwave radiometer options are considered. There is no clear way to include the VIS/IR radiometer. Although some ideas have been articulated for the use of these higher resolution data in a multi-sensor algorithm, they are not yet specific enough to permit quantitative evaluation. Estimates of the uncertainties in these monthly averages will be generated for several different combinations of instruments. Attenuation-based algorithms for radiometers can only be used

Table 16. Instrument Data Rate and Playback Allocation Budget

Instrument			Real-Time Rate (kbps)	
AVHRR (modified)			80	
Precipitation radar			85	
SSM/I			3.3	
ESMR			1.0	
		Total	169.3	
Recorders	**Stored**	**Playback Rate**	**Time**	**Duty Cycle**
2 at 1,000 Mb	990 Mb	2.0 Mbps	8.4 min	1/orbit

over an ocean background. Thus we must consider land and ocean backgrounds separately.

Calculations will be performed for the assumption of a perfect suite of instruments over either land or ocean background. This assumption allows comparison of our results with the sampling studies which assume perfect rain measurements and adjust a scale length to account for the sampling contribution to the total error.

In addition to the radar described earlier in this chapter, we will consider a two-frequency radar which has an additional channel at 24 GHz. The additional channel permits more accurate two-frequency algorithms to be used for low rain rates (below about 16 mm/hr). The simplest radiometer option is the ESMR. The instrument would observe radiation at 19.35 GHz and would image a swath of 700 km from the proposed 350 km orbit of TRMM with a resolution at nadir better than 10 km. A second instrument, which is planned to be included with the ESMR and the radar, is the SSM/I. This instrument would image a swath nearly as wide as the ESMR swath and would permit the use of scattering-based algorithms at high rain rates over either land or ocean backgrounds, as well as extending the attenuation-based algorithms to somewhat lower rain rates over oceans. Its spatial resolution is decidedly poorer than that of the ESMR at their common frequency (19.35 GHz).

The logical beginning point for estimates of rain measurements is a determination of how hard it rains and how often. In Chapter IV, the log-normal distribution (Figure 23) was shown to be a good fit for tropical rainfall (see also Lopez, 1977; Kedem, Chiu, and North, 1987).

For the design of a measurement system, it is important to know what part of the total rain is contributed by which rain rates. For this purpose, we refer back to Equation (3) which showed r_{10}, r_{50} and r_{90}, the rain rates below which 10, 50, and 90 percent of the cumulative rain occurs, respectively, using the GATE data set, where the averaging boxes were 4 km by 4 km, about equal to the resolution of the TRMM radar. In Table 17, the data from Phase I of GATE are expressed in terms of the same log-normal distribution (Kedem, Chiu, and North, 1987). Note that the percentage of time that it rains is rather high (7 percent) and that r_{50} is only 8.8 mm hr^{-1}. For comparison purposes, data are also shown which are derived from a 5-year record of 5-minute averages of a rain gauge at Wallops Island, Virginia (Goldhirsh 1983), and from 13 months of similarly averaged data from a rain gauge on an oil platform in the Gulf of Mexico near Lake Charles, Louisiana. Both of these differ from the GATE data in that the probability of precipitation is much smaller, and associated rain rates are somewhat larger. These differences are consistent with the area average versus point measurement distinction, the climate differences, and the extreme drought in the Southeastern United States that coincided with the Louisiana observation period (August 1985 to September 1986). For our analyses, we will use the GATE distribution; its comparison

Table 17. Log-Normal Parameters for Rain

Data:	P_r	r_0 (mm/hr)	s	r_{10} (mm/hr)	r_{50} (mm/hr)	r_{90} (mm/hr)	$\bar{r}$ (mm/day)
GATE	.07	3.1	1.02	2.4	8.8	32.4	8.8
Virginia	.021	2.2	1.21	2.0	9.5	44.8	2.3
Louisiana	.012	4.1	1.19	3.7	16.9	77.5	2.4

with the Virginia and Louisiana data sets suggests that it is not unreasonable. Results from South Africa, Florida, and Israel and preliminary results from the EMEX monsoon regime (Rosenfeld, personal communication) on the other hand, suggest that, if this data set is unrepresentative of the situations TRMM will encounter, it errs in the sense of a high probability of precipitation and low rain rates.

Even with only two classes of instruments included, two domains must be considered. The swath of the radar will be narrow compared to that of the radiometers because of the geometry of the range measurements. In a central region, along the sub-satellite track, both radar and radiometer data will be available; whereas, over a considerable swath outside of this, only radiometer data are likely. The two regions will be labeled r/r and r/o, respectively. For the purpose of this analysis, we will assume a 200 km swath for the radar and a 600 km swath for the microwave radiometer.

Within each region we will characterize the errors as three different types: sampling, random, and correlated. The sampling errors are discussed in Chapter IV. Simply put, the sampling error results from the approach of measuring only a small fraction of the rain and estimating the total by extrapolation. The random errors represent the noise in the measurement due to instrumental effects, such as thermal emission and Rayleigh statistics as well as local departures from the assumptions on which the algorithms are based. Within the error model, these random errors are assumed to be unbiased. However, in the limit of a great number of observations, the errors will still not average to zero. There will still be a residual of error due to systematic error in the algorithm assumptions and instrumental calibration. To the extent that this error is known, it will be corrected by adjustments to the algorithms, but this correction will never be perfect. The correlated error is the best available estimate of the magnitude of the unknown residual. Minimizing and estimating the correlated error will be the great challenge of the TRMM ground truth program.

It will be seen later that the correlated errors are the dominant source of the instrumental contribution to the total mission error budget. Fortunately, even these correlated errors are random in a sense. Within the r/r portion of the swath, there will be a very intricate mosaic of algorithms used, each having its range of rain rates and incidence angles over which it is valid. The situation within the r/o portion of the swath is similar. It is reasonable to expect that the error residual of one algorithm is unrelated to that for any other algorithm. Moreover, in different portions of the valid range of any given algorithm, different problems can dominate and thus provide an additional degree of independence in the residual errors. For the purposes of this analysis, this form of randomness is approximated by assuming that the correlated errors are independent from one octave (factor of two) of rain rate to the next and the correlated errors in the r/r swath are independent of those in the r/o swath.

Separate estimates of the contribution of each octave of rain rate to the monthly total rainfall for a given 500 km by 500 km cell, R_j, can be generated using observations from the r/o and from the r/r portions of the swath. The two can then be averaged in an optimally-weighted manner and then summed over the octaves of rain rate to arrive at a minimum uncertainty in the net estimate of the monthly total rainfall.

$$R_j = \frac{M}{N_{obs}} \sum_{obs} r = \frac{M}{N_{obs}} = \sum_{octaves} r_i N_i \qquad (4)$$

where M is the length of a month (in hours), N_{obs} is the total number of observations in a month (including those for which there is no rain), r is the rain intensity (per hour) associated with each observation, r_i is the mean value of each octave of rain rate, and N_i is the number of observations of rain rate within each octave. For our purposes, the octaves of rain rate will be 0.5 to 1 mm hr^{-1}, 1 to 2 mm hr^{-1}, ... 64 to 128 mm hr^{-1} for a total of 8 octaves.

The variance of R_j, $\sigma^2(R_j)$, can be expressed as:

$$\sigma^2(R_j) = \frac{M}{N_{obs}} \sum_{octaves} \sigma^2(r_i N_i) \qquad (5)$$

In turn, $\sigma^2(r_i N_i)$ can be expressed as a sum of three contributions:

$$\sigma^2(r_i N_i) = (r_i N_i)^2 \left\{ \frac{1}{\nu_i} + \frac{\rho_i^2}{N_i} + b_i^2 \right\} \qquad (6)$$

Here, the first term represents the sampling error, and ν_i is the number of independent samples in the i'th octave. The second term is the random measurement error and ρ_i represents the fractional random error for measurement of rain rate in the i'th octave. The third term is the contribution to the variance of the underlying bias in the measurements, and b_i is the fractional bias in the measurements in the i'th octave.

For each portion of the swath, the total rainfall is the sum of the contributions from each octave of rain rate, and likewise the variance of the total rainfall is the sum of the variances of the contributions from each octave. The best estimate of the total rainfall in the cell for the month is the average of the estimates from the two portions of the swath weighted inversely to their variance. The variance of this total rainfall is given by:

$$\frac{1}{\sigma^2_{tot}} = \frac{1}{\sigma^2_{r/o}} + \frac{1}{\sigma^2_{r/r}} \qquad (7)$$

In order to estimate ν_i, the number of independent samples, and N_i, the number of observations, in a given rain rate octave, we first note that the satellite will have a ground speed of approximately 7 kms^{-1}. The net width of the r/o portion of the swath is 400 km, and the r/r portion is 200 km. Thus, the satellite will image an area of 7.35×10^9 km^2 per month in the r/o swath and an area of 3.68×10^9 km^2 per month in the r/r swath. The total number of observations by a given instrument is given by:

$$N_o = A/(L_r)_2 \quad (8)$$

and the number of independent samples by:

$$N_i = A/(L_c)_2 \quad (9)$$

where A is the relevant image area, L_r is the instrumental resolution (expressed as a length), and L_c is the correlation length of the precipitation. We will use 10 km as a typical radiometer resolution and 5 km for the radar. A value of 69.9 km is chosen for L_c to match the present results to those of sampling studies for the assumption of a perfect instrument.

The variation of sampling with latitude is ignored; the samples are distributed uniformly over the 864 cells between ± 35 degrees. The samples are distributed among rain rate octaves according to the probability distribution function.

In Table 18, the error constants are given for the combination of the single-frequency radar, the ESMR and the SSM/I. For this table, it is assumed that the sensors are observing rain over an ocean background. Similar tables have been generated for a variety of instrument and background combinations. For the assumption of a perfect instrument, the table contains all zeros for the error terms.

There is admittedly much judgment used in generating such a table, but some comparisons with the results from Nimbus-5 and -7 are possible. Based on the results of Wilheit *et al.* (1977), and Austin and Geotis (1978), the r/o error estimates for the 2-4 and 4-8 mm hr^{-1} octaves appear reasonable for the Nimbus-5 resolution. Similarly, the r/o error estimates for the three highest octaves are consistent with an extrapolation of the results of Spencer *et al.* (1983b), using the Nimbus-7 data. The improved resolution of the TRMM payload would certainly improve the attenuation-based rainfall estimates but has not been used here to lower the error estimates. Thus, it can be argued that the estimates of these error constants are reasonably conservative.

Table 19 lists the results of applying the error model to the various instrument combinations. The 10 percent error listed for the perfect instrument is typical of the results from the sampling studies; if a significantly different number results from the sampling studies, then the correlation length, L_c, can readily be readjusted to match and the error model can be rerun. Note that for all cases with real instrument assumptions, the error estimates are much larger over land than over ocean. This results from the requirement of an ocean background for the attenuation-based algorithms for the radiometers. Although the case of radar only with no radiometers was not calculated, the ESMR over-land case would represent a rather good approximation over both land and ocean backgrounds.

In addition to the error totals it is possible to partition the contributions to the variance from each portion of the swath, each octave of rain rate, and from each of the three error types (sampling, random, and correlated). Table 20 lists these contributions for the ESMR-SSM/I case with a single-frequency radar.

The most striking conclusion that can be drawn from this table is the lack of importance of the random error in the individual measurements. It is also clear that the very lowest rain rates (<1 mm/hr) do not contribute in any meaningful way. This lack of importance of the lower range of rain rates is also the reason the addition of the second radar frequency had so little impact on the net measurement error. If the total error is to be reduced, the measurements of rain rates above about 8 mm hr^{-1} must be improved. This is the rationale for including lower-frequency passive microwave channels, which probably cannot be afforded for TRMM. If they were included on a rain-measuring satellite, channels at 10.7 and 6.6 GHz would extend the upper end of the dynamic range

Table 18. Error Constants for Single-Frequency Radar + ESMR + SSM/I (Ocean Background)

Rain Rate (mm/hr)	Errors r/o		Errors r/r	
	Random	Correlated	Random	Correlated
0.5- 1	.5	.5	.5	.5
1 - 2	.5	.3	.5	.4
2 - 4	.5	.3	.5	.4
4 - 8	.5	.2	.5	.3
8 - 16	.5	.3	.5	.3
16 - 32	.5	.5	.5	.2
32 - 64	.6	.6	.5	.3
64 - 128	.7	.7	.5	.3

Table 19. TRMM Error Estimates for Monthly 5° × 5° Rainfall Totals

Background	Perfect Instruments	ESMR Only (2 frequency radar)	ESMR + SSM/I	ESMR + SSM/I (1 frequency radar)
Land	10% 0.9	22% 1.9	19% 1.65	20% 1.7 mm/day
Ocean	10% 0.9	17% 1.5	13% 1.2	13% 1.2 mm/day

Table 20. Percentage Variance Contributed by Each Error Source—ESMR + SSM/I + Radar Over Ocean

Rain Rate (mm/hr)	Radiometer/Only			Radar/Radiometer		
	Sampling	Correlated	Random	Sampling	Correlated	Random
0.5- 1	< .1	.1	< .1	< .1	< .1	< .1
1 - 2	0.2	0.7	< .1	0.1	0.4	< .1
2 - 4	1.0	4.7	< .1	0.6	2.5	< .1
4 - 8	3.8	6.1	< .1	1.6	3.0	< .1
8 - 16	5.5	10.1	< .1	6.0	5.6	< .1
16 - 32	4.5	7.5	< .1	12.5	1.7	< .1
32 - 64	6.0	2.9	0.1	5.9	0.4	< .1
64 -128	3.7	0.3	0.1	2.2	< .1	< .1

for attenuation-based algorithms from 16 mm hr^{-1} up to 128 mm hr^{-1}. This extension becomes more desirable particularly if the GATE rain rates are lower than many of those actually encountered by TRMM.

ERROR ANALYSIS SUMMARY AND CONCLUSION

An error model has been developed for the TRMM and has been applied to several instrument options. Although the model is preliminary, it does provide a structure which will permit an orderly examination of the assumptions. Ultimately, however, only the TRMM measurements themselves will be adequate for assessment of the TRMM errors.

The mission measurement requirements specified in Chapter III included a 1 mm per day uncertainty in the monthly mean rain rates for 500 km by 500 km cells. To the extent that either the requirement or the error analysis is exact, this requirement can be met over ocean areas by the TRMM with the ESMR-SSM/I for the microwave radiometer. Over land areas, this analysis suggests that the performance of TRMM may fall short of the requirements; it will be necessary to supplement the instrument set investigated here with other satellite-borne measurements and/or with land-based measurements in order to arrive at a complete picture of tropical precipitation. Since the sampling error is by far the largest component of the total error, its reduction by use of data from a microwave-equipped polar orbiter is a realistic and important possibility. Information from the radar may be able to reduce the errors over land, particularly if it becomes possible to increase the radar swath.

VI. RAINFALL RETRIEVAL METHODS AND TESTING

INSTRUMENT COMPLEMENTARITY

Based upon current knowledge of tropical rainfall, together with the state of instrument availability, the instruments selected for TRMM consist of a multichannel passive microwave radiometer, a single frequency radar and a VIS/IR radiometer as described in Chapter V. Each instrument's strengths and weaknesses will be discussed in detail later in this chapter. Although each instrument may be used independently to measure rainfall, this combination of radiometers offers a complement of data which is unprecedented for the estimation of rainfall. This set of instruments was chosen so that the strengths of one will compensate for the weakness of the others, while providing the redundancy needed to give confidence in the results. The complementarity of these instruments is summarized in Table 21.

The ability of ground and airborne radar to map and measure precipitation is well established. Making such measurements from a satellite is quite another matter. If we were not constrained by either antenna size or available transmitter power, one could approach the problem as with a ground-based radar and use a wavelength in the 5 to 10 cm band. But with modest-sized antennas, such wavelengths produce excessively large beams and footprints, and also suffer from the contamination of the weather echoes by ground clutter at large nadir angles. To achieve usable beam widths, TRMM proposes the use of a shorter wavelength and exploits the fact that the attenuation in decibels at such wavelengths is essentially linear with rainfall rate. Most of the radar algorithms are therefore designed to measure attenuation as a proxy for rainfall, although reflectivity will also be used as required. These algorithms are believed to perform best at near-nadir angles for reasons which will become apparent later. Consequently, the purposes of the radar are: first to make rainfall estimates near nadir (± about 20°) and secondly, to improve and/or calibrate the passive microwave methods. Later in this chapter we also discuss an approach which uses the radar in an echo area-only measurement mode which would permit it to be used at larger nadir angles and over larger swath widths.

Table 21. TRMM Payload Complementarity

	Microwave Radiometers (~6 to 9 GHz)	Radar (14 GHz)	VIS/IR Radiometer
Advantages	Quantitative measure of rain	Quantitative measure of rain	Best spatial resolution
	Wide swath	Better spatial resolution	Distinguish between convective and stratiform precipitation
		Vertical profile of rain	Transfer standard to geosynchronous and to polar orbiters
		Can provide layer thickness	
		Works well over land	
Limitations	Less quantitative over land for low rainfall	Narrow swath	Less quantitative measure
	Moderate spatial resolution	Largely untested in space	Obscuration by cirrus shields

Microwave radiation, in the wavelength range of 1 mm to 5 cm, is ideal for the study of precipitation. This is due to the strong interaction between radiation and drops comparable in size to the wavelength. Both active (radar) and passive microwave studies have therefore had good success in detecting and interpreting rainfall intensities. Recent passive microwave studies by Spencer (1986) and Olson (1987) using SMMR data and Kummerow (personal communication) using aircraft data, not only confirm the idea that rainfall retrievals are feasible with the proposed frequencies, but they also point to the improvements which might be achieved with the aid of radar data.

Limited space/time sampling is inherent in TRMM. However, there exists a network of geosynchronous spacecraft with high resolution (~1 km) VIS/IR sensors viewing the entire tropics on a time scale of 1 hour or less. The skill of these sensors for rainfall estimation is markedly lower than

that of microwave radiometers, which measure the rainfall intensity directly. One important reason that the TRMM includes a VIS/IR radiometer is therefore to provide a connection between these geostationary satellites and the more sparsely sampled TRMM measurements.

How best to combine the radar, radiometer, and VIS/IR measurements into a single rain rate will evolve based upon knowledge gained after the aircraft flights with all the TRMM instrumentation are analyzed and still further after the first data are received from the TRMM spacecraft and the "ground truth" information is incorporated. However, based upon past and ongoing studies utilizing satellite microwave, VIS/IR, and ground-based radar data, we can expect this evolving strategy to have certain fundamental features. Current microwave data from either SSM/I or ESMR will be constrained by the VIS/IR data to classify rain only when clouds are present. This will minimize problems such as anomalous propagation and various surface effects, as well as dictate the direction of future research. The active and passive microwave retrievals will be compared for consistency, thus increasing our confidence and knowledge. Ultimately, the measurements can be combined into an inversion scheme to optimize the interpretation of both the passive and active observations simultaneously.

PASSIVE MICROWAVE RETRIEVALS

Background

In the microwave regime, the power emitted by a body in radiative equilibrium is almost exactly a linear function of temperature. This allows one to define an apparent, or brightness temperature (T_B), to be used instead of the measured power. The ability of passive microwave radiometry to infer rainfall depends largely on the contrast between these brightness temperatures observed over raining and non-raining regions.

The ocean has a low emissivity (of the order of 0.5) which does not vary markedly. The brightness temperature from the ocean (temperature times emissivity) is therefore very cold (~150°K), and offers an ideal background to observe the emission from the rain at its equilibrium temperature. Land, on the other hand, has an emissivity of ~0.9 which varies with vegetation, soil moisture, and sundry other parameters. Emission measurements against this warm and variable background are inadequate for retrieving atmospheric constituents such as rain. Large raindrops (in relation to wavelength/2π) and ice particles, such as graupel and hail, scatter microwave radiation, effectively lowering the brightness temperatures by scattering radiation away from the direction of the satellite. This cold signature has shown some promise over both oceans and land (Spencer *et al.*, 1983a, 1983b; Rodgers and Siddalingaiah, 1983), but it depends on some prior knowledge regarding the relationship between large drop and ice particle concentrations to rainfall measurements.

The effectiveness of both absorption/emission as well as scattering tendencies of hydrometeors are strong functions of frequency. Low frequencies are best described in terms of their absorption/emission effects, while high frequencies are best described by their scattering effects. Historically, this has led to the definition of an "emission" regime (<19 GHz) and a scattering regime (>35 GHz). Most recent rainfall retrieval techniques, however, rely on multichannel approaches which make use of the known scattering-to-emission ratios for the various frequencies to determine rainfall.

Many authors have developed radiative transfer models for the interpretation of microwave radiometric measurements for various frequencies under diverse circumstances (Weinman and Guetter, 1977; Wilheit *et al.*, 1982; Wu and Weinman, 1984; Szejwach *et al.*, 1986; Kummerow, 1987; Olson, 1987). It is found that, in addition to rain rate, the microwave brightness temperature depends on many other factors. Beyond the nature of the underlying surface, the most significant of these are: raindrop size distribution (DSD), cloud droplets too small to fall as rain,[16] rain layer thickness, ice above the rain, inhomogeneities within the FOV, water vapor, wind speed at the ocean surface and SST.

As an example, Figure 33 shows one such cloud radiative model (Kummerow & Weinman, 1988) which accounts for the finite horizontal extent of rainshafts. Multichannel techniques can retrieve, along with the rainfall rate, some of the important parameters from the above list, but assumptions must be made about the behavior of the remaining parameters. Following is a brief description of some representative techniques. Some significant improvements which can be achieved by adding radar data to multichannel retrievals will be discussed later in this chapter. Discussion of the error model in Chapter V makes it clear how such a multiplicity of algorithms can be advantageous to the TRMM mission.

Specific Algorithms

Decision Tree Algorithm

Theoretical calculations, as well as observations, reveal that brightness temperatures over the ocean tend to increase with thermal emission for low rainfall rates, saturate, and finally decrease due to scattering from large drops and ice associated with many severe storms. As a result of these relationships, a given brightness temperature at a given frequency will, in general, be consistent with two rain rates. To resolve this ambiguity, one can examine T_B at several frequencies. A typical sequence would be: first to look at the 90 GHz channel and determine two possible rain rates and their associated uncertainties. One would then continue downward through the frequencies, eliminating grossly incompatible possibilities, until one had a single possible rain rate. Knowledge gained in this stepwise procedure can then be used to constrain some of the other unknown parameters, most notably the ice concentration.

Dual Polarization

Another method for resolving the aforementioned ambiguity between low brightness temperatures produced by pre-

[16]Drops must reach 100-300 mm (0.1 to 0.3 mm) to have a large enough terminal velocity to fall through the cloud. Cloud drops, as first formed by condensation, are about 5-10 mm in diameter. It takes about 1 million cloud drops to make one raindrop.

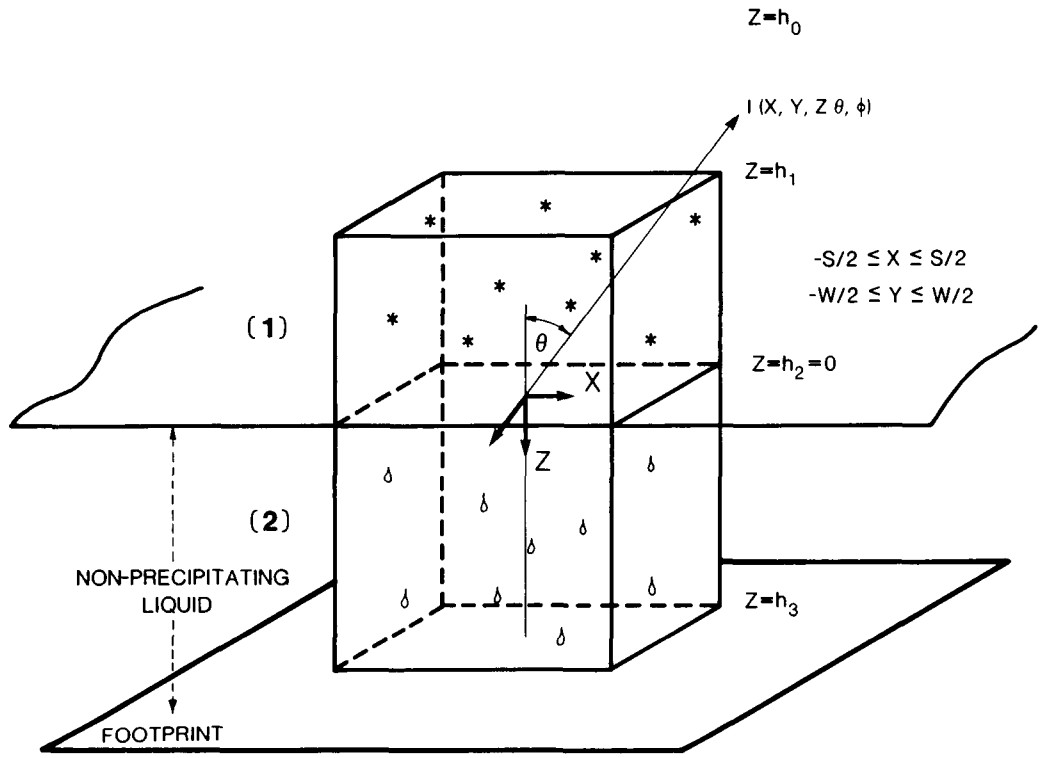

Figure 33. Schematic view of precipitating horizontally finite cloud radiative model. Radiances emerge from the surface of the cloud at points X, Y, and Z in the direction σ, σ.

cipitation, versus those produced by the ocean surface, exploits polarization diversity (Weinman and Guetter, 1977). Because the ocean surface produces radiances that are much more polarized when viewed obliquely than the precipitation, a correction can be made for the degree of polarization. This correction modifies the measured brightness temperatures upward based upon the fraction of the ocean surface shining through the clouds and precipitation. Without clouds or precipitation present, the modification produces T_B equal to the effective radiating temperature of the oxygen and water vapor emission produced by the atmosphere. An SSM/I vertically polarized 85.5 GHz image of a weather disturbance over the south Atlantic Ocean (Figure 34a) shows the effects of clouds, precipitation and clear atmosphere. Non-precipitating cumuliform clouds appear the brightest (highest brightness temperatures), while precipitation regions as well as drier oceanic air to the south appear colder. The ambiguity between the precipitation and the ocean overlain by dry air is eliminated in Figure 34b, where a polarization correction has been performed. Radar testing of this type of algorithm at 37 GHz (Figure 35) has revealed a good correlation between ground-based radar reflectivity and Nimbus-7 SMMR polarization-corrected T_B (Spencer, 1986). While these corrected T_B depressions are related to the amount of precipitation above the freezing level, the form of the relationship between corrected T_B and to rain rate at the surface is more indirect and probably regionally dependent. It can be shown that if the scattering-induced T_B depressions are linearly related to rain rate in the absence of competing ocean effects, then the polarization corrected T_B in the presence of ocean effects will be linear as well (Figure 36). The correction can be applied at any frequency where the ambiguity between precipitation scattering and ocean emission might be expected (generally 20 to 100 GHz). The method is also useful for land retrievals where lakes, rivers, and wet ground exist.

Multichannel Statistical Methods

Microwave brightness temperatures, as pointed out earlier, are not a function of rainfall rate alone, but depend to various degrees on a multitude of atmospheric and cloud parameters. The importance of each parameter in determining the upwelling brightness temperatures, furthermore, depends on the cloud structure, rainfall rate, and frequency in question.

In the absence of detailed measurements relating the above-mentioned variables to the measured brightness temperatures, it is necessary to build radiative transfer models which allow the prediction of upwelling brightness temperatures for any combination of the above variables, including rainfall. A list of such models was presented earlier. Either direct approaches such as Olson (1986), which minimize the difference in observed and calculated brightness temperature by varying the model, or statistical techniques such as Chang and Milman (1982) or Kummerow (1987) using model-generated brightness temperature/rainfall rate relations, can then be used to retrieve rainfall rate. Figure 37 shows the effect of adding channels to the retrieval scheme of Olson. When all frequencies are used, the agreement between radar and SMMR-derived rainfall rates agree within a factor of two, which is probably within the radar error of estimation. Figure 38 shows retrieval errors of 20 percent (over a 22 km by 22 km footprint) achieved by Kummerow by combining 18, 37, and 85 GHz. He used simulated satellite data over both land and ocean. Size and

ORIGINAL PAGE
COLOR PHOTOGRAPH

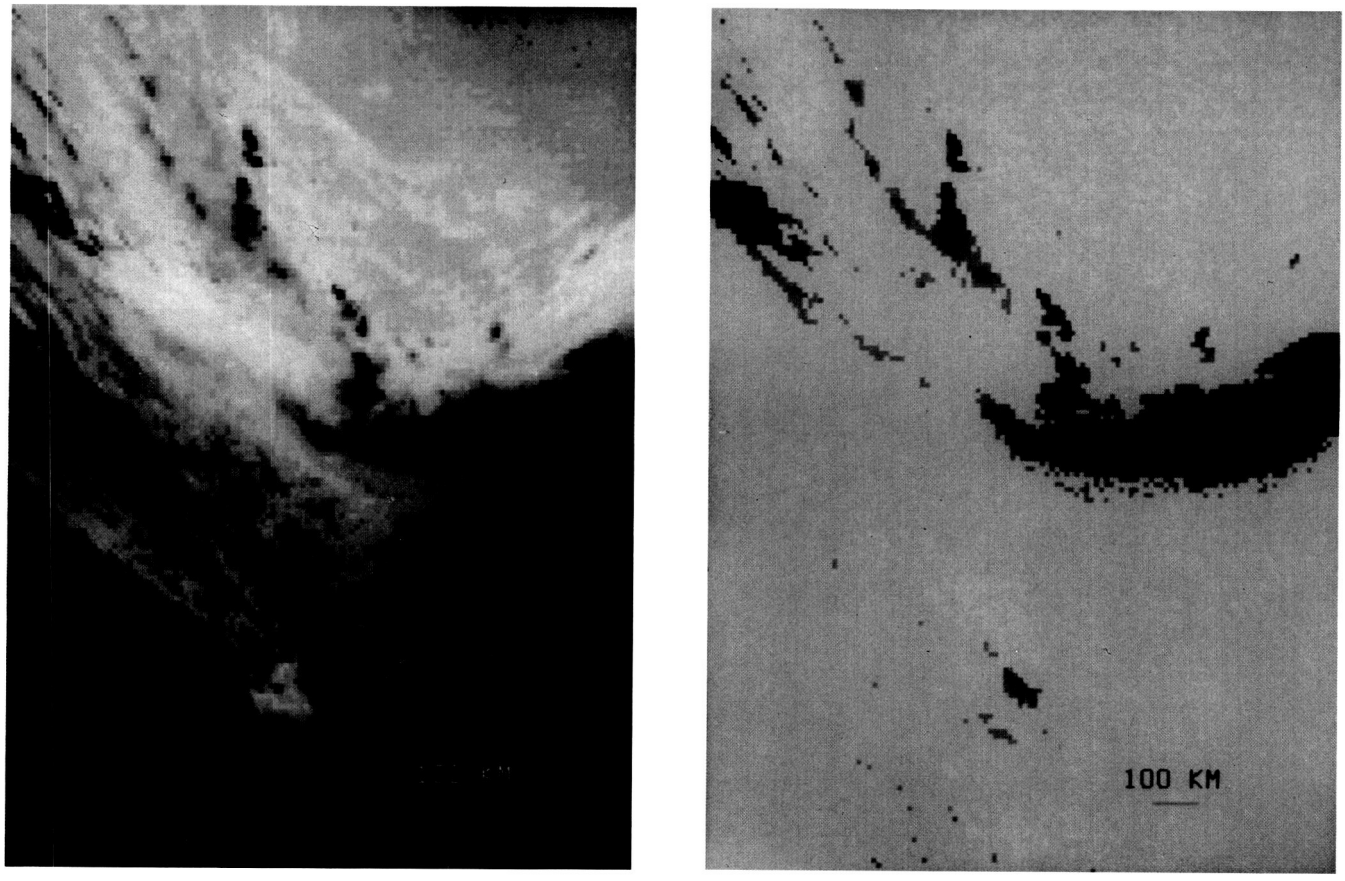

(a) (b)

Figure 34. SSM/I vertically polarized brightness temperature image (a), and polarization corrected image (b) of a weather disturbance over the south Atlantic Ocean near 30°S on July 30, 1987. North is toward the top. The T_B range in (a) is from about 180°K (dark) to 270°K (bright). Dark regions in (b) have polarization corrected T_B below 255°K, and are probably precipitating.

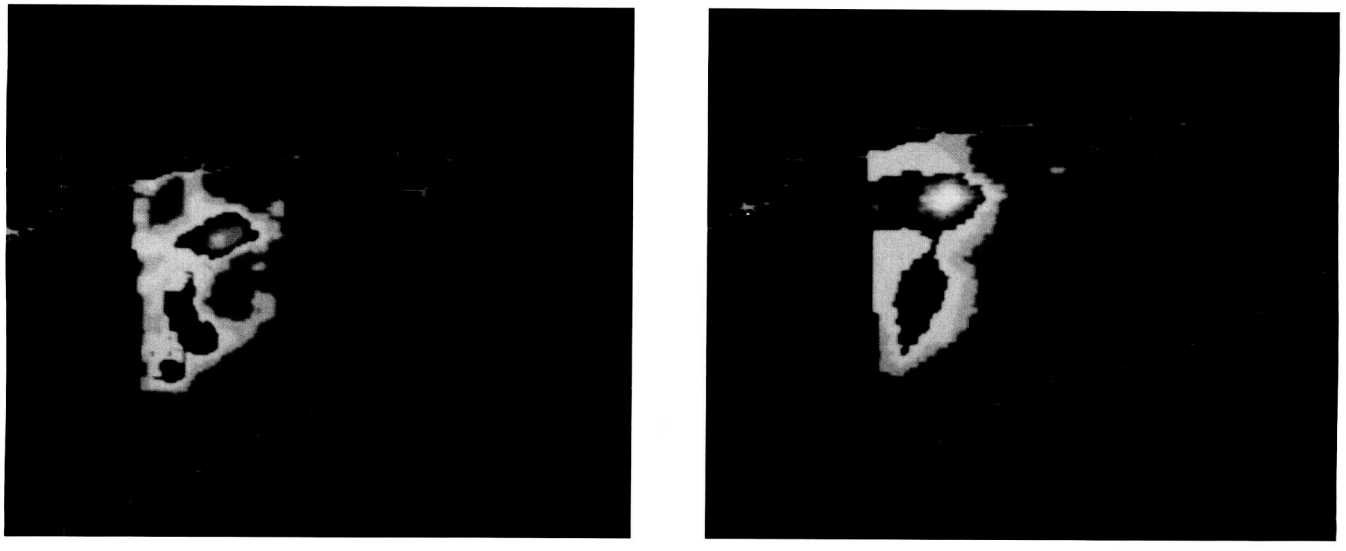

(a) (b)

Figure 35. A comparison between polarization-corrected 37 GHz T_B from the Nimbus-7 SMMR (a), and the WSR-57 radar-derived rain rates at the same time (b), for convection over the coastal waters of the Gulf of Mexico.

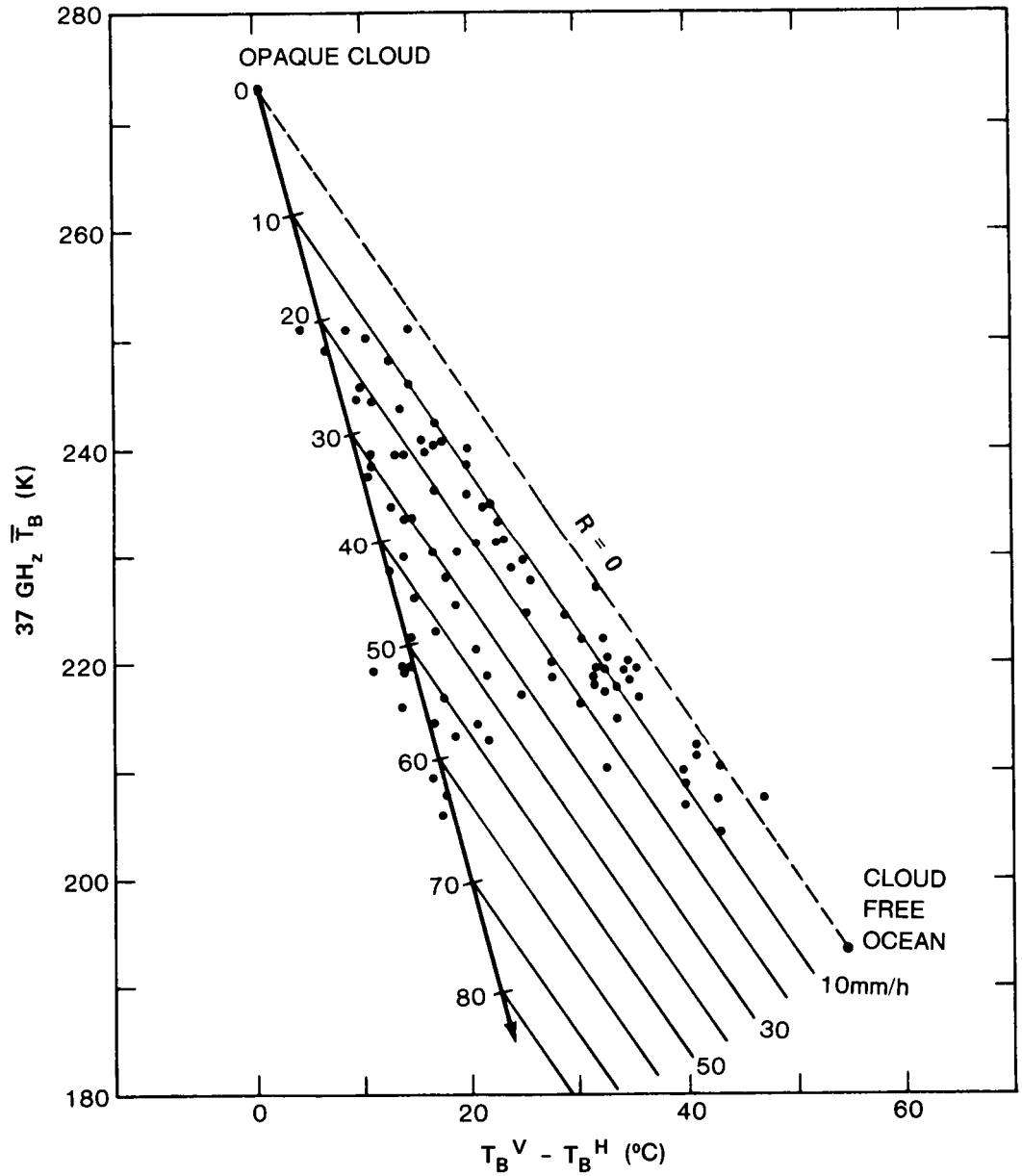

Figure 36. The relationship between dual-polarized 37 GHz brightness temperatures, rain rate, and non-precipitating cloud derived for the Nimbus-7 SMMR. Dots represent SMMR 37 GHz measurements of a squall line over the Gulf of Mexico. Partly because of calibration problems with the SMMR, a corresponding graph for a different satellite instrument (e.g., SMM/I) would be somewhat different.

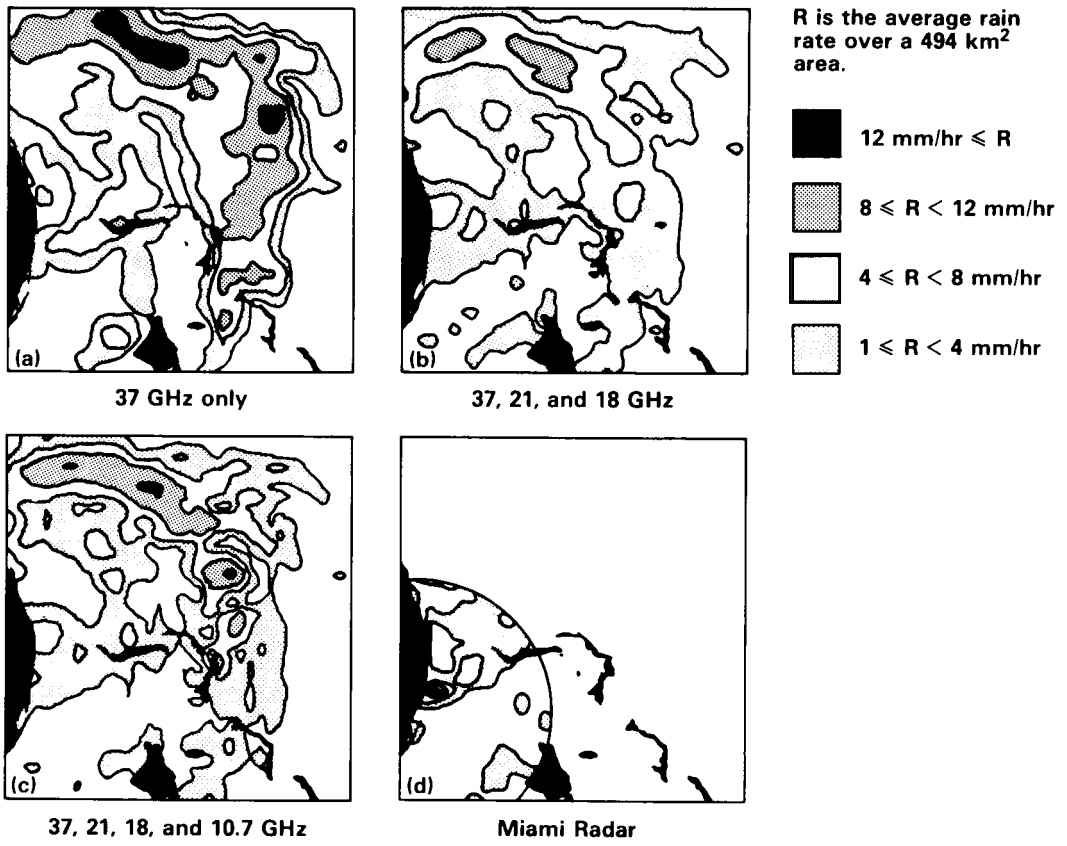

Figure 37. Rainfall rates retrieved from SMMR imagery of Hurricane David compared to radar-derived rain rates at 1644Z on Sept. 3, 1979. Rain retrievals were performed using the method of Olson (1987), incorporating SMMR data from (a) the 37 GHz channels, (b) the 37, 21, and 18 GHz channels, and (c) the 37, 21, 18, and 10.7 GHz channels. Rainfall rates derived from the Miami radar are shown in panel (d).

orientation, as well as rainfall rate and cloud liquid water, were assumed randomly distributed. Results shown in Figure 38 appear to be unbiased. This lack of bias is very satisfying since it confirms that neither the technique itself nor the partial footprint filling introduce any systematic error. Large area-averaged rainfall rates, such as the ones needed for TRMM, will smooth out most of the errors in the individual footprints so long as there is no consistent bias. This result is an important confirmation of the error analysis in Chapter V which assumes that bias can be removed.

TRMM RADAR ALGORITHMS

Introduction

Spaceborne radar differs from conventional radar primarily by the power and antenna size restrictions. The reflectivity to rainfall (Z-R) relations generally require non-attenuating wavelengths (longer than 5 cm), although at shorter wavelengths and lighter rain rates Z-R methods are also applicable. Because the longer wavelengths require currently prohibitively large antenna dimensions to achieve adequate resolution from space, the present radar utilizes a short wavelength of about 2.16 cm (i.e., 14 GHz).

Another advantage of the shorter wavelength is that the attenuation is almost perfectly linear with rain rate and is essentially independent of the DSD. Most of the algorithms which we shall describe are based upon the measurement of attenuation, A, and its relation to rain rate, R. When R becomes small, however, the attenuation also becomes small relative to the measurement errors; then we shall resort to the use of reflectivity, and the appropriate Z-R relationship, as our only alternative.

In general, attenuation by rain is given by

$$A = \int_0^H kR\,dH \qquad (10)$$

where A is the total path attenuation in dB, R is rain rate in mm/hr, k is the attenuation coefficient in db/km per mm/hr, and dH is the incremental path length. In most of what follows we assume that k is independent of R so that we may write $A \approx kRH$ where R is now the path-averaged rain rate, and H is the total path through rain. In order to deduce R we therefore need to measure or estimate H. For most purposes this can be taken as the slant range to the height of the freezing level,

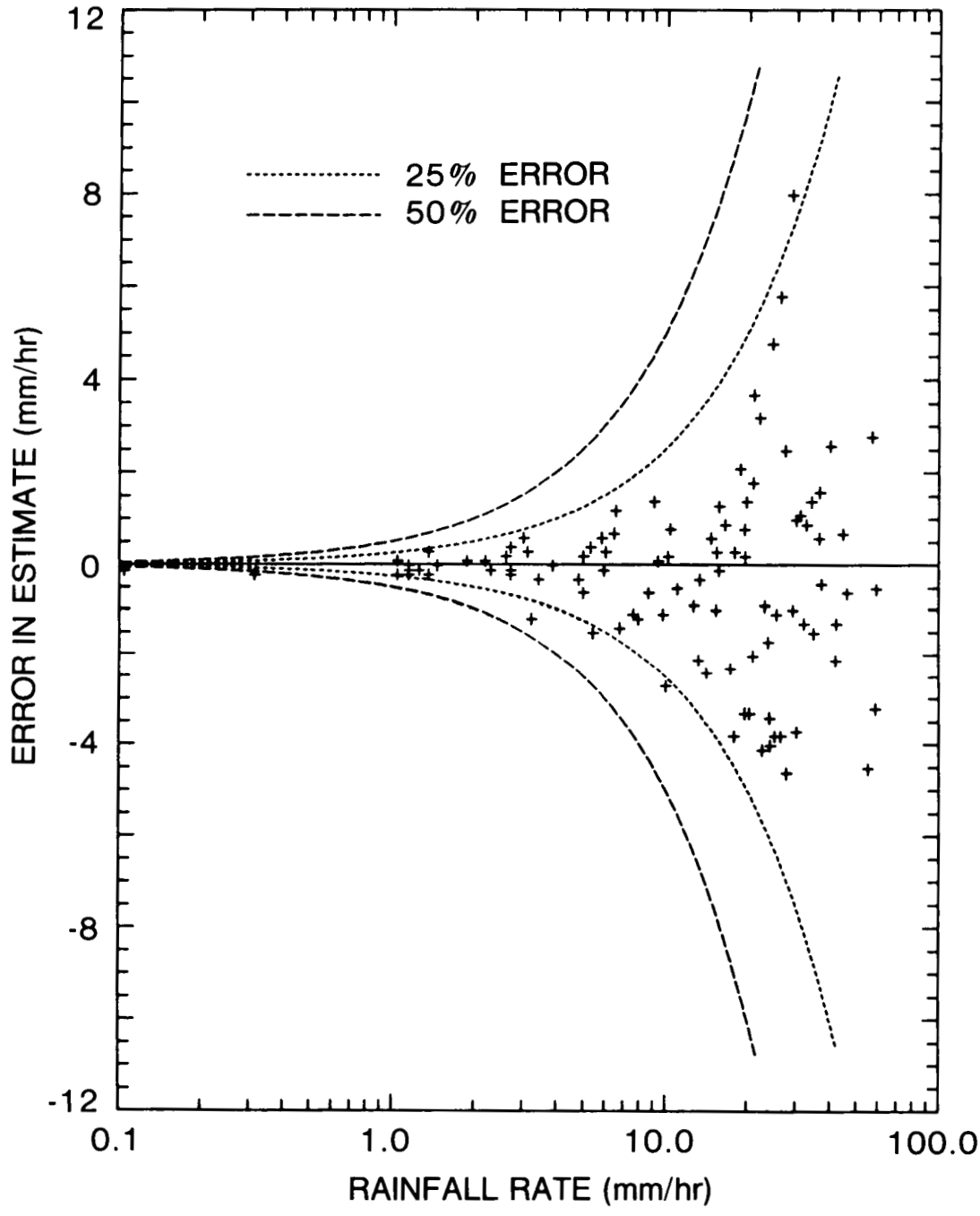

Figure 38. Differences between true footprint-averaged rainfall rate and retrieved rainfall rate over the ocean using 18, 27, and 85.6 GHz simulated data. Retrieval assumes that the rainfall rate, cloud dimensions, cloud liquid water, and surface wind speed are unknown parameters (Kummerow, 1987).

which corresponds to the top of the bright band in stratiform precipitation. This height is also generally known from independent meteorological observations. In convective storms, however, supercooled rain and clouds may occur above the freezing level and then the determination of H is subject to possible errors.

Specific Algorithms and Their Limitations

In what follows we shall discuss both single and dual wavelength algorithms in order to preserve some degree of generality. While only the single wavelength methods will be appropriate with the present design of TRMM, the dual wavelength techniques will be usable on future satellites and on aircraft for the purposes of calibration and intercomparison.

Surface Reference—Single Wavelength

The first method, as illustrated in Figure 39, is the surface target or surface reference method. This and the dual-wavelength analogue have been used with some success in the analysis of airborne radar data obtained from the Communications Research Laboratory (CRL), Japan, and NASA/

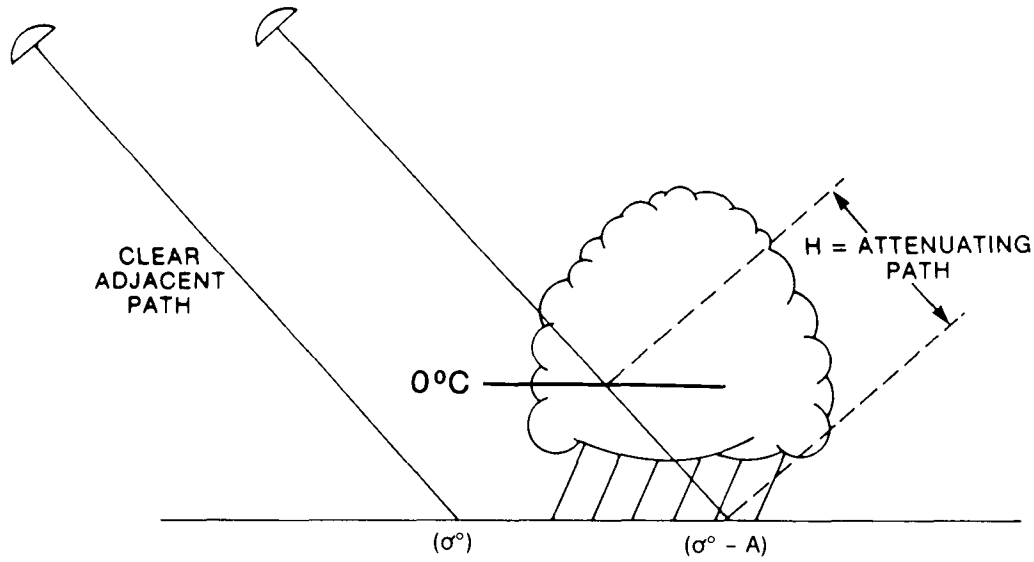

Figure 39. Schematic of the Surface Reference Algorithm showing that the echo from the surface is attenuated by A (dB) below that expected for a normalized radar cross-section (NRCS) of the surface. The NRCS (σ_0) under the storm is estimated from that measured on an adjacent path (Meneghini *et al.*, 1983).

CRL rain measurement experiments (Meneghini *et al.*, 1986). If measurements of the surface return power are made in the presence and absence of rain, the ratio of the powers will be proportional to the path attenuation as long as the surface scattering properties do not change significantly between the two measurements. Advantages of the method are its simplicity and the fact that it estimates a quantity, attenuation, that is highly correlated with rain rate. A possible disadvantage of this method is the uncertainty of the surface scattering in the presence of precipitation. As with most attenuation methods, the accuracy of the surface reference technique is limited at light rain rates where the uncertainties in the measurement are comparable to the quantity to be estimated. For a TRMM-type radar at nadir and a 5 km deep storm over the ocean, the dynamic range is expected to be up to about 90 mm/hr at 14 GHz (Okamoto and Kozu, 1987). The high rain rate limit is due to the signal being attenuated so strongly that the surface is no longer detectable.

The Mirror Image Method

This approach owes its origin to the observations by Atlas and Matejka (1985) showing the occurrence of virtual images of precipitation "below" the surface of the sea due to a double reflection involving energy reflected from the sea surface to the precipitation and back to the radar via a second reflection from the sea. Meneghini and Atlas (1986) have adapted it to a space configuration. Figures 40a and b are schematics of such a configuration with the beam oriented at nadir. Figure 40c shows a vertical profile of the precipitation echoes seen directly down to the surface and those from the surface. Below the surface we show the mirror image of the precipitation echoes seen via double reflection from the surface. The latter echoes are reduced by the double surface reflection and further by the additional two way propagation through the attenuating medium.

The main advantage of this technique lies in the fact that its independent of the effect of raindrops on the surface. Indeed, this approach allows us to explore such rain effects. Of course, the method is not without its limitations. For one, it is probably restricted to use over oceans within a relatively small angle around nadir. Secondly, because it involves an additional two way path through rain, it will lose signal at smaller rain rates than will the other methods.

Conventional Algorithms

The assumption that the rain rate is vertically uniform may sometimes be valid in stratiform precipitation. In such instances, the range-normalized echo power can be related to the rainfall rate if the extinction coefficient (assumed constant in range) is known. This simple idea, first discussed by Atlas and Banks (1951), has been revived by Goldhirsh and Walsh (1982) for application to measurements from space. With a 5 km rain depth, such a system should be capable of observing rain rates up to about 50 mm hr^{-1} at a frequency of 14 GHz.

Radar Performance

In order to get some idea of whether or not the algorithms described above would work in the radar system planned for the TRMM, it is first necessary to determine the signal strengths achievable. Figures 41a and b show the signal to noise ratio versus rain rate computed by Okamoto and Kozu (1987) for 14 and 24 GHz frequencies at nadir incidence. For the 14 GHz TRMM frequency, we note that rain rates of less than 1 mm hr^{-1} are detectable from all ranges within the storm. At large rain rates, on the other hand, the S/N of the rain return falls below 0 dB for rain rates in excess of about 40 mm hr^{-1}, while the surface return falls below the noise level for rain rates over about 90 mm hr^{-1}. The reader is referred to the cited document for detailed characteristics of the radars and the storm model.

Airborne experiments have been conducted using a sensor developed by the Radio Research Laboratory (Okamoto *et*

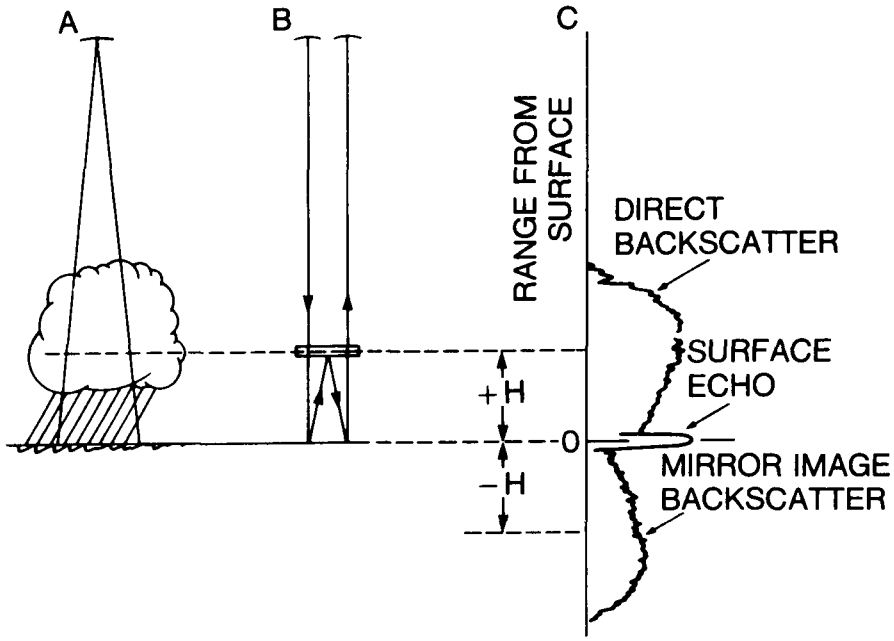

Figure 40. Schematic of the Mirror Image Algorithm for nadir incidence. (A) a beam looking down toward surface through a storm; (B) ray path for mirror image echo from precipitation layer at height H; (C) profile of the echo power received directly from the precipitation and that received via mirror image reflection (Meneghini and Atlas, 1986).

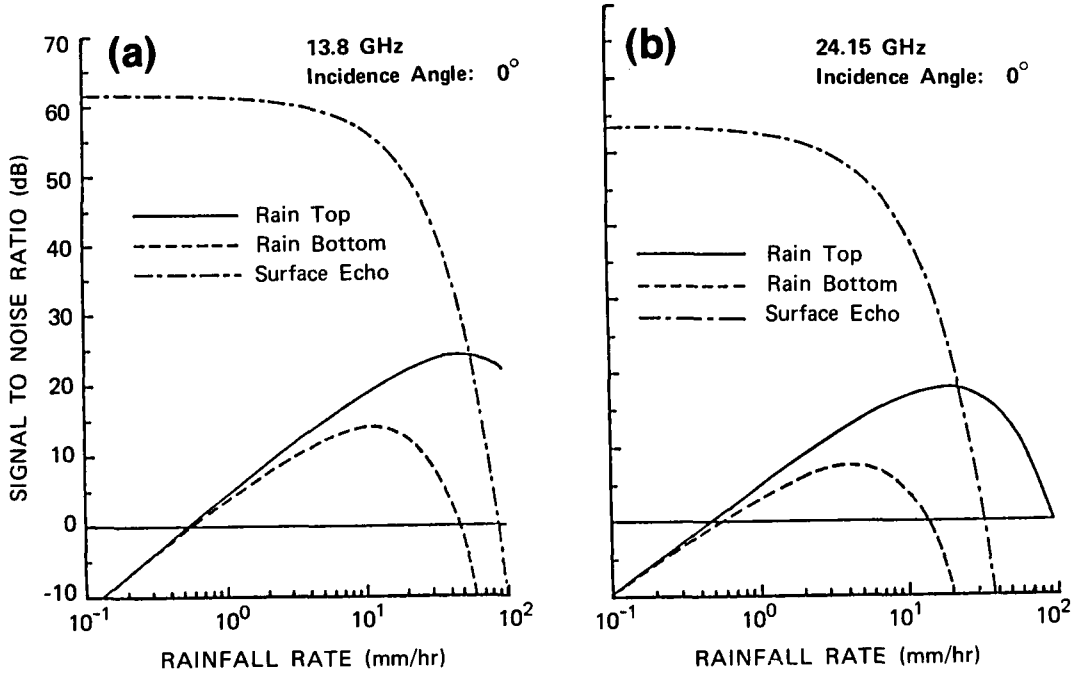

Figure 41. Signal-to-noise ratio versus rain rate from a conceptual TRMM radar operating at (a) ~14 and (b) ~24 GHz (Okamoto *et al.*, 1987).

al., 1982; Fujita *et al.*, 1985; Meneghini *et al.*, 1983). Results from these experiments have been used to aid in the design of the TRMM radar and to test methods of rain estimation from space. The sensor consists of dual frequency radar and a radiometer, where both active and passive sensors operate near frequencies near 10 GHz and 35 GHz. The resolution volumes are matched so that a common volume of rain is viewed nearly simultaneously by the radar and radiometer.

All the algorithms performed reasonably well, although some produced better results than others depending on the

range of rain rates, and in the case of the surface reference techniques, on the nature of the surface. Examples of the performance of two such methods, Figure 42a for the dual wavelength surface reference method (solid curve), and Figure 42b for the corresponding single wavelength method (solid curve), both compared to the rain rates deduced from the use

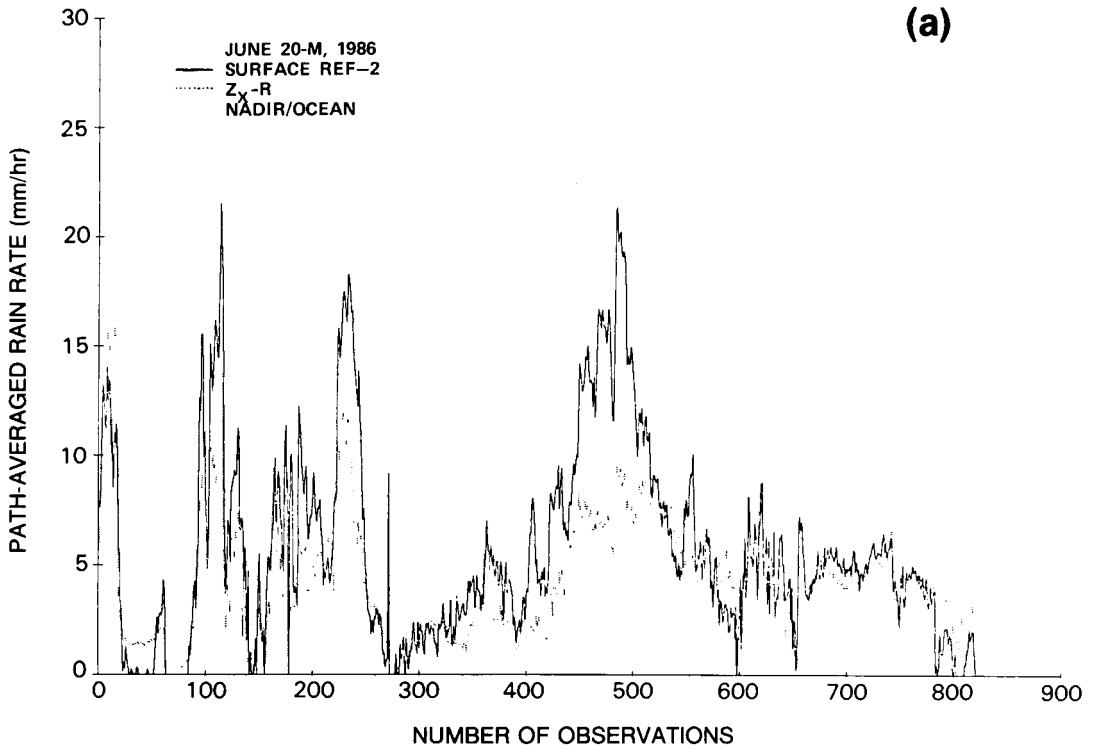

Figure 42a. Comparison of path-averaged rain rates as estimated from the dual-wavelength surface reference technique (solid line) and the Z-R technique (dotted line) as applied to the X-band radar data obtained during the 1986 joint RRL/NASA airborne experiment.

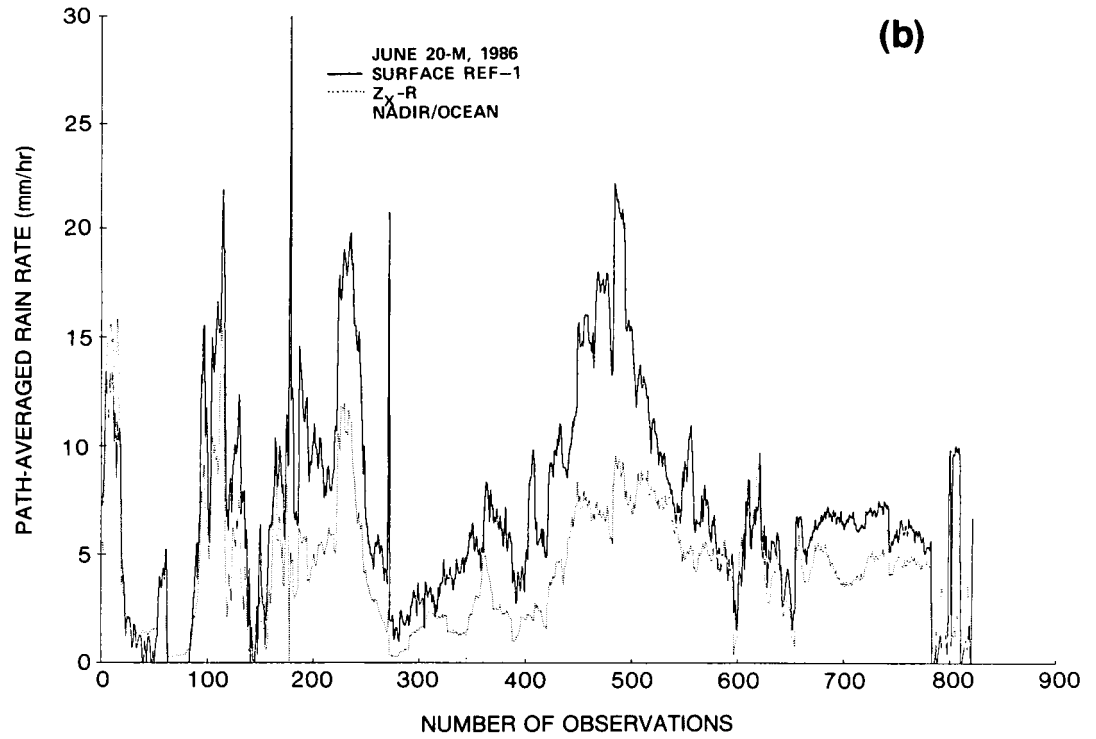

Figure 42b. Same as Figure 42a except using the corresponding single wavelength method.

of the Z-R method at 3 cm wavelength (dotted curves) are shown in the respective figures. The data were taken during the cooperative CRL/NASA rain measuring experiment on June 20, 1986. From these and other results, some conclusions can be drawn:

- Estimates of rain rates using attenuation methods are feasible from a low Earth orbiter.
- Attenuation methods are most accurate in the intermediate range of rain rates where the attenuation is significant but not excessive. For light rain rates, the standard Z-R method is preferable as long as the radar is well calibrated.
- Discrepancies between the rain rate estimates derived from the various methods can sometimes be resolved by an examination of the return power profiles and a knowledge of major error sources.

Plans for further aircraft tests with ground radar/gauge comparisons are outlined later in this chapter.

Radar Rainfall Inference Using Rain Echo Areas and Heights Only—*H*eight *A*rea *R*ainfall *T*hreshold (HART) Technique

Background Relationships

In Chapter IV, the importance of the log-normal distribution of rain rates were noted, though mainly in the context of the sampling problem. Years of research using radar to describe convective cloud systems have shown that many other features of convective cells, such as their heights, areas, and lifetimes are also well fitted by log-normal distributions when an adequate spatial and/or temporal cell sample is considered (Biondini, 1976; Lopez, 1977; Houze and Cheng, 1977). In this subsection, we use these important relationships in summarizing a simple but powerful means to estimate rain volume from spaceborne radar observations, reported in more detail by Atlas *et al.* (1988) and Rosenfeld *et al.* (1988). This technique also exploits well-documented correlations between storm area, height, duration, and total rain volume.

Based upon observations in the Florida Area Cumulus Experiment (FACE), Gagin *et al.* (1985) found remarkably high correlations between the rain volume and storm depth, where the depth is defined as the difference between the radar top and the smallest storm which produces any rainfall whatsoever. Using data in South Dakota, Dennis *et al.* (1975) found similarly good correlations where storm depth was defined relative to the actual cloud base.

The above begins to provide the physical basis for the Area Time Integral (ATI) method of Doneaud *et al.* (1984). They showed that the total rain volume, RV, from a storm is given by the integral

$$RV = \int_t \int_a R \, da \, dt \qquad (11)$$

where R is rain rate, a is area, and t is time. Using A_r as the storm area confined within the 25 dBZ threshold, they found an excellent correlation between A_r and RV, thus permitting them to write

$$RV = R_c \int_0^t A_r \, dt \qquad (12)$$

where R_c represents some climatological time-space average intensity for convective rain in North Dakota. They found R_c = 4 mm/hr. Lopez *et al.* (1983) used a slightly different approach with the FACE data in Florida with a radar threshold of about 18 dBZ. They too reported excellent correlations with R_c = 3.4 mm/hr.

In the case of observations from an orbiting spacecraft, however, we would have observations only twice per day at most, rather than at 5 to 15 minute intervals such as were available to Doneaud *et al.* (1984) and Lopez *et al.* (1983). However, since storm duration is so well correlated with A_r, it was not unreasonable to expect that A_r alone would provide a useful estimate of RV. Using radar data from GATE binned in 4 × 4 km areas, and a variety of thresholds, Chiu (1988) found that the total rain volume, RV, in a single snapshot of the entire GATE area (280 × 280 km) was exceedingly well correlated with the area-wide average rain rate. Indeed, with a threshold of 32 dBZ (about 5 mm/hr) the echo area explained 98 percent of the variance of the rainfall. Also, R_c = 4 mm/hr, identical to that in North Dakota and a bit higher than that in Florida. This provides the promise that individual measurements of storm echo area over a representative domain could provide the desired rainfall estimates. The reason that Doneaud and Chiu were able to estimate the total rainy area and the associated total rain volume is because of the well defined probability density function (log-normal). The area under the pdf which exceeds a preset threshold completely determines the entire area.

Clearly in order to have a well behaved pdf for each realization (i.e., snapshot), we must have a representative number of cells in the domain. We tested this for a Texas data set with R_T = 4 mm/hr and found that the variance of A_r explained increased from 70 to 98 percent as the area of the domain increased from about 10^2 to 1.2 × 10^4 km^2, respectively. With a typical cell size of 50 km^2, this implies about 30 to 40 cells to achieve a stable pdf and 98 percent of the variance.

Because we shall add the measurement of storm height, we shall henceforth refer to the method as the HART technique.

Incorporation of Height and Tests of the Method

In addition to GATE, two other high quality data sets, including both reflectivity and height, were studied: namely, 1) most of the afternoon convective rain in the summer of 1987 at Big Spring, Texas (Rosenfeld and Woodley, 1988), and 2) all the rainfall in the southern summer of 1984/1985 at central South Africa (Rosenfeld and Mintz, 1988). In order to permit comparison of the South Africa and Texas data sets to GATE, we reanalyzed 18 days of the original GATE radar data tapes taken on board the ship Quadra, mainly in Phase III, using identical procedures.

In order to convert the observed reflectivities into rainfall intensity we used Z-R relationships common to each region. These are: 1) South Africa - $Z = 200R^{1.4}$ (Pasqualucci, 1976); 2) Texas - $Z = 383R^{1.615}$ (Smith *et al.*, 1977); and 3) GATE - $Z = 230R^{1.25}$ (Hudlow *et al.*, 1979). The cumulative rain

rate distributions for all areas are shown by the three curves in Figure 43. The Texas rains have the largest median and longest tail consistent with the more intense local forcing, while the GATE data have the lowest median and the smallest tail.

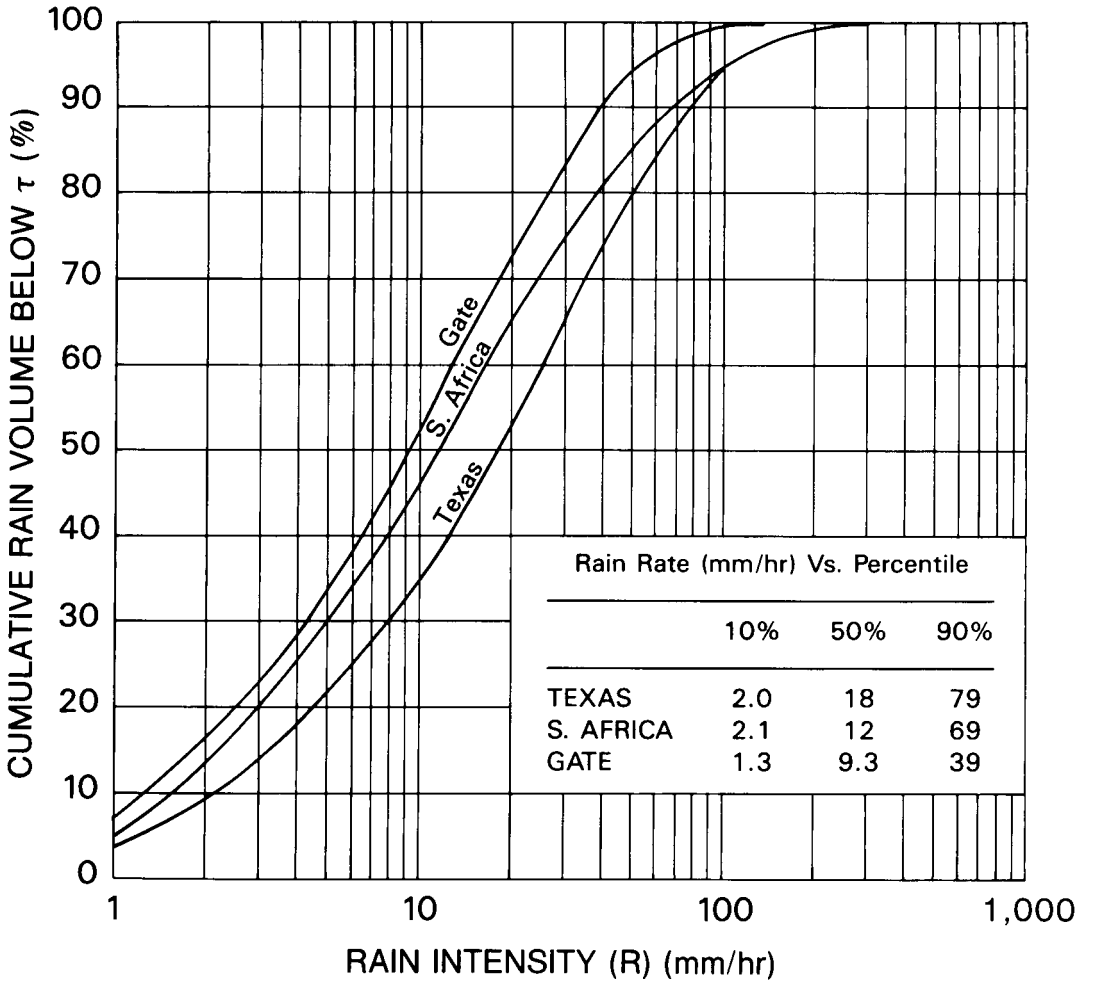

Figure 43. Percent of total rain as a function of rain rate for GATE, Texas, and South Africa as obtained from the original radar resolution (1 degree × 1 km) for the range interval of 31-90 km.

We then obtained the relationships between the total areal rainfall rate and the area covered by intensity greater than R_T mm/hr in a manner similar to Chiu (1988), but for the high resolution radar data in its original polar coordinates.

The actual relationship was calculated as follows. We define the entire area scanned as unity, as shown schematically in Figure 44. The fraction of the area covered by any rain rate greater than zero is F_o. Let F_t be the fraction of the area covered by rain rates greater than the threshold R_T mm/hr.

$$F_t = F_o \int_{R_T}^{\infty} P(R)\, dR \qquad (13)$$

where P(R) is the probability density function (pdf) of R, and the integral represents the rainy area in which $R > R_T$ as a fraction of the total rainy area.

We also assume that P(R) is constant as appropriate to each area. Then, the following expression holds:

$$F_o R_c = F_o \int_{o}^{\infty} R\, P(R)\, dR \qquad (14)$$

where R_c is the average rain rate where it is raining and corresponds to the integral. Since P(R) and R_c are fixed, variations in F_oR_c are due entirely to variations in F_o. We define

$$R_a = F_oR_c \qquad (15)$$

Scattergrams of R_a, the areal averaged rain intensity versus F_t, the fractional area covered by rain rates above threshold

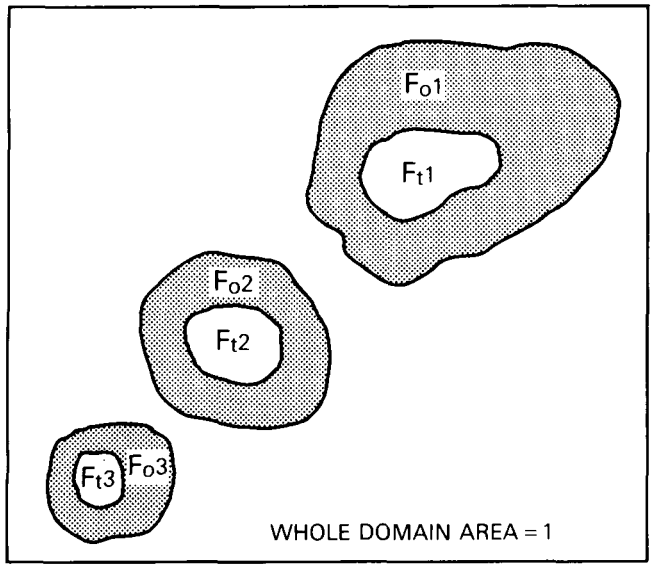

Figure 44. Schematic presentation of the rain intensity distribution in the domain, categorized into the classes below and above the threshold intensity R_T mm/hr.

intensities T ranging from 1 to 10 mm/hr were computed for South Africa, Texas, and GATE. However, Figure 45 shows only those corresponding to R_T = 5 mm/hr for South Africa, Texas, and GATE, respectively. The correlation coefficients were generally very high, and they maximized at R_T values between 5 and 7 mm/hr, to the very high values of r = 0.97 for South Africa and r = 0.99 for Texas and GATE. This is not only in agreement with the findings of Chiu (1988) for GATE, but also demonstrates the generality of the methods for a broad range of convective regimes. We note that the area average rain rate, R_a, is equal to the slope, S_t, of the regression line and increases with the threshold, R_T. This will be clarified later.

Although the correlation coefficients for all three regions are pleasingly high, it must be noted that these large values are due to the small number of points in the rainiest situations. However, for most of the points (i.e., snapshots), which are concentrated near the origin, the standard errors are still of the order of 30 to 50 percent.

Since storm height or depth is so well correlated with rain rate and storm area (Adler and Mack, 1984; Rosenfeld and Gagin, 1988), we utilized the storm depth to develop a parameter which we define as the "Effective Efficiency," E_e, given by

$$E_e = \frac{Q_b - Q_t}{Q_b} \tag{16}$$

Here, the Q's are the vapor mixing ratios at the base and top of the storm as represented by subscripts b and t, respectively. In other words, E_e is the fraction of the water vapor carried up through the cloud base which is potentially available for precipitation. Since Q_t is determined by the actual height which is reached by the storm, the reader will recognize that E_e actually parameterizes a variety of physical factors such as entrainment, mixing, and evaporation which work to prevent a storm column from rising as far as its initial buoyancy would indicate.

By stratifying the data according to both R_T and E_e, we obtained results such as are given in Table 22 for GATE. The data for Texas and South Africa are similar but are not shown. We have underlined the minimum standard errors in each class of E_e and see that the smallest SE's fall along a diagonal along which E_e and the threshold, R_T, increase. Indeed, the percent SE was reduced to 5-10 percent for most snapshot cases including the weakest rains. This means that the pdf is determined to a large extent by the depth and/or the E_e of the rain cloud systems. The conclusion is that storm depth

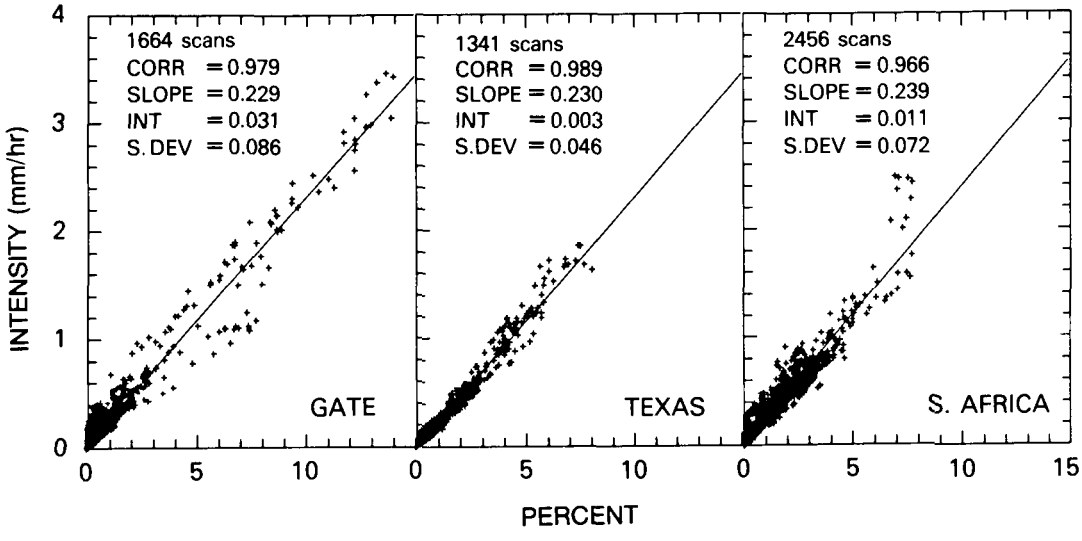

Figure 45. Areal Rain Intensity, R_a, plotted against F_t, percentage of the domain covered by rain intensity >5 mm hr^{-1} for GATE, Texas, and South Africa.

Table 22. The Standard Error of Estimate of Areal Rainfall, R_A, (in mm/hr) from HART Technique for Various Combinations of Rain Intensity Thresholds (R_t) and Effective Precipitation Efficiencies (E_e)

R_T (mm/hr)	Standard Error Without E_e Information	Standard Error for Cases in Selected E_e Intervals				
		3-.4	.4-.5	.5-.6	.6-.7	.7-.8
2	0.190	0.013	0.041	0.211	0.442	0.258
4	0.148	0.016	0.032	0.147	0.290	0.255
6	0.109	0.024	0.033	0.100	0.159	0.162
8	0.103	0.028	0.059	0.107	0.158	0.265
10	0.121	0.031	0.095	0.143	0.209	0.246
Number of cases studied:	1,568	406	336	223	151	65

and area better specify the snapshot area-wide convective rain rate than either parameter alone. This is fortunate because the radar system can provide measures of both parameters. Indeed, the quantitative relationships for all three regimes are very similar.

Comprehensive error analyses have not yet been performed. However, the results are not sensitive to reasonable changes in the Z-R relationships except to the extent that any bias in the threshold, R_T, which might be caused by systematic changes in Z-R or other factors, would result in a corresponding bias in the average rain rate.

With the exception of the need to define a rain rate threshold, the HART method is virtually independent of all the existing algorithms. It simply uses one or more of those algorithms to define a threshold rain rate and substitutes the measurement of the area encompassed within that isopleth, along with measurements of storm height, to estimate the area-wide average rain rate. Moreover, the method has a heritage of observational support which is lacking in the other algorithms. In addition, HART may be used with confidence at greater nadir angles and swath widths, and over a greater range of rain rates, than those to which the present radar algorithms are expected to work.

A critical feature of HART is that, depending upon the number of storms within the observing domain, it has the potential of providing a usefully accurate area-wide rainfall measurement in a single snapshot. Thus, this approach opens the door to a much wider spectrum of research applications than set out in the original TRMM concept, which achieved accuracy by a multiplicity of revisits to the same area over about a month.

On the other hand, HART depends upon the existence of a well-defined and consistent probability density function of rain rate which is also a function of storm height. This makes the method subject to uncertainties such as the variability in the pdf from one region to another, or with time. However, we believe that the appropriate pdf's can be determined by using the combination of the statistical HART method and the physical radar/radiometer algorithms such that the latter are used to "tune" the local statistics. In short, the combination of the HART method with the physical algorithms is expected to provide a much more powerful means of measuring convective rainfall than can either method alone.

HYBRID ALGORITHMS USING RADAR TOGETHER WITH PASSIVE MICROWAVE SIGNALS

Combination of Radiometric Sources

Early attempts to combine radar and passive microwave retrievals have been very successful. Airborne dual frequency radar has been successfully used by Fujita *et al.* (1985) in a range-profiling mode to provide a first approximation to the vertical rainfall structure. When this profile was used as input in a passive microwave radiative transfer equation, the agreement between calculated and observed brightness temperatures was excellent. Using upward viewing radar and passive microwave radiometers at both 10 and 35 GHz, Lü and Hai (1982) have also found a high correlation between the reflectivities measured by the radar, and the emitted energy received by the radiometer. Regression analyses have been performed by these authors, and coefficients reported, for the simultaneous use of the two instruments.

The multichannel linear retrieval schemes described previously in this chapter depend largely on the construction of cloud models which can accurately represent the observed brightness temperatures. If the correct model is used, however, then excellent results obtained from simulated retrievals can be expected (± 20 percent for rainfall over an individual footprint) (see Figure 38). One possible solution to this problem, which relies solely on the passive microwave component of the TRMM complement, is to use a self-consistency approach such as that of Kummerow *et al.* (1988). This technique relies

on the calculated brightness temperatures corresponding to the retrieved geophysical parameters to test the validity of the cloud radiative model used to generate statistics for the particular rain scene of interest. Serious errors, such as those encountered if regression coefficients derived for stratiform rain are applied to measurements corresponding to convective precipitation, can be avoided by such a technique.

With the additional cloud structure information supplied by the spaceborne radar, the cloud model can be further refined to better coincide with the actual rain scene. This, in turn, will allow the passive microwave measurements to yield even more accurate rainfall rate estimates. Results from such a technique, using surface radar and aircraft passive microwave measurements obtained during COHMEX[17] are extremely good. Figures 46 and 47 show the skill of such retrievals for light stratiform rain and severe convective rain respectively. Table 25 summarizes rain retrievals by passive microwave and radar.

Theoretical Analysis of Combined Radio-Radiometer Algorithms for Vertical Hydrometeor Profiling

Outline of the Method

Weinman *et al.* (1988) have simulated the analysis of returned radar signals and the radiances that a multifrequency, dual polarized passive microwave radiometer will provide on a satellite. The combination of radar and radiometer measurements places constraints on the solution of the radar equation which can be used to obtain a vertical hydrometeor profile from a single-wavelength radar. These constraints are:

1. The phase of the mixed liquid/ice hydrometeors and the non-precipitating liquid water are provided as a function of altitude by applying radiative transfer models to the microwave radiances emerging from the precipitating clouds.

2. The mean rainfall rate determined near the surface from the microwave radiances can be used as a first approximation to derive the extinction coefficient near the surface which is used as the boundary condition placed on the solution to the radar equation. This technique is applicable over both land and sea surfaces.

3. The path-integrated extinction can also be used as a constraint on the solution to the radar equation. This quantity can be determined from the radar power reflected from the sea when an aircraft- or satellite-borne radar operates over maritime precipitation. The path-integrated extinction can alternatively be computed from the approximate hydrometeor profile derived from passive radiometry. This latter approach is applicable over both land and sea.

4. In the case of heavy rainfall, the retrieved precipitation profile depends primarily upon the passive microwave radiometric measurements obtained over land and water. The impact of the radar on the retrieval then becomes confined to the upper layers of the precipitating cloud at those higher rainfall rates. Reflection of the radar beam from the sea surface provides a constraint on the radiative transfer model that determines the microwave radiances.

A nadir-viewing radar measures returned power that is described by the radar equation:

$$P(z) = \frac{C\eta \exp(-\gamma \int_{z}^{z^*} k(z')dz')}{(h - z)^2} \qquad (17)$$

where P(z) is the power received by a radar on a platform at height, h, that has been singly scattered from height z. The hydrometeor cloud extends to a height of z*. This height is a function of the rainfall rate at the surface, R(0). The constant, C, contains instrument parameters, such as emitted power, antenna area, efficiency of detection of backscattered power and rain gate length that determines the volume from which the signal is measured. The constant g = .461 converts the extinction coefficients from logarithms based on ten to those based on natural logarithms. The backscattering coefficient, h(z), is the effective reflectivity at 180°. This quantity varies with k(z) and altitude and its value must be obtained *a priori* from information on the phase and density of the hydrometeors provided by the application of radiative transfer models to passive microwave measurements (see Kummerow, 1987).

The total extinction coefficient, k(z), in dB per km is retrieved as a function of altitude. The extinction coefficient consists of three components, namely the extinction coefficients of the liquid hydrometeors, ice hydrometeors, and non-precipitating cloud droplets. The extinction coefficient of the non-precipitating cloud liquid is estimated from the analysis of the passive radiometric data.

Equation (17) can be solved for the extinction coefficient of the hydrometeors only, $\tilde{k}(z)$, as a function of height if a few assumptions are made. Besides knowledge of the non-precipitating cloud water content, it is necessary to relate the effective reflectivity [contained in the function h(z) to the extinction coefficient $\tilde{k}(z)$]. Fortunately, this ratio is relatively insensitive to the density and phase of the hydrometeors. A first guess can be derived from Mie theory computations based upon a rough vertical hydrometeor distribution provided by passive radiometric data.

Surface Rainfall Rate Constraints

The integral nature of Equation (17) further requires the application of a boundary condition on $\tilde{k}$ to determine the solution uniquely. The simplest boundary condition is $\tilde{k}(z^*)$,

[17]COHMEX stands for Cooperative Meteorological Experiment. An Interagency field experiment for the measurement of precipitating cloud systems, it involved NASA, the Federal Aviation Administration (FAA), the National Center for Atmospheric Research (NCAR), and several universities. The NASA ER-2 aircraft was flown at about 20 km altitude with a remote sensing package which included a multichannel microwave radiometer and a polarization lidar.

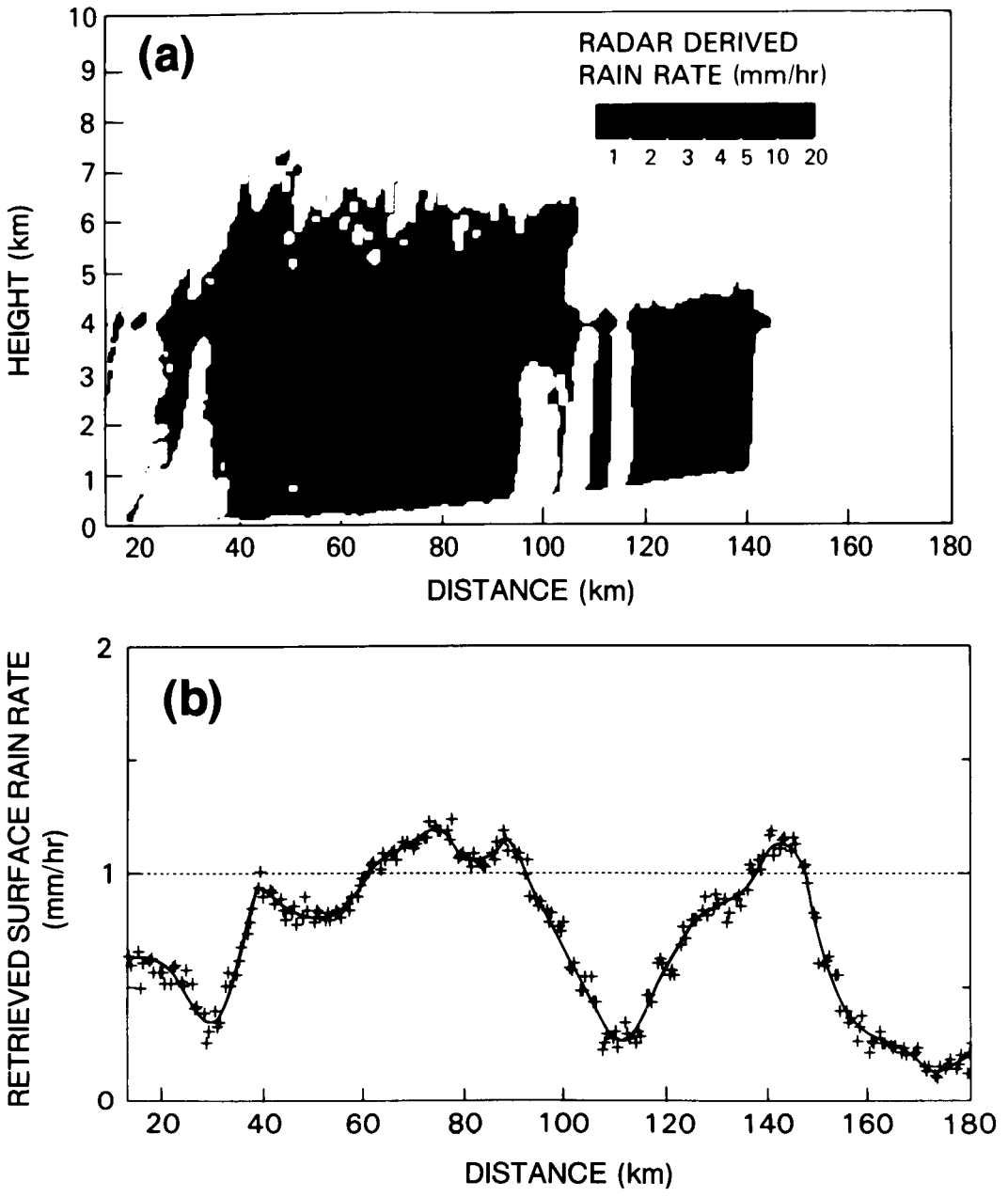

Figure 46. Surface radar-derived rainfall rate (a) over the ocean on July 1, 1986, compared to aircraft radiometer-retrieved rainfall rate (b) from Cooperative Huntsville Meteorological Experiment (COHMEX) '86. Aircraft radiometer footprints are roughly 1 km. Cloud parameters are varied to achieve maximum agreement between observed and deduced brightness temperatures in a statistical sense. The 18 and 37 GHz, dual-polarization channels viewing at 45° ahead of the aircraft are used. This produces a small offset (40 sec) between radar-observed and radiometer-derived rainfall rates.

or the extinction coefficient closest to the radar. This quantity has been measured directly, since attenuation does not affect this measurement. Hitschfeld and Bordan (1954), however, found this solution to be very unstable. That is, small errors in the estimate of $\tilde{k}(z^*)$ tended to produce very large errors in the estimates of $\tilde{k}(z)$ further away from the radar.

A significant advantage of measurements from space, compared to the traditional Hitschfeld and Bordan solution for ground based radars, is the possibility of defining the extinction at a point furthest from the radar at which to apply the boundary condition. This solution has been shown by Klett (1981) to be relatively insensitive to errors in the estimate of the extinction coefficient at the most distant range $\tilde{k}(0)$. A first guess of the value of $\tilde{k}(0)$, the extinction coefficient at the surface, can therefore be derived from the mean rainfall rate between the surface and the 0°C isotherm obtained from the passive microwave retrieval.

This algorithm does not depend on the nature of the surface beneath the cloud; it is equally applicable to precipitation over land and sea.

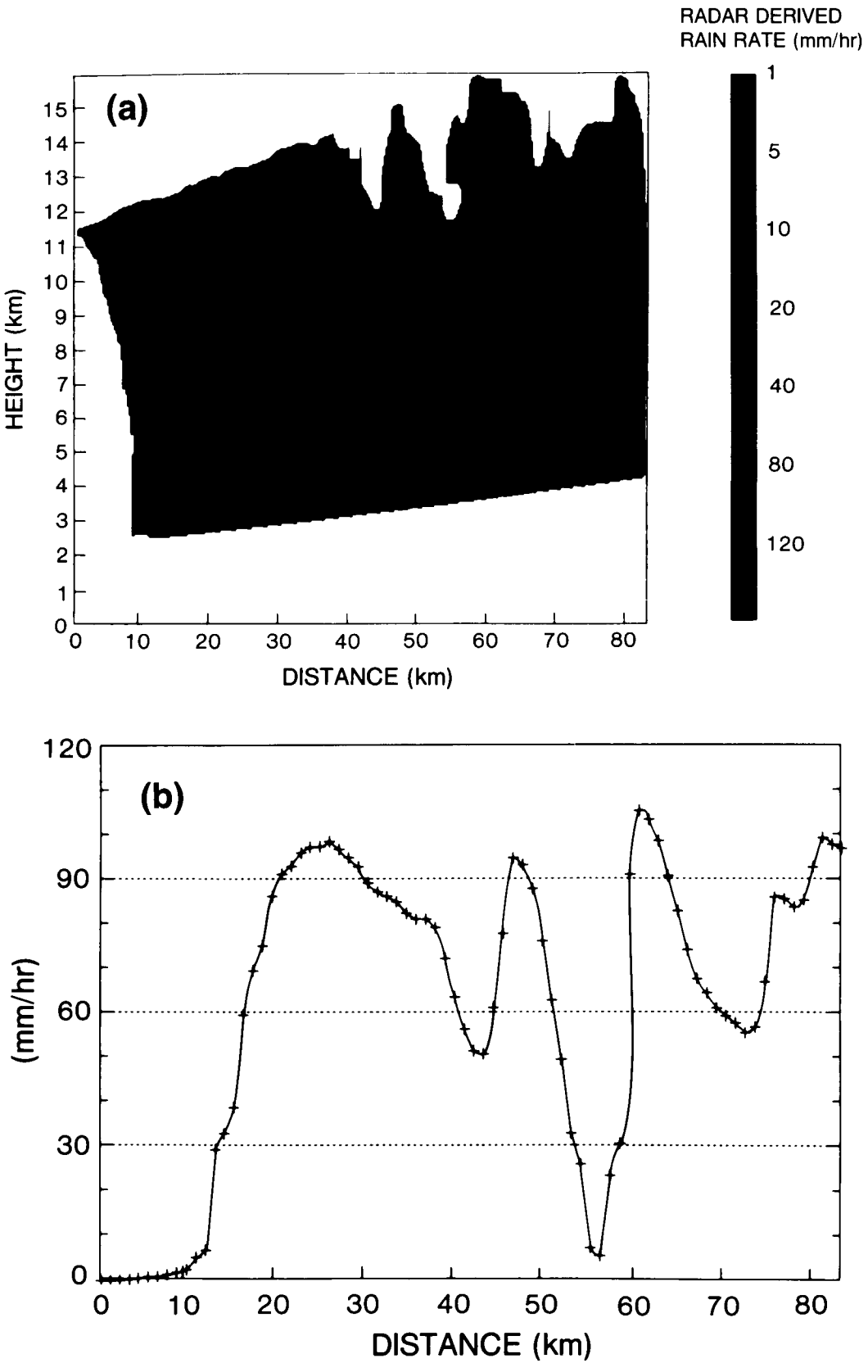

Figure 47. Surface radar-derived rainfall rate (a) over land on June 29, 1986, compared to aircraft radiometer-retrieved rainfall rate (b) from COHMEX '86, using 18 and 37 GHz, dual-polarization channels viewing 45° ahead of the aircraft, and 92 GHz downward-looking channel.

Path Integrated Extinction Constraint

An alternate method of solution involves knowledge of the path integrated extinction, A, defined in Equation (10). Weinman (1988) and Meneghini *et al.* (1983) have shown that the path integrated extinction may be used as a boundary condition instead of the extinction coefficient at a particular height, z. The path integrated extinction can be determined by several methods:

1. The parameter, A, may be measured from the reflection of the radar power from the sea surface. It is noteworthy that Jones *et al.* (1977) showed that the microwave reflection cross section of the ocean surface is independent of the windspeed at a viewing angle of 10° with respect to nadir. If the wind field is assumed to be homogeneous over the swath scanned at several angles by a spaceborne radar, then the multi-angle scan can be used to determine the wind speed and hence the reflectivity of the sea. Once the reflection cross section of the sea is determined, the transmission of the rain column can also be determined from the reflected power.

2. Meneghini and Atlas (1986) have proposed another scheme to measure A that gives broader spatial coverage than the scheme described above and which requires no assumption about the surface roughening but which may be more limited by signal to noise considerations than the previously cited techniques.

3. The previously cited techniques are only applicable over the ocean. Space- and aircraft-borne rain observation systems now utilize or are planned to utilize both radiometers and radars. An estimate of A can be obtained from the approximate hydrometeor profile that can be derived from the radiometric data only. Such a technique is applicable over both land and sea.

VIS/IR USE AND LIMITATIONS

Although TRMM rainfall estimates will depend primarily on the passive and active microwave components, the VIS/IR data should aid in the final determinations in several important ways, among them confirming the presence of clouds and measuring their height. Furthermore, these data will be useful to study high resolution cloud structure and possibly the environment of the rain systems. Most important, however, is the role of the TRMM VIS/IR data set as a bridge between the TRMM system's rain estimate and the high temporal resolution geosynchronous rain estimates, which are limited to VIS/IR.

Despite the fact that VIS/IR rain estimates are necessarily inferential (precipitation is inferred from cloud observations), interest in making such estimates remains strong. The reason for this is the short duration and high temporal variability of precipitation events; observations with high spatial and temporal resolution are thus needed. Recent work in VIS/IR rain estimation is summarized in Table 23.

Perhaps the simplest approach to rainfall estimations is that of Arkin and Meisner (1987), who found that a climatological rainfall rate applied to rain areas delineated approximately by cold cloud top temperatures was adequate to account for much of the variance of tropical rain. As a limiting case (with radar to give a more accurate rain area outline), Chiu (1987) explained 90 percent of the variance of rainfall in the GATE area.

Inoue (1987) has used a split window technique to delineate raining areas from AVHRR imagery. The principle that underlies this technique is that while both cirrus and cumulonimbus clouds may be cold and bright, the spectral dependence of the emissivity of ice and water clouds differs in the infrared window. By comparing the difference in the brightness temperatures at 11 and 12 m to the mean value, the two phases can be readily discriminated. The presence of precipitation was identified by comparisons with radar. Figure 48 shows an example of rainfall distribution obtained by this technique.

The CST of Adler and Negri (1988) defines convective cores and assigns rain rate and rain area to these features based on the IR brightness temperature (T_B) and the cloud model approach of Adler and Mack (1984). It identifies the associated anvil stratiform rainfall area by a threshold T_B, the value of which is calculated from the satellite data itself. The use of a one-dimensional cloud model (Cheng, 1981) to account for ambient temperature, moisture, and shear conditions provides a stronger physical, less empirical basis for the cloud-height/rain relationships. It potentially allows for the transportability of the technique to various climatological regimes. Figure 49 illustrates a comparison between the results of the CST and calibrated radar estimates of rainfall. Bellon and Austin (1986) and Wu *et al.* (1985) used VIS and IR data. This additional information appears to improve the retrieval skill. Because nocturnal precipitation is significant in the tropics, a nocturnal VIS sensor is being considered for TRMM.

TRMM rain retrievals are summarized in Table 24.

ROLE OF CLOUD MODELING AND AIRCRAFT EXPERIMENTS IN ALGORITHM DEVELOPMENT

It is necessary to test and improve the rain retrieval algorithms as much as possible before the TRMM satellite is launched. One way to do this is to simulate a raining cloud or field of clouds, overfly the simulated situation with an imaginary satellite, and calculate the field of brightness temperature, T_B, from a radiative transfer model. Next, one or more of the retrieval methods just described can be used to derive the rain rate from the T_B field over various-sized FOV's. Finally, the retrieved rain is compared with that predicted by the simulation over the same area.

Fortunately, meteorologists' ability to simulate how cloud motions initiate hydrometeors and the dynamical/microphysical interactions throughout cloud life cycles has advanced enough in the past five years (Cheng, 1981; Lin *et al.*, 1983; Rutledge and Hobbs, 1984; Soong and Tao, 1980; Tao and Soong, 1986; Tao *et al.*, 1987) to permit useful simulations of rain retrievals by remote sensing. However, restrictions posed by still arbitrary modeling assumptions, limited computer power, and a wide variety of cloud conditions require that the simulated results be compared with actually measured brightness temperatures in several channels under as many conditions as possible. This means that a series of high-altitude aircraft overflights with radiometers must be made in locations where carefully calibrated radars, gauges, and other sensors

Table 23. Recent Research in VIS/IR Satellite Rain Estimation

Study	Thrust
Adler and Mack, 1984	A cloud modeling approach to cloud height/rain-rate relationships
Adler and Negri, 1988	Convective-stratiform technique (CST): Relationship between gradient and minimum of IR brightness temperature only as a function of rainfall
Arkin and Meisner, 1987	Threshold approach for climatological purposes
Bellon and Austin, 1986	Two-channel approach, using VIS brightness with IR temperatures
Inoue, 1987	Difference between two IR window channel T_B's versus average window T_B is related to rain area
Martin and Howland, 1986	A multi-spectral time dependent technique for tropical daily rainfall
Tsonis and Isaac, 1985	Multi-spectral classification of rain/no-rain
Wu *et al.*, 1985	Multi-spectral/multi-textural analysis of satellite imagery

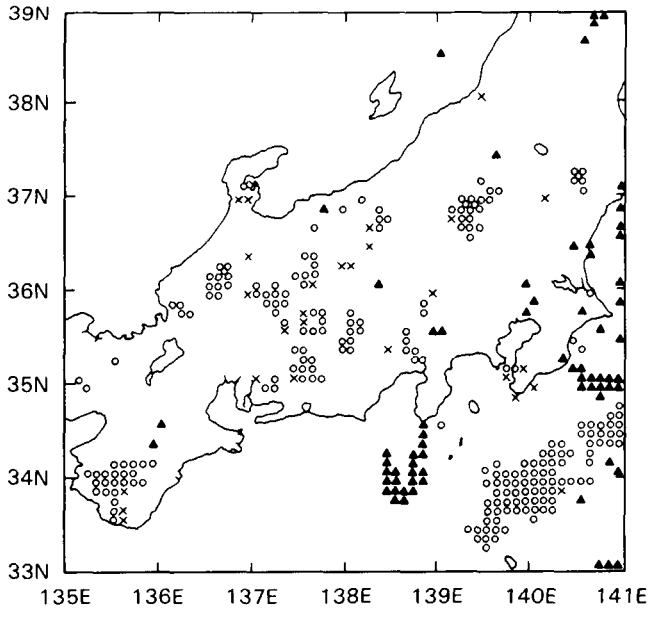

Figure 48. The verification map of Inoue's split window technique for the case of July 27, 1984. The hit, false alarm, and miss are indicated as a circle, a triangle, and a cross, respectively.

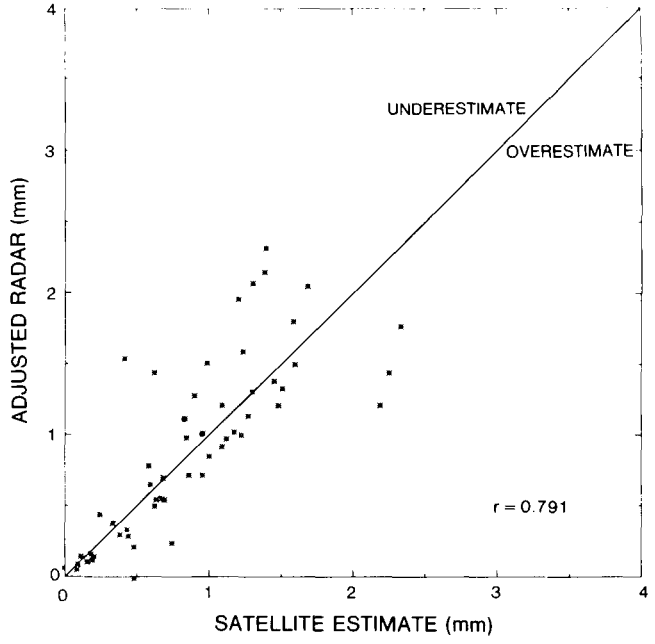

Figure 49. Scatter plot of CST estimates of FACE area average rain depth (mm) from half-hour interval IR data on 4 days using gauge-adjusted radars as ground truth.

provide "ground truth". The interactive procedure whereby cloud microphysical-dynamical models are coupled with cloud radiative models and used with observations to support each other is outlined by a flowchart in Figure 50.

Since 1979, NASA has been developing a high-altitude aircraft program with a remote sensing package for examining cloud and precipitation properties, with the ultimate goal of using these for space-based studies of cloud radiation, rainfall, severe storms, and other cloud-related aspects of Earth system science.

During the summer of 1986, a series of flights by NASA's ER-2 aircraft (20-km operating altitude) was made as part of COHMEX. The aircraft carried a number of remote sensing instruments, including the Microwave Precipitation Radiometer (MPR), with dual-polarized channels at 18 and 37 GHz with an along-track view at 45° from nadir toward the front of the aircraft. The Advanced Microwave Moisture Sounder (AMMS) scans across the aircraft track ±45° from nadir at 92 GHz and at 3 channels centered arounded 183, i.e., ±2 GHz, ±5GHz, ±9 GHz. Data obtained from the MPR and

Table 24. Rain Retrieval Summary*

Passive Microwave

Piece-wise linear regression using plane parallel radiative model—or horizontally finite cloud model

Model inversion scheme using finite geometries

Dual polarization technique

Multi-channel decision tree to select single channel look-up table

Radar

Algorithms based on backscatter power (Z-R) relations — light rain

Algorithms based on attenuation — moderate rain

- Single- or dual-wavelength** surface reference method
- Conventional dual wavelength**
- Single wavelength attenuation profiling with surface reference or radiometric bound
- Mirror-image method
- Echo-area and height correlated with rain rate — Height Area Rainfall Threshold (HART)

Combinations of Instruments

Combination of radar, multichannel passive microwave measurements places constraints on radar equation to obtain vertical hydrometeor profile from single wavelength radar

Consistency between radar and passive microwave

Use VIS/IR to resolve some of footprint filling problems

*Rain rates from light to heavy—calibrate with other algorithms.

**In TRMM, we shall utilize only single wavelength methods.

AMMS, along with ground based radar, have been used already to develop the new rain retrieval technique discussed previously in this chapter. Furthermore, the cloud population model of Tao was able to successfully reproduce the cold temperatures obtained by the passive microwave over the most intense convective core (see Figure 51) observed during COHMEX (Simpson *et al.*, 1988) giving assurance of its value in future TRMM simulations. This result is important because cloud population models will be needed to help obtain vertical profiles of latent heat release from the TRMM radar data, which will provide the vertical profiles of rain rates.

In the 1988-1990 period it is intended to begin flying an instrument package increasingly similar to the planned TRMM complement on a single DC-8 or T-39 aircraft. This aircraft will also have *in situ* instruments such as the Knollenberg 2-D and 3-D particle samplers for slow ascent through the clouds. By 1992, an airborne TRMM rain radar under design at the Jet Propulsion Laboratory is expected to be ready for participation in a planned mid-Pacific joint field experiment with the TOGA program.

SUMMARY AND CONCLUSIONS

Our conclusions at this time are that the retrievals are sufficiently far advanced and tested to meet the basic requirements of TRMM goals with the minimum payload outlined. A larger range of passive microwave frequencies, however, would be highly desirable on future rain-measuring satellites. The additional low-frequency channels (6.6 and 10 GHz) would be useful because of their more linear response to high rainfall rates. Extra frequencies would also provide added confidence to the retrievals, as well as calibration for satellites already making rainfall measurements.

Concerning the radar, extension of the dynamic range and the addition of a second frequency, which would add to the available algorithms and refine vertical profiling, appear to be out of sight for TRMM. This first exploratory mission must be designed within limitations of power, space, weight, and resources, which can be relaxed considerably when a rainfall package is designed for future platforms, such as the Space Station. A most important improvement of radar capability

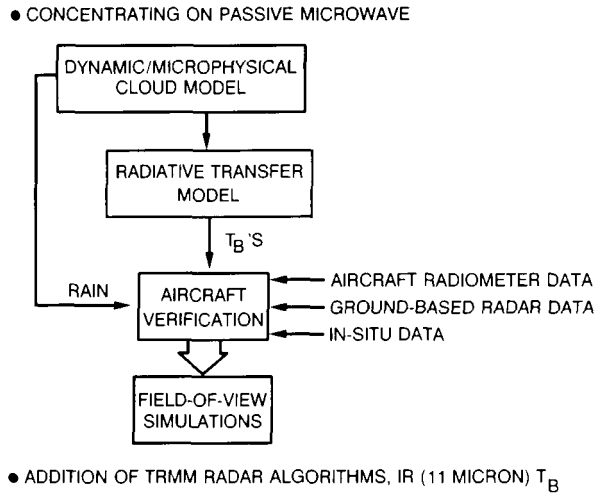

Figure 50. Flowchart showing how cloud dynamical-microphysical models are used together with a cloud radiative model and aircraft and other data to test and improve rain retrieval algorithms. To date, this approach has been used only with passive microwave algorithms (Simpson *et al.*, 1988).

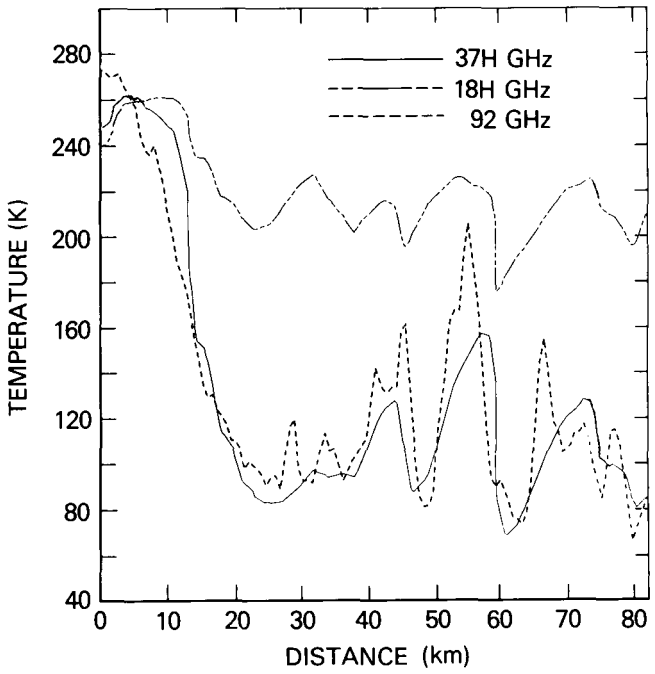

Figure 51. Traces from passive microwave channels as the ER-2 high-level aircraft flew over the cumulonimbus towers (radar echoes shown in Figure 46) on June 29, 1986. T_B is plotted against time for each channel. The top curve is from the 18 GHz channel. The middle curve is from the 37 GHz channel and the lowest curve is from the 92 GHz channel. Instrument viewing offsets have been corrected, so that low temperatures coincide in all three channels (Simpson *et al.*, 1988).

would lie in the increase of the scan angle to cover the whole 600 km swath. Even if the results outside the ± 20 near-nadir swath are of poor quality, the extension is worthwhile firstly, if it does not compromise the data quality within ± 20 of nadir and secondly, if the rain echo areas can be delineated over the whole extent of the sampling swath. This swath extension would enable the HART technique to be applied over the entire viewing field of the passive microwave observations, leading to more powerful hybrid retrievals. Table 25 summarizes TRMM rainfall and latent heat profile retrievals.

Table 25. Summary of TRMM Rainfall and Latent Heat Profile Retrievals

I. Passive Microwave Multichannel Retrievals

A. Improved plane parallel radiative models tested in a few cases by aircraft, surface radar data using coupled microphysical/dynamical cloud population models. Other multichannel retrievals tested with SMMR data.

B. Horizontally finite cloud radiative model, tested on simulated SSM/I data. Being coupled with cloud microphysical/dynamical model to test with actual SSMM/I data, together with surface radar.

II. Radar

Family of four algorithms developed, three of which have been tested by aircraft flights, and good results obtained.

III. Hybrid Retrievals

A. Radar and microwave combined analysis: Preliminary aircraft tests by Japanese and with COHMEX data, good results; vertical profiling simulation being developed, report in 1988.

B. Use of HART technique together with other radar and multichannel passive microwave algorithms — in progress, report in 1988.

IV. 1988 on: Aircraft Program with all TRMM Instruments: Two Heavily Instrumented Sites with Multi-Parameter Radars (Florida, Mid-Pacific, and Darwin, Australia)

A. Retrieval techniques (single and combined) will be applied with the aircraft remote data and tested over both land and ocean validation sites.

B. Cloud models will be used and aircraft *in situ* data obtained as resources permit.

VII. GROUND TRUTH

GOAL AND OBJECTIVES

The goal of the ground truth component of the TRMM is to provide rainfall measurements which will allow the validity of the TRMM measurements to be established within specified limits. Such rainfall measurements must be made at a number of sites which are representative of the major tropical rainfall regimes of the globe. The validation measurements must furthermore be made over a range of time and space scales which adequately reflect the rainfall and the sampling characteristics of the TRMM.

The ground truth goal is developed in three stages, each with distinct objectives:

1. Pre-mission
   - development of a central facility for precipitation research and to calibrate rain measuring instrumentation and techniques (algorithms);
   - development of transfer standards;
   - development of rain climatologies; and
   - development of mission validation sites.
2. Mission
   - validation of mission measurements;
   - calibration of mission measurements; and
   - provision of supplemental data.
3. Post-mission
   - interpretation of results; and
   - definition of second generation requirements.

The most pressing concern early on is the pre-mission phase. Efforts in this area must be accelerated if we are to adequately support the mission by the mid-90's time frame.

BACKGROUND AND GENERAL STRATEGY

The technology for detecting precipitation through remote sensing is reasonably well in hand. However, the real challenge is in interpreting the spaceborne measurements because of the kind of sampling that results from the extreme variability of rainfall in space and time. Furthermore, to be meaningful in terms of latent heat release, the vertical structure of the precipitation is almost as critical as the horizontal distribution. Thus, for a space rainfall project to be truly successful, well instrumented and calibrated validation sites must be established within the area of satellite coverage. Such data can also make an important contribution to climate diagnostics as well as enhancing the space data set. This end objective requires a substantial pre-mission program because there remain serious limitations regarding the measurement of rainfall by conventional means, particularly over extended areas. The pre-mission program objectives must also include understanding of physical processes associated with rainfall and its regional characteristics and variability, studying sampling and statistical approaches, developing climatologies of key validation sites and supporting measurements for instrumentation and algorithm development. Equally as important is establishing a transfer standard of measurement technology and procedures for the mission validation sites. The critical dependence on a well-developed surface-based rainfall observational program to ensure credible rainfall products from space was recognized early on at a workshop on the Measurement of Precipitation from Space in 1981 (Atlas and Thiele, 1981).

Rainfall, unlike other key atmospheric parameters, is extremely variable in space and time. Not only is rainfall unevenly distributed in occurrence, but the rate is highly variable even over a single convective rain system. In the tropics, of course, the rain originates mainly from convective systems. For these reasons, rain has always been an elusive parameter to measure. There still remain substantial uncertainties with the best available rain gauges even for point measurements, and, when attempting to quantify areal rainfall, the uncertainties begin to magnify significantly. Thus, a fundamental task of the "ground truth" strategy is precipitation *measurement* research. Better ways must be found to obtain reliable area averaged rainfall to properly verify the quality and usefulness of space measurements.

A general strategy for accomplishing the three stages of mission activities described earlier is outlined in Table 26. However, the focus here will be on the two main components of the validation programs, i.e., pre-mission and mission, as envisioned at the first TRMM workshop (Thiele, 1987). Although the end objective is to provide reliable comparative data during the mission for area and time averaged rainfall representative of the tropics, instantaneous comparisons will be attempted as well. To achieve the end objective, however, a strong pre-mission program is critical and must be organized and implemented without delay. Thus, initially, the emphasis is on the pre-mission phase. Not only must we be prepared to acquire reliable validation data when the mission begins, but we must also learn how to do it beforehand. Support of mission development activities is a requirement as well. Elements of the validation program are outlined in Figure 52.

PRE-MISSION STRATEGY

The pre-mission strategy will encompass a variety of activities: 1) development of primary rain measurement standards at a primary first order test facility, 2) development of transfer standards, 3) the establishment of second order test sites in representative rainfall regimes, and 4) development of cooperative agreements to establish additional "ground truth" sites for the mission. Figure 53 shows the location of planned and potential sites relative to TRMM spacecraft coverage. More explicitly, the pre-mission phase must focus on rain measurement research, state-of-the-art measurements for rain processes, variability studies, and development of measurement and procedural techniques for calibrating the mission

Table 26. Experimental Rainfall Methods

Device	Advantages
Optical rain gauge	Fast response, wide dynamic range
Zenith pointing VHF-UHF doppler rain gauge	Explicit vertical velocity, drop size distribution (DSD), rainfall rate, level of diabatic heating
Scanning doppler radar	Mesoscale vertical motion, profiles of condensate production and fallout
Multiple frequency polarized radar	Observations over water, semi-independent estimates of rainfall
Microwave attenuation	Calibration of radar statistics over land and observations over water
Satellite beacon attenuation	Sampling over remote (ocean) areas
Airborne doppler radar	Sampling over oceans/remote areas
Underwater hydrophones	Sampling over oceans, integration of rainfall over a surface area
Profilers	Vertical structure in and near convective cloud systems

ground truth sites. Other important functions of the test sites are to support flight instrumentation and algorithm development and to collect long term climatological rainfall data bases for their respective regimes.

Primary Standard

No adequate methods exist for the measurement of rainfall at the surface and in the atmospheric column. Concurrently, estimates of absolute standards and estimates of error of the measurement of rainfall are deficient or absent. These deficiencies and the objectives of TRMM can best be served by the establishment of a world class test facility for the calibration and testing of both new ground based and remote sensing instruments on aircraft and the TRMM including the algorithms used with them to give rainfall estimates.

We believe that no single method for the measurement of rainfall will provide an adequate estimation of rainfall on the range of time and space scales that are required. We thus believe that a hybrid system must evolve.

Such a *hybrid* system must be based upon *current techniques* such as radar reflectivity combined with rain gauges but must be capable of including new techniques. However, a fundamental improvement and understanding of the Z-R relationship is a must if we are to derive reliable quantitative rainfall amount from radar reflectivity measurements. It is becoming increasingly evident that a dedicated coherent radar with *polarization diversity* is required at the primary test facility for this improvement. In addition to rain measurement research such a radar is of fundamental importance for all components of precipitation research, especially the microphysics in rain system, and for transfer technologies as well.

The design of a world class test facility must be based upon both a broad knowledge of potential measurement techniques and an in-depth statistical analysis of sampling methodology of tropical convective rainfall. We believe that such a statistical analysis, designed to optimize the observational network of the test facility as well as subsequent field facilities, is essential.

We wish also to stress that there is an urgent need to acquire a detailed rainfall data base comparable to or better than that obtained during the GARP GATE. We believe that the GATE rainfall data set can be improved upon by increasing time and space resolution, the number of techniques employed, and the length of time covered by the observations. We recommend below that the Primary Rainfall Test Facility (PRTF) be based in Florida in the vicinity of the Kennedy Space Flight Center; we wish in particular to stress the need to make open ocean rainfall measurements. Thus, emphasis must be placed upon measurement of rainfall over the ocean adjacent to the PRTF where calibration over land can be accomplished with a large number of properly distributed rain gauges. The ability to make rainfall measurements out to 200 km offshore will be sought. Fortunately, the Cape Canaveral area is in an ideal location for this purpose.

Transfer Standard

The PRTF is seen as a test bed for new techniques. Facilities to test new methodologies should be provided together with the requirement that the validity of all new techniques should be demonstrated through inter-comparisons conducted at the facility. Table 26 outlines a number of experimental rainfall measurement techniques and anticipated advantages.

Some of these, notably Doppler and polarimetric radar and profilers, are expected to be important measurement tools for investigating the vertical structure of rainfall. In the validation of TRMM observations, the vertical structure is essentially as important as area averaged rainfall. To model the effect of released latent heat on global circulation, the height at which it occurs must be known. Thus, for vertical structure measurements, including phase, and to develop reliable reflectivity

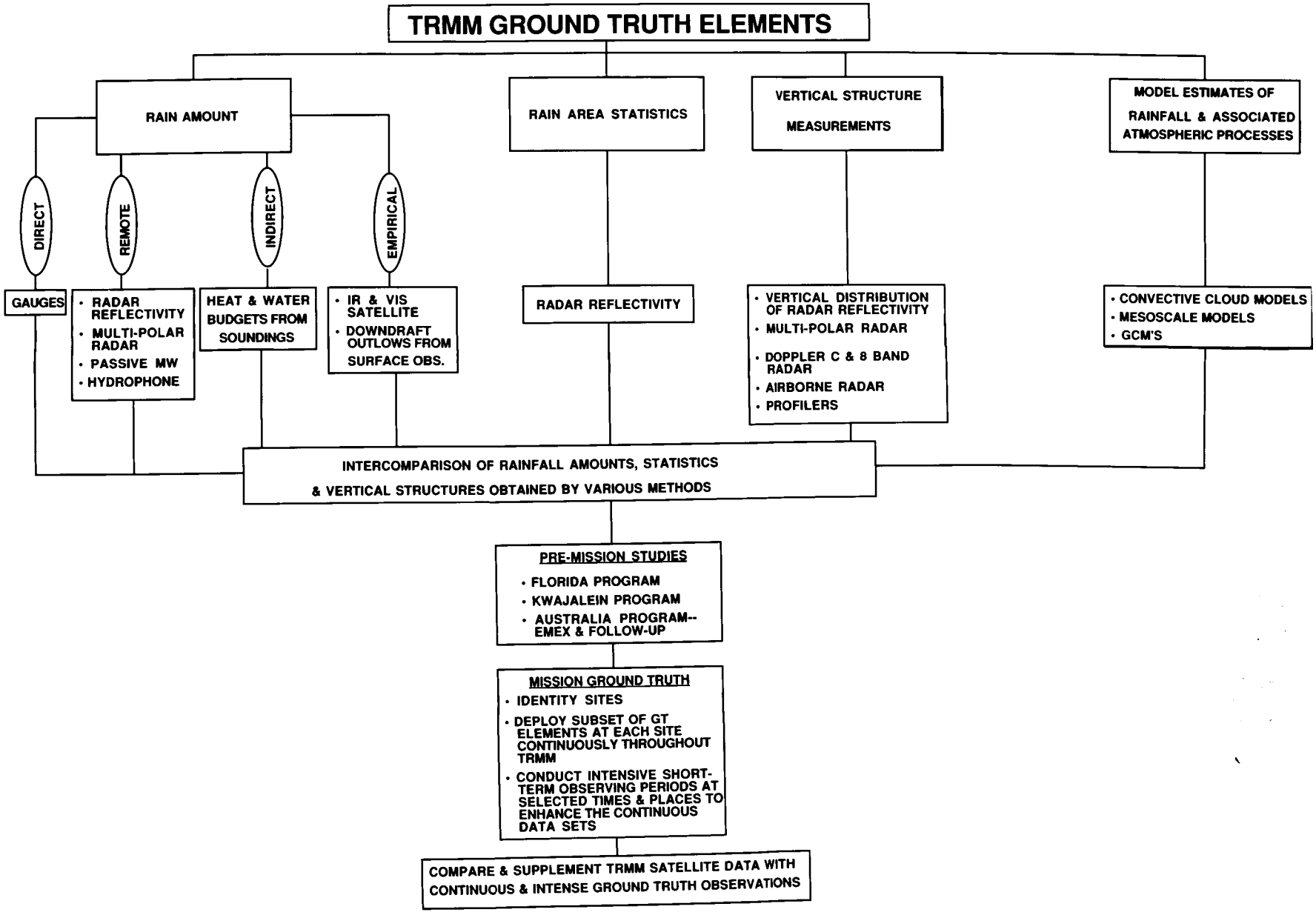

Figure 52. Hierarchy of activities necessary to validate TRMM observations.

ORIGINAL PAGE
COLOR PHOTOGRAPH

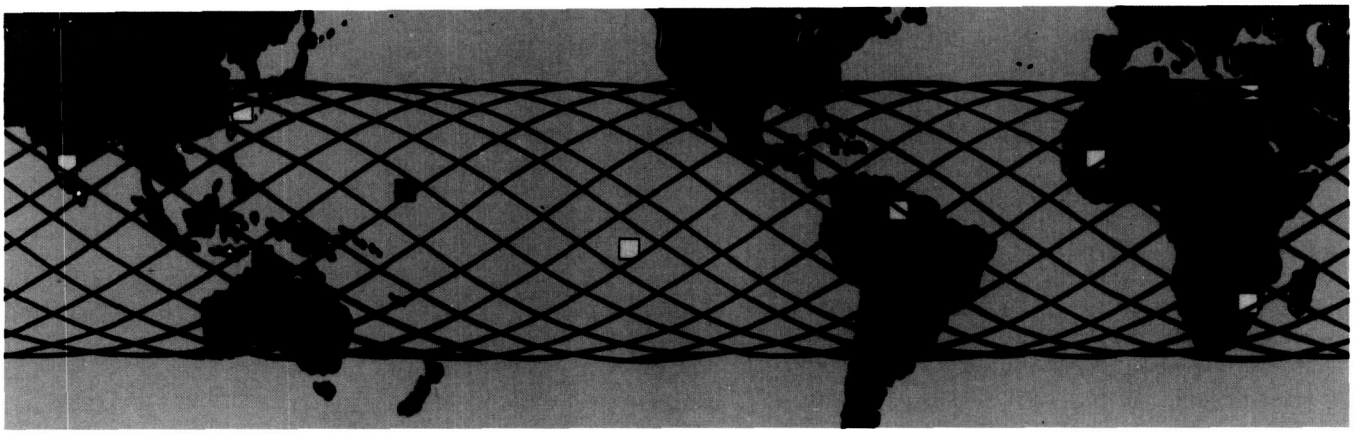

Figure 53. The red square shows the location of the primary test facility (central Florida). The secondary test sites are identified with green squares and potential sites for other representative rain regimes are indicated with yellow squares. Radar and rain gauge data are already being collected at the Florida, Australia, and Kwajalein sites and observations are expected to begin in Thailand during 1989.

relationships, the need for a dedicated multi-parameter radar for the primary test site cannot be overemphasized. Plans are already underway for a profiler to be installed at the Kennedy Space Center (KSC) to support weather forecasting for shuttle operations. The profiler also promises to be an important tool in vertical structure studies.

For improving surface measurement techniques, a small scale experimental rain measurement research facility, Figure 54, is being developed to determine the best methods and equipment to deploy at the primary test site. A polarized multi-frequency microwave attenuation link will be the key component of the facility. Attenuation of horizontally propagating microwave radiation is strongly related to the intensity of intervening precipitation and less sensitive than radar Z-R to rain DSD (Crane, 1985; Ulbrich and Atlas, 1985). If this technique can be successfully developed it will provide an accurate way of determining mean rain rates over large areas.

Under the microwave transmission path will be a number of state-of-the-art rain gauges for calibration. Also, at least two new "gauge" techniques will be investigated, i.e., an optical rain gauge and an upward looking Doppler rain gauge. The CRL of Japan is planning to participate in this research.

Two other methods of obtaining corroborative rain data are through inference from mass, heat, and moisture budgets derived from surface wind measurements or rawinsonde data. In one technique, convective outflow at the surface is related to rainfall (Ulanski and Garstang, 1978a, 1978b, 1978c). The downward vertical velocities are integrated over time and space to estimate downward mass transport which in turn can be directly related to rainfall. Over much larger areas surface fluxes of precipitation are inferred from heat and moisture budgets calculated from upper air soundings describing a large volume of atmosphere. (See, for example, Brummer, 1978.) This budget method is one of the few techniques that can provide an estimate of rainfall amount on the largest scale of interest to TRMM.

A goal at the PRTF is to develop a hybrid system which will, in turn, lead to a standard or set of procedures to transfer to other sites. The test facility must, therefore, provide the opportunity for the measurement and estimation of rainfall via a wide range of possible techniques. It is probable that a variety of measurement techniques will be employed at the individual sites to yield estimates of rainfall. The key functions of the PRTF are summarized as follows:

- Rain measurement technique development;
- Precipitation research, e.g., physical processes/variability/distribution characteristics, etc.;
- Sampling and statistical studies/error estimation;
- Data assimilation methodologies;
- TRMM scale climatology development;
- Support to instrumentation and algorithm development;
- Development of a hybrid system as a transfer standard; and
- Major "ground truth" site during the mission (maximum overflights occur near the latitude boundaries of the orbit).

Secondary Test Sites

An important parallel task during the pre-mission stage is to identify and begin to develop secondary ground truth test sites. These secondary test sites, of course, will become primary validation sites during the mission. Three important tropical rainfall regimes should be represented in the location of the secondary sites, aside from the higher latitude convective regime represented by the PRTF, to provide baseline climatologies and to support specialized field experiments. The three regimes are:

1. ITCZ rainfall
   - oceanic
   - continental

2. Monsoon rainfall

3. Dry zones (minimal rainfall area)

Evidence exists that the rainfall characteristics at the surface and with height are distinctly different in each of the three regimes identified above. Time and space relationships of rainfall are different in each regime. The amount and rate of rainfall varies for different rain producing systems even when these systems consist primarily of intense convective cores. The amount of rain produced in the core and in the anvils shows large variation (Houze, 1981; Houze and Hobbs, 1982). Failure to monitor these variations for validation of TRMM measurements could lead to considerable uncertainty or even serious error. Sampling of at least one dry region in the tropics is suggested to guard against errors of over estimation.

Candidate sites for some of the above rainfall regimes already exist. For example:

- Kwajalein Atoll
- Darwin, Australia
- Thailand
- Amazon Basin
- Sahel

Other locations where reasonably reliable rain data is being collected need to be identified.

MISSION STRATEGY

During the mission we view the ground truth strategy to be embedded within a hierarchical structure of rainfall measurements. Most important are:

- primary (first order) validation sites (e.g., central Florida; northern Australia, western Pacific (Kwajalein), northern Thailand;
- second order validation sites (e.g., central South America, India, Africa, eastern Mediterranean (Israel), etc.);
- coordinated near instantaneous as well as integrated measurements for validation between latitudes 35°N and S;
- use of airborne doppler radar for instantaneous validation measurements over oceans; and
- infrared estimates of rainfall in the tropics and to high latitudes from geosynchronous satellites.

The ultimate utility of the mission and the range of scientific questions that can be addressed depends critically on the effective handling of the combination of these data. The TRMM instruments capture instantaneous rainfall rates and their height distribution at tropical locations several times a day. The validation of this system may be attempted in two ways:

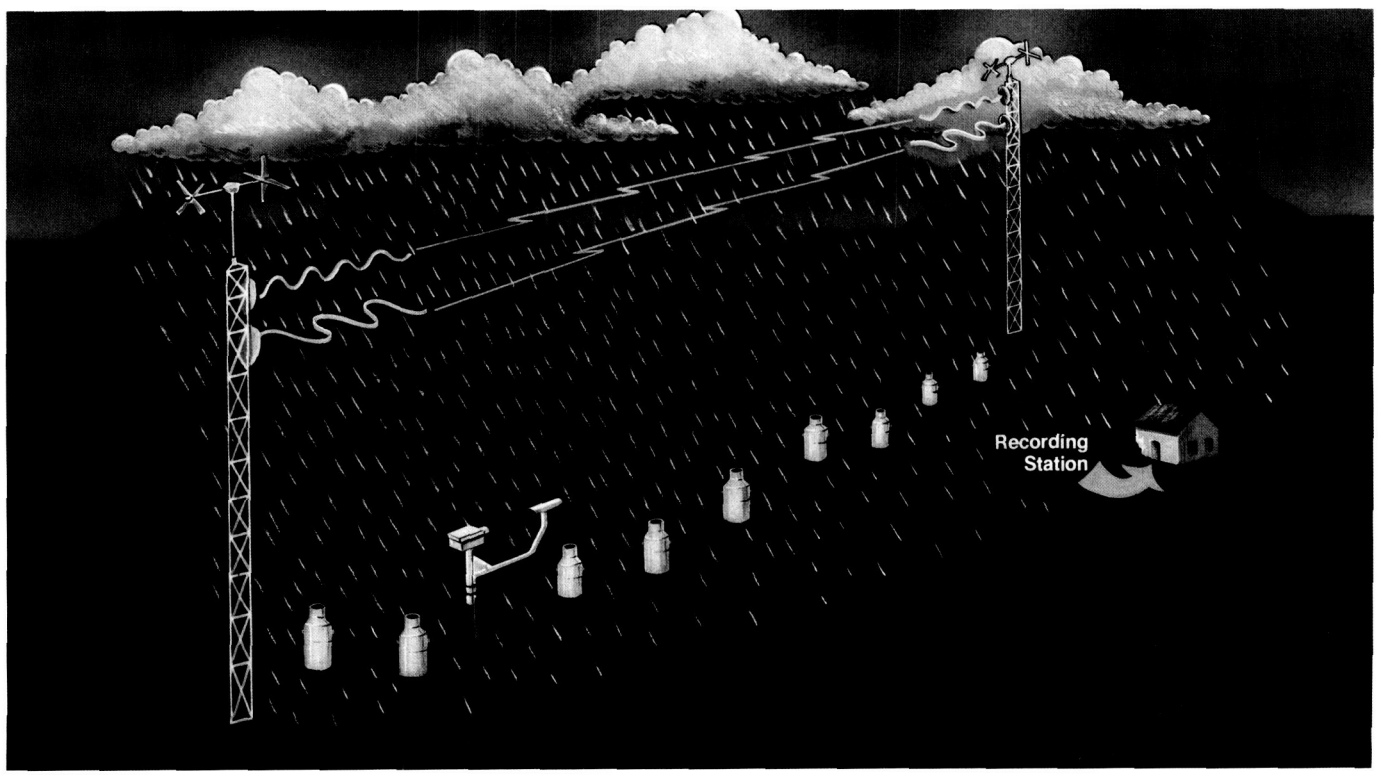

Figure 54. Artist's concept of attenuation link indicating vertical and horizontal polarization and supporting rain gauges. Planned frequencies are 8, 25, 38, 80, and 240 GHz. CRL (Japan) plans to furnish the 80 and 240 GHz systems.

1. average the TRMM rainfall data for several months over large areas (600 × 600 km) and compare with climatological values, and

2. compare both the rainfall and height distribution data from TRMM with the instantaneous values observed at one or more "ground truth" stations.

Both of these strategies depend on the availability of high quality "ground truth." The climatological schemes might work with gauge network data alone if a dense enough network were deployed over an entire 600 × 600 km box. The instantaneous calibration scheme, however, depends on the availability of four-dimensional precipitation data with radar for the key rainfall regimes in the tropics. The second strategy has the advantage that it will verify the accuracy of the TRMM instruments much more rapidly than the climatological approach and will allow the more rapid development of sophisticated algorithms. It also verifies the height distribution data.

The Geostationary Operational Environmental Satellite (GOES) data perform an essential link in allowing the TRMM instruments to be used to contribute to a variety of techniques which can be used to give global precipitation estimates of known accuracy in near real time. This step allows a hierarchical scheme such that:

1. ground truth at one or a few locations calibrates TRMM, and

2. TRMM calibrates global rainfall estimates from GOES sensors.

Operating any of these schemes without the others will necessarily produce rainfall estimates that have more limited accuracy and coverage than will be otherwise possible.

The mission strategy for validation must also include those indirect methods that have proved to be useful in the pre-mission intercomparisons (see Figure 52). Budget studies as well as comparisons to model-estimated precipitation amounts may serve as sensitivity tests placing bounds upon the acceptability of the TRMM observations.

FIELD EXPERIMENTS

Pre-mission field experiments are required to serve a multiplicity of research and mission development objectives, i.e., aircraft flights for radar and radiometer instrument/system development, algorithm development and testing, basic research on physical processes related to rainfall initiation and distribution characteristics, verification of cloud models, and, not least, the development of primary and transfer standards leading to establishment of large area "ground truth" observational systems for the mission.

In addition to limited and specialized field studies tailored to TRMM needs, the program will take advantage of and participate in other major field experiments such as the proposed storm activities tentatively planned for the summer of 1990 and a western Pacific experiment presently being discussed for the early 1990's under the sponsorship of the TOGA program.

During the mission, carefully designed field experiments will be necessary to assess, understand, and possibly enhance the data sets that are to be developed.

POST MISSION STRATEGY

We wish to stress the fact that the value of the TRMM measurements extends well beyond the direct measurement of rainfall at the ground. The real scientific value of these measurements lies in their contribution to the understanding of atmospheric processes ranging from local release of latent heat in the atmospheric column to synoptic and planetary scale water vapor, and heat and energy budgets. Successful TRMM measurements will be incorporated into model calculations and will serve as a check of model estimates of precipitation. A substantial effort should be planned to ensure that the TRMM measurements are fully utilized.

We believe that in the ground truth response to TRMM, substantial advances in our understanding of rainfall and our ability to measure rainfall will have been made. Furthermore, it is realistic to assume that these achievements will form the foundation for validating other space-based measurements such as those from the Eos. The support fabric constructed for TRMM should be applied to these efforts.

The measurement of precipitation from space is an extremely difficult problem under the best circumstances, and validation (probably calibration as well) of the space measurements is crucial to a successful TRMM program. Therefore, substantial project resources will be required for the entire ground validation program.

VIII. SCIENCE DATA PROCESSING/MANAGEMENT

BACKGROUND

The tasks of processing and managing the science data are likely to be more complex for TRMM than for most previous science missions because of the sheer volume of data. Individual processing of the high-rate data from each instrument is in itself a formidable task, but added to that is the complication of interrelated processing of the data from several instruments because no single instrument provides all of the information necessary to develop the most complete and accurate rainfall data product. Furthermore, the science data processing system will have to accommodate the almost equally complex task of assimilating the wide variety of "ground truth" observations that will be acquired from many representative regions in and near the tropics. A complement of surface-based rainfall data products similar to the space observations will have to be produced to validate, calibrate, and even enhance the TRMM data sets.

Inherent in the definition and development of a science data processing system of this scope is the parallel development of complex algorithms. In addition to a sophisticated theoretical approach to the problem, the algorithm development effort will include a strong experimental component involving instrumentation testing with aircraft, precipitation measuring technique research, etc., through various field experiments.

While the focus of this chapter will be on the science data processing system concept for TRMM, a brief outline of the total data system, including data acquisition and the Level 0 data processing procedure is described. Figure 55 shows the overall TRMM data flow.

DATA ACQUISITION AND LEVEL 0 PROCESSING

The TRMM spaceborne sensors will collect data at a total rate of 185 kbps and store the data on on-board recorders. The recorded data will be played back twice per orbit at a 5 Mbps rate via the Tracking and Data Relay Satellite System (TDRSS). TDRSS will relay the data to the Payload Operations Control Center (POCC) at the Goddard Space Flight Center via the NASCOM, as shown in Figure 56. TDRSS will provide command, telemetry, and tracking support for TRMM. There will be a dedicated facility at the POCC to handle high-rate TRMM data. The spacecraft (non-science) telemetry data will be processed by the POCC and displayed in the Mission Operations Room (MOR) for the Project Flight Operations Team (FOT). The FOT will be responsible for the health, safety, and operation of the spacecraft. Commands generated in the POCC will be transmitted to TRMM via NASCOM and TDRSS. Spacecraft attitude data will be decommutated in the POCC and transmitted to the Flight Dynamics Facility (FDF) as an element in the computation of the spacecraft orbit. Orbit maneuver support will also be provided by the FDF to place and maintain TRMM in the mission orbit. The Command Management System (CMS) will prepare stored command loads based on inputs from the FOT. The command loads will be sent to the POCC for transmission to TRMM.

Data from the spacecraft tape recorders will be processed by the Sensor Data Processing Facility (SDPF). Level 0 processing of the data includes data capture, recording, tape recorder playback, overlap removal, time ordering, quality checking, annotation of missing data, and decommutation of data for each sensor. The decommutated Level 0 sensor data and ephemeris data will be transmitted to the Science Data Processing Center (SDPC) at a minimum 1 Mbps data transfer rate for further data processing and analysis. The Level 0 processing will differ to some extent if packetized telemetry data is the mode of operation during the TRMM time frame. A procedure that will make TRMM data available to Japan at the same time is being sought.

Tracking or ephemeris data for processing the science data can be provided in two ways. At present, it appears that the most economical method is TDRSS tracking for spacecraft position information and is therefore the first option. A second option is the Global Positioning System (GPS) which provides on-board position data that becomes part of the science data stream and ensures non-ambiguous Earth location. In order to provide similar rapid processing (as with GPS) the TDRSS ephemeris data must be routed back to the spacecraft and recorded with the science data for simultaneous playback. Either scheme requires an on-board computer and one of these two approaches must be used if data are to be re-routed in real-time for immediate processing in Japan. An on-board computer will also be required if packetized mission data is used.

SCIENCE DATA PROCESSING

Objective

The science data processing effort must be organized to ensure that 1) data will meet the requirements of the scientists involved in the experiment, and 2) the data approved for archiving will meet the highest possible quality standards. The responsibility for overseeing this objective rests with the TRMM Science Team, which is composed of participating scientists, who in many cases are members of the individual calibration, algorithm, and data validation teams.

The TRMM science data will be processed by the TRMM Science Data Processing Team (SDPT). The SDPT will operate a central SDPC for developing and implementing the TRMM data processing software, producing science data products from TRMM, processing and cataloging data from the data validation team, storing and cataloging correlative data, and distributing TRMM science data and other relevant data to Science Team members. When approved by the TRMM Science Team, SDPT will deliver Levels 1 to 4 data (Table 27) to NSSDC and other participating data centers for archiving and distribution. The SDPC will include a computing facility and necessary personnel to operate and maintain the facility. The SDPT will interface with members of the TRMM Science Team, which includes the Instrument Calibration Team (ICAT), Science Algorithm Teams (SAT), Validation Teams, and the NSSDC. The SDPT will receive technical direction from the TRMM Science Team.

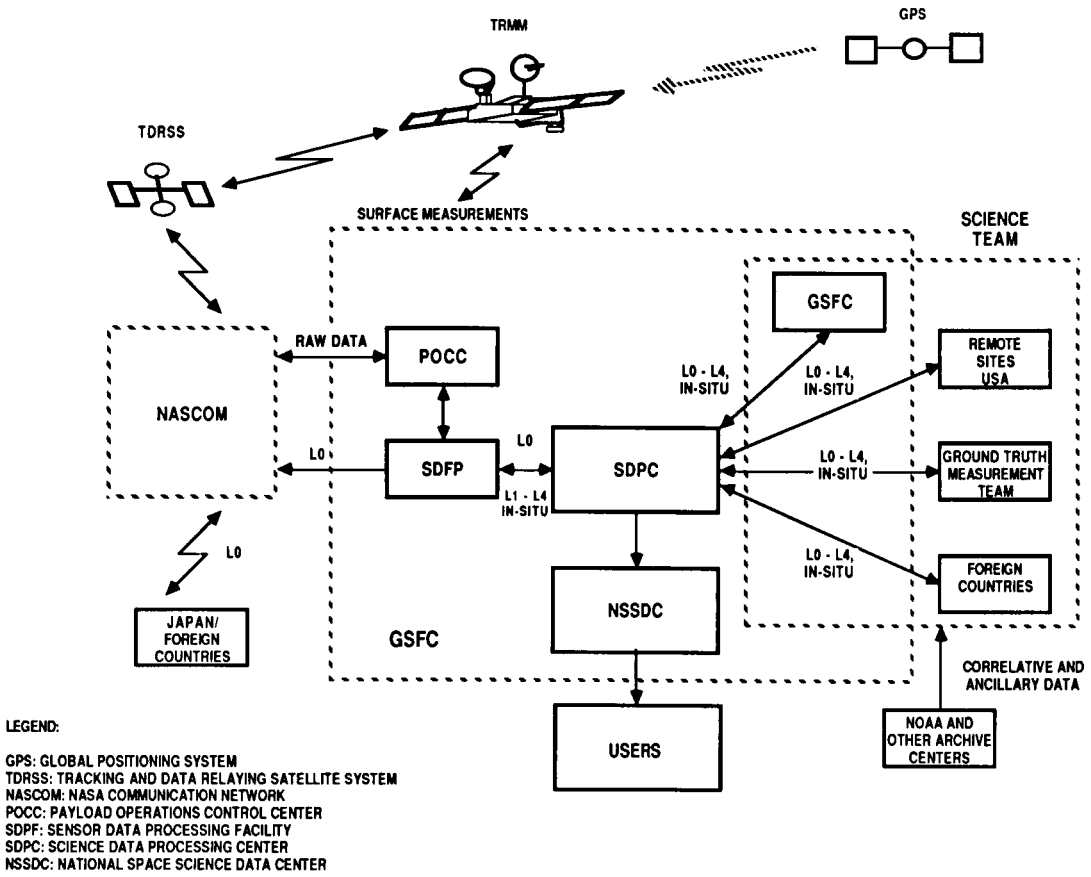

Figure 55. TRMM end-to-end data flow.

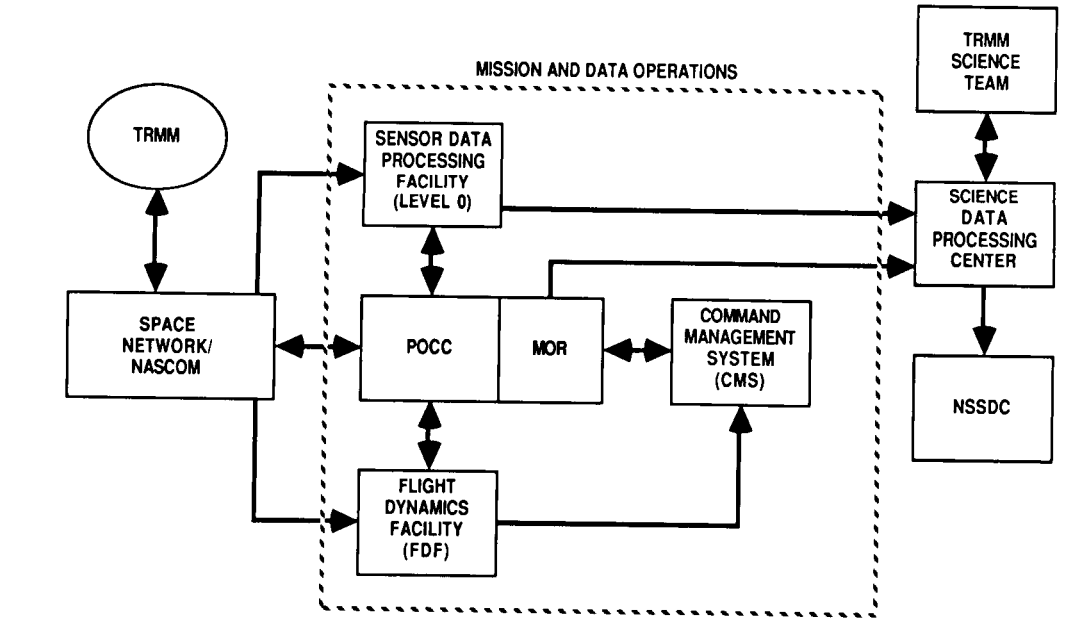

Figure 56. TRMM operational space/ground system.

Table 27. Definition of Data Levels

Level 1A	Instrument data in full resolution, reconstructed, and redundancy removed. Radiometric and geometric calibration, i.e., platform ephemeris, computed and appended, but not applied to Level 0 data. It is possible to reconstruct Level 0 data from Level 1A data.
Level 1B	Instrument data in full resolution with calibration and Earth location computed. It may not be possible to reconstruct Level 1A from Level 1B.
Level 2A	Derived physical parameters in full resolution.
Level 2B	Derived physical parameters with some averaging process applied. Will preserve orbital structure.
Level 3	Space- and/or time-averaged data product. Mapped on the Earth grids.
Level 4	Model and analysis results.

Data Sources and Products

The TRMM instrumentation complement presently planned includes 1) a two-channel VIS/IR radiometer (modified AVHRR), 2) a single-channel ESMR, 3) a multifrequency microwave radiometer (SSM/I), and 4) a rain radar. In addition, there are the surface-based data sources from the validation (ground truth) network.

A wide range of data products can be derived from the proposed instrumentation, especially at the higher levels. At this point, however, only a rather basic group of parameters has been identified to help size the problem. These products, generally referred to as Level 2 products, are physical parameters at the highest practical time and space resolution. The initial 13 TRMM-generated parameters, four validation parameters, and two other parameters necessary to produce TRMM data products are listed in Table 28.

The Data Processing Steps

Science data processing begins with reception of decommutated Level 0 science and ephemeris data from the SDPF, which should take place within a few hours after transmission from the satellite. It should be noted here that the processing software system will be in place 6 months before launch in order to have had time for extensive simulation processing with initial algorithms that were developed many months earlier. This will ensure a timely startup, but characteristically, many iterations and refinements will follow, with interactive participation by algorithm and calibration teams before satisfactory products are produced routinely. *This explicitly requires that the processing hardware be capable of handling both processing and reprocessing at the same time.*

The first step of science data processing is Level 1A (refer to Table 27 for a definition) data production. The Level 1A data set is the most fundamental data record that will be archived, and it is the foundation upon which subsequent data sets are produced. The Level 1A data record is, however, fully reversible to Level 0. There will be a separate Level 1A data set for each TRMM instrument.

The primary function of Level 1A processing is to merge instrument data with ephemeris data and generate a data set with location and attitude information appended. However, the location of each FOV may not be computed in order to save computational time and storage space. Instead, an interpolation method will be used. In case an interpolation scheme is used, the scheme will be tested beforehand to make sure that the interpolated location will meet the mission accuracy requirements.

The Level 1A data will be immediately processed to Level 1B data and transferred to off-line storage media to lessen the on-line data storage requirement. Calibration data and other engineering data necessary for calibration will be extracted from the Level 1A data and stored separately for further analysis.

Level 1B data sets will likewise be developed for each TRMM instrument. The Level 1B software processes instrument data in terms of radiance temperatures and reflected power with fully corrected Earth locations and with instrument calibration algorithms applied. The Science Team is responsible for providing these algorithms. The Level 1B data will be processed to Level 2A immediately if the processing does not require any other ancillary data, i.e., data other than TRMM data. Until Level 2A processing is completed, Level 1B data will be stored on-line. Once the Level 2A processing is completed, Level 1B data will also migrate to off-line storage media. It should be noted, however, that under no circumstance will Level 1B data be stored on-line more than 24 hours. That is, if the ancillary data set is not available within 24 hours after Level 1A generation, the data will be routed to off-line storage until the ancillary data set is available.

Level 2 data are geophysical parameters computed from the Level 1B record and other necessary data sets, using algorithms developed and provided by the TRMM Science Team. These data are at the first level that is directly usable for most scientific purposes. There are generally two stages for Level 2 data. One stage preserves the original instrument resolution and the other stage averages the data to produce data sets which have different spatial and/or temporal resolutions from the original instrument resolutions.

Table 28. Level 2 Physical Parameters

AVHRR	TRMM
Cloud cover	Composite rain rate (all instruments)
Rain estimate (area averages)	Vertical profile of rain
ESMR-SSM/I	**Ground Truth/Other Ancillary Data**
Rain rate (19 GHz)	Radar rain rate
Rain rate (37 GHz)	Rain gauge—rain rate
Rain rate (85.5 GHz)	Composite rain rate (each site)
Composite microwave radiometer rain rate	Experimental instruments—rain rate
	Other satellite rain estimates
Radar	Special meteorological data
Profiled rain rate	
Path-averaged rain rate	
Liquid water content	
Storm height	
Well-defined bright band (Y/N)	

At least 6 months of the Level 2 data generated with the most-current algorithms will be stored on-line for further analysis and fine tuning of the algorithms.

Level 3 data, produced from Level 2 data, are generally conceived to be mapped representations on a fixed-Earth grid system or representations in the form of histograms. The primary climatological data set for TRMM will be monthly averaged rainfall over 600 × 600 km grid boxes (approximately). The Level 3 data will be stored on-line for the mission life time.

Level 4 products will be derived products from models or analysis results based on inputs from TRMM observations. A wide variety of products are anticipated from modeling and analysis efforts. The Level 4 data sets can be produced at the SDPC if the Science Team members provide necessary modeling and/or analysis tools, or they can be produced at the Team members' computing facilities and delivered to the SDPC.

A challenging task for science data processing is to handle the high volume of about 20 Gigabits of output data per day. An equally challenging task is to handle data processing at an estimated 100 million instructions per second. Data handling and processing of this magnitude and speed are not trivial tasks and require extremely careful planning.

DATA ACCESS AND DISTRIBUTION

The TRMM Science Team will, of course, have immediate and direct access to all levels of data as they are being processed at the SDPC. The methods of access cannot be realistically defined now, but it is anticipated that scientists away from the processing center will have terminals and that reasonably high-speed data links will be commonly available at that time. Other methods of distribution, such as physical transfer of high-density storage media, are currently being considered.

SDPC will store, maintain, and distribute data to members of the Science Team during the mission life time. Other satellite data and *in situ* data, as approved and provided by the Science Team, will also be stored to offer immediate access to related data bases.

It is intended to make the TRMM data available to the general scientific community as quickly as possible. However, it cannot be determined this early how long each processing step will take. Algorithms and quality control procedures will have to be refined and other unanticipated problems will surely arise. Nevertheless, the NSSDC will participate from the beginning with the SDPT to implement and manage data catalogs and inventories, ensuring that they conform with NSSDC's standards and formats. Once the TRMM mission is over, the NSSDC will take over the TRMM archival data sets, catalogs, and other data bases and will be responsible for general distribution.

The NSSDC serves as the long-term archive and distribution center for data obtained from NASA Space and Earth Science flight investigations. In addition to direct distribution, a number of services will be available to participating science users through the NASA Climate Data System (NCDS). The NCDS functions as an interactive scientific information management system which provides an integrated set of tools for locating, manipulating, and displaying climate research data. TRMM products will be included in the NCDS as rapidly as the data sets are approved by the TRMM Science Team.

The NCDS supports a number of research and development data sets normally available from the NSSDC and several correlative data sets usually available only from other archives. It provides comprehensive information about available data, via catalogs and inventories, and flexible, easy access to the supported data sets. The NCDS's capabilities enable scientific users to locate data of interest, preview the data sets using graphical and statistical methods, and extract subsets of interest for further analysis at their own sites. The functions of the NCDS are illustrated in Figure 57.

Participating scientists can gain access to the NCDS in one of several ways: via dial-in lines, via the Space Physics Analysis Network (SPAN), via GTE Telenet, or via terminals linked directly to the computer system.

SUMMARY—DATA PROCESSING

The data acquisition process of converting raw data to Level 0, though complex, is relatively straightforward because of NASA's extensive experience with spaceborne science missions. (It will require an upgraded system to handle the high TRMM data rates.) Similarly, the NSSDC archiving and distribution system provides the advantage of well-organized procedures and facilities for handling such large volumes of data as TRMM will produce. Also, advancing technology should further streamline these functions, making data access even more timely and efficient in the future.

The real challenge, obviously, is in the science data processing. Here, we are moving into an arena of many new unknowns. Not only are we faced with totally new space instrumentation, i.e., space-borne rain radar, but we are seeking to measure one of the most elusive of all weather parameters. Rainfall, because of its extreme space, time, and intensity variability, cannot be measured completely nor directly with any straightforward techniques. We must develop many individual algorithms and combined algorithms using information from many sources, based not only on the complementarity of the TRMM instruments, but on other satellite- and surface-based observations as well, to arrive at credible rain estimates. And, of course, there are many related parameters that are of concern as well, particularly those associated with the vertical structure of rain. Thus, one can see why planning a comprehensive science data processing system for TRMM is exceedingly difficult and why only a general concept can be envisioned at this time.

Although progress is being made with statistical and algorithm studies, it is abundantly clear that the support task of theoretical and experimental research and associated software development is a huge one. If we are to have a smoothly running and effective science data processing system at launch time, a major effort will have to begin well in advance so that an initial algorithm/processing software system can be in place for substantial testing 6 to 9 months beforehand.

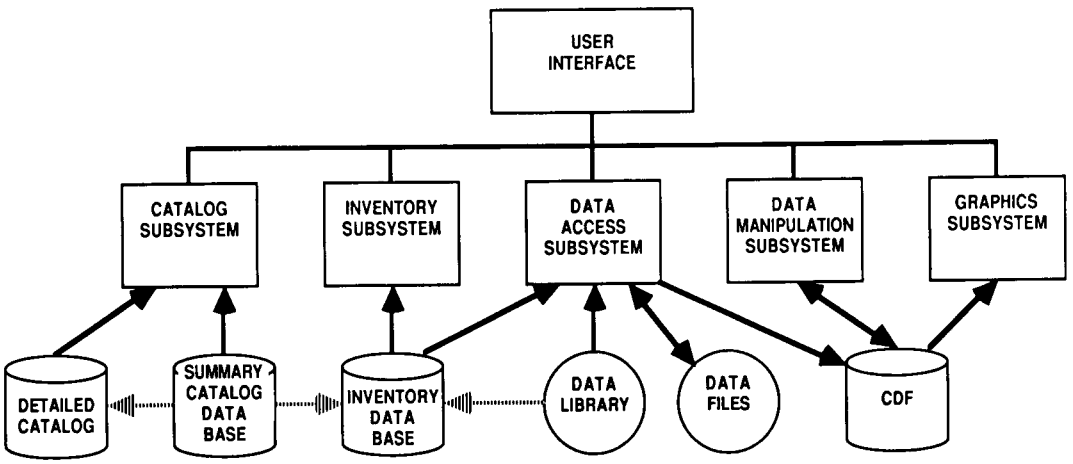

Figure 57. NASA climate data system.

REFERENCES

Adler, R. F., and R. A. Mack, 1984: Thunderstorm cloud height-rainfall rate relations for use with satellite rainfall estimation techniques. *J. Clim. Appl. Meteor., 23,* 280-296.

Adler, R. F., and A. J. Negri, 1988: A satellite infrared technique to estimate tropical convective and stratiform rainfall. *J. Appl. Meteor., 27,* 30-51.

Albright, M. D., E. E. Recker, R. J. Reed, and R. Dang, 1985: The diurnal variation of deep convection and inferred precipitation in the central tropical Pacific during January-February 1979. *Mon. Wea. Rev., 113,* 1663-1680.

Arkin, P. A., 1979: Relationship between fractional coverage of high cloud and rainfall accumulations during GATE over the "B" scale array. *Mon. Wea. Rev. 107,* 1382-1387.

Arkin, P. A., and B. Meisner, 1987: The relationship between large-scale convective rainfall and cold cloud over the western hemisphere during 1982-1984. *Mon. Wea. Rev., 115,* 51-74.

Arkin, P. A., V. E. Kousky, J. E. Janowiak, and E. A. O'Lenic, 1986: Atlas of the tropical and subtropical circulation derived from the national meterological center operational analysis. *NOAA Atlas No. 7,* U. S. Dept. of Commerce, Washington, D.C., 95 pp.

Atlas, D., and H. C. Banks, 1951: The interpretation of microwave reflections from rainfall. *J. Meteor., 8,* 271-282.

Atlas, D., and T. J. Matejka, 1985: Airborne doppler radar velocity measurements of precipitation in ocean surface reflection. *J. Geophys. Res., 90,* 5820-5828.

Atlas, D., D. Rosenfeld, and D. A. Short, 1988: The estimation of convective rainfall by area integrals. Part I: The theoretical and empirical basis. To be presented at the Amer. Meteor. Soc. Mesoscale Precipitation Conf., Boston, September 13-16, 1988.

Atlas, D., and O. W. Thiele, eds., 1981: Precipitation measurements from space. Workshop Report, D. Atlas and O. W. Thiele, Editors, NASA/Goddard Space Flight Center, Greenbelt, MD.

Augustine, J. A., 1984: The diurnal variation of large-scale inferred rainfall over the tropical pacific ocean. *Mon. Wea. Rev., 112,* 1745-1751.

Austin, P. M., 1947: Measurement of approximate raindrop size by microwave attenuation. *J. Meteor., 14,* 121-124.

Austin, P. M., and S. G. Geotis, 1978: Evaluation of the quality of precipitation data from a satellite-borne radiometer. Final report under NASA grant NSG 5024.

Balsley, B., W. L. Ecklund, D. A. Carter, A. C. Riddle, and K. S. Gage, 1988: Average vertical motions in the tropical atmosphere observed by a radar wind profiler on Pohnpei (7° N latitude, 157° E longitude). *J. Atmos. Sci., 45,* 396-405.

Bates, R. J., 1973: A generalization of the CISK theory. *J. Atmos. Sci., 30,* 1509-1511.

Battan, L. J., 1973: *Radar Observation of the Atmosphere.* 2nd Ed. Univ. of Chicago Press. Chicago and London. 324 pp. (See esp. pp. 175-178.)

Bell, T. L., 1987a: A space-time stochastic model of rainfall for satellite remote-sensing studies. *J. Geophys. Res., 92,* 9631-9643.

Bell, T. L., 1987b: Statistical problems in rainfall measurements from space. Invited lecture at the Joint Statistical Meetings of the American Statistical Assoc., August 17-20, 1987, San Francisco.

Bell, T. L., A. Abdullah, R. S. Martin, and G. R. North, 1987: A Monte Carlo study of sampling errors for satellite-derived tropical rainfall with a space-time stochastic model. (in preparation).

Bellon, A., and G. L. Austin, 1986: On the relative accuracy of satellite and rain gauge rainfall measurements over middle latitudes during the daylight hours. *J. Clim. Appl. Meteor., 25,* 1712-1724.

Betts, A. K., and W. Ridgway, 1988: Coupling of the radiative, convective, and surface fluxes over the equatorial pacific. *J. Atmos. Sci., 44,* 522-536.

Biondini, R., 1976: Cloud motion and rainfall statistics. *J. Appl. Meteor., 15,* 205-224.

Bjerknes, J., 1969: Atmospheric teleconnections from the equatorial Pacific. *Mon. Wea. Rev., 97,* 163-172.

Brier, G. W., and J. Simpson, 1969: Tropical cloudiness and rainfall related to pressure and tidal variations. *Quart. J. Roy. Met. Soc., 95,* 120-147.

Brummer, B., 1978: Mass and energy budgets of a 1 kilometer high atmospheric box over the GATE C-scale triangle during undisturbed and disturbed weather conditions. *J. Atmos. Sci., 35,* 997-1011.

Chang, A. T. C., and A. S. Milman, 1982: Retrieval of ocean surface and atmospheric parameters from multichannel microwave radiometric measurements. *IEEE Trans. on Geoscience and Remote Sensing, 20,* 217-224.

Cheng, C. P., 1981: Numerical simulation of the dynamics, cloud microphysics and radar echo structure of tropical and mid-latitude convection. Ph.D. dissertation, University of Washington, 271 pp.

Chesters, D., L. W. Uccellini, and W. D. Robinson, 1983: Low-level water vapor fields from the VISSR Atmospheric Sounder (VAS) split window channels. *J. Clim. Appl. Meteor., 22,* 725-743.

Chiu, L. S., 1987: Estimating Areal Rainfall from Rain Area. Int'l Symposium on Tropical Precipitation Measurements, Tokyo, October 28-30.

Chiu, L. S., 1988: Rain estimation from satellites: Areal rainfall-rain area relation. Third Conf. on Satellite Meteor. and Oceanog., Feb. 1-5, Amer. Meteor. Soc., Anaheim, CA, 363-368.

Crane, R. K., 1985: Comparative evaluation of several rain attenuation prediction models. *Radio Science, 20,* 843-863.

Dennis, A. S., A. Koscielski, D. E. Cain, J. H. Hirsch, and P. L. Smith, Jr., 1975: Analysis of radar observations of a randomized cloud seeding experiment. *J. Appl. Meteor., 14,* 897-908.

Doneaud, A. A., S. Ionescu-Niscov, D. L. Priegnitz, and P. L. Smith, 1984: The area-time integral as an indicator for convective rain volumes. *J. Clim. Appl. Meteor., 23,* 555-561.

Fennessy, M., L. Marx, and J. Shukla, 1985: General circulation model sensitivity to 1982-83 equatorial Pacific SST anomalies. *Mon. Wea. Rev., 113,* 858-864.

Fujita, M., K. Okamoto, S. Yoshikado, and K. Nakamura, 1985: Inference of rain rate profile and path-integrated rain rate by an airborne microwave rain scatterometer. *Radio Science, 20,* 631-642.

Gadgil, S., P. V. Joseph, and N. V. Joshi, 1984: Ocean-atmosphere coupling over monsoon regions. *Nature, 312,* 141-143.

Gagin, A., D. Rosenfeld, and R. E. Lopez, 1985: The relationship between height and precipitation characteristics of summertime convection cells in south Florida. *J. Atmos. Sci., 42,* 84-94.

Garstang, M., 1972: A review of hurricane and tropical meteorology. *Bull. Amer. Meteor. Soc., 53,* 612-630.

Garstang, M., and G. D. Emmitt, 1983: Anatomy of drought. Paper presented at Symposium on Atmospheric Sciences, Oct. 18-20, 1983, Pretoria, Rep. of S. Africa.

Gill, A. E., 1980: Some simple solutions for heat-induced tropical circulation. *Quart. J. Roy. Met. Soc., 106,* 447-462.

Goldhirsh, J., 1983: Yearly variations of rain rate statistics at Wallops Island and their impact on modeled slant path attenuation distribution. *IEEE Trans. Antennas Propagat. AP 31,* 918-921.

Goldhirsh, J., and I. Katz, 1974: Estimation of rain drop size distribution using multiple wavelength radar systems. *Radio Sci., 9,* 439-446.

Goldhirsh, J., and E. J. Walsh, 1982: Measurement of precipitation with a TOPEX-class dual frequency satellite altimeter. Proceedings of URSI Commission F, Multiple Parameter Radar Measurements of Precipitation. Bournemouth, UK.

Hakkarinen, I. M., and R. F. Adler, 1987: Observations of convective precipitation at 92 and 183 GHz: Aircraft results. *Meteor. and Atmos. Phys.* (in press).

Harriss, R. C., S. C. Wofsy, M. Garstang, E. V. Browell, L. C. B. Molion, R. J. McNeal, J. M. Hoell, Jr., R. J. Bendura, S. M. Beck, R. L. Navarro, J. T. Riley, and R. L. Snell, 1988: The Amazon boundary layer experiment. [ABLE 2A]: Dry season 1985. *J. Geophys. Res., 93,* 1351-1360.

Hartmann, D. L., H. H. Hendon, and R. A. Houze, Jr., 1984: Some implications of the mesoscale circulations in tropical cloud clusters for large-scale dynamics and climate. *J. Atmos. Sci., 41,* 113-121.

Hayashi, Y. Y., and A. Sumi, 1986: The 30-40 day oscillations simulated in an "aqua planed" model. *J. Meteor. Soc. Japan, 61,* 812-828.

Hitschfeld, W., and J. Bordan, 1954: Errors inherent in the radar measurement of rainfall at attenuating wavelengths. *J. Meteor., 11,* 58-67.

Horel, J. D., and J. M. Wallace, 1981: Planetary scale atmospheric phenomena associated with the southern oscillation. *Mon. Wea. Rev., 109,* 813-829.

Houze, R. A., Jr., 1981: Structure of atmospheric precipitation systems: A global survey. *Radio Science, 16,* 671-689.

Houze, R. A., Jr., 1982: Cloud clusters and large-scale vertical motions in the tropics. *J. Meteor. Soc. Japan, 60,* 396-410.

Houze, R. A., Jr., and A. K. Betts, 1981: Convection in GATE. *Rev. Geophys. and Space Phys., 41,* 541-576.

Houze, R. A., Jr., and C. P. Cheng, 1977: Radar characteristics of tropical convection observed during GATE: Mean properties and trends over the summer season. *Mon. Wea. Rev., 105,* 964-980.

Houze, R. A., Jr., and D. D. Churchill, 1987: Mesoscale organization and cloud microphysics in a Bay of Bengal depression. *J. Atmos. Sci.* (in press).

Houze, R. A., Jr., S. G. Geotis, F. D. Marks, Jr., and A. K. West, 1981: Winter monsoon convection in the vicinity of North Borneo. Part I: Structure and time variation of the clouds and precipitation. *Mon. Wea. Rev., 109,* 1595-1614.

Houze, R. A., Jr., and P. V. Hobbs, 1982: Organization and structure of precipitating cloud systems. *Advances in Geophysics, 24,* 225-315.

Hudlow, M. D., R. Arkell, V. Patterson, P. Pytlowany, F. Richards, and S. Geotis, 1979: Calibration and intercomparison of the GATE C-band radars. NOAA Technical Report EDIS 31.

Hudlow, M. D., and V. L. Patterson, 1979: GATE radar rainfall atlas. NOAA special report, U.S.G.P.O., Washington, D.C.

Inoue, T., 1987: An instantaneous delineation of convective rainfall areas using split window data of NOAA-7 AVHRR. *J. Meteor Soc. of Japan., 65,* 469-481.

Jaeger, L., 1976: Monatskarten des Niederschlags fur die ganz Erde. *Berichte des Deutschen Wetterdienstes, 18,* No. 139. Im Selbsverlag des Deutschen Welterdienstes, Offenbach, W. Germany.

Janowiak, J. E., A. F. Krueger, and P. A. Arkin, 1985: Atlas of outgoing longwave radiation derived from NOAA satellite data. NOAA Atlas No. 6, U.S. Dept of Commerce, 44 pp.

Jastrow, R., and M. H. Thompson, 1972: Astronomy: fundamentals and frontiers. John Wiley & Sons, Inc., New York, 404.

Johnson, R. H., and Hamilton, 1987: The relationship of surface pressure features to the precipitation and air flow structure of an intense mid-latitude squall line. Submitted to *Mon. Wea. Rev.*

Johnson, R. H., and R. A. Houze, Jr., 1987: Precipitating cloud systems of the Asian monsoon. In Reviews in Monsoon Meteorology, C.-P. Chang and T. N. Krishnamurti, Eds. (in press).

Jones, W. L., L. C. Schroeder, and J. L. Mitchell, 1977: Aircraft measurements of the microwave scattering signature of the ocean. *IEEE Trans. Ant. Prop., AP-25 (1),* 52-61.

Jorgensen, D. P., 1984: Mesoscale and convective scale characteristics of mature hurricanes. Part I. General observations by research aircraft. *J. Atmos. Sci., 41,* 1268-1285.

Kedem, B., L. S. Chiu, and G. R. North, 1987: Estimating time mean areal average rainfall: A mixed distribution approach. Submitted to *J. Geophys. Res.*

Klett, J. D., 1981: Stable analytical inversion solution for processing lidar returns. *Appl. Opt., 20,* 211-220.

Knutson, T. R., and K. M. Weickmann, 1987: 30-60 day atmospheric oscillations: Composite life cycles of convection and circulation anomalies. *Mon. Wea. Rev.* (in press).

Kraus, E. B., 1963: The diurnal precipitation change over the sea. *J. Atmos. Sci., 20,* 546-551.

Krishnamurti, T. N., 1971: Tropical east-west circulations during the northern summer. *J. Atmos. Sci., 28,* 1342-1347.

Krishnamurti, T. N., M. Kanamitsu, W. J. Koss, and J. D. Lee, 1973: Tropical east-west circulations during the northern winter. *J. Atmos. Sci., 30,* 780-787.

Kummerow, C., 1987: Microwave radiances from horizontally finite, vertically structured precipitating clouds. Ph.D. thesis, Univ. of Minnesota, Minneapolis, MN, 146 pp.

Kummerow, C., R. A. Mack, and I. M. Hakkarinen, 1988: A self-consistency approach to improved microwave rainfall rate estimation from space. *J. Appl. Meteor.* (submitted).

Kummerow, C., and J. A. Weinman, 1988: Determining microwave brightness temperatures from precipitating horizontally finite and vertically structured clouds. *J. of Geophys. Res., 93,* 3720-3728.

Lavoie, R. L., 1963: Some aspects of the meteorology of the tropical Pacific viewed from an atoll. Rep. No. 27, Institute of Geophysics, Univ. of Hawaii, 76 pp.

Lau. K.-M., and P. H. Chan, 1985: Aspects of the 40-50 day oscillations during the northern winter as inferred from outgoing longwave radiation. *Mon. Wea. Rev., 113,* 1889-1909.

Lau, K.-M., and P. H. Chan, 1986: The 40-50 day oscillation and the El Niño/southern oscillation: A new perspective. *Bull. Amer. Meteor. Soc., 67,* 533-534.

Lau, K.-M., and P. H. Chan, 1987: Intraseasonal and interannual variations of tropical convection: A possible link between the 40-day mode and ENSO? *J. Atmos. Sci.* (in press).

Lau, N.-C., and K.-M. Lau, 1986: The structure and propagation of intraseasonal oscillations appearing in a GFDL general circulation model. *J. Atmos. Sci., 43,* 2023-2047.

Lau, K.-M., and M.-T. Li, 1984: The monsoon of East Asia and its global associations — A survey. *Bull. Amer. Meteor. Soc., 65,* 114-125.

Lau, K.-M., and L. Peng, 1987: Origin of low frequency (intra-seasonal) oscillations in the tropical atmosphere. Part I: The basic theory. *J. Atmos. Sci.,* 950-972.

Lau, K.-M., and T. J. Phillips, 1986: Coherent fluctuations of extratropical geopotential height and tropical convection in intraseasonal time scales. *J. Atmos. Sci., 43,* 1164-1181.

Lau, K.-M., C. H. Sui, and L. Peng, 1987: A theory of low-frequency oscillations in the tropical atmosphere. Proceedings of the 17th Conf. on Hurricanes and Tropical Meteorology, Miami, FL, 401-404.

Lau, K- M., G. J. Yang, and S. Shen, 1987: Seasonal and intraseasonal climatology of monsoon rainfall over East Asia. *Mon. Wea. Rev.* (in press).

Laughlin, C. R., 1981: On the effect of temporal sampling on the observation of mean rainfall. Precipitation Measurements from Space, D5-D66, Workshop Report, ed. by D. Atlas and O. Thiele. NASA publication, available from Goddard Space Flight Center, Greenbelt, MD 20771.

Leary, C. A., and R. A. Houze, Jr., 1979: Melting and evaporation of hydrometeors in precipitation from the anvil clouds of deep tropical convection. *J. Atmos. Sci., 36,* 669-679.

Leary, C. A., and R. A. Houze, Jr., 1980: The contribution of mesoscale motions to the mass and heat fluxes of an intense tropical convective system. *J. Atmos. Sci., 37,* 784-796.

Leith, C. E., 1973: The standard error of time-average estimates of climatic means. *J. Appl. Meteor., 12,* 1066-1069.

Lin, Y.-I., R. D. Farley, and H. D. Orville, 1983: Bulk parameterization of the snow field in a cloud model. *J. Clim. Appl. Meteor., 22,* 1065-1092.

Lopez, R. E., 1977: The log-normal distribution and cumulus cloud populations. *Mon. Wea. Rev., 105,* 865-872.

Lopez, R. E., J. Thomas, D. O. Blanchard, and R. L. Holle, 1983: Estimation of rainfall of an extended region using only measurements of the area covered by radar echoes. 21st Conf. on Radar Meteor. Amer. Meteor. Soc., Edmonton, Canada, Sept. 19-23, 681-686.

Lorenc, A. C., 1984: The evolution of planetary-scale 200 mb divergent flow during the FGGE year. *Quart. J. Roy. Meteor. Soc., 110,* 427-441.

Lü, D., and L. Hai, 1982: Annual Report, Institute of Atmos. Phys., Academia Sinica, 91-97.

Madden, R. A., and P. R. Julian, 1971: Detection of a 40-50 day oscillation in the zonal wind in the tropical Pacific. *J. Atmos. Sci., 28,* 702-708.

Madden, R. A., and P. R. Julian, 1972: Description of global scale circulation cells in the tropics with a 40-50 day period. *J. Atmos. Sci., 29,* 1109-1123.

Malkus, J. S., 1962: Large-scale interactions. *The Sea: Ideas and Observations on Progress in the Study of the Seas. Chap. 4, 1,* 88-294, Interscience Publishers. New York and London.

Malkus, J. S., 1963: Tropical convection: Progress and outlook. Proc. Symposium on Tropical Meteor. Rotorua, New Zealand, 247-277.

Malkus, J. S., and H. Riehl, 1964: Cloud structure and distributions over the tropical Pacific Ocean. University of California Press. Berkeley and Los Angeles, 229 pp.

Martin, D. W., and M. R. Howland, 1986: Grid History: A geostationary satellite technique for estimating daily rainfall in the tropics. *J. Clim. Appl. Meteor., 25,* 184-195.

McConnell, A., and G. R. North, 1987: Sampling errors in satellite estimates of tropical rain. *J. Geophys. Res., 92,* 9567-9570.

McGarry, M. M., and R. J. Reed, 1978: Diurnal variations in convective activity and precipitation during phases II and III of GATE. *Mon. Wea. Rev., 106,* 101-113.

Meneghini, R., and D. Atlas, 1986: Simultaneous ocean cross section and rainfall measurements from space with a nadir-looking radar. *J. Atmos. and Ocean Tech., 3,* 400-413.

Meneghini, R., J. Eckerman, and D. Atlas, 1983: Determination of rain rate from spaceborne radar using measurements of total attenuation. *IEEE Trans. on Geoscience and Remote Sensing, GE-21,* 34-43.

Meneghini, R., K. Nakamura, C. W. Ulbrich, D. Atlas, T. D. Clem, and S. R. Kostic, 1986: Comparisons of methods using data from an airborne dual wavelength radar. Preprint Vol., 23rd Conf. on Radar Meteor., and the Conf. on Cloud Physics, Amer. Meteor. Soc., Snowmass, CO, 100-103.

Mintz, Y., and C. Leovy, 1969: Numerical simulation of the atmospheric circulation and climate of Mars. *J. Atmos. Sci., 26,* 1167-1190.

Mooley, D. A., and J. Shukla, 1987: Variability and forecasting of the summer monsoon rainfall over India. *Reviews in Monsoon Meteorology,* Eds. C. P. Chang and T. N. Krishnamurti, Oxford Monograph Geological and Geophysics, No. 7, Oxford University Press, 26-59.

Nakazawa, T., 1987: Analysis of super cloud cluster by geostationary meteorological satellite infrared 3-hourly data. International Symposium on Tropical Precipitation Measurements, Tokyo, October 28-30.

NASA Advisory Council, 1986: Earth system science overview: A program for global change, NASA, Washington, D.C., 48 pp.

National Academy of Sciences, 1980: Atmospheric precipitation: Prediction and research problems. National Research Council, Washington, D.C.

National Academy of Sciences, 1985: A strategy for Earth science from space in the 1980's, Part II: Atmosphere and interactions with the solid Earth, oceans and biota. Committee on Earth Sciences of the Space Science Board, National Research Council, Washington, D.C.

National Academy of Sciences, 1986: U. S. Participation in the TOGA program: A research strategy. National Academy Press, Washington, D.C., 24 pp.

National Academy of Sciences, 1986a: Global change in the geosphere-biosphere: Initial priorities for an IGBP. U. S. Committee for an International Geosphere-Biosphere Program of the Commission on Physical Sciences, Mathematics and Resources, National Research Council, Washington, D.C.

Nitta, T., 1987: Convective activities in the tropical western Pacific and their impact on the northern hemisphere southern circulation. *J. Meteor. Soc. Japan, 65,* 373-390.

Okamoto, K., and T. Kozu, 1987: Conceptual design of TRMM radar. Unpublished report, Radio Res. Lab., Japan, April 3, 1987.

Okamoto, K., T. Kozu, K. Nakamura, and T. Ihara, 1987: Tropical rainfall measuring mission rain radar. International Symposium on Tropical Precipitation Measurements, Tokyo, October 28-30, (to appear in Proceedings).

Okamoto, K., S. Yoshikado, H. Masuko, T. Ojima, N. Fujono, K. Nakamura, J. Awaka, and H. Inomata, 1982: Airborne microwave rain-scatterometer/radiometer. *Int. J. Remote Sens., 3,* 277-294.

Olson, W. S., 1986: Model-based retrieval of tropical cyclone rainfall rates using the Nimbus-7 SMMR. Preprint Vol., Second Conf. on Satellite Meteor./Remote Sensing Applications. Amer. Met. Soc., Williamsburg, VA, 438-443.

Olson, W. S., 1987: Estimation of rainfall rates in tropical cyclones by passive microwave radiometry. Ph.D. Thesis. Univ. of Wisconsin, Madison, WI, 282 pp.

Olson, W. S., 1988: Physical retrieval of rainfall rates over the ocean by multi-spectral microwave radiometry—application to tropical cyclones (in preparation).

Palmer, T. N., and J. S. Owen, 1986: A possible relationship between some severe winters in North America and enhanced convective activity over the tropical west Pacific. *Mon. Wea. Rev., 114,* 648-651.

Pasqualucci, F., 1976: Drop-size distribution in unicell, multicell and squall-line storms. Intern'tl Cloud Phys. Conf. July 26-30, Amer. Meteor. Soc. Boulder, CO, 522-525.

Philander, S. G. F., 1979: Variability of the tropical oceans. *Dyn. Oceans Atmos., 3,* 191-208.

Piola, A. J., and A. L. Gordon, 1984: Pacific and Indian Ocean upper-layer salinity budget. *J. Phys. Oceanogr., 14,* 747-753.

Ramage, C. S., 1968: Role of a tropical "maritime continent" in the atmospheric circulation. *Mon. Wea. Rev., 96,* 365-370.

Ramanathan, V., 1987: Atmospheric general circulation and its low frequency variance: Radiative influences. Submitted to *Jour. Japanese Meteor. Soc.*

Rasmusson, E. M., 1985: El Niño and variations in climate. *American Scientist, 73,* 168-178.

Rasmusson, E. M., 1987: Global climate change and variability: Effects on drought and desertification in Africa. *Drought and Hunger in Africa: Denying Famine a Future.* M. H. Glantz, Editor, Cambridge University Press, Cambridge, U.K., pp. 3-22.

Rasmusson, E. M., and P. A. Arkin, 1985: Interannual climate variability associated with the El Niño/southern oscillation. Coupled Ocean-Atmosphere Models. Elsevier Science Publishers B.V., Amsterdam, 697-725.

Rasmusson, E. M., and T. H. Carpenter, 1982: Variations in tropical sea surface temperature and surface wind fields associated with the southern oscillation/El Niño. *Mon. Wea. Rev., 110,* 354-384.

Riehl, H., 1954: *Tropical Meteorology.* McGraw-Hill Book Co., New York, 392 pp.

Riehl, H., and J. S. Malkus, 1958: On the heat balance in the equatorial trough zone. *Geophysica, 6,* 503-535.

Riehl, H., and J. Simpson, 1979: The heat balance of the equatorial trough zone, revisited. Contributions to *Atmos. Phys., 52,* 287-304.

Riehl, H., T. C. Yeh, J. S. Malkus, and N. E. LaSeur, 1951: The north-east trade of the Pacific Ocean. *Quart. Jour. Roy. Met. Soc., 77,* 598-626.

Rodgers, E. B., and H. Siddalingaiah, 1983: The utilization of Nimbus-7 SMMR measurements to delineate rainfall over land. *J. Clim. Appl. Meteor., 22,* 1753-1763.

Rogers, R. R., 1979: *A Short Course in Cloud Physics.* 2nd Ed. Pergamon Press, Oxford, 235 pp. (see esp. p. 88).

Rosenfeld, D., D. Atlas, and D. Short, 1988: The estimation of convective rainfall by area integrals. Part II: The Height Area Rainfall Threshold (HART) Method. To be presented at the Amer. Meteor. Soc. Mesoscale Precip. Conf., Boston, September 13-16, 1988.

Rosenfeld, D., and A. Gagin, 1988: The factors governing the total rainfall yield of continental convective clouds. Accepted by *J. Appl. Meteor.*

Rosenfeld, D., and Y. Mintz, 1988: Evaporation of rain falling from convective clouds as derived from radar measurements. *J. Clim. Appl. Meteor., 27,* 209-215.

Rosenfeld, D., and W. L. Woodley, 1988: The effect of cloud seeding for dynamic effects in west Texas, Part I: Individual cells. Submitted to *J. Appl. Meteor.*

Rutledge, S. A., and P. V. Hobbs, 1984: The mesoscale and microscale structure and organization of clouds and precipitation in mid-latitude clouds. Part XII: A diagnostic modeling study of precipitation development in narrow cold frontal bands. J. Atmos. Sci., 41, 2949-2972.

Schiffer, R. A., 1987: Global energy and water cycle experiment (GEWEX). Int'l Symposium on Tropical Precipitation Measurements, Tokyo, Japan, Oct 28-30, 1987. (to appear in Proceedings).

Sellers, W. D., 1969: A global climatic model based on the energy balance of the Earth-atmosphere system. *J. Appl. Meteor., 8,* 392-400.

Shin, K.-S., and G. R. North, 1987: Sampling error study for rainfall estimates by satellites using a stochastic model. Tenth Conference on Probability and Statistics, October 4-5, Edmonton, Alberta, Canada. Published by the American Meteorological Society, Boston.

Shin, K.-S., and G. R. North, 1988: Sampling error study for rainfall estimates by satellites using a stochastic model. *J. Appl. Meteor.* (in press—to appear in August issue).

Shukla, J., 1984: Predictability of time averages: Part II: The influence of the boundary forcings. *Problems and Prospects in Long and Medium Range Weather Forecasting,* Eds. D. M. Burridge and E. Keller, Springer Verlag, London, 155-206.

Shukla, J., 1987: Variability of rainfall over tropical oceans: Scientific basis and justification for TRMM. Proceedings of the International Symposium on Tropical Precipitation Measurements, Tokyo, Japan, 1987.

Shukla, J., and J. M. Wallace, 1983: Numerical simulation of the atmospheric response to the equatorial pacific sea surface temperature anomalies. *J. Atmos. Sci., 40,* 1613-1630.

Simmons, A. J., J. M. Wallace, and G. W. Branstator, 1983: Barotropic wave propagation and instability and atmospheric teleconnection patterns. *J. Atmos. Sci., 40,* 1363-1392.

Simpson, J., 1972: Use of the gamma distribution in single-cloud rainfall analysis. *Mon. Wea. Rev., 100,* 309-312.

Simpson, J., R. F. Adler, and G. North, 1988: A proposed tropical rainfall measuring mission (TRMM) satellite. *Bull. Amer. Met. Soc., 69,* 278-295.

Simpson, J., R. L. Holle, and R. W. Reeves, 1977: On the cloud structure in the GATE B-scale array. Proc. 11th Tech. Conf. on Hurricanes and Tropical Meteor., Amer. Met. Soc., Miami Beach, FL, December 13-16, 339-346.

Simpson, R. H., and H. Riehl, 1981: The hurricane and its impact. Louisiana State University Press. Baton Rouge and London, 398 pp.

Simpson, J., and G. Van Helvoirt, 1980: GATE cloud-subcloud layer interactions examined using a three-dimensional cumulus model. *Beiträge zur den Physik der Atmosphäre, 53,* 106-134.

Simpson, J., G. Van Helvoirt, and M. C. McCumber, 1982: Three-dimensional simulations of cumulus congestus clouds on GATE day 261. *J. Atmos. Sci., 39,* 126-145.

Smith, T. B., R. L. Peace, and S. N. Howard, 1977: Radar evaluation of Big Spring weather modification program. *T.D.W.R. LP-5,* Texas Dept. of Water Resources, Austin, TX.

Soong, S.-T., and W.-K. Tao, 1980: Response of deep tropical cumulus clouds to mesoscale processes. *J. Atmos. Sci., 37,* 2016-2034.

Spencer, R. W., 1986: A satellite passive 37 GHz scattering-based method for measuring oceanic rain rates. *J. Clim. and Appl. Meteor., 25,* 754-766.

Spencer, R. W., B. B. Hinton, and W. S. Olson, 1983b: Nimbus-7 37 GHz radiances correlated with radar rain rates over the Gulf of Mexico. *J. Clim. and Appl. Meteor., 22,* 2095-2099.

Spencer, R. W., D. W. Martin, B. B. Hinton, and J. A. Weinman, 1983a: Satellite microwave radiances correlated with radar rain rates over land. *Nature, 304,* 141-143.

Spencer, R. W., W. S. Olson, R. Wu, D. W. Martin, J. A. Weinman, and D. A. Santek, 1983a: Heavy thunderstorms observed by the Nimbus-7 scanning multi-channel microwave radiometer. *J. Clim. and Appl. Meteor., 22,* 1041-1046.

Spencer, R. W., W. S. Olson, R. Wu, D. W. Martin, J. A. Weinman, and D. A. Santek, 1983b: Heavy thunderstorms observed by Nimbus-7 scanning multi-channel microwave radiometer. *J. Clim. and Appl. Meteor., 22,* 1041-1046.

Stephens, G. L., and P. J. Webster, 1984: Cloud decoupling of surface and upper radiation balances. *J. Atmos. Sci., 41,* 681-686.

Szejwach, G., 1982: Determination of semi-transparent cirrus cloud temperature from infrared radiances: Application to METEOSAT. *J. Appl. Meteor., 21,* 384-393.

Szejwach, G., R. F. Adler, I. Jobard, and R. A. Mack, 1986: A cloud model-radiative model combination for determining microwave T_B-rain rate relations. Preprint Vol., Second Conf. on Satellite Meteor./Remote Sensing and Applications, Amer. Met. Soc., Williamsburg, VA, 444-449.

Taft, B. A., and W. S. Kessler, 1987: On the effects of salinity on the dynamics of the Pacific Ocean tropical circulation. *Tropical Ocean-Atmosphere Newsletter, 41,* 8-10.

Tanaka, H., K. Kato, S. Saitoh, G. Liu, and Y. Ishizaka, 1987: Large and mesoscale characteristics of the Baiu front. Int'l Symposium on Tropical Precipitation Measurements, Tokyo, Japan, Oct. 28-30, 1987. (to appear in Proceedings).

Tao, W.-K., and J. Simpson, 1984: Cloud interactions and merging: Numerical simulations. *J. Atmos. Sci., 41,* 2901-2917.

Tao, W.-K., and J. Simpson, 1988: Modeling of tropical squall-type convective line. *J. Atmos. Sci.,* conditionally accepted.

Tao, W.-K., J. Simpson, and S.-T. Soong, 1987: Statistical properties of a cloud ensemble: A numerical study. *J. Atmos. Sci., 44,* 3175-3187.

Tao, W.-K., and S.-T. Soong: 1986: The study of the response of deep tropical clouds to mesoscale processes: Three-dimensional numerical experiments. *J. Atmos. Sci., 43,* 2653-2676.

Thiele, O. W., Ed. 1987: On requirements for a satellite mission to measure tropical rainfall. NASA Ref. Pub. 1183, 49 pp.

Tsonis, A. A., and G. A. Isaac, 1985: On a new approach for instantaneous rain area delineation in the mid-latitudes using GOES data. *J. Clim. Appl. Meteor., 24,* 1208-1218.

Ulanski, S. L., and M. Garstang, 1978: Some aspects of Florida convective rainfall. *Water Resources Research, 14,* 1133-1139.

Ulanski, S. L., and M. Garstang, 1978a: The role of surface divergence and vorticity in the life cycle of convective rainfall, Part I: Observations and analysis. *J. Atmos. Sci., 35,* 1047-1062.

Ulanski, S. L., and M. Garstang, 1978b: The role of surface divergence and vorticity in the life cycle of convective rainfall, Part II: Descriptive Model. *J. Atmos. Sci., 35,* 1063-1069.

Ulanski, S. L., and M. Garstang, 1978c: Some aspects of Florida convective rainfall. *Water Resour. Res., 14,* 1133-1139.

Ulbrich, C., and D. Atlas, 1985: Extinction of visible and infrared radiation in rain: Comparison of theory and experiment. *J. Atmos. and Oceanic Tech., 2,* 331-339.

Walker, G. T., and E. W. Bliss, 1932: World Weather V., *Mem. Roy. Meteor. Soc., 4,* 53-84.

Wallace, J. M., and D. S. Gutzler, 1981: Teleconnections in the geopotential height field during the northern hemisphere winter. *Mon. Wea. Rev., 109,* 784-811.

Wang, J.-T., D. Rosenfeld, G. R. North, and S. Nakamoto, 1988: The effect of spatial resolution on the correlation structure of GATE III rainfall fields. (manuscript to be submitted).

Webster, P. J., 1981: Mechanisms determining the atmospheric response to large-scale sea surface temperature anomalies. *J. Atmos. Sci., 38,* 554-571.

Webster, P. J., 1982: Seasonality of atmospheric response to sea-surface temperature anomalies. *J. Atmos. Sci., 39,* 29-40.

Webster, P. J., 1987a: Elements of ocean-atmosphere interaction: Scientific strategies for TOGA. Submitted to *Quart. J. Roy. Met. Soc.* Presented as The Adrian Gill Memorial Lecture, IUGG, Vancouver, Aug. 14, 1987.

Webster, P. J., 1987b: The role of hydrological processes in ocean-atmosphere interaction. International Symposium on Tropical Precipitation Measurements. Tokyo, Japan, Oct. 28-30, 1987. (to appear in Proceedings).

Webster, P. J., and G. L. Stephens, 1980: Tropical upper-troposphere extended clouds: Inferences from winter MONEX. *J. Atmos. Sci., 37,* 1521-1541.

Weickmann, K. M., G. R. Lussky, and J. E. Kutzbach, 1985: Intraseasonal (30-60 day) fluctuations of outgoing longwave radiation and 250 Mb streamfunction during northern winter. *Mon. Wea. Rev., 113,* 941-961.

Weinman, J. A., 1988: The derivation of atmospheric extinction profiles and wind speed over the ocean from a satellite borne lidar. Submitted to *Appl. Opt.*

Weinman, J. A., and P. J. Guetter, 1977: Determination of rainfall distribution from microwave radiation measured by the Nimbus-6 ESMR. *J. Appl. Meteor., 16,* 437-442.

Weinman, J. A., and C. D. Kummerow, and C. A. Atwater, 1988: An algorithm to derive precipitation profiles from a downward viewing radar and a multifrequency passive radiometer. Submitted to *IGAARS 88.*

Wilheit, T. T., A. T. C. Chang, M. S. V. Rao, E. B. Rodgers, and J. S. Theon, 1977: A satellite technique for quantitatively mapping rainfall rates over the ocean. *J. Appl. Meteor., 16,* 551-560.

Wilheit, T. T., J. L. King, E. B. Rodgers, R. A. Nieman, B. M. Krupp, A. S. Milman, J. S. Stratigos, and H. Siddalingaiah, 1982: Microwave radiometric observations near 19.35, 35, 92 and 183 GHz of precipitation in tropical storm Cora. *J. Appl. Meteor., 21,* 1137-1145.

Williams and Houze, 1987: Satellite-observed characteristics of winter monsoon cloud clusters. *Mon. Wea. Rev., 115,* 509 -515.

Woodley, W. L., A. R. Olsen, A. Herndon, and V. Wiggert, 1975: Comparisons of gage and radar methods of convective rain measurements. *J. Appl. Meteor., 14,* 909-928.

World Climate Research Program, 1985: 1985 scientific plan for the tropical ocean and global atmosphere program. *W.C.R.P. Publication Series 3,* World Meteorological Org., Geneva, 146 pp.

World Climate Research Program, 1987: Space system possibilities for a global energy and water cycle experiment. (WCP- 137), Columbia, MD, January 19-23, 1987.

World Climate Research Program, 1988: Validation of satellite precipitation measurements for the global precipitation climatology project. (WCRP-1) WMO/TD-No. 203, Washington, D.C., November 17-21, 1986.

Wu, R., and J. A. Weinman, 1984: Microwave radiances from precipitating clouds containing aspherical ice, combined phase, and liquid hydrometeors. *J. Geophys. Res., 89,* 7170-7178.

Wu, R., J. A. Weinman, and R. T. Chin, 1985: Determination of rainfall rates from GOES satellite images by a pattern recognition technique. *J. Atmos. Ocean Tech., 2,* 314-330.

Wyrtki, K., 1975: El Niño - the dynamic response of the equatorial Pacific Ocean to atmospheric forcing. *J. Phys. Oceanogr., 5,* 572-584.

ACRONYMS

ABLE	Amazon Boundary Layer Experiment
AMEX	Australian Monsoon Experiment
AMMS	Advanced Microwave Moisture Sounder
ATI	Area-Time-Integral
AVHRR	Advanced Very High Resolution Radiometer
C&DH	Command and Data Handling
CISK	Conditional Instability of the Second Kind
CMS	Command Management System
COHMEX	Cooperative Huntsville Meteorological Experiment
CRL	Communications Research Laboratory
CST	Convective-Stratiform Technique
DMSP	Defense Meteorological Satellite Program
DSD	Drop Size Distribution
ELV	Expendable Launch Vehicle
EMEX	Equatorial Mesoscale Experiment
ENSO	El Niño-Southern Oscillation
Eos	Earth Observing System
ESA	European Space Agency
ESMR	Electrically Scanning Microwave Radiometer
FAA	Federal Aviation Administration
FACE	Florida Area Cumulus Experiment
FDF	Flight Dynamics Facility
FGGE	First GARP (Global Atmospheric Research Program) Global Experiment
FOT	Flight Operations Team
FOV	Field of View
GARP	Global Atmospheric Research Program
GATE	GARP (Global Atmospheric Research Program) Atlantic Tropical Experiment
GCM	General Circulation Model
GEWEX	Global Energy and Water Cycle Experiment
GLAS	Goddard Laboratory for Atmospheric Sciences
GOES	Geostationary Operational Environmental Satellite
GPS	Global Positioning System
GSFC	Goddard Space Flight Center
GTE	General Telephone and Electronics
HART	Height Area Rainfall Threshold
ICAT	Instrument Calibration Team
IEEE	Institute of Electrical and Electronic Engineers
IFOV	Instantaneous Field of View
IR	Infrared
ITCZ	Intertropical Convergence Zone
ITT	International Telephone and Telegraph (Corporation)
KSC	Kennedy Space Center
MMS	Multimission Modular Spacecraft
MONEX	Monsoon Experiment
MOR	Mission Operations Room
MPR	Microwave Precipitation Radiometer

ACRONYMS (continued)

NASA	National Aeronautics and Space Administration
NASCOM	NASA (National Aeronautics and Space Administration) Communications (Network)
NCAR	National Center for Atmospheric Research
NCDS	NASA (National Aeronautics and Space Administration) Climate Data System
NEDT	Noise Equivalent Delta Temperature
NOAA	National Oceanic and Atmospheric Administration
NRCS	Normalized Radar Cross-Section
NSSDC	National Space Science Data Center
OBC	On-Board Computer
OLR	Outgoing Longwave Radiation
pdf	Probability Density Function
PNA	Pacific-North America
POCC	Payload Operations Control Center
PRTF	Primary Rainfall Test Facility
RV	Rain Volume
SAT	Science Algorithm Team
SDPC	Science Data Processing Center
SDPF	Science Data Processing Facility
SDPT	Science Data Processing Team
SMA	S-Band Multiple Access
SMMR	Scanning Multichannel Microwave Radiometer
S/N (SNR)	Signal-to-Noise (Ratio)
SPAN	Space Physics Analysis Network
SPCZ	South Pacific Convergence Zone
SSA	Single-Band Single Access
SSG	Science Steering Group
SSM/I	Special Sensor Microwave/Imager
SSO	Sun-Synchronous Orbit
SST	Sea Surface Temperature
T_B	Brightness Temperature
TDRSS	Tracking and Data Relay Satellite System
Tiros	Television and Infrared Observation Satellite
TMR	TRMM (Tropical Rainfall Measuring Mission) Microwave Radiometer
TOGA	Tropical Ocean and Global Atmosphere
TRMM	Tropical Rainfall Measuring Mission
TWTA	Traveling Wave Tube Amplifier
VHF	Very High Frequency
VIS/IR	Visible/Infrared
VISSR	Visible-Infrared Spin Scan Radiometer
WCRP	World Climate Research Program
WOCE	World Ocean Circulation Experiment
WSGT	White Sands Ground Tracking
WWW	World Weather Watch